



Department für Biotechnologie



Vorstand:

Ao.Univ.Prof. Dipl.-Ing. Dr.rer.nat. Reingard Grabherr

Betreuer:

Assoc. Prof. Dipl.-Ing. Dr. Johannes Grillari

Differentially secreted miRNAs in senescent fibroblasts and their impact on skin aging

Dissertation

zur Erlangung des Doktorgrades

an der Universität für Bodenkultur

Eingereicht von

Dipl.-Ing. Lucia Terlecki-Zaniewicz

Wien, April 2017

I. Danksagung

Nicht die Glücklichen sind dankbar. Es sind die Dankbaren, die glücklich sind.

Francis Bacon

II. Abstract

Human skin as a first line of defense, is constantly attacked by extrinsic and intrinsic factors driving signs of skin aging leading to wrinkles, skin thinning, pigment irregularities as well as to deterioration of skin barrier function. The presence of up to 20% of senescent cells in aged skin and their accumulation with age contribute to the development of systemic tissue dysfunctions and age-related diseases. A major culprit for the derogatory effects of senescent cells, is their acquisition of a senescence-associated secretory phenotype (SASP). It is characterized by an increased secretion of pro-inflammatory and matrix-remodeling factors that are supposed to exert negative effects on neighbouring cells and tissue, while their transient presence enhances wound healing and regeneration. Recently, miRNAs packaged into extracellular vesicles (EV-miRNAs) have been found as novel paracrine communicators and mediators acting on the transcriptional machinery of recipient cells. Here, we identified small EV-miRNAs as part of the SASP and investigated if abundantly and specifically packaged EV-miRNAs modulate keratinocyte functionality.

We revealed a selective packaging mechanism and identified prominent candidates that might be able to confer a biological role on recipient cells. EV-miRNA mediated paracrine crosstalk between human fibroblasts and keratinocytes was confirmed by the uptake of a *C.elegans* specific miRNA enclosed in EVs derived from fibroblasts in monolayers and in *in-vivo* mimicking skin-equivalents.

Finally, we evaluated how EVs derived from senescent fibroblasts influence the differentiation potential and wound healing capacity of keratinocytes and identified miR-23a-3p as a crucial 'miRdiator' of the miR-SASP. To summarize, our data indicate that EV-miRNAs of senescent fibroblasts are *bona fide* members of the SASP and suggest the term 'miR-SASP'. The selective sorting of specific senescence-associated EV-miRNAs contributes to the communication between fibroblasts and keratinocytes and impair their epidermal homeostasis. However, the biological role of other abundantly and selectively secreted senescence-associated miRNAs and their implications *in vivo* and in age-associated diseases remain to be determined.

III. Zusammenfassung

Der erste Abwehrmechanismus des menschlichen Körpers, die Haut, wird kontinuierlich von äußeren und inneren Einflussfaktoren beansprucht. Dies fördert die Entstehung von Zeichen der Hautalterung und beeinträchtigt die natürliche Hautbarriere. In alter Haut wurde die Ansammlung von 20% seneszenten Zellen beobachtet, welche zu systemischen Fehlfunktionen und alters assoziierten Krankheiten führen können. Es wird vermutet, dass die Entstehung des seneszenz-assoziierten sekretions Phänotyp den Großteil der negativen Effekte des Alterns steuert. Dieser Phänotyp, auch SASP genannt, zeichnet sich durch eine erhöhte Sekretion von pro-inflammatorischen und Matrix-veränderten Stoffen aus, die auf die umliegenden Zellen und Gewebestrukturen nachteilig wirken. Widererwartend, kann die kurzzeitige Sekretion die Wundheilung und die Regenerationsfähigkeit verbessern. Erst kürzlich wurde darauf aufmerksam gemacht, dass mikro (mi)RNAs verpackt in extrazellulären Vesikel (EV-miRNAs), die Fähigkeit haben die parakrine Kommunikation zwischen Zellen zu vermitteln und dabei in die Regulation der Transkription eingreifen können.

In dieser Arbeit haben wir EV-miRNAs von seneszenten humanen Fibroblasten (HDF) als neue Faktoren des SASP entdeckt und untersucht ob spezifisch verpackte miRNAs die Funktion von Keratinozyten (NHEK) beeinflussen können.

Wir haben in HDF einen alterungsspezifischen und selektiven Verpackungsmechanismus von EV-miRNAs identifiziert und konnten eine parakrine EV-miRNA Kommunikation zwischen HDF und NHEK in einschichtigen sowie 3D Kulturen bestätigen.

Schlussendlich, haben wir die EV von seneszenten HDF mit NHEK behandelt und eine verbesserte Wundheilung, aber ein gestörtes Differenzierungspotential festgestellt. Dieser Mechanismus wird von miR-23a-3p, ein entscheidender ‚miRdiator‘ des SASP, gefördert.

Zusammenfassend zeigen wir, dass EV-miRNAs ein Teil des SASP von HDF sind (miR-SASP). Die selektive Sekretion von EV-miRNAs trägt zur Kommunikation zwischen HDF und NHEK bei und beeinträchtigt dessen Funktionen. Nun bleibt es, dessen Relevanz *in vivo* und in altersbedingten Krankheiten zu ermitteln.

I. Content

I.	Danksagung	2
II.	Abstract	3
III.	Zusammenfassung.....	4
I.	Content.....	5
1.	Introduction.....	8
1.1.	Building blocks maintain skin integrity – The structure & function of skin	8
1.1.1.	The dynamic fine-tuning of epidermal homeostasis	10
1.1.2.	Programmed fine-tuning allows healing	11
1.1.3.	Heterogeneity of cellular skin residents	12
1.1.4.	The dialog between inside and outside – intrinsic and extrinsic signs of skin aging	13
1.1.5.	Turn the light on – ROS induced skin signaling triggers an inflammatory cascade.....	14
1.2.	Causes and Consequences of Aging – What is cellular senescence?.....	15
1.2.1.	The SASP – cell-non autonomous signaling during cellular senescence	17
1.2.2.	Shall we appreciate the presence of senescent cells?	19
1.3.	short communicators with a profound impact – micro RNAs	20
1.3.1.	miRNAs at the edge between aging and longevity	21
1.3.2.	Friends or enemies? miRNAs in the skin.....	22
1.3.3.	Message in a bottle - Circulating miRNAs in aging.....	25
1.4.	Extracellular vesicles - smart transport vehicles with physiological function	26
1.4.1.	The versatility of EVs.....	27
1.4.2.	Should I stay or should I go now - Vesicle biogenesis and secretion	28
1.4.3.	The butterfly effect - RNA sorting and trafficking.....	30
1.4.4.	The versatile functions of EVs	32
1.4.5.	EVs for therapy – a new area?	34
2.	Objective	35
3.	Results	37
	Part A	37
3.1.	Extracellular vesicles of stress-induced premature senescent fibroblasts are part of the SASP.....	37
3.1.1.	Stimulation of stress-induced premature senescence mirrors hallmarks of cellular senescence .	37
3.1.2.	Small extracellular vesicles are part of the senescence associated secretory phenotype of senescent cells.....	41
3.2.	Are EV-miRNAs novel factors of the senescence-associated secretory phenotype?	44
3.2.1.	The miR-SASP	45
3.2.2.	The miR-SASP targets pro-apoptotic mediators	49
3.2.3.	Differential miRNA loading per vesicle upon SIPS and over time	51
3.2.4.	Differential transcription of intracellular miRNAs identifies skin aging associated miRNAs	53
3.3.	Are specific EV-miRNAs selectively secreted or retained after entry into senescence?	57
3.3.1.	Specific EV-packaging of miRNAs is directed by cellular senescence	58

Part B	61
3.4. EV mediated miRNAs crosstalk between fibroblasts and keratinocytes	61
3.4.1. EV-miRNA crosstalk in 2D monolayer cultures	61
3.4.2. EV-miRNA crosstalk in 3D human skin equivalents	62
3.4.3. Implications for the presence of extracellular vesicles and multivesicular bodies in human skin	64
3.5. The EV-miR-SASP and its impact on keratinocyte's functionality.....	68
3.5.1. The transient presence of the in vitro EV-miR-SASP increases wound healing of keratinocytes ..	68
3.5.2. The chronic presence of the EV-miR-SASP impairs keratinocyte differentiation	70
3.6. miR-23a-3p a skin aging associated 'miRdiator' of the miR-SASP	72
3.6.1. miR-23a-3p mimics the wound healing mediated effects of SIPS EVs.....	73
3.6.2. miR-23a-3p and its effect on keratinocyte differentiation	75
3.7. miR-21-5p an 'oncomiR' as part of the SASP?	75
3.7.1. Stress resistance of miR-21 knockout cells against various stress stimuli – pre-screening	77
3.7.2. miR-21 knockout cells are stress resistant against Cisplatin.....	80
3.7.3. Oxidized lipids impair the growth advantage of miR-21 knockout cells	81
4. Discussion	84
4.1. Why studying skin aging is important?	84
4.2. Specifically packaged miRNAs in extracellular vesicles are novel members of the senescence-associated secretory phenotype	85
4.3. Extracellular vesicles as paracrine communicators between skin residents.....	88
4.4. The EV-miR SASP of fibroblasts modulates the wound healing capacity and differentiation of keratinocytes	90
4.5. miR-23a-3p a mediator of the miR-SASP.....	92
4.6. Aging or dying? Is the miR- SASP a mediator of apoptosis resistance?	93
5. Material and Methods.....	96
Cell Biology Methods.....	96
5.1. Primary cell culture	96
5.2. Induction of stress and stress-induced premature senescence	99
5.3. Human Skin equivalents	100
5.4. Annexin-V-/PI staining.....	100
5.5. BrdU incorporation.....	100
5.6. Senescence associated (SA) β -Gal staining	101
5.7. Isolation of small extracellular vesicles (EVs)	101
5.8. EV Treatment of Keratinocytes	101
5.9. Nanoparticle tracking analysis	102
5.10. Electron microscopy	102
5.11. miRNA transfections.....	102
5.12. Wound Healing Assay.....	103
5.13. Cellular proliferation and activity using AlamarBlue®	103
Molecular Biology Methods	104
5.14. Protein quantification, western blot and antibodies	104

Content

5.15.	RNA Isolation,	105
5.16.	cDNA synthesis	106
5.17.	Quantitative Real Time PCR (qPCR)	107
5.18.	Illumina small RNA cDNA library preparation	109
5.19.	Illumina, miRNA next generation sequencing	109
5.20.	Statistical analysis.....	110
6.	Supplementary Tables	112
6.1.	Summary and evaluation of secreted miRNAs by qPCR panel	112
6.2.	miRNAs from customized qPCR panel.....	113
6.3.	Significantly differentially secrete miRNAs from SIPS cells from two timepoints D7 and D21 after the SIPS treatment.....	120
6.4.	Table to different composition of miRNAs per vesicle between Q and SIPS cells from two timepoints 130	
6.5.	Differentially transcribed miRNAs (intracellular)	132
6.6.	Correlation of intracellular to extracellular miRNAs	138
6.7.	miRNA - gene interaction from pathways analysis	142
7.	References	143
8.	Appendix A	172
8.1.	Cells	172
8.2.	List of Figures.....	172
8.3.	List of Tables	174
8.4.	Abbreviations.....	175
9.	Appendix B Manuscripts.....	180
9.1.	Accepted and published Manuscripts	180
9.2.	Submitted Manuscript	181
9.3.	Submitted Manuscript – Co-author.....	201
10.	Appendix C Contributions during the Phd	218
10.1.	Talks and Posters	218
	Talks.....	218
	Short Poster talks	218
	Posters and Abstracts.....	219
10.2.	Prizes and Scholarships.....	220
10.3.	Visits abroad	220
10.4.	Students.....	220
11.	Appendix D Curriculum vitae	221

1. Introduction

'I think science has begun to demonstrate that aging is a disease. If it is, it can be cured'

Tom Robbins

With increasing medical research and the advanced development of biopharmaceuticals for the treatment of a plethora of (age-associated) disease we are currently faced with an increased life expectancy while most often the average health-lifespan remains unchanged. In order to increase the population of so-called 'wellderlies' (Scott & DeFrancesco 2015) and thereby the extension of average health span, the future of biopharmaceutical developments should shift their focus to holistic treatments to target the systemic environment of aged cells. Promising insights from the selective removal of senescent cells were gathered in mouse models showing a later onset of age-associated diseases leading to an increase in a healthy lifespan (Baker et al. 2016). Presumably, first strategies in humans are currently under investigation.

Therefore, as Tom Robbins indicated, the idea emanates to classify aging as a 'disease' according to the International Statistical Classification of Diseases and Related Health Problems (ICD-11) (Zhavoronkov & Bhullar 2015).

It might be intriguing to think that the most natural cause of life should be declared as a disease. However, the underlying idea beyond should stress stakeholders of pharmaceutical and regulatory organizations to disclose the natural process of aging as an elementary multifactorial system and as the crucial culprit and driver of many age-associated diseases that restrict the health life span leading among others also to financial and ecological issues. However, the notion, 'aging as a disease, that needs to be cured' increased manifold discrepancies in the aging community, on 'patients' as well as on stakeholders.

Some researcher believe to lose the tumor-suppressive effect of senescence. Elderlies do not want to be declared as 'ill' only due to their advanced age, and stakeholders struggle with financial frictions.

Nonetheless, whether it is a point of money, medical definitions or part of the philosophy of 'being', it should fade into the background to allow successful aging with the focus to remain mentally and physically healthy, starting as early as possible as it opens the stairway to a 'wellderly'.

1.1. Building blocks maintain skin integrity – The structure & function of skin

Skin, the largest organ of human body is constituted with a protective lifelong sensing function against external and internal attacks. Its compartmentalization and hierarchical organization comprises three main layers, each with its own specific characteristics and functions. The most inner sub-cutaneous layer is the hypodermis. It is below the dermis and mainly composed of white adipose tissue that stores nutrients and energy to maintain thermoregulation and to protect the connective tissue against environmental disturbances (reviewed by Driskell et al. 2014).

Introduction

The dermis consists of the extracellular matrix (ECM), composed of collagens, long-lived elastic fibres and various proteoglycans that form a mesh-like network (reviewed by Naylor et al. 2011). Collagens, present in several isoforms, are the most abundant proteins in the dermis. They form bundles or weave-basket-like structures and are an essential element for mechanical strength, while insoluble elastic fibres form a highly organized and cross-linked amorphous matrix to provide both, resilience and deformability (reviewed by Langton et al. 2010). The 'ground substance' of the ECM spans through the entire dermis and shapes a gel-like structure, consisting of proteoglycans, glycoproteins, water and hyaluronic acid, which maintain nutrient supply and hydration (reviewed by Tobin 2006).

The third and outermost layer of the skin is the epidermis. It prevents loss of insulation and forms a stratified avascular tissue with an essential barrier function against pathogenic entry. The stratum (S.) basale is the first lower layer of the epidermis. The formation of dermal-epidermal junctions (DEJ) allows the connection with the dermis. These so-called rete ridges are assembled in a interdigitated finger-like structure and increases the epidermal surface (reviewed by McGrath & Uitto 2008). They direct the exchange of nutrients and oxygen and allow the crosstalk between dermal and epidermal cells (reviewed by Lawlor & Kaur 2015).

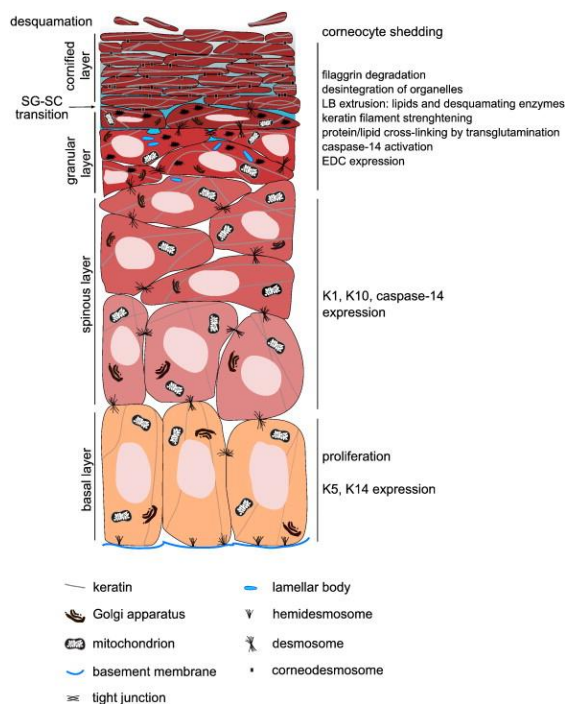


Figure 1 Different building blocks involved in the terminal differentiation of keratinocytes. Each layer is constituted with specific proteins and characteristics and direct the formation of a fully functional skin barrier. From Eckhart L. et al. 2013, BBA

The main cell type located in the epidermis are keratinocytes.

The S.basale populates transiently amplifying cells with stem cell renewal properties. Once they left the basement membrane, they start a progressive differentiation process through S.spinosum, S.granulosum and finally traverse into the most upper part, the S.corneum. Each sub-layer acquires a brick like structure and is characterized by a specific morphology and by the expression of distinct keratins (K). In the basal layer, the detection of K5 and K14 indicates the presence of highly proliferating keratinocytes, while the expression of K1 and K10 activates the onset of maturation and thus initiates the formation of an insoluble cornified envelope (CE) (Poumay & Pittelkow 1995).

Multiple, highly conserved structural proteins involved in differentiation and cornification are encoded by the epidermal-differentiation complex (Mischke et al. 1996; Marenholz et al. 2001). The assembly of the CE is a holistic crosslinking process catalyzed by the calcium dependent transglutaminase (TG)

family (reviewed by Eckert et al. 2005). Involved in the early steps of cornification and substrate of many TGs is involucrin. Together with TG1 (Nemes et al. 1999) and TG5 (Candi et al. 2001) it forms crosslinks with the cell membrane anchored proteins evoplakin (Ruhrberg et al. 1996) and periplakin (Ruhrberg et al. 1997) and provides a scaffold for the subsequent maturation of the CE. In the granular layer ceramides (Marekov & Steinert 1998) are linked to ester-bonds and are incorporated into the involucrin-periplakin-evoplakin complex to form a protective barrier against pathogenic entry (Sevilla et al. 2007) as well as to keep hydration balanced. Mainly TG1 and TG3

mediated, the small proline-rich proteins, loricrin, filaggrin and keratin filaments are crosslinked to components of the desmosomes to support CE assembly. Finally, the release of cellular organelles transform the viable transdifferentiating keratinocytes to mature corneocytes. They lose their nuclei and degradation of filaggrin and cellular debris is mediated by caspase-14 activation (reviewed by Eckhart et al. 2013). It contributes to the formation of a flattened, stratified and insoluble cornified envelope that builds a valuable protective barrier for the skin. To maintain the balance of constantly renewing cells and to remove extrinsic damage, corneocytes are constantly shed off, a process known as desquamation (reviewed by Kalinin et al. 2001; Candi et al. 2005).

1.1.1. The dynamic fine-tuning of epidermal homeostasis

The epidermis forms a dynamic network to facilitate mechanical strength and barrier function as well as repair in response to injury. A key mechanism in this context is the fine-tuning of a continuous amplification and differentiation. It is highly organized and controlled by gradually increasing calcium (Ca^{2+}) concentrations, reaching its peak in the S.granulosum and declining sharply in the S.corneum (Menon et al. 1992; Elias et al. 2002).

The main anchoring junctions of epithelial cells, are desmosomes and adherens junctions, that link actin (adherens) and cell type specific intermediate filaments (desmosomes; in epithelial cells 'keratin intermediate

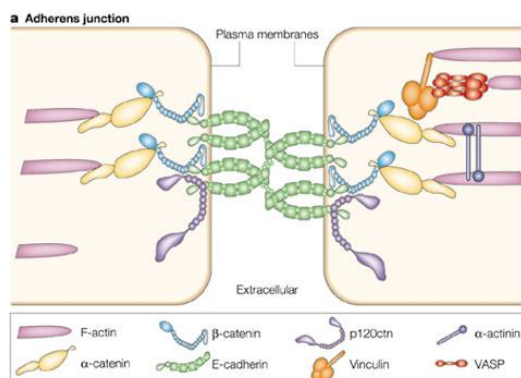


Figure 3 Adherens junction between adjacent cells. Cadherins provide anchorage and stabilization between actin filaments of two cells. From Fuchs & Raghavan 2002

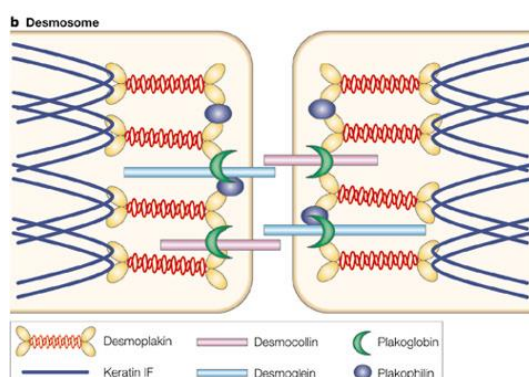


Figure 2 The desmosomes between two cells are formed by the cadherins desmocollin (Dsc) and desmoglein. . From Fuchs & Raghavan 2002

filaments') to cadherins. They are a large family of cohesive proteins (Nollet et al. 2000) and maintain tissue integrity and facilitate cytoskeleton reorganization and signaling (reviewed by McGrath & Uitto 2008; Alberts 2008). The loss of epithelial specific cadherins triggers epithelial to mesenchymal transition (EMT), mainly observed during development and pathophysiological processes, such as tumor migration and metastasis as well as upon injury and inflammation (reviewed by Lamouille et al. 2014). The classical E-cadherins bridge cell -- actin-cytoskeletal networks and are stabilized by α - and β -catenin (Figure 3) while the 'button-like' connections of desmosomes are connected by specific cadherins, the desmocollin (Dsc) and desmoglein (Figure 33). They are the core proteins within the extracellular space and associate with the desmosomal plaque proteins desmoplakin, plakoglobin and plakophilin (Kowalczyk et al. 1999). They provide a scaffold and mediate tethering to cytoplasmic keratin intermediate filaments, preserve protection and barrier maintenance and their elementary function becomes evident in autoimmune and hereditary blistering diseases (reviewed by Kottke et al.

2006) such as epidermolysis bullosa and bullous pemphigoid (Valeski et al. 1992). But also infectious diseases and bacterial toxins confer various pathogenic phenotypes associated with desmosomal alterations (reviewed Payne

et al. 2004). Studies in transgenic mice, either after modulation of Dsc1 (Chidgey et al. 2001) or after disruption of Dsc3 localization (Hardman et al. 2005) outlined the pivotal importance of functional desmosomes in epidermal morphogenesis as well as their high abundance in keratinocyte differentiation. In addition, a growing body of literature examined the integral function of rigid hyper-adhesive desmosomes and their flexibility in response to wounding (Watt et al. 1984; Berika & Garrod 2014).

Both are intertwining functions of the dynamic turnover of the epithelial tissues during normal and injured conditions. Hyper-adhesive desmosomes were first described in frog tissue (Borysenko & Revel 1973) and their function in cell-culture models was demonstrated in Madin-Darby canine kidney cells (Wallis et al. 2000). They are characterized by a vast stiffness, insensitive to disruption by calcium chelating agents such as EGTA (reviewed by Garrod & Tabernero 2014), which is indispensable for most, if not all desmosomes in adult tissue. Thus, it is intriguing to ask, whether Ca^{2+} independent hyper-adhesive desmosomes are compatible with wound healing induced migration and re-epithelialization? In particular, how do they release the tight connection to accommodate migration?

1.1.2. Programmed fine-tuning allows healing

Wound healing is a highly orchestrated and complex process, necessary to retain the protective function of skin

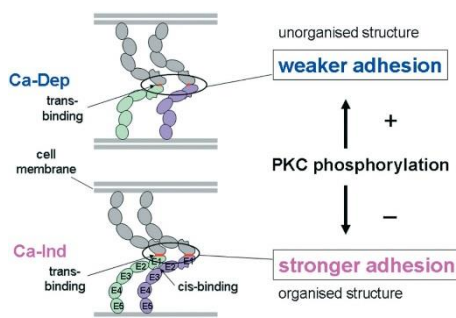


Figure 4 Hyper-adhesive Ca^{2+} -independent (Ca-Ind) desmosomes are disrupted by the phosphorylation of PKC- α , leading to loosening of the adhesion, which allows healing and repair. From Garrod & Kimura 2008.

after injury. Four subsequent, timely overlapping phases engage inflammatory blood cells, epithelial, endothelial and specialized α -smooth muscle actin (α -SMA) activated fibroblasts (Singer & Clark 1999; Darby & Hewitson 2007). Injured cell sheets or intact epidermis force a rapid switch from hyper-adhesive to Ca^{2+} depended desmosomes that favour infiltration and colonization of the wounded area. The transition is achieved by attraction of protein kinase C (PKC- α) and its subsequent signaling induced phosphorylation of specific components of the desmosomal plaque (reviewed by Garrod & Kimura 2008) (Figure 4). Consequently, the

mere addition of EGTA permits the detection of non-hyper-adhesive Ca^{2+} depended desmosomes *in vitro* (Garrod 2013). They demonstrated that impaired and delayed re-epithelisation is directly linked to the cytoplasmic presence of PKC- α , while its translocation to the desmosomal plaques assures mobilization of keratinocytes and proper healing (Thomason et al. 2012).

In general, the culprits for chronic wounds are manifold. Alterations in vascularization, excessive inflammatory burden or increased apoptosis are only few to be mentioned (reviewed by McGrath & Uitto 2008). It results in a modulated and distracted autocrine and paracrine communication with the consequences of a prolonged and complicated healing process. The fascination to understand the cellular and molecular physiology of cutaneous wound healing attracted not only scientists, but also biopharmaceutical industries. This comes from the notion that elderly and immune-compromised people are highly susceptible to improper healing rates, although the knowledge to the underlying mechanism are quiet advanced, we still miss efficient and long lasting therapeutic

interventions. Additionally, also miRNAs were integrated into the holistic approach of wound healing and emerged as prominent candidates for therapeutic interventions or as biomarkers (reviewed by Miller et al. 2015; Banerjee 2015).

1.1.3. Heterogeneity of cellular skin residents

Imaging the huge surface of the skin with its versatile functions, the mere presence of two cell types seems suspicious. Hence, besides keratinocytes the epidermis hosts melanocytes, Langerhans cells and Merkel cells (reviewed by Dayan 2008). Melanocytes reside normally in the S.basale and produce the pigmenting source melanin to protect against UV light. Langerhans cells are antigen-presenting cells involved in the immunosurveillance. Their immunomodulatory functions are dampened by persistent UV irradiation and increases the susceptibility to inflammatory cutaneous conditions. Merkel cells or 'the brain of keratinocytes', are specialized nerve cells responsible for the neural development and tactile sensation (reviewed by White & Yager 1995).

The DEJ at the S.basale gives rise to a defined interface between dermis and epidermis, while hair follicles form specialized appendages and span through the dermis and epidermis. They both form a niche, harbouring a diverse population of epidermal-, hair - and melanocyte stem cells to maintain the high turnover of the epidermis (reviewed by Heath & Carbone 2013). Equally important is the skins' ability to recruit its immunosurveillance against pathogens and infections coming from outside. A vast diversity of immune cells embedded in the ECM direct the adaptive and innate immune system. They are interspersed in the dermis and so-called appendages function as focal points linking arrector pili muscles, sensory neurons and blood vessels to dermal and epidermal signaling (reviewed by Hsu et al. 2014).

The main residents in the dermis are fibroblasts, sub-divided in two distinct types named after their location and endowed with divergent morphological and secretory characteristics (Harper & Grove 1979; Schafer et al. 1985). *In vivo*, they represent a scarcely dividing post-mitotic population embedded in the dermal matrix. The papillary fibroblasts are closest to epidermis, while the reticular layer is in contact with the adipose tissue of the hypodermis. Examining their proliferation *in vitro*, revealed an increased proliferation and clonogenic capacity of the papillary cell type. They maintain a spindle-like shape morphology and are able to reach higher cell densities. Their counterparts in the reticular dermis are characterized by a flattened and enlarged morphology, a slow growing pace and an earlier induction of contact inhibition that abrogates high cell densities when compared with papillary cells (Sorrell 2004). It was long thought that these features are restricted to *in vitro* cell culture until their embedding in artificial *in vivo* mimicking 3D skin equivalents, pointed to an impaired skin integrity when built with reticular cells (Sorrell et al. 2004). Moreover, El Ghalbzouri and co-workers identified differentially regulated genes present in the reticular and papillary layer and validated their specificity in *in vivo skin* sections (Janson et al. 2012). Interestingly, papillary-like characteristics were less pronounced after several divisions in culture and resembled the features of reticular cells, while their counterparts remained to be mostly unaffected (Mine et al. 2008). This finding, suggest an age-related transition of papillary to reticular (PRT) cells prior induction of replicative senescence (Lämmermann et al. in progress).

1.1.4. The dialog between inside and outside – intrinsic and extrinsic signs of skin aging

Skin at the boundary between inside and outside serves as a first line of defense and shields inner organs from cumulative harm. It is constantly attacked from environmental sources that leave silent traces on a cellular and molecular level. For a long period hardly visible, but the cellular brain remembers the engraved insults from outside that sooner or later result in signs of skin aging. However, they are not the mere results of environmental and lifestyle habits, it is an inevitable and rather synergistic product of intrinsic and extrinsic factors that contribute to systemic deteriorations.

Intrinsic aging is a genetically determined process and relies on endogenously produced reactive oxygen species (ROS) that affect the entire organism. Once the antioxidant system is exhausted, accumulation of ROS causes damage within all cellular compartments and tissues leading to gradual changes in structural skin integrity (reviewed by Farage et al. 2008).

In addition, substantial amounts of exogenous ROS are derived from xenobiotics, pollutants and UV radiation that synergistically increase the oxidative burden leading to extrinsic signs of aging. In the context of skin, UV induced photo-aging, is seen as the principal culprit and driving force leading to age-related cutaneous conditions. Importantly, while UVA is able to penetrate deeper layers of the skin, UVB only affects the epidermis.

Molecular changes:

Intrinsically, the most apparent structural changes of aged skin are prominent expression lines, fine wrinkles, sagging, skin atrophy and pale appearance. They are indicators of a wide and loose remodelled matrix network, loss of subcutaneous fat tissue, reduced support from bones and muscles as well as changes of the hormonal activity (reviewed by Puizina-Ivić 2008). In particular the reduction of estrogen in post-menopausal women (reviewed Stevenson & Thornton 2007) drives the decline of hyaluronan (Röck et al. 2012) and contributes to loss of elasticity and hydration (Henry et al. 1997).

Photo-aging reinforces signs of intrinsic aging and is manifested with apparent deep wrinkles, thickening of epidermis and hyperpigmentation (reviewed by Zouboulis & Makrantonaki 2011). In deeper layers of the skin, the dermis undergoes profound functional and structural changes, triggered by remodelling of the ECM that interferes with correct fibrillogenesis and accumulation of dystrophic elastic fibres, a feature known as solar elastosis (Wilson et al. 2014; Bernstein et al. 1994; Kligman 1989). But it is not only the accumulation of dysfunctional elastic tissues leading to advanced glycation end products over time (Verzija et al. 2000), but also matrix metalloproteases (MMP) degrade and promote disorganization of the ECM (reviewed by Langton et al. 2010). This imbalance and reduced amounts of fibrillins force the gradual flattening of rete ridges that decrease the epidermal to dermal surface necessary for exchange of nutrients and intercellular signaling (Watson et al. 1999).

Epidermal turnover decreases, the disruption of the Ca^{2+} gradient (Denda et al. 2003) changes the lipid composition of the CE (Rinnerthaler et al. 2013) and thus impairs barrier integrity. Aged epidermis is less hydrated, has an extended barrier recovery after injury and an increased susceptibility to allergies and irradiations (Farage et al. 2009).

Changes on a cellular level and immunity:

Clinical and molecular signs of skin aging are associated with changes of cellular functions and morphology. A decreased ratio of papillary to reticular fibroblasts and skin atrophy further contribute to increased sensitivity and to a reduction of nerve endings (reviewed by Zouboulis & Makrantonaki 2011). A dysfunctional dermis derived from reticular (Mine et al. 2008; Janson et al. 2013) or aged (Weinmüller et al in preparation) fibroblasts is unable to support the formation of a functional epidermis. It is probably the release of distinct cytokine and growth factor that are considered to modulate keratinocyte proliferation and differentiation (Sorrell et al. 2004). Owing to that, the keratinocytes appear larger but less uniform and disrupt the highly organized 'building block-like shape'. The number of corneocytes decrease, likewise less Langerhans cells and blood vessels aggravate the immunosurveillance leading to a higher susceptibility against infections (reviewed by McGrath & Uitto 2008). Changes in the dermal network impair T cell functionality and restrain their mobility and circulation through the matrix. These findings provide a convincing explanation for the acquiring of a deteriorated immunosurveillance with age, known as immunosenescence (reviewed by Moreau et al. 2016).

The major hallmarks of extrinsic and intrinsic aging reflects their huge imbrications between their main mediators (ROS) and changes on a molecular and cellular level. In addition, ROS signaling initiates an inflammatory cascade and contributes to altered signaling between dermal and epidermal cells.

1.1.5. Turn the light on – ROS induced skin signaling triggers an inflammatory cascade

UV induced ROS trigger oxidative damage of multiple cellular components and major DNA lesions most strongly involved in skin pathogenesis are cyclobutane pyrimidine dimers (CPDs) and (6–4) pyrimidine-pyrimidone photoproducts (6-4PP). They are created in a wavelength dependent manner and interaction with tryptophan containing proteins can form oxidative base alterations known as 8-hydroxyguanine (8-oxo-7,8-dihydroguanine, 8-oxoG) (reviewed by Pfeifer 2011). Mutations in the nucleotide excision repair (NER) pathway are the major causes for many hereditary disorders characterized by a high photosensitivity, abnormal pigmentation and cancer predisposition. However, individuals diseased of cockayne and UV-sensitive syndromes carry specific deficiencies in the transcriptional coupled repair pathway, a sub-pathway of NER. They only develop a mild skin phenotype with a high susceptibility against UV light leading to sun burning, freckles, inflammation and premature signs of aging, while no incidence of cancer have been observed (reviewed by Spivak & Hanawalt 2015).

On a molecular level, UV radiation induced oxidative stress, stimulates a cytokine or growth factor regulated signaling cascade and activates NF- κ B and AP-1 transcription (Fisher et al. 1996). Although NF- κ B and AP-1 are governed by distinct mechanism, it is assumed that similar signaling pathways and stimuli initiate and enhance their activation. A key inducer is the mitogen-activated protein kinases/ERK kinase-1 (MEKK1). It stimulates three sub-pathways, either/and ERK, p38 and c-Jun amino-terminal kinase (JNK) (reviewed by López-Camarillo et al. 2012). While NF- κ B is activated upon phosphorylation of its inhibitors known as I- κ B, the activity of AP-1 is transcriptionally dependent and regulated by the assembly with the Fos (c-Fos, FosB, Fra1, and Fra2) and Jun (c-Jun, JunB, and JunD) families (reviewed by Rittié & Fisher 2002).

AP-1 transcription is a crucial for the dermal and epidermal response against stress stimuli and modulates proliferation, apoptosis and differentiation. However, differences in expression and stability of AP-1 in keratinocytes and fibroblasts have been observed (Offord et al. 1993), pointing to a dynamic crosstalk between keratinocytes and fibroblasts.

In fibroblasts, UV induced AP-1 signaling triggers MMP1 (interstitial collagenase) and MMP3 (stromelysin) secretion that hinders collagen synthesis and further promotes ECM remodeling and ROS generation (Fischer 1997). In the epidermis, AP-1 transcription regulates the fine-tuning between proliferation and differentiation, to maintain proper wound healing and epidermal homeostasis (reviewed by Angel et al. 2001)

Oxidative stimuli such as H₂O₂ (Vollgraf et al. 1999) normally stimulate NF-κB and AP-1 signaling processes that pave the way for inflammatory skin diseases such as psoriasis or age-related skin conditions . Gradually increasing levels of AP-1 and NF-κB with age have been observed in gastric mucosa cells isolated from old rats compared to young animals (Xiao & Majumdar 2000). In addition, also a skin rejuvenating effects was connected to AP-1 and NF-κB levels. UVB induced wrinkle formation in hairless mice was alleviated upon treatment with three different compounds derived from garlic (Kim et al. 2013). The scavenging of UVB induced ROS levels restored pro-collagen synthesis, decreased MMP secretion and concomitantly reduced the activity of AP-1, NF-κB as well as cyclooxygenase-2 (COX-2) and nitric oxide synthase (iNOS) (Kim et al. 2013). These findings nicely demonstrated a strong correlation between a modulated inflammatory phenotype and its effect on intrinsic and extrinsic signs of skin aging.

AP-1 and NF-κB are both involved in multiple intertwining cellular functions and an imbalanced activity contributes to the development of benign skin conditions (Dhar et al. 2002). Contrary, reduction of ROS levels with antioxidants inhibited AP-1 and NF-κB activity and abrogated transformation of human keratinocytes (Dhar et al. 2002).

To conclude, endogenously or exogenously produced ROS impair the signaling cascade of the key players AP-1 and NF-κB. Age related deprivation of endogenous antioxidant mechanism cannot control elevated ROS levels anymore, causing a cumulative burden of oxidative stress leading to aggravation of inflammatory age-related cutaneous conditions.

1.2. Causes and Consequences of Aging – What is cellular senescence?

The uttermost interest in cellular and organismal aging derives from the conviction to actively restore the functional decline of tissues and organs and to maintain a youthful appearance while preventing frailty. Nine hallmarks of aging describe the causes and consequences of advanced age, whereby cellular senescence and altered communication are the ones on the crossroad of both (López-Otín et al. 2013).

Cellular senescence is a state of permanent cell cycle arrest and can be triggered by multiple stimuli. Either by the most natural cause of critically short telomeres (Harley et al. 1990; d'Adda di Fagagna et al. 2003) or by an array of exogenous stimuli, such as, hyperoncogenic signaling (Serrano et al. 1997), modulation of chromatin structures (Ogryzko et al. 1996; Munro et al. 2004), chemotherapeutic drugs (Schmitt et al. 2002) , vanishing of the deoxyribo nucleotide pools (Mannava et al. 2013) accumulation of DNA damage (reviewed by Grillari et al. 2007)

and other oxidative stressors (von Zglinicki 2000). The underlying molecular pathways to enter a state of senescence-associated growth arrest are either the a p53/CDKN1A(p21) or Rb/CDKN2A(p16) axis, though few exceptions exist (Olsen et al. 2002).

Telomere attrition, genotoxic stress and overexpression of specific oncogenes alert the DNA damage response system (DDR) and trigger a p53/CDKN1A(p21) dependent growth arrest to hinder impaired cells from proliferation. Stabilization of p53 is required to activate its downstream target CDKN1A, a cycline dependent kinase inhibitor and thus a universal mediator of a reversible growth arrest. Consequently, depended on the damage and the repair capacities, the cells are either repaired, marked for degradation or irreversibly growth arrested for entry into cellular senescence (reviewed by Ben-Porath & Weinberg 2005; Campisi 2001; Beauséjour et al. 2003 and many others).

On the other side, independently of the DDR, upon persistent damage, replicative senescence or oncogene induced senescence, the formation of senescence associated heterochromatin foci activate the CDKN2A(p16) axis (Kosar et al. 2011) that similarly induces and maintains a senescence-associated growth arrest. Activation of pro-survival pathways enhance a resistance against apoptosis and the cells undergo growth arrest. Consequently, they are not proficient to re-enter the cell cycle at a later time point, besides few exceptions showing oncogene induced escape of senescence and instead tumor progression (reviewed Liu & Sharpless 2012), and gradually deepen their senescent phenotype. They show an increased activity of lysosomal β -Galactosidase activity (Lee et al. 2006), a known biomarker of senescence and detectable at pH 6 (Dimri, X. Lee, et al. 1995). In addition, reorganization of the cytoskeleton structures and changes in gene expression further enhance the development of the senescent phenotype and the cells acquire a flat and enlarged morphology. However, they remain metabolically more active (reviewed by Wiley & Campisi 2016) than corresponding young or early passage cells and contribute to an imbalanced tissue metabolism (Goldstein et al. 1982; Bittles & Harper 1984; James et al. 2015). This metabolic switch is an elementary part of the senescent phenotype and contributes to the loss of cell type specific functionalities leading to partial de- or transdifferentiation (Bremnes et al. 2011; Parrinello et al. 2005), decline in the replicative potential required for tissue regeneration and the development of a senescence-associated secretory phenotype (SASP) (reviewed by Davalos et al. 2010).

The stimuli to change their secretory behaviour emanates independently of p16 and rely mainly on the DDR, besides few exceptions of acute senescence, as for instance during embryonic development (reviewed by Muñoz-Espín & Serrano 2014).

However, the mere overexpression of CDKN2A is not sufficient to induce a SASP, weather this is owing to spontaneous silencing events of CDKN2A upon long time cultivation or due to missing damage stimuli remains a matter of speculations (reviewed by Coppé et al. 2010).

Based on these definitions, mainly derived from cell culture experiments, the presumably most detrimental consequence of cellular senescence is their presence at sites of age-associated diseases and their accumulation with age in various tissues of rodents (Denchi et al. 2005), primates (Herbig et al. 2006) and humans (Dimri, X. Lee, et al. 1995). Importantly, they contribute to organismal aging, while their removal in mice or by senolytics (Zhu et al. 2016; Wang et al. 2016; Chang et al. 2016; Eirin et al. 2014; Roos et al. 2016; Zhu et al. 2015; Yi Zhu et al. 2017) impact beneficially on the healthy lifespan (Baker et al. 2016) , which leads to a later onset of several age-

associated diseases (Yosef et al. 2016). Thus, strategies to remove senescent cells in humans are currently under investigation (reviewed by Kirkland & Tchkonja 2015; and Ovadya & Krizhanovsky 2016). However, it should be noted that although the inactivation of CDKN2A in transgenic mice attenuated age-related phenotypes, the incidences of tumor progression increased. This highlights the significance of cellular senescence and the validity of the antagonistic pleiotropic theory of aging, meaning to preserve tissue integrity and health early in life, while having detrimental consequences at later timepoints, promoting tumor progression, diseases and inflammation. Thus, the current emerging strategies face to disrupt or attenuate the SASP, which is thought to be root cause of age-associated dysfunctions.

1.2.1. The SASP – cell-non autonomous signaling during cellular senescence

The SASP is probably the most powerful attribute of senescent cells with creating a chronically inflamed and pro-tumorigenic environment. Not only the mere cell-cell contact, but also cell-non autonomous effects induce senescence and thus reinforcing the negative effects on tissue homeostasis and regeneration. It is in particular the wide-ranging effects and the over-proportional persistent secretion of a potent mixture of SASP factors that are considered to act in a paracrine manner on neighboring cells and on matrix components. The core elements are growth factors, cytokines, chemokines (Coppé et al. 2008; Hubackova et al. 2012) as well as remodeling enzymes (West et al. 1989; Millis et al. 1992). It is a progressive and dynamic process and its composition is dependent on the senescent stimuli as well as on the cell type (reviewed by Rodier & Campisi 2011), although substantial overlaps revealed a high conservation throughout the elementary factors (Coppé et al. 2008). Mainly induced in an NF-kB depended manner, prominent cytokines such as IL-1 α , IL-6 and IL-8 participate in a vicious cycle of transdifferentiation, inflammation and migration. Similarly, chemoattractive substances from the CXCL and CCL family (reviewed by Nedoszytko et al. 2014) recruit the immune system in an inducible manner, while acting constitutively on developmental processes. To support migration and adhesion, fibronectin interacts with integrins, growth factors such as vascular endothelial growth factor, fibroblast growth factor and the binding proteins from the insulin growth factor (IGF) family facilitate angiogenesis and regulate proliferation or differentiation. In addition, tissue reorganization and degradation of the surrounding matrix are orchestrated by an interplay of multiple matrix metalloproteinases (MMP) (Liu & Hornsby 2007). The main culprit of collagen degradation is MMP-1, and thus highly involved in skin atrophy and wrinkle formation. It is not only highly expressed and secreted in intrinsically aged skin, but substantially activated upon UV radiation that is even amplified in smokers (Lahmann et al. 2001) and after exposure to tobacco extract in human fibroblasts (Yin et al. 2000).

Besides the impact on tissue functionality, the inflammatory and growth promoting capacity of the SASP potentially modulate dermal and epidermal crosstalk. Crucial targets in this context are the superfamily of insulin growth factor binding proteins (IGF-BP). They consist of 6 well characterized isoforms (Hwa et al. 1999), while others were reported (Kutsukake et al. 2008), have a broad binding spectrum and act as activators, modulators or repressors. IGF-BPs are part of the SASP and aberrantly secreted in fibroblast senescence (Micutkova et al. 2011; H. H. Yang et al. 2011; Hampel et al. 2005). Depended or independently after binding to IGF-I or IGF-II or even after

Introduction

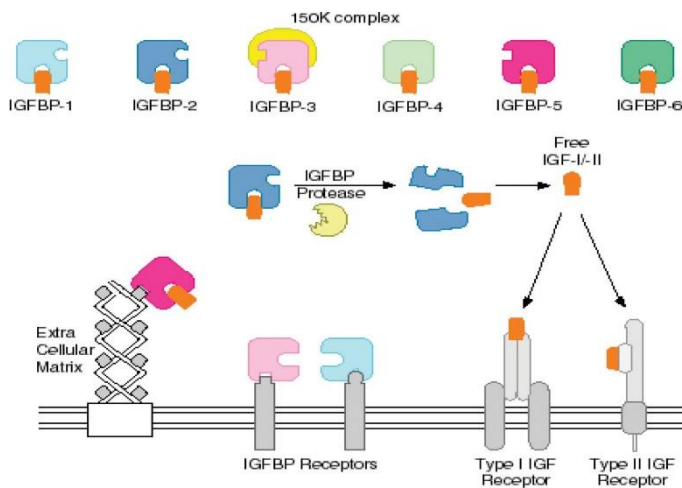


Figure 5 binding partners of IGF-BP. Adapted from (Beattie et al. 2006)

ECM docking, they interfere with receptor occupancy and initiate multiple processes ranging from proliferation, differentiation, apoptosis as well as migration (Figure 5) (reviewed by Firth & Baxter 2002; and Hwa et al. 1999). Notably, keratinocytes express IGF-I receptor, but lack mRNA transcripts to synthesis IGF-I (Tavakkol et al. 1992) and rely on exogenous supply from fibroblasts to maintain epidermal homeostasis after UVB radiation (Lewis et al. 2008). However, reduced expression of IGF-I in replicate and stress-induced senescent fibroblasts, as well as in the

dermis of elderly reduces the resistance of keratinocytes against UVB (Lewis et al. 2010). The nucleotide excision repair pathway is impaired (Loesch et al. 2016) and loss of p53 phosphorylation drives the inability to undergo apoptosis. Therefore, proliferation of damaged cells increase the susceptibility for skin malignancies. When focusing on their binding proteins, it is intriguingly, that most IGF-BP are commonly upregulated in the supernatants of senescent fibroblasts (Micutkova et al. 2011), endothelial cells (Hampel et al. 2006) and mesenchymal cells (Severino et al. 2013), while differences in the abundance of IGF-I and IGF-II in senescent endothelial cells were reported (Kim et al. 2007). Thus, the increased abundance of IGF-BP, most probably maintain the protective function of senescent cells and convey senescence to neighboring cells (H. H. Yang et al. 2011; Elzi et al. 2012; Kim et al. 2007). However, their accumulation and aberrant signaling during the SASP increase the load of IGF-BP in the microenvironment and trigger uncontrolled proliferation of injured cells and prevents their apoptosis.

Summarizing so far, it becomes clear that the mere accumulation of senescent cells, even in the absence of overt injury or infections resemble a state of chronic, low-grade inflammation. It allows crosstalk and tissue reorganization in a cell non-autonomous manner. It attracts immune cells to clear injured and senescent cells and to facilitate tissue renewal. However, the burden of accumulating senescent cells rise with age and the concomitant weakening of the innate and adaptive immunity allow impaired cells to escape. Consequently, the risk for systemic deterioration increases steadily and provides the source for the development of age-associated diseases. Nonetheless, it will never exceed the load of an acute inflammation, it is rather an age-related phenomenon of an imbalanced pro-inflammatory and growth promoting network that was therefore intuitively termed 'inflammaging' (Franceschi et al. 2000).

1.2.2. Shall we appreciate the presence of senescent cells?

On the contrary, to the persistent accumulation of senescent cells, the phenomenon of acute senescence and the acquisition of a SASP impinges beneficially on wound healing, tissue regeneration and plasticity (Demaria et al. 2014; Ritschka et al. 2017; J. Il Jun & Lau 2010).

The underlying mechanism relies on the transient presence of senescent cells and their subsequent removal by the immune cells, when no longer required. Primarily discovered during embryonic development, the detection of senescent myofibroblasts at sites of wounded areas enhanced the healing process and prevented fibrosis (Demaria et al. 2014). The key-regulator involved in this process is primarily the matricellular protein CCN1 (J.-I. Jun & Lau 2010a; J. Il Jun & Lau 2010). Activated in response to injury, it stimulates ROS mediated senescence and takes advantage of the SASP to initiate matrix degradation, proliferation, tissue renewal as well as immunoclearance to eliminate senescent cells. It is a highly organized process directed by the crosstalk of immune cells, endothelial cells and fibroblasts and their secreted compounds. Fibronectin serves as a substrate for dermal attachment and migration, its binding to platelet derived growth factor (PDGF)-BB promotes proliferation (Gilchrist et al. 2015) and PDGF-AA enhances myofibroblast differentiation (Demaria et al. 2014). However, the chronic presence of senescent cells at injured lesions (Mendez et al. 2017; Vande Berg et al. 2005) and a depleted immunity with advanced age, is considered to delay the closure of wounds and to drive morbidity and mortality in elderly.

Similarly, the growth promoting effects of the SASP activate transdifferentiation to enhance proliferation and tissue regeneration. The evidence for these findings was recently demonstrated after transient exposure to conditioned media derived from oncogene induced senescent mouse keratinocytes. Increased colony formation capacity and activation of stem cell markers *in vitro* and *in vivo* enabled tissue regeneration after engrafting and stimulated hair follicle development *in vivo*. However, long time exposure induced bystander senescence, which counteracted the regenerative potential (Ritschka et al. 2017).

These findings and other processes of acute senescence revolutionized the view of the SASP function, while strengthening the antagonistic pleiotropic theory of aging. In addition, it highlights the significance of senescent cells and illustrates the potency of a prolonged SASP signaling.

Thus, the strategy to preserve senescence, but to attenuate the long lasting negative effects of the SASP are conceivable. Many efforts have been made and an attractive approach are SASP inhibitors that dampen the transcriptional activity of SASP components. Among those are glucocorticoids (Laberge et al. 2012), metformin, rapamycin (Laberge et al. 2015) and JAK inhibitors (M. Xu et al. 2015) that target NF- κ B and p38 the actual root mediators of the SASP (reviewed by Prattichizzo, De Nigris, et al. 2016). Another strategy tested the selective elimination of senescent cells in transgenic mice or with senolytic substances. We contributed to that approach and observed an improvement of skin functionality in human skin equivalents and a concomitant de-repression of known SASP components such as IL-8 (CXCL8), MCP-1 (CCL2), RANTES (CCL5), GRO α (CXCL1), INHBA (Lämmermann et al in preparation).

Taken together, we are far closer to understand the holistic causes and consequences of aging. However, in order to target and attenuate the dark side of the SASP, it is of great importance to dissect and identify the disposition of existing and novel SASP components and their impact on neighboring cells and on tissue homeostasis. Recently,

so called ‘inflamma-miRs’ were implicated in the fine-tuning mechanism of the SASP (reviewed by Olivieri et al. 2015; Olivieri et al. 2013). Considering their differential expression in response to aging and diseases, and their manifold effects intracellularly, it remains to be determined to what extent they affect their surroundings. In addition, whether they act as signaling molecules to regulate transcriptional activity and intensity of the SASP, or if they are themselves aberrantly secreted and harmful remain elusive.

1.3. short communicators with a profound impact – micro RNAs¹

miRNAs are single stranded, typically 19 – 24 nucleotides (nt) long small noncoding RNAs (sncRNAs), with regulatory and modulatory functions that are implicated in the fine-tuning of a broad range of biological processes. They are highly conserved and have been detected in all eukaryotic cells as well as in plants (reviewed by Reinhart et al. 2002). They account for 3% of all human genes and it is estimated that they regulate the expression of around 30% of protein-encoding genes (Lewis et al. 2005). More than 20 years ago, the first miRNA, encoded by the gene *lin-4* was discovered in *C.elegans* and changed the traditional view of gene to protein expression radically (Lee et al. 1993). Since then, miRNA biogenesis and functions have been extensively studied.

The transcription of precursor transcripts, so called pri-miRNAs from genes or intronic sequences is initiated by polymerase II or III. They are typically monocistronic or polycistronic precursor RNAs with a length of several 100 nt that encompasses multiple mature miRNA sequences (reviewed by Sarnow et al. 2006). They form imperfect hair-loop structures and contain 5' 7-methylguanosine (m⁷) caps and 3' polyA tails. The double stranded (ds) RNA binding protein DGCR8 (DiGeorge syndrome critical region 8) and its association into a microprocessor complex with the endonuclease Drosha, mediates the cleavage into 70 nt long pre-miRNAs with a recognition pattern of 2 nt at the 3' overhang (reviewed by Filipowicz et al. 2008). They are subsequently incorporated into exportin-5-Ran and GTP hydrolysis facilitates the export of the pre-miRNA from the nucleus. In the cytoplasm, the endoribonuclease Dicer complexes with the ds RNA-binding protein TRBP and cleaves the stem loop, leading to the generation of the ds mature miRNAs (reviewed by Winter et al. 2009). After helicase unwinding and strand separation the thermodynamically less stable (passenger) strand is degraded, while the guide and complementary strand associates with Argonaute (Ago2) proteins. Incorporation into the RNA-induced silencing complex (RISC) directs the binding to the 3' UTR, in rare incidences to 5' UTRs of a target mRNA. The strength and complementarity of base pairing ('seed' region) determines the further fate leading either to degradation, translational repression due to steric hindrance of the ribosomal subunit or to deadenylation (reviewed by Bartel 2009). This imperfect binding to a target mRNAs entails the remarkable diversity of up to 100 mRNA targets per miRNA and is an explanation for the pleiotropic roles of one miRNA on a plethora of biological process with distinct consequences in different cell types. Consequently, miRNAs are implicated in normal cellular and developmental processes, but changes in miRNA expression patterns have also been detected in response to stress stimuli, diseases and aging.

¹ the respective miRNA isoform is indicated with '3p' or '5p' when stated in the original resources. If not indicated no information regarding the strands were given.

1.3.1. miRNAs at the edge between aging and longevity²

The first substantial age related effects of miRNA regulation were achieved after overexpression of *lin-4* in *C.elegans*. It extended the life span by targeting the IGF1/insulin signaling pathway, while its loss reduced the life span and favoured tissue deterioration and signs of aging (Boehm & Slack 2005). Other *C.elegans* specific miRNAs involved in the fine-tuning between elongation of lifespan and stress resilience were identified to interact not only with the insulin signaling pathway, but also to modulate the DNA damage checkpoint system (de Lencastre et al. 2010). On the other hand, also the dampening of miRNA activity emerged as a strategy to modulate the lifespan in mammalian cells. The inhibition of miR-21-5p was the first miRNA with a life span prolonging effect in mammalian cells and its upregulation was associated with endothelial senescence (Hanna Dellago et al. 2013). Interestingly, miR-21-5p as one of the most published miRNA, it is also known for its oncogenic traits and aberrantly regulated in pathophysiological process and malignant transformations (reviewed by Krichevsky & Gabriely 2009). Similarly, miR-17-5p, as part of the miR-17-92 cluster, is a miRNA on the crossroad between cancer and longevity (reviewed by Dellago et al. 2016) and commonly downregulated in organismal and cellular senescence (Hackl et al. 2010; reviewed by Grillari et al. 2010). Contrary, its overexpression in transgenic mice promoted longevity by inhibiting the induction of a senescence-induced growth arrest (Du et al. 2014). Also the highly conserved miR-34 family and its implication in neurodegenerative diseases (reviewed by Aw & Cohen 2012) regulates the life and health span of many organism. In the fly, it is scarcely detectable at early developmental stages and maintains brain homeostasis to promote healthy aging (Liu et al. 2012). However, with increasing age, it is found upregulated, not only in the fly, but also in the brain of adult mice (Bak et al. 2008), in the liver of rats (Li et al. 2011), in *C.elegans* (J. Yang et al. 2013; Ibanez-Ventoso et al. 2006) and in the dermis of elderly (Li et al. 2016). Besides, the miR-34 family, the miR-17-92 cluster and miR-21, many other miRNAs, among those are for instance the miR-16 family, the let-7 family and the miR-143/145 cluster that fit into the antagonistic pleiotropic theory of aging, acting either as tumor suppressor or oncogene (reviewed by Negrini et al. 2009; Kent & Mendell 2006).

In addition, miRNA profiling of several studies identified differentially transcribed miRNAs within various senescent cell types and tissues (reviewed by Grillari & Grillari-Voglauer 2010). As for instance in human dermal fibroblasts (Greussing et al. 2013; B. R. Zhou et al. 2013), bone marrow derived stem cells (Yoo et al. 2014), foreskin fibroblasts (Hackl et al. 2010), endothelial cells (Hanna Dellago et al. 2013) and in aged tissue derived from skeletal muscle, brain or skin sections (Li et al. 2016). Different miRNA patterns were also obtained from various age-associated diseases when compared with young and/or healthy controls. Among those are cardiovascular diseases, neurodegenerative diseases, age related cartilage and bone fractures, diabetes, autoimmune disorder as well as skin conditions (reviewed by Grillari & Grillari-Voglauer 2010). Interestingly, most of these disorders are characterized by an imbalanced inflammatory signalling, which probably reflects the SASP of senescent cells at lesion sites.

The particular importance of miRNA regulation in aging, was demonstrate upon dicer knockout, which impaired the entire mature miRNA synthesis. It resulted in the accumulation of senescent cells at the limbs of the fetuses.

² the respective miRNA isoform is indicated with '3p' or '5p' when stated in the original resources. If not indicated no information regarding the strands were given.

They showed a retarded embryonic development and signs of premature senescence *in vitro* as well as an early onset of organismal aging *in vivo* (Mudhasani et al. 2008).

1.3.2. Friends or enemies? miRNAs³ in the skin

The skin is an impressive and complex model system to study miRNA regulation in response to intrinsic or extrinsic stimuli. Particularly, because dermal and epidermal cells are derived from two distinct germ layers, from the ectoderm and mesoderm, and are involved in a dynamic turnover during the self-renewal capacities of the skin. Distinct miRNA abundances obtained from the dermis and the epidermis shows a strong involvement of the miR-200 family members in epidermal cells, while the members of the miR-199 family were predominately found in post mitotic dermal cells (Yi et al. 2006). But also *dicer*, as a key enzyme and marker for miRNA maturation, was shown to be differentially present in the different layers of the skin. Inhibition of *dicer* in K14 positive epithelial cells impaired only hair follicle development (Andl et al. 2006), while the homeostasis between proliferation and differentiation of epidermal cells was not affected (Yi et al. 2006). This highlights the profound differences of the two layers and underscores that the high turnover of the epidermis, developmental process during skin morphogenesis and dermal modelling are strictly separated pathways governed by different posttranscriptional processes. Thus, the spatiotemporal presence of specific mature miRNAs regulates the balanced mRNA to miRNA ratio to maintain functional skin homeostasis within different layers and cell types (reviewed by Botchkareva 2012). It is therefore not surprisingly that (i) skin aging associated changes and (ii) age-related problems during the fine-tuning of overlapping wound healing phases are regulated by the transient or constitutive presence of specific miRNAs.

The crosstalk of several miRNAs governs the dynamic fine-tuning of wound healing

The inducing of excisional wounds at back skin of mice gave substantial insights into the dynamic regulation of several differentially expressed miRNAs after 7 days post injury (T. Wang et al. 2012). Comparable results and a similar abundance of miR-21-5p, miR-203a and miR-31-5p was found in cells derived from fibrotic scar tissues of previous acute injuries (P. Li et al. 2015a). miR-21-5p is involved in multiple stages of the entire healing processes, although with different expression intensities (T. Wang et al. 2012) and at different spatial sites of the dermis and epidermis (Ahmed et al. 2011; T. Wang et al. 2012). At early stages, transforming growth factor β (TGF- β) activates miR-21, which subsequently enhances keratinocyte migration (X. X. Yang et al. 2011), wound contraction (T. Wang et al. 2012) and re-epithelisation, essentially for the regeneration of skin barrier (X. X. Yang et al. 2011). However, miR-21 inhibition in keratinocytes, disturbed the switch from proliferation to differentiation leading to an increased epidermal thickness due to multiple layers of compromised non-differentiated epithelial cells (T. Wang et al. 2012). Similarly, impaired collagen disposition and the lack of crosslinks between newly formed matrix proteins disturbed the last phase of re-epithelisation (T. Wang et al. 2012). This dynamic regulation and spatial temporal presence of miR-21 indicates the urgent prevalence for an interplay with other miRNAs.

³ the respective miRNA isoform is indicated with '3p' or '5p' when stated in the original resources. If not indicated no information regarding the strands were given.

One candidate could be miR-31. It is predominantly present in the epidermis and gradually increases within the first 7 days after injury. Comparison to miR-21, discloses again TGF- β as an inducer of miR-31 expression. It stimulates keratinocyte proliferation and migration by downregulation of one of its direct target epithelial membrane protein 1 (D. Li et al. 2015).

Another example of a crucial regulator involved in the different wound healing phases is miR-203, likewise upregulated after 7 days post excisional injury (X. X. Yang et al. 2011). It is a keratinocyte specific miRNA, and was originally discovered as a key mediator in switching between epidermal proliferation and differentiation. Responsive to differentiation stimuli, PKC induces miR-203 and enhances differentiation (Sonkoly et al. 2010) via its downstream target p63, the guardian of stem cell like properties (Yi et al. 2008; Lena et al. 2008). Intriguingly, only involucrin and no other early or late differentiation marker, such as filaggrin, K10 or loricrin were detectable upon miR-203 overexpression. From this point of view, the question arises, how miR-21, miR-31 and miR-203 expressions behave to each other. However, until now, no study examined their crosstalk during wound healing phase, although they were found to be commonly upregulated in samples derived from psoriatic lesions (Sonkoly et al. 2007).

miRNAs in age-related and inflammatory diseases

Accordingly, psoriasis is an autoinflammatory disease, still poorly understood and lacking promising and long lasting prospects of treatment (reviewed by Laws & Young 2012). It is enhanced by genetic dispositions and thought to be triggered by environmental stimuli, whereby the crosstalk between infiltrating immune cells and keratinocytes is impaired. Activation of tumor necrosis factor alpha (TNF- α) contributes to the secretion of proinflammatory cytokines and chemokines, which affect the entire skin homeostasis leading to an imbalance between hyperproliferation and differentiation of keratinocytes (reviewed by Wagner et al. 2010). The EVer phenotype is characterized by elongation of rete ridges, reduced nutrient supply and enhanced epidermal thickness leading to epidermal lesions and hyperplasia (reviewed by Elder et al. 2010). Although miRNA profiling from skin biopsies of moderate to EVer psoriatic lesion sites identified a unique, psoriatic specific miRNA signature (Sonkoly et al. 2007), most of their targets and their impact are still unknown reflecting the complex and multifactorial pathogenesis of this disease (reviewed by Hawkes et al. 2016).

The downstream targets of miR-21, miR-203 and miR-31 are all involved in a complex inflammatory cascade. Inhibition of miR-21 in patients-derived xenotransplants of mouse tissue decreased epidermal thickness and alleviated the secretion of cytokines involved in psoriasis development (Guinea-Viniegra et al. 2014). Similarly, a collective dampening effect of NF- κ B driven cytokine signalling was also observed upon miR-31 inhibition (Xu et al. 2012). In addition the suppressor of cytokine signaling 3 is targeted by miR-203, which sustains STAT3 activation (signal-transducer and activator of transcription 3), the main inducer of psoriatic plaque formation (Sonkoly et al. 2007). A similar effect was achieved with TNF- α antagonists, which is still the therapeutic agent most commonly used against the inflammatory response during this disease. Intriguingly, besides its clinical application, TNF- α ameliorated the secretory phenotype of endothelial cells suggesting that the psoriatic inflammatory phenotype renders the secretory behaviour of senescent cells or vice versa (Prattichizzo, Giuliani, et al. 2016).

In addition to miR-21, miR-203 and miR-31 other interesting candidates were identified. Among those miR-146a, a prominent inflamma-miR', induced by NF- κ B (Taganov et al. 2006), reduced after treatment with TNF- α antagonist (Prattichizzo, Giuliani, et al. 2016) and involved in the fine-tuning mechanism of several SASP components (Bhaumik et al. 2009). miR-17-5p, not only on the crossroad between aging and cancer (Dellago et al. 2016), but also reported to regulate keratinocyte proliferation and differentiation (Wu et al. 2012). Notably, it is still challenging to find consistent marker to discriminate between keratinocyte senescence and differentiation (Narzt et al in preparation).

What is known so far about miRNAs in skin aging?

Besides miRNA regulation during diseases and acute injuries, also normal physiological processes, as cellular and organismal aging, are target of miRNA deregulation. Many skin specific differentially expressed miRNAs of replicatively (Holly et al. 2015; Hackl et al. 2010) and premature senescent dermal (Greussing et al. 2013) and epidermal cells (Shin et al. 2011; Rivetti di Val Cervo et al. 2012; Lena et al. 2012) have been identified (reviewed by Mancini et al. 2014). There are accumulating evidences that specific senescence-associate miRNA patterns of dermal and epidermal skin cells *in vitro*, strongly correlate to miRNA regulation in skin sections of elderly (Li et al. 2016), extrinsically aged and young individuals (reviewed by Mancini et al. 2014). Based on age depended changes in extracellular matrix organization, recent studies elucidated whether aberrantly regulated miRNAs contribute to collagen degradation or impaired activity of fibrillogenesis.

In particular, senescence-induced upregulation of miR-29 family members was repeatedly associated with reduction of collagen synthesis by directly targeting distinct collagen isoforms (Maurer et al. 2010; Yumin Zhu et al. 2017; Takahashi et al. 2012; Yu et al. 2015; Li et al. 2012) or desmosomal functions (Kurinna et al. 2014). Similarly, miR-196a, miR-152, miR-181a overexpression induced senescence and suppressed collagen production in fibroblasts (Mancini et al. 2012). Another miRNA repeatedly involved in skin aging and found to be upregulated in senescent dermal fibroblast as well as skin samples of elderly (≥ 60 years old) is miR-23a-3p (Röck et al. 2014). It contributes to loss of elasticity by directly targeting hyaluronic acid synthase 2 (HAS2), which impairs the synthesis of the unbranched glycosaminoglycan hyaluronic acid (HA) (Röck et al. 2014). HA is a main component of the ECM and guarantees hydration, nutrient and ECM assembly (reviewed by Stern & Maibach 2008) and is reduced in an estrogen and UVB dependent manner (Dai et al. 2007). Another target of miR-23a-3p is lamin B1 (Dreesen, Chojnowski, et al. 2013). It is known to be reduced in cellular senescence of fibroblasts (Freund et al. 2012) and keratinocytes *in vivo* and *in vitro* (Dreesen, Chojnowski, et al. 2013), either depended or independent of miRNA binding.

To this end, skin-(aging) associated research apparently lack comparative studies of dermal and epidermal miRNA abundances. One recent study, however, found miR-15b-5p, low abundant in the dermis and highly expressed in epidermis, while it was significantly alleviated in photo-aged epidermal skin. *In vitro* it is commonly downregulated in senescent fibroblasts, either after UV (Greussing et al. 2013; Lang et al. 2016), gamma irradiation (Lang et al. 2016), oxidative stress (Li et al. 2009) or dysfunctional mitochondria-induced senescence (Lang et al. 2016) as well as in replicatively aged fibroblasts (Holly et al. 2015; Dhahbi et al. 2011). Its downregulation was consistently found in different models of aged fibroblasts, derived from lung (Holly et al. 2015), skin (Hackl et al. 2010) or foreskin

(Lang et al. 2016; Greussing et al. 2013; Hackl et al. 2010) tissue and points to a robust miRNA pattern of miR-15b-5p in aging. A possible explanation for the consistent downregulation of miR-15-5p could be a channeling of a NF- κ B mediated SASP activity (Kang et al. 2015), which is a process highly depended on a plethora of fine-tuning mechanism.

To summarize, skin as a two germ layer cell system with a dynamic turnover in cell renewal, is a complex model system to study miRNA regulation during normal and pathophysiological processes.

1.3.3. Message in a bottle - Circulating miRNAs in aging

While, much is known about cell, tissue and disease specific aberrantly regulated miRNAs, the discovery of circulating miRNAs present in conditioned media (Valadi et al. 2007) human plasma (Hunter et al. 2008) and bodily fluids (Cogswell et al. 2008) unravelled their potential as biomarker, therapeutic target and as a new form of intercellular communication (reviewed by Chen et al. 2012b). They were found in the systemic and tissue environment of 12 different body fluids (Weber et al. 2010). The remarkable stability of secretory miRNAs, present in mammalian serums was tested against harsh conditions after exposure to low/high pH levels, DNA and RNA degrading enzymes, freezing-thawing cycles and boiling (Chen et al. 2008). Quantitatively still detectable, their outstanding preservation constitutes from their protective association with RNA binding proteins such as nucleophosmin (Wang et al. 2010) and argonaut associated proteins (Arroyo et al. 2011) or from their encapsulation in several types of extracellular vesicles (reviewed by Turchinovich et al. 2012) or lipoproteins (Vickers et al. 2011a) (Figure 6).

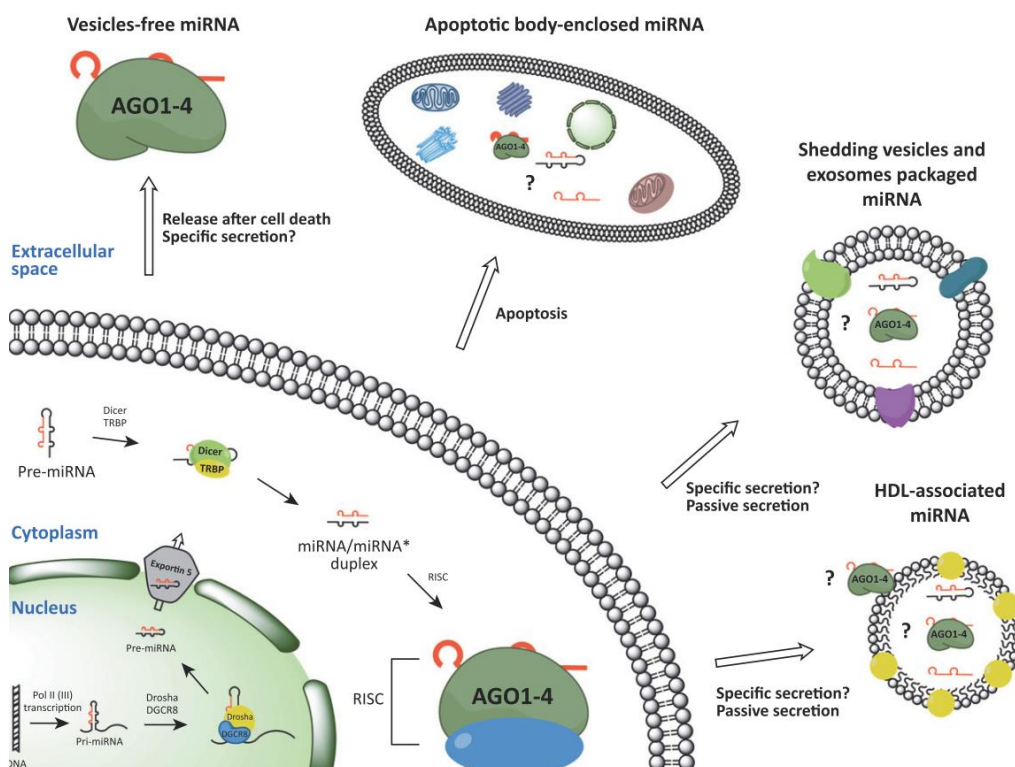


Figure 6 miRNA biogenesis, secretory miRNAs and their regulatory functions from Turchinovich et al. 2012

Presumably, circulating miRNAs emerged as powerful and suitable biomarker applicable for routine testing in clinics or other repositories and many discovery studies contributed to the development of commercially available testing kits to assess prognosis, risk and response to therapeutic strategies (reviewed by Hackl et al. 2016).

At the forefront of biomarker development are primarily cancer-associated miRNA studies, with promising results from multiple stages and types of benign or malignant cancer forms, mainly classified by a specific miRNA pattern found in serum rather than in blood. This was observed after comparing differences in miRNA signature of cancer patients derived from serum and blood samples, while they were absent in samples from the healthy cohort. Even after tumor resection the miRNA expression levels were reduced, indicating a strong impact of secretory compounds and metastasising capacities of cancer cells (Chen et al. 2008) and underscores the importance of tissue or cell of origin. In the context of accumulating senescent cells and their secretory factors, it is thus extremely likely to find an enrichment of senescence-associated miRNAs in the circulation of healthy and frailty elderly. High throughput miRNA profiling of samples from healthy-middle aged young (20 - 49 years), long lived centenarians and cardiovascular diseased patients revealed substantial evidences for the presence of the 'inflamma-miRs', miR-21-5p and miR-146a (Bhaumik et al. 2009) as important age-related miRNAs present in the systemic environment of aged individuals. Contrary, the retrospective longevity studies from ElSharawy and Serna identified a preserved longevity associated miRNA (ElSharawy et al. 2012; Serna et al. 2012) and small noncoding RNA signature (Serna et al. 2012), while a follow-up study, started 1958, to correlate the 'longevimiRs' with life span of study participants (Vikos et al. 2016).

With increasing medical support and advanced therapies, we are close to increases the amount of centenarians. Although the genetic predisposition of the most of us might not change, it will consequently increase the incidences of age-related diseases. In order to identify specific circulating miRNAs of age-associated diseases rather than for changes responsive to normal physiological aging (Erusalimsky et al. 2015), many studies collected a plethora of expression profiles from cardiovascular diseases (Min & Chan 2015) with or without atherosclerotic lesions (Andreou et al. 2015), mild or severe cognitive impairments (reviewed by Aw & Cohen 2012), age related cartilage and bone fractures (Kocijan et al. 2016; reviewed by Hackl et al. 2016), obesity and diabetes (reviewed by Guay & Regazzi 2013)(reviewed by Weilner et al. 2013).

Finally, we are close to answer, whether the mere abundance and detection of specific secretory miRNAs, either abundantly, differentially or temporally present, are sufficient to differ between pathological and physiological inflammatory processes of aging.

Circulating miRNAs need to be protected to allow delivery of their messages. But what is the 'bottle' of miRNA-based messages?

1.4. Extracellular vesicles - smart transport vehicles with physiological function

EVs are small multifaceted components involved in the paracrine communication between heterotypic cells and tissues. They are surrounded by a double lipid membrane and serves as protective vehicles for the transport of lipids, proteins and nucleic acids through the extracellular space where they modulate and activate intracellular

signalling cascades. They have been found throughout the tree of life, which in turn solidifies their biodiversity and importance throughout all cellular processes (Deatherage & Cookson 2012).

Since their discovery as a novel form of intercellular communication, many researches from various fields endowed their work to disclose the impact of EVs and their cargo down to the molecular level. To preserve the knowledge and broad range of collected data, the establishment of databases guarantees the recording of the manifold EV cargo molecules as well as EV markers detected in eukaryotes as well as in prokaryotes respectively. To date Vesiclepedia (Kalra et al. 2012) lists entries of 92.897 proteins, 4.934 miRNAs and 584 lipids detected within 33 species. In conjunction with EVpedia (Kim et al. 2015) the integration of comprehensive analysis tools allows the systematic dissection of myriad EV components identified within 6.879 publications (Database access 9th, March 2017).

Going back in history, EVs are not a phenomenon of the 2000s. They were originally identified as 'platelet dust' present in normal plasma and were further identified as 'vesicles/particles' during bone calcification (Anderson 1969) and tumor shedding (De Broe et al. 1975). Several years later the fusion of endosomal membrane compartments with the plasma membrane and the subsequent exocytotic release of transferrin receptor unveiled a different mechanism for vesicle shedding (Harding et al. 1983; Harding et al. 1984).

1.4.1. The versatility of EVs

EVs are surrounded by a double lipid membrane and differ significantly in density and size. It is their biogenesis that is used for a rough classification in three main subtypes, even though we still lack specific marker of the different classes of EVs (reviewed by Mathivanan et al. 2010).

Exosomes, microvesicles/ectosomes and apoptotic bodies. The latter are blebs and remnants of late apoptotic cells, within a broad size range of 50 – 500 nm. Microvesicle, ectosome or shedding vesicles, are a versatile group in size ranging from 100 – 1000 nm that share the same secretion mechanism by budding from the plasma membrane of the parental cell (reviewed by Cocucci et al. 2009). Exosomes are the smallest particles, with a narrow size range between 30 to 150 nm. They are among the most published nanoparticles and several researches endeavour to work with them (reviewed by Raposo & Stoorvogel 2013; Colombo et al. 2014; Kowal et al. 2014; and Kalra et al. 2016).

Current available isolation methods such as filtration, size exclusion chromatography, differential centrifugation in combination with a density gradient, focus primarily on discrimination based on size and/or density, which in turn leads to co-purifying of distinct vesicle subtypes. Therefore, the mere isolation of small vesicles around 100 nm does not implicate endosomal origin. The appearance of so-called 'exosome-like vesicles' budding directly from the plasma membrane was spread through the vesicle field and caused confusion and misleading. Therefore, the demand to unify and standardize vesicle nomenclature increased (discussed by Gould & Raposo 2013). This comes from the notion that one single cell secretes all sorts of vesicles that even change their appearance and function in response to exogenous stimuli or pathophysiological conditions (Pallet et al. 2013; Aatonen et al. 2014; Kowal et al. 2016; Brouwers et al. 2013).

Marker of EVs

In general the membrane of almost all vesicles is enriched in saturated fatty acids, cholesterol and sphingomyelene and contains proteins with distinct glycosylation patterns (Kapsogeorgou et al. 2005) and cell specific lipid compositions derived from the parental cell (reviewed by Record et al. 2014). This is of particular importance to identify the cellular source of circulating EVs within body fluids during clinical routines (Lynch & Ludlam 2007). In addition, the presence of 70 kDa heat shock proteins, antigen presenting proteins such as MHC-II and the tetraspanin CD63 are specific for the majority of EVs from various cells. The identification of endosomal derived proteins involved in MVB biogenesis such as tumour-susceptibility protein (TSG)101, Alix, Sphingomyelase, accessory proteins involved in transport and fusion (Rab GTPases, ect) and the tetraspanin family (mainly CD63, CD9, CD81 and CD82) were long considered to be specific for exosomes. However, it became clear that the 'former' *bona fide* exosome proteins CD63, CD9, CD81 are also detectable in microvesicles and apoptotic bodies (Kowal et al. 2016 and many others).

For that reason, Kowal and colleagues reviewed the protein composition of small EVs after the 'classical' differential centrifugation isolation method and suggested a new categorization to discriminate between endosomal and non-endosomal small EVs. Within this study, they revealed a coexistence of all three tetraspanins CD63, CD81, and CD9 combined with TSG101 and syntenin-1, which represent together a valid combination specific for small endosomal EVs. On the other side, the enrichment of several transmembrane integrins and actins (Gordon-Alonso et al. 2012) can be used to discriminate between non-endosomal (micro)vesicles in various sizes (Kowal et al. 2016). However, their reactivity was tested on EVs derived from primary dendritic cells and their validity needs to be determined on EVs from other cell types, sources and upon different isolation techniques.

1.4.2. Should I stay or should I go now - Vesicle biogenesis and secretion

The secretion of EVs from different subcellular location and their cargo selection depend on cellular condition of the parental cell and on exogenous triggers such as hypoxia or stress (de Jong et al. 2012; Eldh et al. 2010).

Microvesicles are normally shed from the plasma membrane by protrusion followed by fission. This is stimulated by PKC, and sphingomyelinase (Bianco et al. 2009), p38 (Curtis et al. 2009) and a cytoplasmic increase in Ca^{2+} concentration (reviewed by Cocucci & Meldolesi 2015). The local disassembly of cytoskeleton structures by degrading proteases such as calcium-activated calpains (Miyoshi et al. 1996) allows the sorting of genetic material into the immature vesicle. The externalization of phosphatidylserine is mediated by flippase and/or scramblase and activates the outward budding (reviewed by Cocucci et al. 2009; and Kalra et al. 2016). Secretion can be triggered by a signalling cascades initiated by GTP-binding protein ADP-ribosylation factor 6 (ARF6) that leads to pinching off through actomyosin contractions (Muralidharan-Chari et al. 2009).

Exosomes are the most published EVs and the gravest difference to other sorts of EVs is their biogenesis through the endosomal network. The inward budding of early endosomal membranes forms intraluminal vesicles (ILV), which are incorporated into multivesicular bodies (MVB). The presences of endosomal sorting complexes required for transport (ESCRT) complexes and its associated proteins (Babst 2005), lipids such as ceramides or sphingomyelin and tetraspanins are just few to be mentioned and are on the crossroad to define the prospective

fate of MVB and thereby the biogenesis of exosomes. While the presence of specific lipids such as endosomal marker lysosomal-associated membrane protein LAMP (Wubbolts et al. 2003; Brouwers et al. 2013) or ubiquitinated MHC class proteins (Buschow et al. 2009) are associated with the degradative process, the enrichment of tetraspanins such as CD9 or cholesterol molecules appear to direct the fusion with the plasma membrane leading to exocytic release of ILV, from now on termed 'exosomes'. If intended for degradation, MVB are sequestered within lysosomal organelles to allow enzymatic degradation, which might be necessary to regulate intracellular signaling, as do so for instance to reduce growth factor signalling (Miller et al. 1986; Sorkin & Goh 2009).

For the formation of MVB and the subsequent releases of ILV two distinct mechanisms have been described.

ESCRT, ceramides and tetraspanins mediated exosome release

The idea that distinct pathways regulate ILV formation and exosomes secretion was confirmed by Kosak and co colleagues. They showed that the knockdown of ESCRT components does not affect the neutral sphingomyelinase (nSMase2)-induced ceramide dependent secretion of EV-miRNAs, suggesting two clearly separated pathways of exosome biogenesis (Kosaka et al. 2013).

The ESCRT dependent mechanism governs the internalization of ubiquitinated cargo by the sequential assembly of multiple ESCRT protein complexes (ESCRT-0, ESCRT-I, ESCRT-II, ESCRT-III) and their accessory proteins (such as Hrs-STAM, binding to phosphatidylinositol-3-phosphate and the 3,5-bisphosphate, TSG101, Alix, etc). Deubiquitination and recycling of the ESCRT is executed by AAA-ATPase Vps4 machinery and MVB are transferred to the plasma membrane for exocytic release (reviewed by Kalra et al. 2016).

An alternative pathway, still proficient to form functional MVB, even in the absence of ESCRT proteins, is the ceramide dependent pathway (Stuffers et al. 2009). SMase synthesised lipid rafts are ceramide and cholesterol enriched domains that trigger the inward bending of the endosomal membrane and therefore ILV formation (Trajkovic et al. 2008).

The tetraspanin CD63 guided process of pre-melanosoma formation, mediates the packaging of ILV independently of the ceramide and ESCRT mechanism (van Niel et al. 2017). The generation of a CD9 knockout mouse model showed a reduced exosomes secretion in bone marrow dendritic cells (Chairoungdua et al. 2010) and an impaired sperm egg fusion (Miyado et al. 2008). Interestingly, overexpression of CD81 can rescue this sort of cell fusion after loss of CD9. This observation is consistent with several reports that propose an intertwining function of CD9 and CD81 in the fusion processes of different cells (Takeda et al. 2003; Tachibana & Hemler 1999; Martin et al. 2005), indicating a symbiotic mode of action of those tetraspanins. On the other side, CD63 as a major component of the lysosomes and the endosomes (Pols & Klumperman 2009), seems to function in a different manner. Although, CD63 disruption did not induce lysosomal dysfunctions, suggesting a compensating mechanism by other tetraspanins or accessory proteins, it rather induced a severe phenotype of kidney deficiency characterized by an abnormal water homeostasis (Schroder et al. 2009). These and several other studies implicate a fundamental role of the EV tetraspanins CD9, CD81 and CD63, in packaging and sorting of exosomes as well as their implications in various cellular processes.

However, it is still unknown, which mechanism or if a combination of the ESCRT, ceramide and/or tetraspanin depended pathways direct ILV formation and exosome secretion.

Still, for the subsequent exosome secretion, the reorganization of cytoskeleton structures, docking and fusion with the plasma membrane a coordinated co-working of several components from the Rab GTPases family (e.g. RAB27A, RAB27B, and RAB11), tetraspanins and SNARES are inevitable. several studies outlined a Rab dependent secretion mechanism that modulates vesicle homeostasis. For example, inhibition of RAB27A increased the size of MVB (Ostrowski et al. 2010) and modulated the distribution of specific tetraspanins showing less CD63, while CD9 expression was not affected (Bobrie et al. 2012). Interestingly, RAB27A was recently reported to govern miRNA secretion in tumor models to favour metastasis and invasion (Ostenfeld et al. 2014), indicating that cancer induced secretion goes in line with intracellular deregulations.

1.4.3. The butterfly effect - RNA sorting and trafficking

Even though, it was long thought that intercellular signaling is mediated by secreted soluble proteins, the first evidences of functional transfer of RNAs enclosed in EVs between different cell types and their power to regulate recipient's cell behaviours (post) transcriptionally and in a functional manner, raised the paradigm of cell-non-autonomous regulation to the next level. The first milestones of a shuttling of functional mRNAs enclosed in EVs and their translatability into new proteins were demonstrated in mast cells (Valadi et al. 2007) and human brain microvascular endothelial cells (Skog et al. 2008). The physiological relevance of EV containing RNAs and their communication during immune responses became evident in the study of Pegtel et al., by revealing the inhibitory capacity of EBV virus derived EV miRNAs on a target mRNA in dendritic cells (Pegtel et al. 2010). In a comparable EV-miRNA study the authors noticed changes in EV miRNA composition during different maturation states of the cells (Montecalvo et al. 2012), indicating that physiological stimuli may change the loading of EVs. Since then, EVs and their RNA cargo has been implicated in a various biological processes under physiological and pathophysiological processes. But not only mRNAs and miRNAs are protected within EVs, also other small non coding RNA species, such as vRNA, yRNA, tRNA, rRNA, snoRNA, snRNA, piwi-interacting RNAs, mtRNAs and lncRNAs (Nolte'T Hoen et al. 2012; Tosar et al. 2015; Ji et al. 2014; van Balkom et al. 2015;) have been identified in cellular culture supernatants and in human plasma (Huang et al. 2013), which were recently summarized by Fritz and colleagues (Fritz et al. 2016). In this context, the enrichment of vRNA, yRNA, snoRNA, scRNA and mRNA degradation products were attributed to EVs (Nolte'T Hoen et al. 2012; van Balkom et al. 2015) and differentially distributed miRNAs with 3p, 5p and stem loop fragments (van Balkom et al. 2015), pointed to a specific, motif dependent miRNA packaging mechanism rather than to a random process.

Specifically, EV-miRNAs are among the most studied sncRNAs of current and past research, with the main focus on functional or mechanistic miRNA trafficking processes. Accordingly, accumulating reports gave evidence that the extracellular environment does not simply mirror the cytoplasmic landscape of the donor cell, and the identification of specific guiding patterns and motifs (EXOmotif) gave insights into the packaging machinery of EV-miRNAs (Villarroya-Beltri et al. 2013). several sequence depended and independent RNA binding proteins and their post transcriptional modifications were found to direct miRNA packaging and are summarized in Table 1

Table 1 Overview of RNA packaging mechanism into EVs (Villarroya-Beltri et al. 2013; Koppers-Lalic et al. 2014; Shurtleff et al. 2016; Santangelo et al. 2016; McKenzie et al. 2016; Wang et al. 2010; Iavello et al. 2016; Melo et al. 2014; Jaé et al. 2015; Gibbings et al. 2009).

Sort of function	Mediator	Modification	Reference
Sequence depended, binding to 'EXOmotifs'	RNA-binding protein hnRNP A2B	sumoylated	Villarroya-Beltri et al. 2013
		addition of non-template terminal nucleotides rich in 3' uridylation	Koppers-Lalic et al. 2014
	synaptotagmin-binding cytoplasmic RNA-interacting protein (SYNCRIP/hnRNP-Q/NSAP1)		Santangelo et al. 2016
Sequence depended binding to miR-223	RNA-binding protein Y-box protein (YBX1) Y-box proteins		Shurtleff et al. 2016
sequence independent mechanism ('suggested') Interaction with accessory proteins involved in MVB biogenesis and membrane trafficking	Ago2 (eventually with GW182 Gibbings 2009)	Inhibitory phosphorylation	McKenzie et al. 2016
	distinct ribonucleoproteins relevant for RNA stability and transport, such as nucleophosmin		Wang et al. 2010
	Alix		Iavello et al. 2016
	TSG101		Melo et al. 2014
	Rab proteins		Jaé et al. 2015
	neutral sphingomyelinase		Kosaka et al. 2010
	Ago2 (eventually with GW182 Gibbings et al. 2009)	Inhibitory phosphorylation	McKenzie et al. 2016

However, none of these mechanism disclosed if this process is part of the 'cellular byproduct hypothesis' also known as 'disposal theory', or an active paracrine way of communication to transmit signals to their surrounding environment (reviewed by Turchinovich et al. 2016). However, it is intriguing to speculate that the many changes in recipient cell behaviour after EV mediated uptake of miRNAs (Mittelbrunn et al. 2011; reviewed by Zhang et al. 2015) would not require specifically regulated packaging mechanism. In particular, differences in miRNA patterns in tumour cell lines under basal (Eldh et al. 2014; Guduric-Fuchs et al. 2012; Ohshima et al. 2010) or benign conditions (Pigati et al. 2010; Xiao et al. 2012) exist. Hence, the reaction against endogenous stimuli or changes in mRNA expression seem to regulate miRNA packaging. This theory was tested by Guduric-Fuchs and colleagues, by mimicking the stimulus with the overexpression of miR-146a-5p in HEK293 cells. They observed an enrichment of several EV-miRNAs, while others remained constant, with a balanced ratio between endogenous and extracellular miRNA abundance (Guduric-Fuchs et al. 2012). Concludingly, it seems that only specific miRNAs react to exogenous signals. Similarly, even provocation by vaccination initiated the release of miRNAs to regulate gene expression in lymphocytes *in vitro* and *in vivo* (de Candia et al. 2013). In cancer models the release of tumor-suppressive miRNAs is considered to maintain tumor progression (Ostenfeld et al. 2014; Cha et al. 2015; Ohshima et al. 2010), while the secretion of specific miRNAs initiated pro-metastatic inflammatory responses and consequently favours metastatic behaviour (Fabbri et al. 2012). Squadrito and colleagues explain the selective disposal of miRNAs, as a redistribution mechanism to maintain a balanced homeostasis between endogenous mRNA to miRNA ratio (Squadrito et al. 2014). However, the term 'selective disposal' in this context raises confusion, since it seems to be a 'real' intercellular communication with a purpose. Contrary, the selective secretion of degradation products and

misfolded RNA fragments, which are not functional to fulfil paracrine communication is a valid example of the disposal theory (van Balkom et al. 2015). To sum up, most of these studies point into the direction of a selective packaging mechanism induced in response to physiological stimuli and/or under pathophysiological conditions. Nonetheless, recent studies raise serious doubts as to whether EV-miRNAs indeed confer a 'hormone-like' impact on recipient cells. This comes from the notion that around 90% of all secretory miRNAs, at least the one in serum and plasma, travel vesicle-free and are instead incooperated into Ago proteins (Arroyo et al. 2011). This, however, does not necessarily implicate that co-purification of EV-enclosed Ago proteins (Gibbings et al. 2009) was considered for that estimation and that on average less than one copy of miRNA was found per exosome after correlating nanoparticle tracking analysis (NTA) and qPCR data (Chevillet et al. 2014). On the other hand, by comparing qPCR derived standard curves of synthetic spiked in miRNAs with the endogenous concentration of miR-146a, it yielded in one miRNA copy per exosome in bone marrow derived dendritic cells (Alexander et al. 2015). Similarly around 10 to 50 copies, dependent on the quantification technique, were calculated for miR-1246, most abundantly present in human neural stem cells (Stevanato et al. 2016). Considering the vast increase of around 500 exosomes per cell (Alexander et al. 2015), it is thought to be sufficient to amplify the abundance of extracellular miRNAs to be higher than 100 copies per cell (Mullokandov et al. 2013; Brown et al. 2007) and thus potent enough to elicit a regulatory and/or inhibitory function on a target mRNA. In addition, miRNAs are normally more abundant than their target mRNAs and can reach around 10.000 copies per 1000 μm^3 cell, which corresponds to around 22 μM of a miRNA (Ragan et al. 2011). Whether this might fit to a clinical relevant dose of 100 nM per mg/kg body weight of RNAi therapy (Martinez et al. 2014) is however a matter of debate (Stevanato et al. 2016). Finally, both theories, either the 'waste disposal theory' or the 'selective secretion hypothesis for cell-cell communication' have many supportive evidences, for and against them. However, which theory holds true remains a matter of debate and paves the way for many exciting pursuing studies. In addition, whether the 'hormonal activity' of secretory miRNAs enclosed in EVs convey sufficient potential to regulate cell non – autonomous signalling or if other forms of protective extracellular miRNA carrier, such as nucleophosmin (Wang et al. 2010), Ago2 (Arroyo et al. 2011) or high density lipoproteins (HDL) (Vickers et al. 2011a) govern the intercellular miRNA crosstalk needs to be addressed in the upcoming future.

1.4.4. The versatile functions of EVs

EVs are secreted by most if not all cells and the encapsulation of cytosolic cargo allows protected transport through the extracellular space leading to the detection of EVs adjacent to tissues as well as in various body fluids such as blood, plasma, serum, cerebrospinal fluid, urine, semen, saliva, breast milk and amnion (reviewed by Foster et al. 2016; B. Zhang et al. 2016; Turchinovich et al. 2011 and many others).

Within in the last years the immunomodulatory roles (reviewed by Robbins & Morelli 2014; and Hwang 2013) of exosomes derived from blood cells have been extensively studied, probably due to their elementary role as a defense barrier against exogenous hazards (Wisgrill et al. 2016; Beer et al. 2015; Sódar et al. 2016; and many others Cheng et al. 2014; Montecalvo et al. 2012). They can serve as storage vacuoles for MHC-II class proteins to facilitate antigen presentation at a later timepoint (Kleijmeer et al. 2001). They can carry MHC proteins, co-stimulatory ligands and adhesion molecules to stimulate T cell priming and to confer bystander effects necessary for a robust

T cell activation. Notably, studies on immature and activated dendritic cells revealed not only a distinct set of co-stimulatory ligands but also a rather aggravated immune stimulatory function between the two cell conditions (reviewed by Robbins & Morelli 2014).

But where are they going? Although many research groups exploited fluorescence labelling methods (reviewed by Gangadaran et al. 2017) to monitor vesicle uptake by endocytosis, membrane fusion, phagocytosis or micropinocytose, the clear mechanism of EV uptake and in particular their distribution *in vivo* remains elusive (reviewed by Hwang 2013; and Mulcahy et al. 2014). However, few substantial sights to EV tracking in mouse models were already provided and will be discussed later (reviewed by Zomer et al. 2016; Ridder et al. 2014).

EVs in pathophysiological processes

EVs are versatile physiological all-rounders and do not only participate in normal physiological functions such as stem cell and tissue maintenance, vascular biology, coagulation and immune regulation, but are highly involved in certain diseases and pathophysiological conditions (reviewed by El Andaloussi et al. 2013; and Yànez-Mo et al. 2015). Especially their implication in metastasis and tumor progression is of high interested and allows the identification of novel mechanism enhancing tumorigenesis.

Within the crosstalk between normal and malignant stroma cells (Bremnes et al. 2011), the shedding of EVs from the plasma membrane favours the establishment of a pre metastatic tumor niche (Castellana et al. 2009) and thereby the expression of angiopoietic components. Transfer and spreading of oncogenic traits transmitted via EVs confers drug-resistance and promote matrix degradation within the tumor stroma to enliven invasion, motility and spreading (Camussi et al. 2011). A major perpetrator involved in matrix degradation and immune response is EMMPRIN, or basigin/CD147, encased in shedded tumor vesicles (Sidhu et al. 2004) and able to trigger the release of MMPs in fibroblasts and to induce α -smooth muscle actin depended transformation into cancer associated fibroblasts (CAF) (Xu et al. 2013). Since CAFs occupy up to 80% of solid tumor tissue and their acquired secretory phenotype is comparable to the SASP of senescent fibroblasts, it is tempting to speculate that extracellular vesicles resides on the edge between cancer and aging of fibroblasts and are thus key inducer of antagonistic pleiotropic features (Bremnes et al. 2011; Gascard & Tlsty 2016). Moreover, a-SMA induced myofibroblast differentiation is an essential transition necessary for proper wound healing and relies mainly on cell autonomous and non-autonomous communication between skin residents (Demaria et al. 2014).

Intriguingly, elevated EV levels were repeatedly associated with general stress conditions and have been shown to rely on increasing amounts of ATP (Bianco et al. 2005). In particular, ATP stimulation activates a p38 MAPK signalling cascade and induces the mobilisation of acid sphingomyelinase, a key component involved in EV biogenesis, and thus enhances EV shedding (Bianco et al. 2009). Consequently, elevated EV secretion observed in cancer cells does occur surprisingly, since their ATP generation is accelerated and shifted to 'aerobic glycolysis', even in presence of excess oxygen (Warburg 1956). The same holds true for serum starved cells (Muturi et al. 2013), which reflects a stress condition and an unconventional strategy to induces 'senescence' induced growth arrest (Weebadda et al. 2005). The very first report on EVs in cellular aging, showed indeed an increase of EVs in replicatively senescent fibroblasts and in irradiation-induced senescent prostate cancer cells (Lehmann et al. 2008), probably mediated by p53 activation in response to irradiation/DNA damage (Yu et al. 2006). Similarly, chronic

inflammation and stress stimuli, such as hypoxia observed in cardiomyocytes (Chistiakov et al. 2016) and lung fibroblasts (Moon et al. 2015) stimulated EV secretion. Moreover, the increase of EVs in cerebrospinal fluid from Alzheimer disease patients (Agosta et al. 2014) where also senescent astrocytes were encountered to contribute to the SASP (Bhat et al. 2012). EVs were also visualized in atherosclerotic aortas (Perrotta & Aquila 2016) a model system to study age associated cardiovascular diseases, since senescent endothelial (Minamino 2002) and vascular smooth muscle cells (Fenton et al. 2001; Baker et al. 2016) have been located at lesion sides. Those and many more findings anticipate the physiological relevance of EVs in age- associated diseases and it is intriguing to speculate that senescent cells might also secrete more EVs *in vivo*.

1.4.5. EVs for therapy – a new area?

The implication of EVs in many diseases allows the transmission of pathogenic traits. Presumably, the reversion of these traits lead to the development of strategies to alleviate disease progression. They comprise the inhibition of EVs upon diseases. Either by reducing (i) excess production and (ii) release; (iii) prevent uptake of EVs and (iv) block the uptake of specific EV components by direct targeting of surface receptors, such as FAS ligand or phosphatidylserine (reviewed by El Andaloussi et al. 2013).

Although, it has been shown that these approaches are feasible, it is intriguingly to think that the ideal exploitation point to vesicles as a functional therapeutic. One reason for that, might be their capacity to spread between heterogenic cell types and to induce vessel formation and angiogenesis, and thus render EVs to a formidable tool as a therapeutic target and vehicle for gene transfer (reviewed by El Andaloussi et al. 2013). It is in particular the tissue regenerating, antigen presenting and immunomodulatory roles of stem cell derived vesicles and their cargo that were recently endorsed for clinical studies (reviewed by B. Zhang et al. 2016; reviewed by Lener et al. 2015). The curing potential of MSC derived vesicles is mostly used in systems of myocardial infarcts (Lai et al. 2010) and kidney diseases (Bruno et al. 2012), graft versus host disease (Le Blanc et al. 2004) and in several sorts of injuries (Rani & Ritter 2016; reviewed by Rani et al. 2015). The successful immortalization of MCS and the establishment of an EV producer cell line (Yeo et al. 2013; Lamparski et al. 2002) are solely the beginnings for a new area of regenerative medicine.

In addition EVs are constituted with a delivery feature and offer a convenient way to transport and transmit drugs or molecules for targeted therapy and this is probably the most promising trait of EVs. Since current gene therapy methods rely mostly on viral delivery vectors, the benefits of EVs in regard to safety and biocompatibility are striking. The general approach aims the endogenous or exogenous loading of mRNA, miRNAs, shRNAs or specific drugs into EVs, which can then be tested *in vitro* or by injection in *in vivo* systems. First evidences for the delivery of EV cargo after passing the blood brain barrier were already conducted six years ago (Alvarez-Erviti et al. 2011). Thereby, EVs were engineered to expose the brain specific peptide sequence (rabies virus glycoprotein (RVG)-derived peptide) on their surface prior loading of EVs with siRNA. Interestingly, the RNAi induced effects were present throughout the brain but with minor effects in the spleen and liver (Alvarez-Erviti et al. 2011). This reflects the potency of EVs upon release into circulation. However, to use the full potential of EVs we still lack precise knowledge about specific targeting strategies.

2. Objective

The multifaceted phenomena of cellular senescence *in vitro* has been extended to the conviction that accumulation of senescent cells with age contribute to the functional decline of organs and tissues, while their removal in transgenic mice (Baker et al. 2011) or by senolytic compounds (Zhu et al. 2016; Wang et al. 2016; Chang et al. 2016; Eirin et al. 2014; Roos et al. 2016; Zhu et al. 2015; Yi Zhu et al. 2017) have been shown to promote healthy aging. The skin as a first line of defense, is the most exposed organ and shields the organism from environmental harm and lifestyle habits, known as intrinsic and extrinsic sources of skin aging. Thus, its progressive functional deterioration result in cellular and clinical signs of skin aging and contributes to the development of acute and chronic systemic diseases. In the skin of aged primates up to 20% of the fibroblasts show signs of cellular senescence (Herbig et al. 2006; Jeyapalan et al. 2012) and mounting evidences suggests that the acquisition of a senescence-associated secretory phenotype (SASP) negatively impacts on tissue homeostasis and regeneration *in-vivo*, while its transient presence favors wound healing (Demaria et al. 2014), tissue development (Ritschka et al. 2017), and even embryogenesis (reviewed by Muñoz-Espín & Serrano 2014).

While many SASP factors have been identified, miRNAs and extracellular vesicle are under severe suspicion to contribute to the cell autonomous and non-autonomous communication during cellular senescence (Bonafè & Olivieri 2015; Olivieri et al. 2013; Olivieri et al. 2015). This comes from the notion that EVs are reported to be increasingly secreted in response to acute or chronic stress stimuli (Wang et al. 2010; Arscott et al. 2013; de Jong et al. 2012; Eldh et al. 2010), diseases (Chistiakov et al. 2016; Joshi et al. 2014) or in replicatively senescent prostate cancer cells (Lehmann et al. 2008). In addition, selected EV packaged miRNAs and proteins in aging (Effenberger et al. 2014; Weilner, Keider, et al. 2016) have been shown to modulate the transcriptional and post transcriptional machinery of neighbouring cells.

However, whether these EV-miRNAs are selectively packaged or retained in response to physiological stimuli is still not entirely clear. So far it is known that either under basal (van Balkom et al. 2015), tumorigenic (Pigati et al. 2010; Xiao et al. 2012; Fiskaa et al. 2016; Kogure & Lin 2011) or stress conditions (Yentrapalli et al. 2017; Baglio et al. 2015) some miRNAs are indeed selectively packaged into EVs. However, only few reports cover changes in EV-miRNA packaging due to external stimuli including KRAS mutation status (Cha et al. 2015) or after irradiation (Yentrapalli et al. 2017), while no reports exist that compared changes in intracellular and vesicular miRNA abundance after induction of senescence.

We thus hypothesize that dysfunctional signaling in skin aging is also influence by specifically secreted EV-miRNAs from senescent cells. Consequently, part one of the study (A) will cover the following aspects:

(Ai) We aim to identify differentially secreted EV-miRNAs as part of the SASP from stress-induced premature senescence (SIPS) fibroblast and address,

(Aii) whether specific EV-miRNAs are selectively packaged or retained after entry into SIPS.

Objective

Having identified prominent regulators of EV mediated miRNA secretion in fibroblasts' senescence, the second part (B) explores the functional impact of differentially secreted miRNAs on keratinocytes.

Striking evidences for the impact of vesicular crosstalk between different skin cells were recently presented and confirmed the existence of a functional EV-mediated effect on recipient cells (Wäster et al. 2016; Huang et al. 2015). However, these reports focused on keratinocyte derived EVs and their effect on fibroblasts and evaluated the uptake of melanocyte derived EVs and their consequences on keratinocytes, while to our knowledge no other studies evaluated the fibroblast to keratinocyte EV-crosstalk and the physiological effect of miRNA uptake.

In order to achieve this, we will initially test

(Bi) if dermal and epidermal cells indeed communicate via an EV mediate miRNA crosstalk within *in vitro* and *in vivo* mimicking cell culture systems. As they do so, we will then

(Bii) evaluate keratinocyte specific functionality and

(Biii) miRNA expression levels after exposure to senescent EVs. In order to identify the most pivotal mediators, we will mimic the impact of SIPS derived vesicles by overexpression of single miRNAs in keratinocytes.

With the end of this study, we will have identified a signature of senescence-associated EV-miRNAs that are causally involved in age dependent regulatory functions such as wound healing and differentiation of keratinocytes as well as their stress resistance in cells derived from a knockout mice model.

3. Results

Part A

3.1. Extracellular vesicles of stress-induced premature senescent fibroblasts are part of the SASP

Human dermal fibroblast (HDF) scarcely divide and telomere attrition as a consequence of the replicative end problem might not represent a valid model to study dermal aging. Supportive data observe only marginal differences of telomere loss in skin sections of differentially aged donors (Krunic et al. 2009) and no correlation of the replicative life span to donor age was found (Cristofalo et al. 1998). Contrary, age-dependent reduction of telomere length in the dermis is considered to be a consequence of extrinsic aging (Sugimoto et al. 2017).

Mimicking extrinsic dermal aging by repeated sub-toxic concentrations of oxidative stressors is thus an accepted model system. Common agents used to trigger stress-induced premature senescence (SIPS) are H_2O_2 (Chen & Ames 1994; von Zglinicki 2000), ethanol (Dumont et al. 2002), t-BHP (Toussaint et al. 1994), organic peroxides (Fransen et al. 2012), paraquat (Jung et al. 2009) and UV radiation (Rodemann et al. 1989). Among those, we selected two different stimuli and tested their potency in HDF, derived from three different healthy donors. We established a SIPS protocol using the traditional H_2O_2 based protocol (Fripiat et al. 2001) and tested the efficiency of the natural herbicide paraquat. It is able to diffuse across the cell membrane and is thus considered to confer toxicity intracellularly (Bus & Gibson 1984).

3.1.1. Stimulation of stress-induced premature senescence mirrors hallmarks of cellular senescence

For the optimization of a paraquat-triggered SIPS protocol, several parameters, ranging from different concentrations, seeding densities prior treatment and amount of days and duration of doses were evaluated. We observed a very narrow concentration range, between, no induction of senescence and cytotoxicity (Figure 8) that was in addition dependent on the donor (Figure 7)

Microscopic examination of HDF85 and HDF161 indicated a distinct response to the similar treatment, showing either a stressed and thin morphology in HDF85, while almost no effect on HDF161 was visible. This observation is in line with the detection of three fold more apoptotic cells in HDF85 compared to HDF161 at either timepoints (Figure 8).

Results

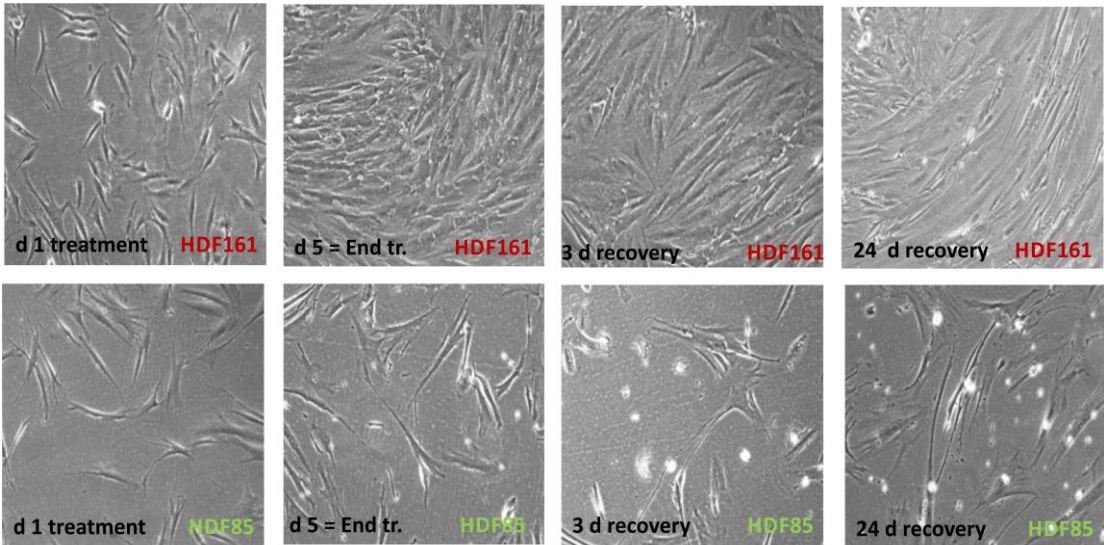


Figure 7 Donor depended impact of paraquat-induced stress. Incubation wit 60 μ M paraquat on three consecutive days induced either no senescent phenotype (HDF161) or a cytotoxic effect on (HDF85).

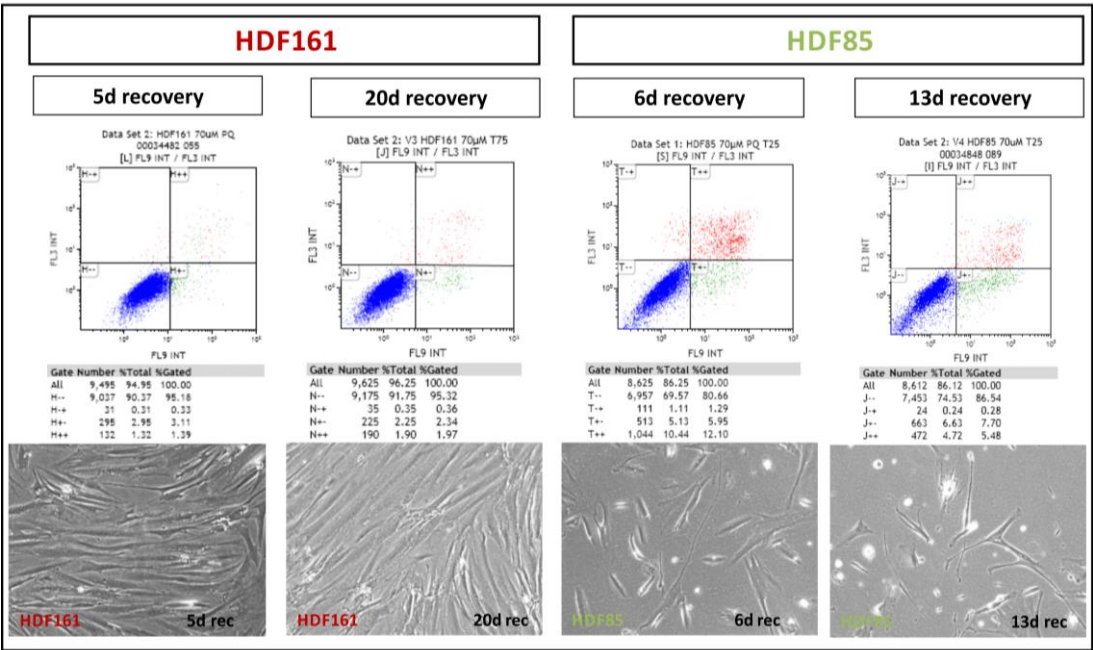


Figure 8 Annexin-V/PI staining shows an increase in apoptosis of HDF85, while no cytotoxic effect on HDF161 was detectable

In addition, long term follow-up showed a delayed response to the treatment showing a cytotoxicity effect after 11 days post stress (p5) that was reverted by the recovery of the cells leading consequently to passaging.

Results

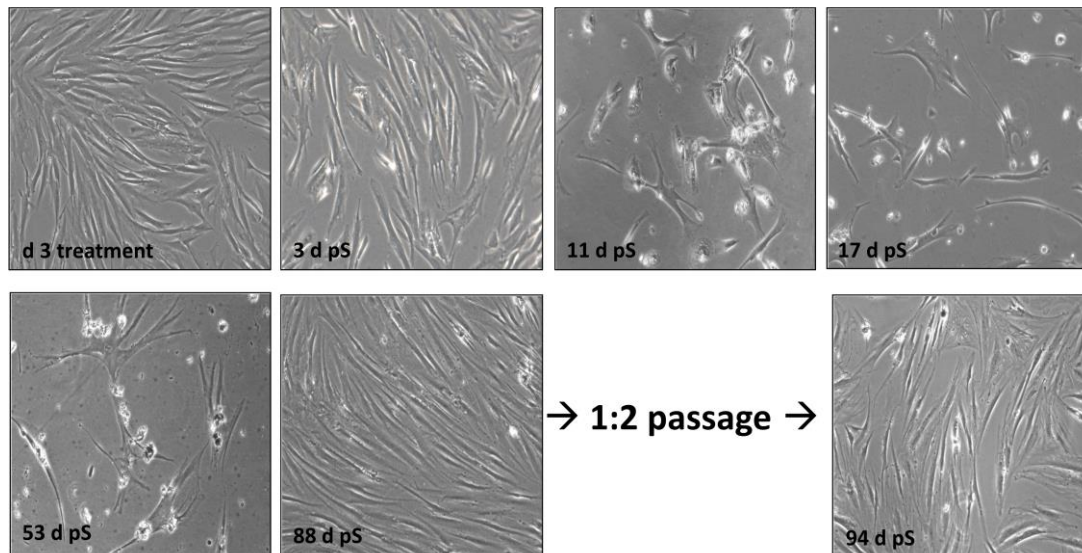


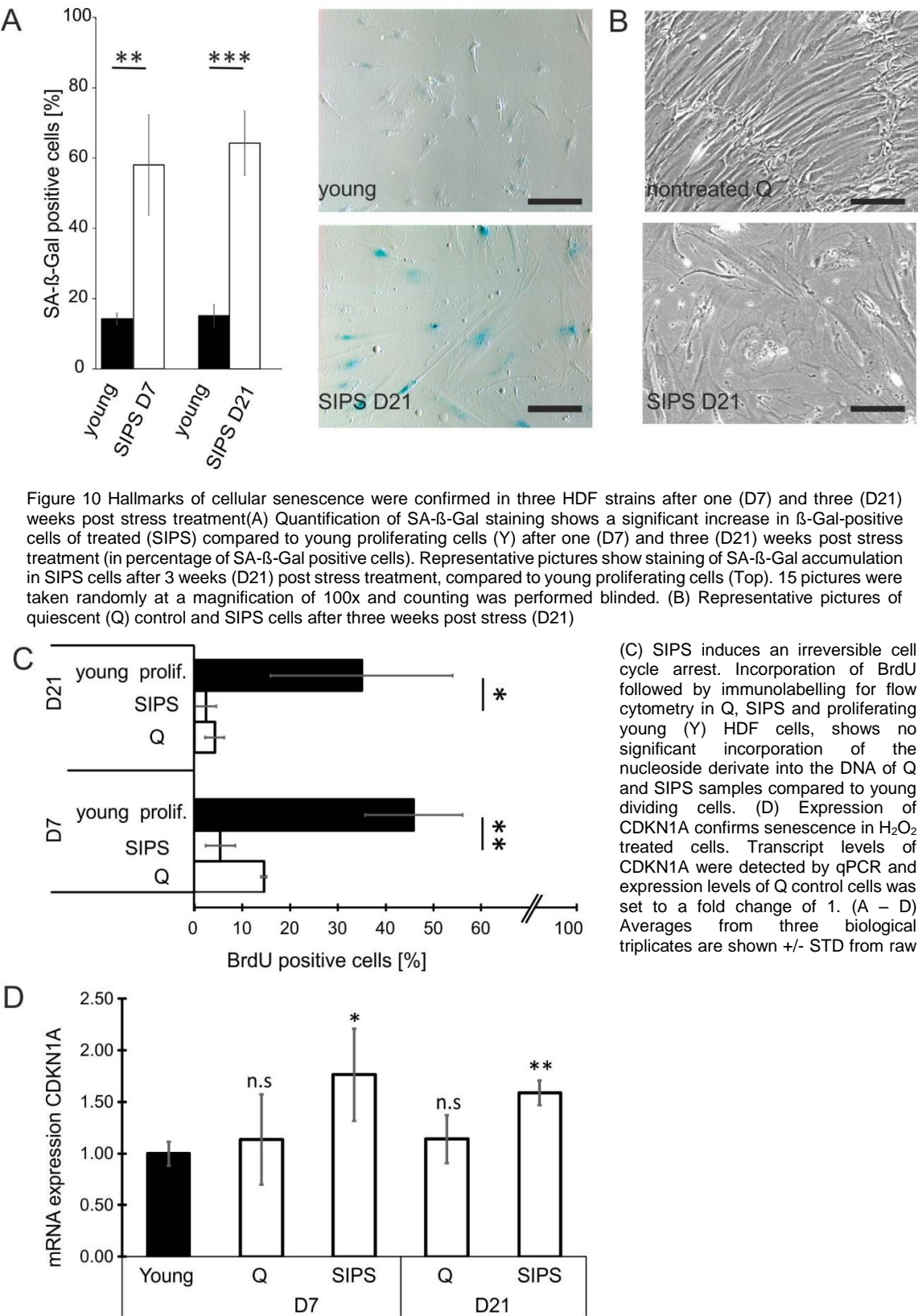
Figure 9 Long term follow up of paraquat treated cells (HDF76) show a delayed response to the agent.

The unpredictable toxicity of paraquat is exhibited by activated oxygen (superoxide anion, hydrogen peroxide, hydroxyl radical) and by the stimulation of NADPH that further promotes ROS generation. This might be the reason for its delayed response. Initially the cellular antioxidant mechanism counteract the oxidative burden until its complete deprivation, which leads to a postponed potency visible after 11 days post treatment.

Thus, we concluded that paraquat is not suitable to induce SIPS in fibroblasts and we decided to go back to H_2O_2 -induced senescence and established a protocol using $100\ \mu\text{M}$ H_2O_2 for 1 hour on 9 days, with a recovery of 2 days in between.

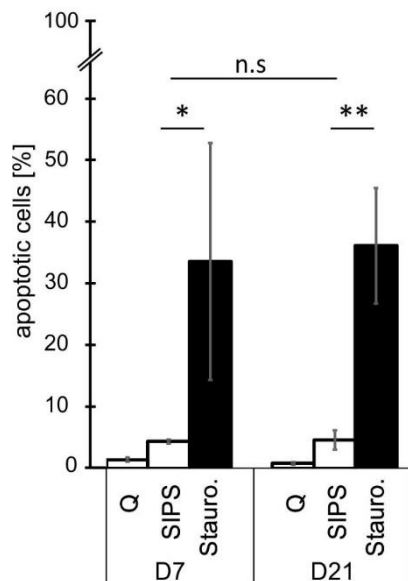
The cells of all three donors were repeatedly treated with chronic low doses of H_2O_2 , while nontreated control cells were allowed to reach quiescence (Q) by contact inhibition. Major hallmarks of cellular senescence were confirmed at early (after one week/seven days post stress = D7) and late stages (after three weeks/21 days post stress = D21) of cellular senescence. Senescent cells acquired a flattened and enlarged morphology, while nontreated control cells maintained a spindle-like shape morphology (representative pictures Figure 10B). Induction of cell cycle inhibitor CDKN1A (Figure 10D), significantly increased activity of SA- β -Gal (Figure 10A) and irreversible growth arrest (Figure 10C) in senescent versus young cells confirmed entry into SIPS.

Results



In order to exclude the presence of apoptotic bodies in the purified EV fractions, cell viability was assessed by trypan blue exclusion resulting in almost 100% viable cells (data not shown). In addition, no significant difference in the basal amount of 5% apoptotic cells and over time was detected (Figure 11). This finding is in agreement with

Results



the amount of cells present in sub-G1 peak upon staining with propidium iodide (PI). We summarized detailed data of the characteristics of all SIPS and control Q HDF cell strains in Table 2 and continued with the evaluation of the extracellular environment from all donors and conditions.

Figure 11 SIPS treatment is sub-lethal. SIPS and Q control cells do not show a substantial increase in early and late apoptotic cells when comparing with positive-control, treated with 300 nM staurosporin (+) for 24 hours.

	1 week recovery (D7)												3 week recovery (D21)																
Donor	early and late apoptotic (Annexin + PI positive)			BrdU positive cells [%]			Sub-G1 peak (PI staining) [%]			CDKN1A mRNA Expression. Normalized Fold changes			SA-βGal positive cells [%]		Apoptosis (Annexin & PI positive) [%]			BrdU positive [%]			Sub-G1 peak (PI staining) [%]			CDKN1A mRNA Expression. Normalized Fold changes			SA-βGal positive cells [%]		
	Q	S	+	Q	S	Y	Q	S	Y	Q	S	Y	Y	S	Q	S	+	Q	S	Y	Q	S	Y	Q	S	Y	Q	S	Y
HDF161	1,7	4,3	49,2	15,0	5,0	55,0	2,5	3,9	0,6	1,1	0,9	16,1	50,2	1,1	2,8	39,7	4,5	1,5	35,0	0,8	3,3	1,2	1,3	13,0	69,7	1,2	1,3	13,0	69,7
HDF85	1,1	4,1	12,1	14,0	2,8	35,0	0,7	4,8	1,3	1,7	1,0	13,0	74,4	0,7	5,4	25,5	3,8	0,4	16,0	1,2	3,2	1,1	1,5	13,8	69,2	0,8	1,4	18,7	53,7
HDF76	1,5	4,7	39,6	15,0	8,0	48,3	1,2	3,3	1,2	1,9	0,8	13,8	49,3	0,6	5,6	43,3	3,5	1,1	54,0	1,3	6,8	0,8	1,4	18,7	53,7	0,8	1,4	18,7	53,7

Table 2 Characteristics of fibroblast (HDF) cell strains: Confirmation of characteristics of cellular senescence after 7 (D7) and 21 days (D21) after the last H₂O₂ application in cells of three donors.

3.1.2. Small extracellular vesicles are part of the senescence-associated secretory phenotype of senescent cells

The SASP is thought to be a crucial driver of age-associated diseases. While the transient presence of senescent cells and the secretion of pro-inflammatory growth factors, cytokines, chemokines and extracellular matrix remodeling factors have been shown to act beneficially on wound healing (Demaria et al. 2014; J. Il Jun & Lau 2010), their chronic presence contributes to tissue remodeling and to an impaired homeostasis of the surrounding environment. Recently, extracellular vesicles have been shown to be progressively secreted in response to various acute or chronic stress stimuli such as serum starvation (Wang et al. 2010), irradiation (Arscott et al. 2013) hypoxia (de Jong et al. 2012), oxidative stress (Eldh et al. 2010), diseases (Chistiakov et al. 2016) or in aged related conditions (Joshi et al. 2014) or cellular senescence (Lehmann et al. 2008). However, whether EVs and their cargo are part of the SASP of human dermal fibroblasts has not been investigated yet.

Therefore, small (< 220 nm) EVs from all three fibroblasts cell strains were pelleted by ultracentrifugation and resuspended either with PBS for functional studies or with Trizol for subsequent EV-miRNA profiling. EVs were characterized by nanoparticle tracking analysis (NTA), transmission electron microscopy (TEM), and immunoblotting. Size distribution as assessed by NTA revealed a vesicle population below 220 nm (Figure 12A)

Results

within an average size range of 65 – 80 nm (Figure 12B), while no significant difference in vesicle size harvested from SIPS versus Q cells was identified.

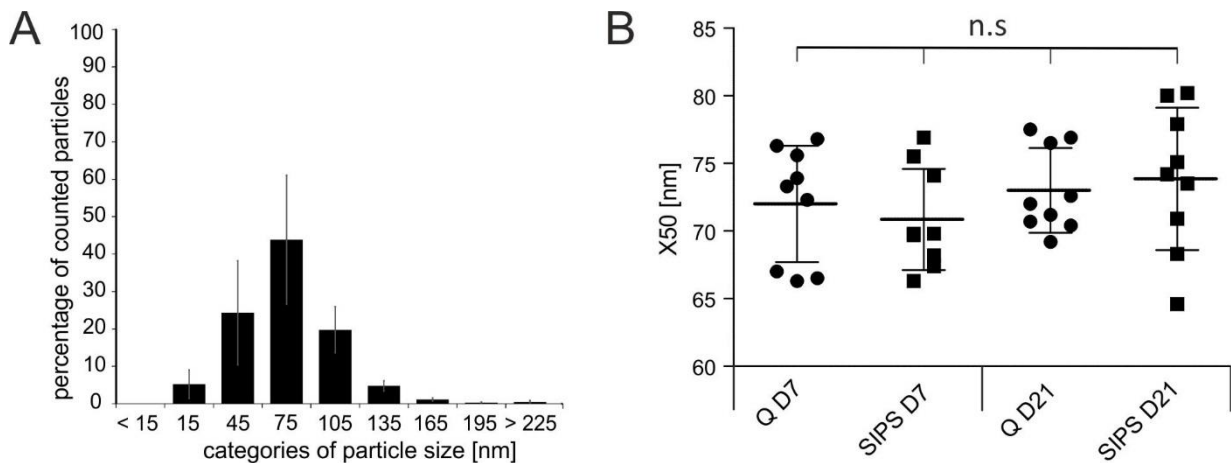


Figure 12 Vesicles from quiescent/contact inhibited control (Q) and SIPS cells from three different donors and two timepoints were measured in triplicates by nanoparticle tracking analysis (NTA). (A) Size of EVs are in an average size range of +/- 80 nm in diameter. Average values from peak analysis are indicated +/- STD. (B) NTA reveals a vesicles population below 220nm. Size distribution of vesicles determined by NTA shows number of total counted particles against their size in nm.

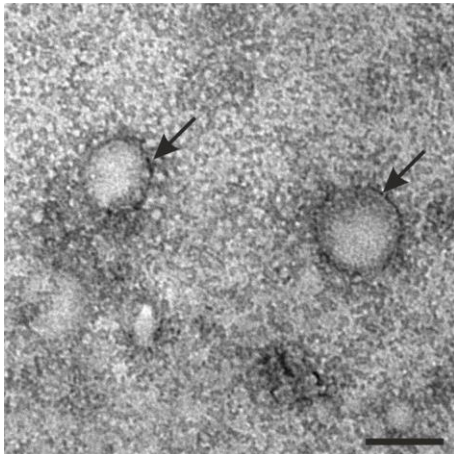


Figure 13 Representative image of negative stain preparations for Transmission electron microscopy (TEM) of EVs isolated from SIPS cells. Vesicles are in a size range of 50 – 100 nm and are surrounded by a double lipid membrane

Size was further confirmed by TEM, showing in addition a clearly visible lipid bilayer in fibroblasts' vesicles (Figure 13). Interestingly, vesicles harvested from non-treated cells appeared more electron dense than SIPS derived vesicles (Figure 14), indicating differences in the molecular composition between SIPS and Q vesicles. Given the fact that phosphotungstic acid (PTA), used for contrast staining is known to interact with lipoprotein structures (Rames et al. 2014; Zhang et al. 2013) and based on differences between intracellular lipid composition of SIPS and Q cells (Gruber lab and unpublished) we assume to see this effect also between senescent and control derived EVs. A similar phenotype was recently observed in a study on EVs from senescent platelets (Pienimaeki-Roemer et al. 2015) and comparable pictures, showing exosomes with obscured double lipid membranes

secreted from U87 and HMVEC cells (Sharghi-Namini et al. 2014), and in bovine milk exosomes (Reinhardt et al. 2012) were also reported.

Results

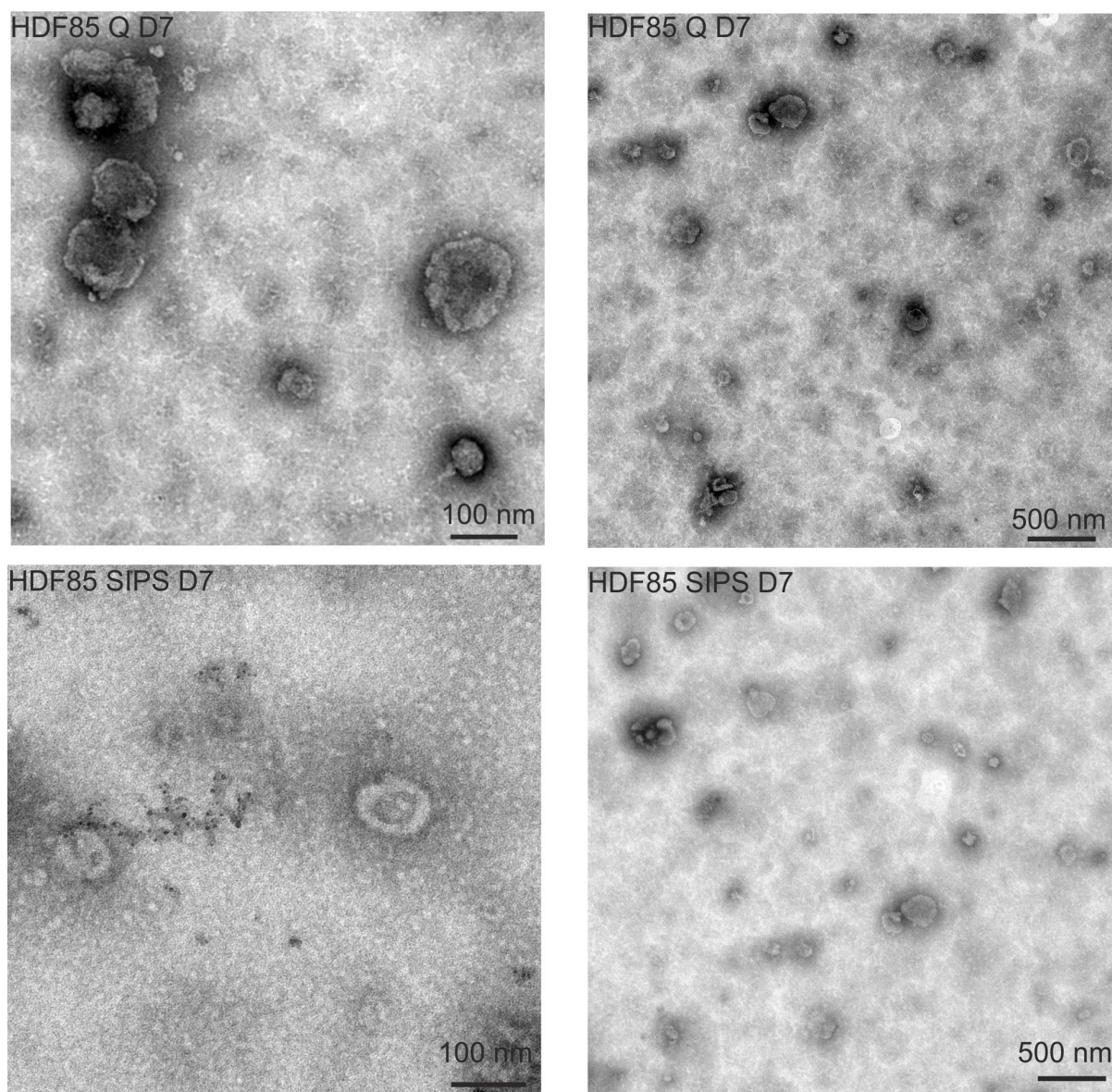


Figure 14 Images of contrast stain preparations for Transmission electron microscopy (TEM) of EVs isolated from Q (top) and SIPS (bottom) cells after 7 days post stress. Vesicles are in a size range of 50 – 220 nm. Vesicles from Q cells appear more electron dense than vesicles isolated from SIPS HDF. Both are surrounded by a double lipid membrane- 100 nm, m and 500 nm as represented by size scale.

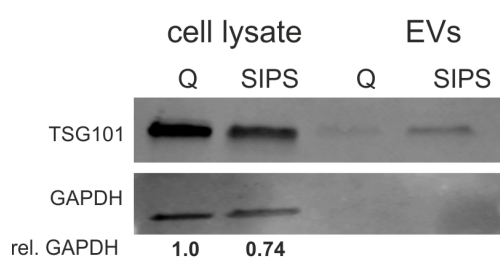


Figure 15 Representative Western blot image shows expression of TSG101 (top) and GAPDH (below) in total cells and vesicles from Q and SIPS cells (right lane).

We next tested for the presence of TSG101, a known marker for exosome-like vesicles synthesized via the endosomal network (reviewed by Colombo et al. 2013). Intracellular TSG101 levels were normalized to GAPDH and revealed a reduced expression of TSG101 in SIPS cells. Extracellularly, we ensured equal loading of vesicles as determined by BCA assay (data not shown) and surprisingly we detected the opposite, namely an increased expression of TSG101 in SIPS derived vesicles (Figure 15). Still the detection of other EV specific markers such as the tetraspanins CD63 and CD81, needs to be done.

Results

Presumably, these characteristics and the particular isolation procedure pointed towards exosome-like vesicles, hereinafter collectively called, EVs (EVs) that we further used for miRNA-profiling.

In order to determine differences in vesicle secretion between Q and SIPS cells, we quantified the amount of EVs using NTA and found an four fold increased secretion of EVs per cell in all three donors from both timepoints tested (Figure 16). It is thus, intriguing to speculate, that a reduction of TSG101 in senescent cells is due to its increased secretion of TSG101 positive EVs.

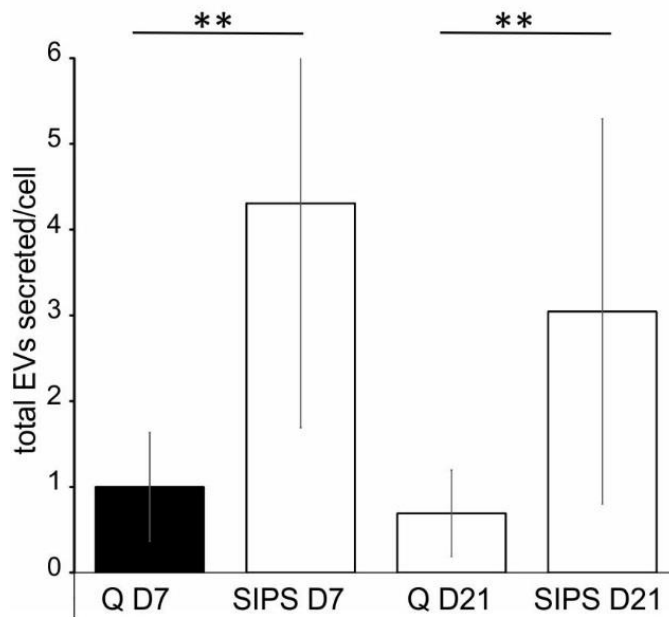


Figure 16 Senescent cells secrete more small EVs per cell than Q cells. Total concentration of counted particles was normalized to total cell number used for secretion. Vesicles from Q and SIPS cells from three different donors after 7 (D7) and 21 (D21) days post stress were measured in triplicates. Fold changes relative Q control cells are shown. Unpaired students t-test was applied on raw values. **P < 0.01;

Considering the phenomenon of increased senescence-associated secretion of proteins summarized under the term SASP and earlier findings on elevated EV secretion in response to stress, our findings suggest that small EVs are *bona fide* members of the SASP. We next decided to focus on their miRNA composition and to identify specific senescence-associated miRNAs enclosed in EVs (EV-miRNAs).

3.2. Are EV-miRNAs novel factors of the senescence-associated secretory phenotype?

In order to identify the quantity of secreted EV-miRNAs we performed a preliminary screening with EV from one donor and two conditions, covering 752 ubiquitously expressed human miRNAs included in the ready to use Human Panel I and II, supplied by Exiqon. From 752 miRNAs tested, 542 (72%) were detectable in both or either conditions, respectively (Figure 17). In order to include only reliably detectable miRNAs, 368 miRNAs with two Ct-values above detection limit (Ct-values < 38) in either conditions were selected for further analysis. In addition, we included Even miRNAs detectable just in one conditions but with interesting publication record and designed a customized qPCR panel for the subsequent discovery study using cells of three different donors and two timepoints.

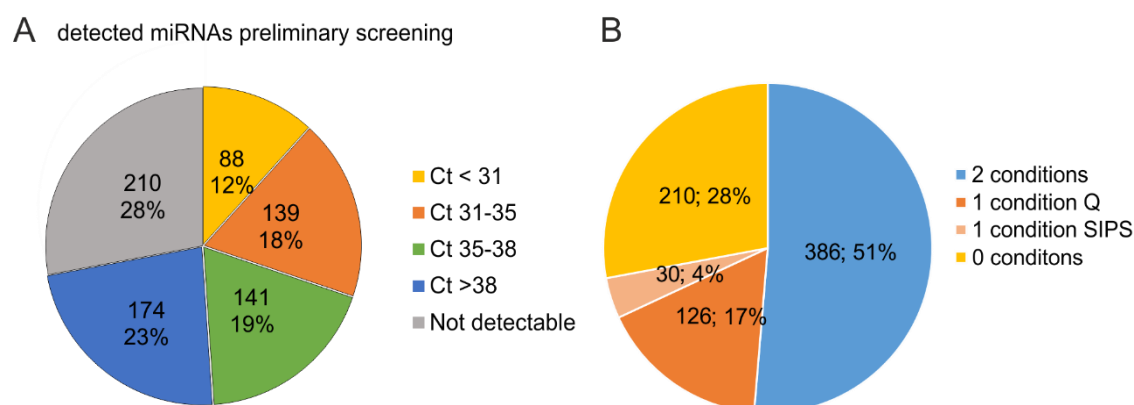


Figure 17 Quantity of secreted vesicular miRNAs was evaluated in an initial screening using one HDF cell strain in both conditions Q and SIPS from one timepoint (D21). (A) Screening of 752 miRNAs included in the qPCR ready to use panels supplied by Exiqon. 543 (72%) secreted miRNAs were detectable. (B) Categorization of secreted miRNAs by Ct-values shows 368 miRNAs with an average signal < 38 in one or both conditions (Q, SIPS) tested

3.2.1. The miR-SASP

Consequently, we designed a qPCR panel comprising 375 miRNAs to quantify EV-miRNAs in three different fibroblast cell strains in non-treated control (Q) and senescent (SIPS) cells from two different time points (D7 and D21) after the last H₂O₂ treatment. Technical robustness was monitored using five synthetic spike-ins controlling for RNA extraction (Unisp2, Unisp4, Unisp5), cDNA synthesis (Unisp6, cel-miR39) and qPCR efficiency. In addition, each plate contained a negative control and two interplate calibrator (IPC) to control and correct fluctuations from the pipetting machine. Summarizing the signals of spike-ins and IPC revealed a constant signal within all 12 samples and calibration based on IPC was performed using GenEX software (Figure 18).

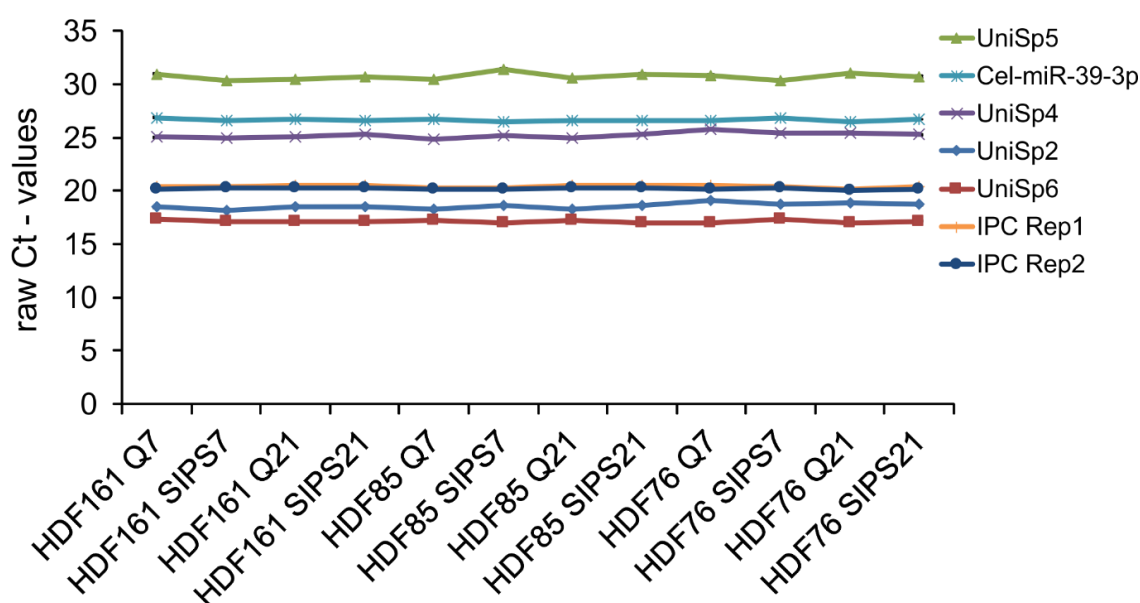


Figure 18 (C) Monitoring of synthetic RNA-spike-ins confirms technical coverage of the discovery study within 12 samples extravesicular RNA from three different donors and two timepoints each. For quality control each qPCR plate contained primer for synthetic RNAs that were added prior RNA isolation (Unisp2, Unisp4, Unisp5) and cDNA synthesis (Unisp6, cel-miR-39). The detection of two inter-plate calibrator per panel and an empty negative control, monitored accuracy of the pipetting machine. The difference of the highest and lowest Ct-signal was used to evaluate constant expression. A value below 1.5 was used as a quality cut-off value.

Results

From 375 miRNAs screened, 371 gave signals in both conditions. Within that, 285 miRNAs were detected in all three HDF cell strains in both conditions and at both time points. For the subsequent bio statistical analysis, only those miRNAs with a complete dataset for both conditions were included (352 miRNAs).

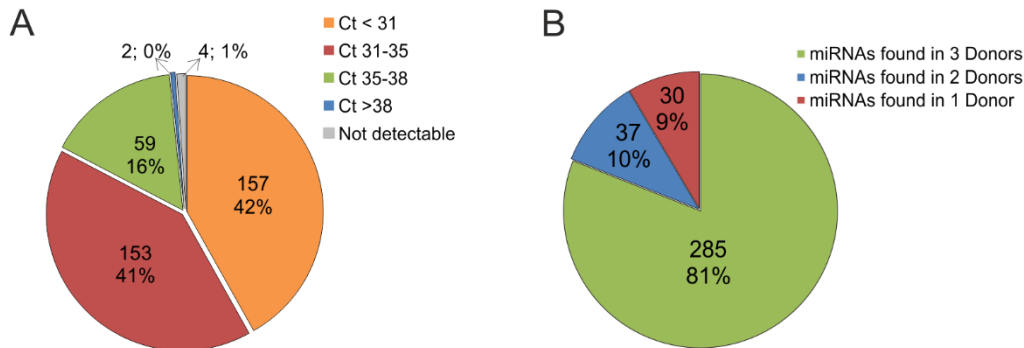


Figure 19 (A) % of detected miRNAs and number of total miRNAs detected within the discovery study. In total 375 miRNAs were screened. miRNAs with an average Ct-value < 31, between 31 and 35, between 35 and 38, > 38 and not detectable are shown. (B) For statistical analysis, 353 miRNAs detected in both conditions were further analysed. Averages from D7 and D21 are presented. 81% (285) of miRNAs were detectable in all 3 donors SIPS and Q control. 10% (37) of miRNAs were detected in at least 2 donors and 9% (30) of miRNAs were detected in one donor.

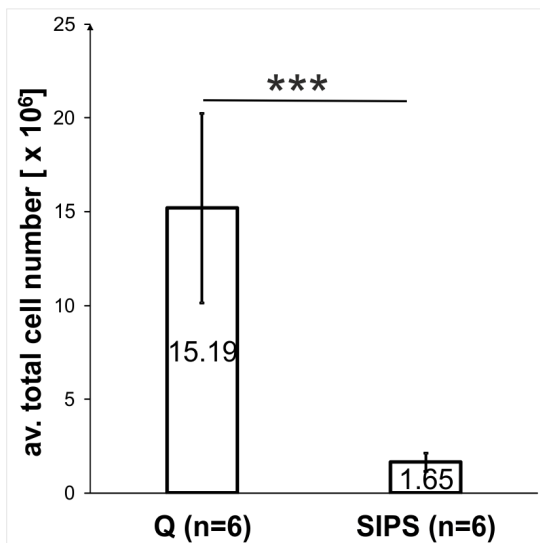


Figure 20 Average differences in total viable cell number between quiescent (Q) and senescent cells (SIPS) from both timepoints, as determined with Vi-CELL XR. Raw Ct-values of EV-samples from discovery study were normalized to corresponding cell number.

Due to the absence of a robust extracellular housekeeping miRNA and the lack of knowledge of non-regulated miRNAs secreted by fibroblasts, we decided to use standardized secretion times and equal working volumes for all subsequent steps and normalized the data to total viable cell number of each samples (Figure 20 averages from Q and SIPS are shown) Multivariate analysis on the 371 EV-miRNAs clearly distinguished between SIPS and Q, as depicted by principal component analysis (PCA) (Figure 21A) and hierarchical clustering (Figure 21B).

Intriguingly, the color gradient from the heatmap suggest an increased secretion of almost all miRNAs from SIPS cells.

Results

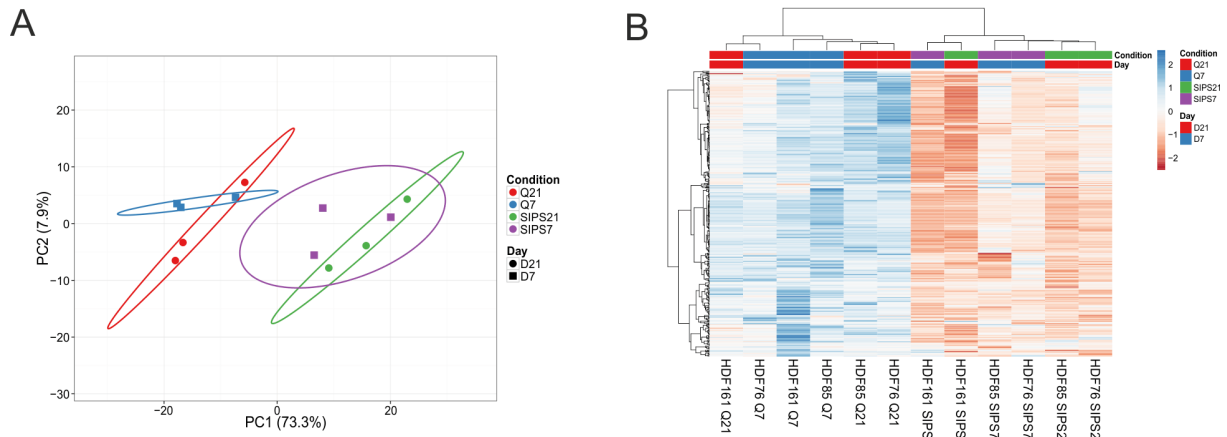


Figure 21 (A) Principal Component analysis of extracellular miRNAs from SIPS and Q control cells from D7 and D21 recovery. Exploratory analysis was performed with ClustVis. The expression matrix shows the clustering of 12 samples and 371 miRNAs screened. Values of biological triplicates ($n=3$) were averaged. Ellipses indicate a confidence level of 95% that a new observation will fall into it. Illustrated 2D-biplot explains a variance of 73.3% in principal component 1 and 7.9% in principal component 2, respectively. Red Q21: quiescent HDF at day 21 recovery; blue Q7: quiescent HDF at day 7 recovery; green SIPS21: SIPS HDF at day 21 recovery; purple SIPS7: SIPS HDF at day 7 recovery. Circle: Day 21 recovery, rectangular: day 7 recovery. (B) Heatmap and hierarchical clustering of EV-miRNAs after D7 and D21 post SIPS treatment. The 2D matrix shows the dendrogram and heatmap of 12 samples and 371 miRNAs screened. Unit variance scaling was applied and rows are centered. MiRNAs were clustered according to correlation distance and Ward linkage. Samples in columns are clustered using Euclidean distance and Ward linkage method. (Colors in matrix: red = low-Ct values, blue = high Ct-values)

Finally, statistical evaluation confirmed our first observation and we identified 221 (59%) miRNAs significantly higher secreted on day 7, and 321 (85%) on day 21, while none were down-regulated significantly (Figure 22).

To reconsider our results and to deal with challenges in finding a suitable normalization method for EV-miRNAs (van Balkom et al. 2015; Zeringer et al. 2013; Schageman et al. 2013; Hill et al. 2013) we tested other normalization methods based on differences in total cell size and volume (blue dotted line in Figure 22 and Figure 23A,B), and total intracellular RNA content (red dotted line in Figure 22 and Figure 23 C,D). However, it did not abrogated our first observation showing still an overall trend of increased EV-miRNA secretion.

Results

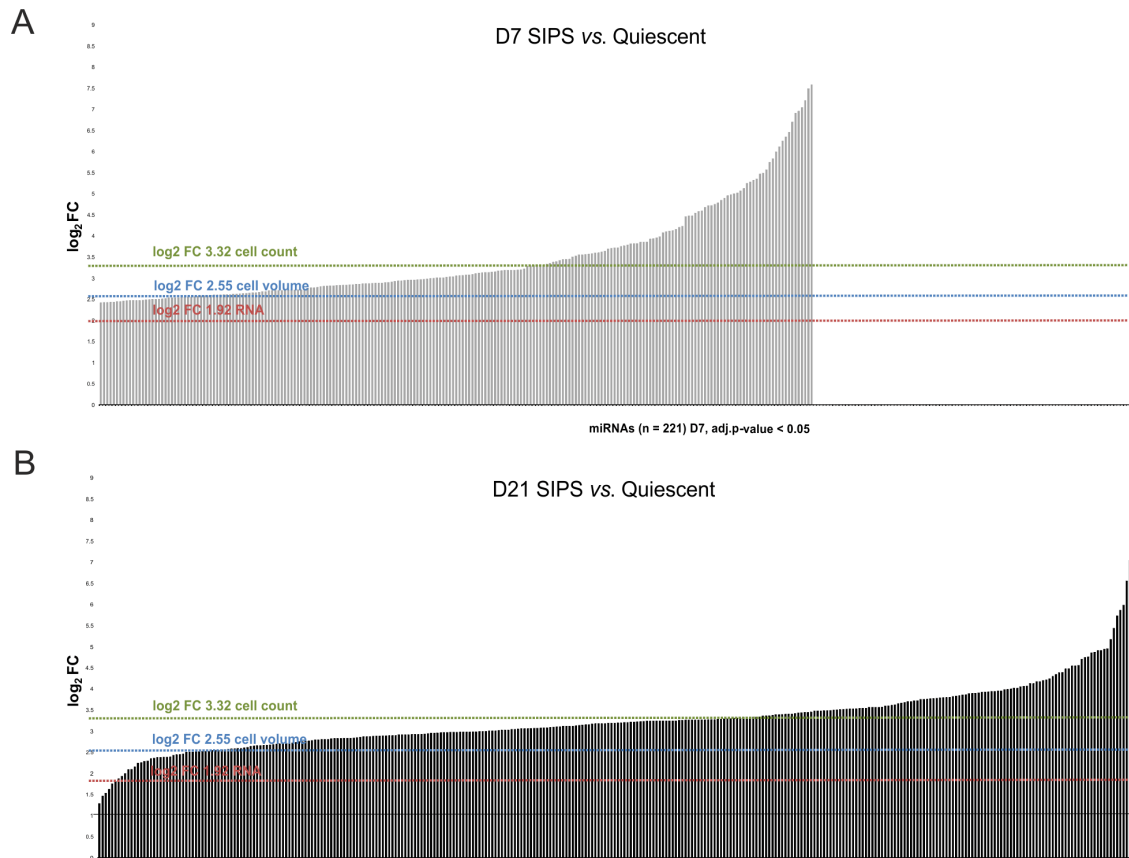


Figure 22 (A) Bar chart of significantly higher secreted miRNAs in SIPS fibroblasts on day 7 (D7) and (B) Day 21 (D21) post treatment. Log₂FC values from three biological triplicates were calculated and plotted on y-axis. Bars plotted on y-axis show all miRNAs reaching an adjusted p-value < 0.05 after applying the BE method for FDR. On D7, 221 miRNAs and on D21, 321 miRNAs passed the adjusted p-value. Dotted lines represent difference in cell number (log₂FC 3.32 = FC 9.2 green), cell volume (log₂FC 2.55 = FC 5.9 blue) and total RNA concentration averaged from Nanodrop and Bioanalyzer (log₂FC 1.92 = FC 3.5 red).

We therefore concluded that despite taking potential pitfalls of different methods in normalizing the data into account, we identified substantial differences in the miRNome of senescent and quiescent contact inhibited skin HDF of the three different donors.

Altogether, these findings suggest EV-miRNAs as new members of the SASP. Thus, as already discussed (Bonafè & Olivieri 2015; Olivieri et al. 2014), but not experimentally validated earlier, we and others propose that secreted miRNAs are active components of the senescent secretome and that they might be able to influence the surrounding microenvironment on the same level as other reported protein SASP factors (Davalos et al. 2010; Freund et al. 2010). Therefore, we propose to use the terms 'miR-SASP' and 'senescence-associated EV-miRNAs (SA EV-miRNAs)'.

Results

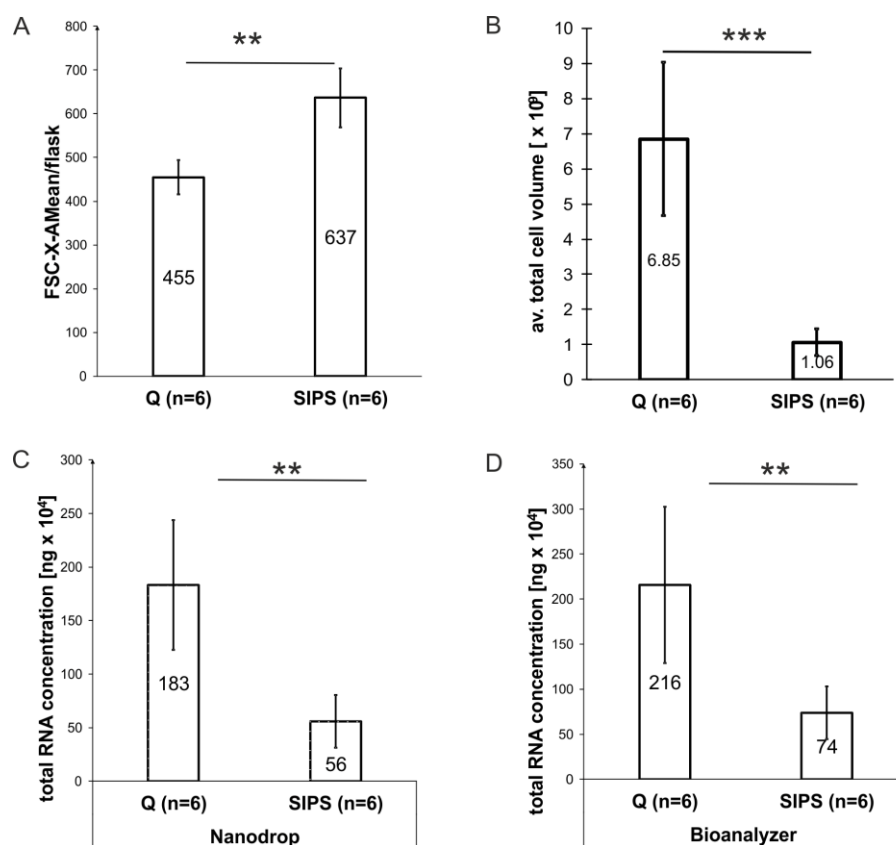


Figure 23 (A) Differences in size between Q and SIPS cells was determined by quantitation of arithmetic mean of FSC (measurement for size) analyzed by FACS. (B) Differences in total cell volume calculated by total viable cell number and FSC from FACS between Q and SIPS cells. (C) Differences in total intracellular RNA concentration of Q and SIPS cells used for secretion of EV-RNA as quantitated by Nanodrop spectrometer. (D) Differences in total RNA concentration of Q and SIPS cells used for secretion of EV-RNA as quantitated by Agilent Bioanalyzer spectrometer.

3.2.2. The miR-SASP targets pro-apoptotic mediators

Based on the fact that single senescent cells do secrete high amounts of EVs in comparison to quiescent cells, we were now interested in the most abundant and highly secreted miRNAs that we consider to have the biggest functional impact on recipient cells when taken up. Therefore, we focused on the top 20 of the most abundantly highly secreted miRNAs identified in our discovery study (Figure 24A) and screened for validated miRNA/mRNA target pairs. We identified 11.588 target interactions comprising in total 5.437 genes.

Results

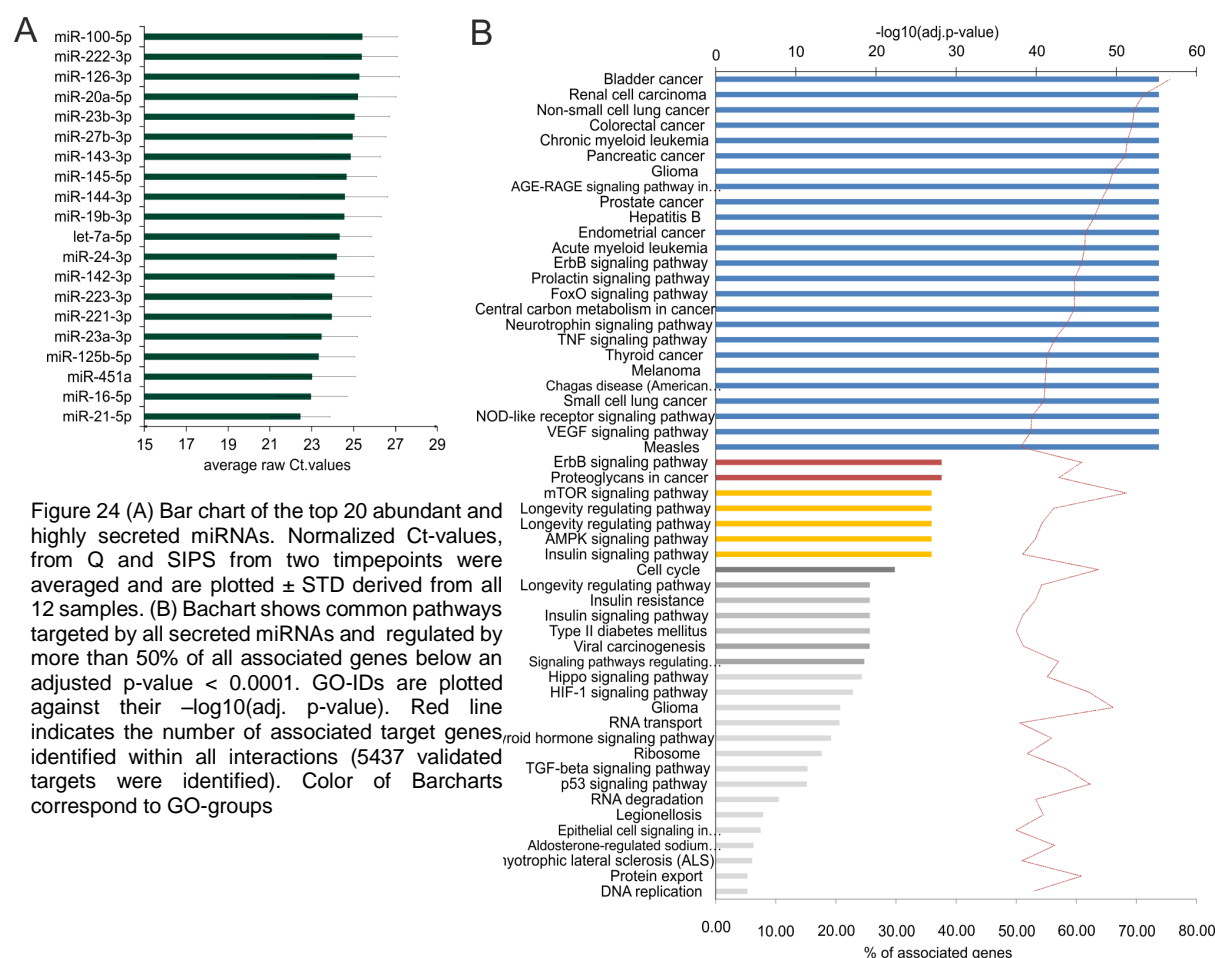


Figure 24 (A) Bar chart of the top 20 abundant and highly secreted miRNAs. Normalized Ct-values, from Q and SIPS from two timepoints were averaged and are plotted \pm STD derived from all 12 samples. (B) Bar chart shows common pathways targeted by all secreted miRNAs and regulated by more than 50% of all associated genes below an adjusted p-value < 0.0001 . GO-IDs are plotted against their $-\log_{10}(\text{adj. p-value})$. Red line indicates the number of associated target genes, identified within all interactions (5437 validated targets were identified). Color of Bar charts correspond to GO-groups

To evaluate potential regulated pathways, enrichment analysis of all annotated interactions between miRNAs and genes, discovered 125 GO terms with an adjusted p-value below 0.0001, among those, 54 comprise more than 50% of all associated genes (Figure 24B). Interestingly, we found several gene modules that participate repeatedly in several pathways, indicating a crosstalk of pleiotropic genes involved in various cellular activities. In addition, we also discovered series of cellular activities such as signaling, which use more than one gene module. Based on that finding, we built large metapathways (Fertig et al. 2013; Higareda-Almaraz et al. 2013; Higareda-Almaraz et al. 2016) and identified a complex, but predominant network that points to an interplay of signaling, longevity and cancer, which are supposed to be orchestrated by the secreted miRNAs and their target genes (Figure 25).

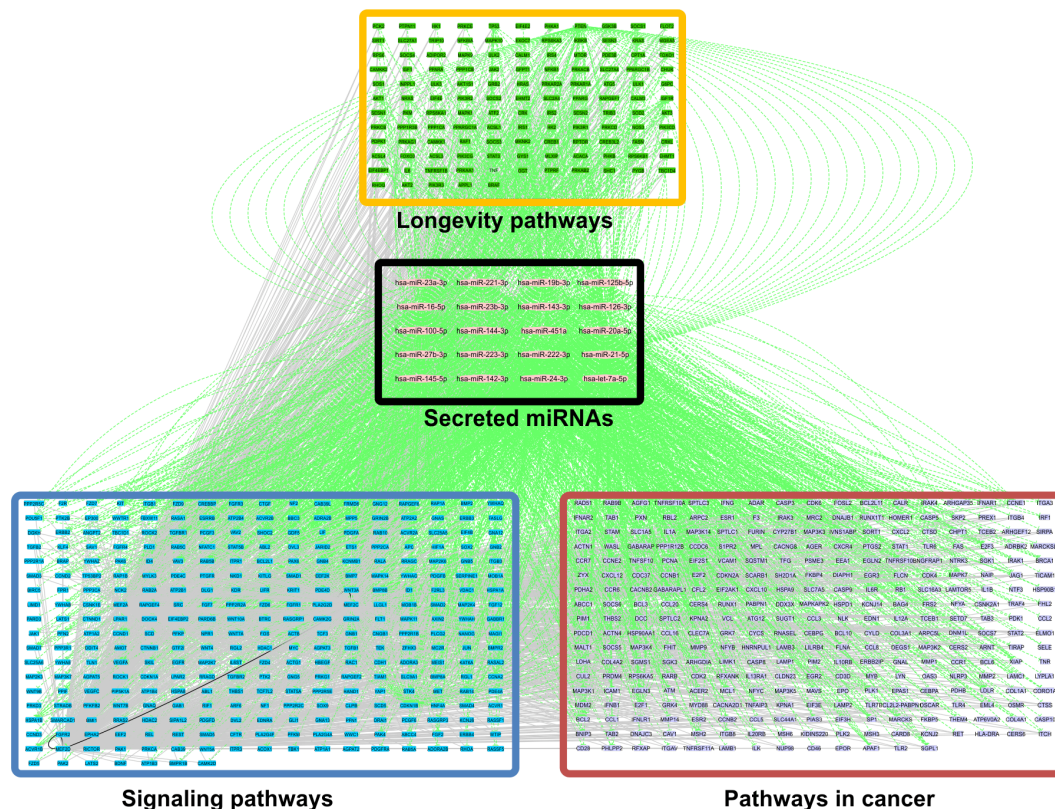


Figure 25 (C) Secreted miRNAs regulate a dynamic crosstalk of three prominent metapathways by interacting with various genes and cellular activities. Longevity (colour), cancer (colour) and signaling pathway (colour) modules are shown. Green edges represent miRNA regulation over their targets across different pathways. Grey edges represent PPI and transcriptional regulation.

Finally, we identified PTEN, P53, APAF-1, CDKN1B and MYC as prominent targets, heavily regulated by all secreted miRNAs and involved in the dynamic crosstalk of all three cellular activities. Finding only pro-apoptotic targets strengthens the protective function of EVs (Y. Zhou et al. 2013; Zhao et al. 2017) and miR-21-5p, highly secreted from senescent fibroblasts might be a key mediator of this process (Xiao et al. 2016; Zhang et al. 2011).

3.2.3. Differential miRNA loading per vesicle upon SIPS and over time

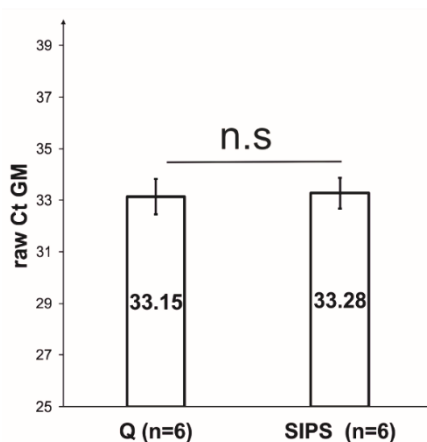


Figure 26 Average raw Ct-values used for global mean normalization.

Bearing in mind that senescence induces increased secretion of proteins and miRNAs enclosed in EVs, we were now interested if miRNA composition of a single vesicle changes upon SIPS and when senescence is fully established. Therefore, we applied the mean-centering restricted (MCR) method (Mestdagh et al. 2009, Wylie et al. 2011; Deo et al. 2013) and normalized raw-Ct-values to the global mean (Figure 26) of each sample, which we assume to reflect the average miRNA content of one EV. Statistical analysis revealed a typical Volcano plot with a symmetric distribution of all miRNAs (Figure 27) showing 31 SA-EV miRNAs differentially present in single EVs on D7, and 32 miRNAs on D21, respectively. However, none of those reached

Results

the 0.05 cut-off value for the FDR of an adjusted p-value and we took only those into account that pass a p – value < 0.05.

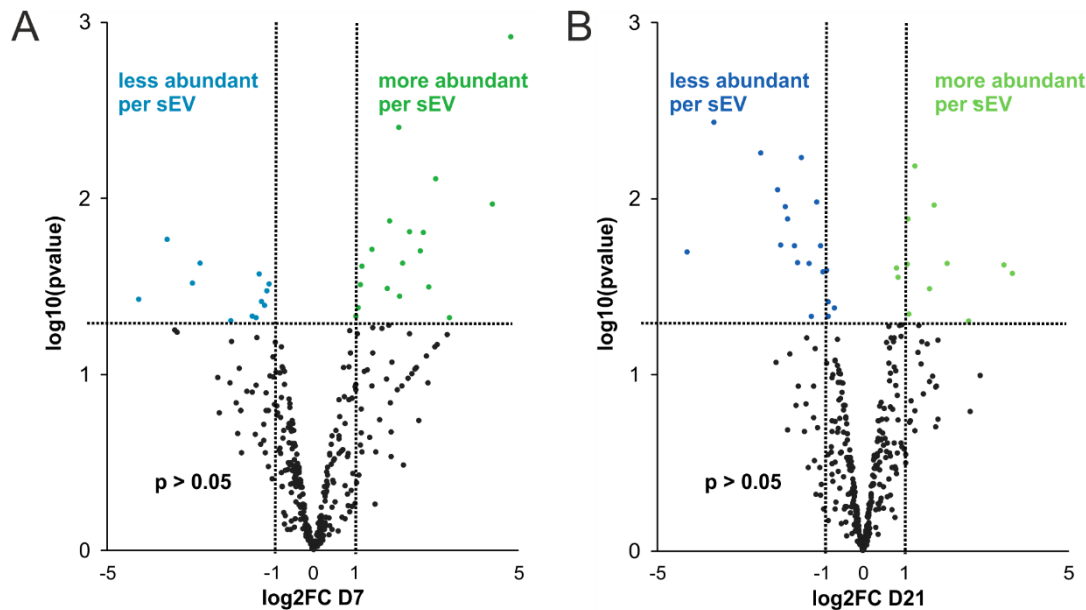


Figure 27 Changes in miRNA composition per vesicle as quantified after normalization with the MCR method. Volcano plot of significantly different compositions of all senescence-associated (SA-) EV-miRNAs after (A) D7 and (B) D21. Raw Ct-values were normalized to the global mean and averaged (n=3). Log2FC of stress-induced premature senescent (SIPS) relative quiescent contact inhibited control (Q) cells were calculated. Values from day 7 (left D7) and day 21 (right D21) recovery are plotted on x-axis against their individual -log₁₀ (p-value) on y-axis. Horizontal dotted lines indicate a separation between miRNAs passing a p-value higher or lower than 0.05. Vertical dotted lines separate secreted miRNAs with log₂FC > 1 or log₂FC < 1. MiRNAs reaching a p-value < 0.05 are illustrated with white dots and miRNAs with a p-value > 0.05 are shown in black.

Thus, comparing the composition of SIPS vesicles from D7 and D21, we consistently identified 2 SA-EV-miRNAs (miR-23a-5p, miR-137) more abundantly present in EVs at both time points and 5 miRNAs (miR-17-3p, miR-625-3p, miR-766-3p, miR-199b-5p, miR-381-3p) to be less abundant on day 7 and day 21 recovery (Figure 28)

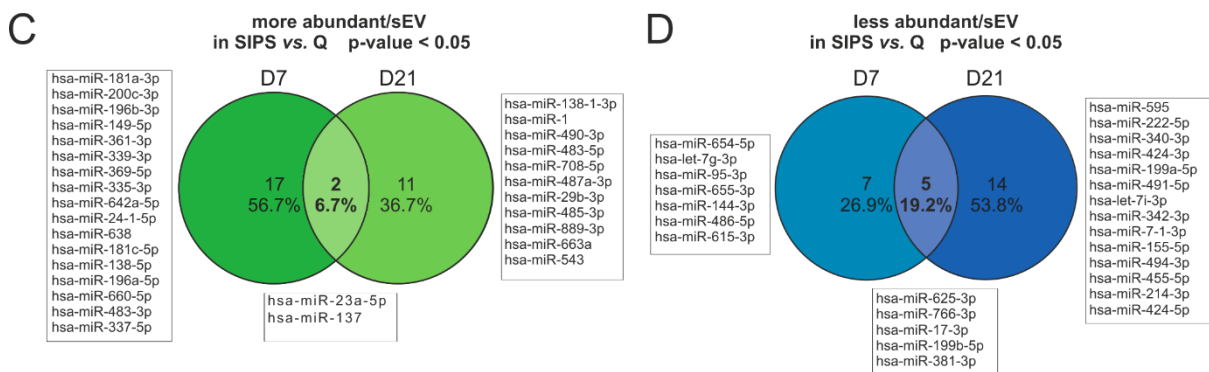


Figure 28 (C) Venn diagram shows miRNAs more abundantly present in single vesicles of stress-induced premature senescent (SIPS) cells. Log₂FC were calculated and significantly (p-value < 0.05) miRNAs from D7 and D21 were compared. (D) Venn diagram of less preferentially present miRNAs in stress-induced premature senescent (SIPS) cells. Log₂FC were calculated and significantly (p-value < 0.05) lower abundant miRNAs on D7 and D21 post stress were identified.

Results

To investigate time depended changes of EV composition, we evaluated differences between day 21 relative to day 7 in SIPS and Q at early and late stages of senescence. In total, we observed a balanced miRNA composition over time between SIPS (6 miRNAs) and Q cells (6 miRNAs). Interestingly, however, we detected 14 miRNAs that changed the composition of SIPS derived vesicles on D21 relative to D7 (Figure 29), while we identified only 3 miRNAs in Q cells.

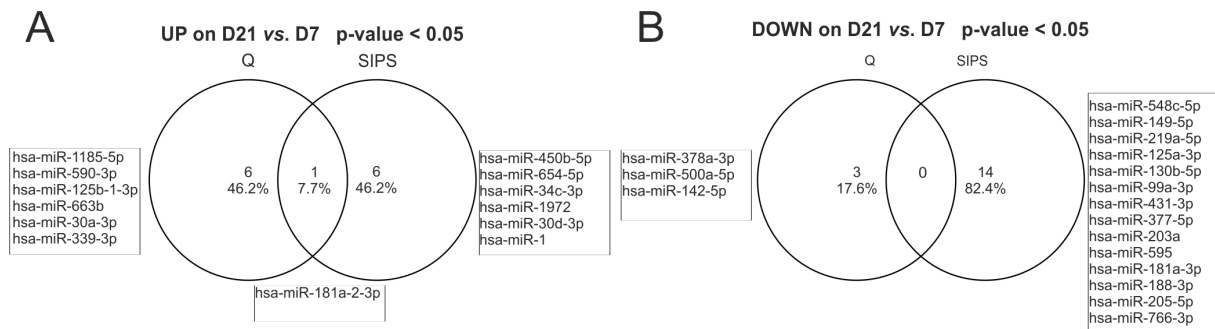
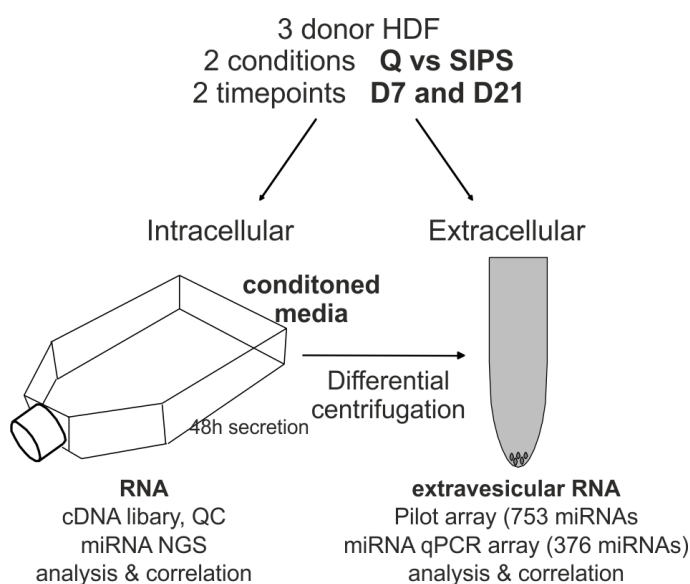


Figure 29 (A) Venn diagram shows a balanced secretion of miRNAs over time. MCR-normalized Ct-values from biological triplicates were averaged and log2FC relative day 7 recovery were calculated. (p-value < 0.05). (B) Venn diagram shows changes in miRNA composition per vesicle over time. Average Ct-signals were normalized to global mean and log2FC values were calculated relative to D7. (p-value < 0.05).

Summarizing our knowledge about miRNAs enclosed in EVs so far, indicate that even though all miRNAs are in their entirety upregulated per cell, also the miRNA composition per EV changes upon entry into senescence. We next asked, if changes in miRNA secretion might be due to differential transcription or processing, or if it is regulated at the level of miRNA packaging into EVs. We therefore decided to quantitate first the intracellular miRNAs of all cell strains and conditions and then to correlate their abundance with extracellular miRNA secretion.

3.2.4. Differential transcription of intracellular miRNAs identifies skin aging associated miRNAs



In order to quantify intracellular miRNA transcription of SIPS versus Q HDF, we synthesized cDNA libraries for Illumina next generation sequencing (NGS) using RNA extracted from the same cells at the same time points, from which we harvested EVs for miRNA analysis (Figure 30). RNA concentration was quantitated by Nanodrop and Agilent Bioanalyzer and cDNA library was

Figure 30 Scheme of experimental design. SIPS was induced in three donors of primary human dermal fibroblasts (HDF) by repeated H₂O₂ doses. 7 days (D7) and 21 days (D21) after the last H₂O₂ treatment, intracellular RNA was harvested and cDNA library for NGS was synthesized. Correspondingly, the vesicular RNA was isolated from supernatants by differential centrifugation.

Results

synthesized with the NEBNext Multiplex Small RNA Library Prep Set for Illumina. Successful adapter ligation and PCR amplification was controlled by Bioanalyzer (Figure 31A) and in order to select only sncRNAs the cDNA library was separated on a 10% TBE gel. Corresponding sncRNA fragments between 18 and 36 basepairs (bp) were cut (Figure 31B), gel purified and again quality controlled on Bioanalyzer (Figure 31C).

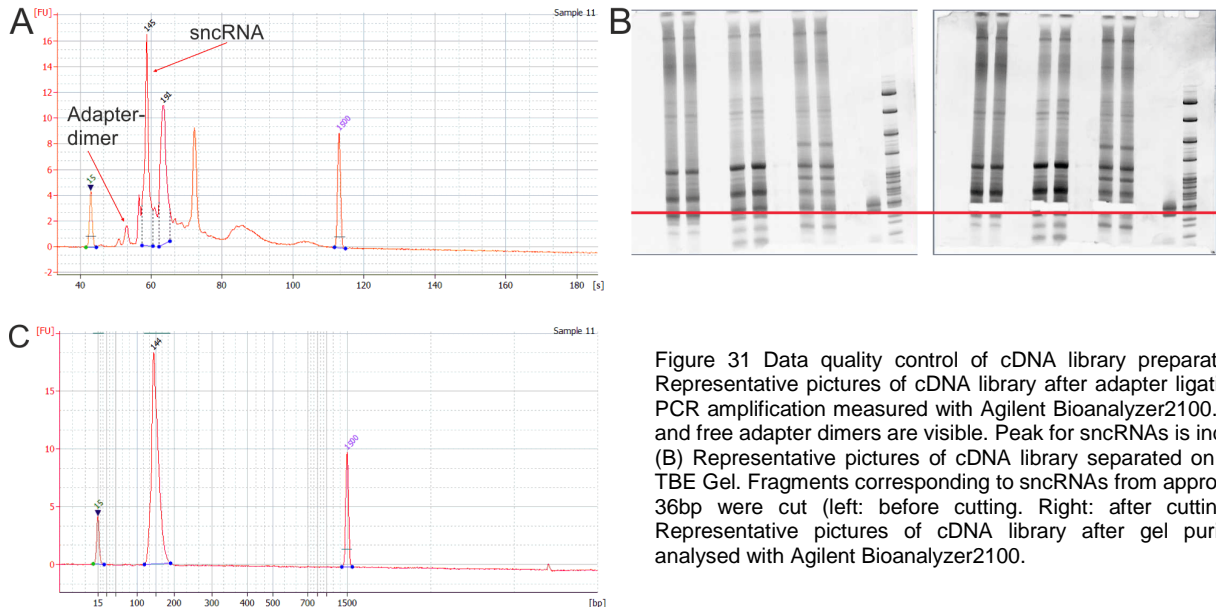


Figure 31 Data quality control of cDNA library preparation (A) Representative pictures of cDNA library after adapter ligation and PCR amplification measured with Agilent Bioanalyzer2100. Bound and free adapter dimers are visible. Peak for sncRNAs is indicated. (B) Representative pictures of cDNA library separated on a 10% TBE Gel. Fragments corresponding to sncRNAs from approx. 18 to 36bp were cut (left: before cutting. Right: after cutting). (C) Representative pictures of cDNA library after gel purification analysed with Agilent Bioanalyzer2100.

Finally, the cDNA libraries were pooled and sent to Exiqon for NGS sequencing and quality control. Quality control (only HDF samples are shown) included intensity correction, base calling and assigning the quality score (Q-score) to predict the probability of an incorrect base call. All samples showed good quality indicated by a Q-score > 30, which indicates an accuracy of 99.9% for base calling (data not shown) (Cock et al. 2010). Adapter trimming after sequencing was part of base calling and revealed distinct peaks showing miRNAs (~18- 22 nt) and some longer sequences representing other sncRNAs, such as rRNA, tRNA and mRNA fragments (~30 – 50 nt).

After adapter trimming, the sequence reads were mapped and classified according to the following: outmapped (polyA and polyC homopolymers), unmapped/unaligned (no alignment possible) and genome (aligning to reference genome), which should yield approx. 40 -60% of miRNAs to be assigned as qualitatively high and efficient (Figure 32). In total, we obtained approximately 17.6 million reads per sample and identified isomiRs and novel miRNAs which we annotated according to miRBase 20 and miRNA NGS data from differentially transcribed miRNAs in stress-induced premature senescence (SIPS) have been deposited to the GEO repository under the accession number GSE95354 <https://www.ncbi.nlm.nih.gov/geo/query/acc.cgi?token=ytojsgmknpqbtix&acc=GSE95354>. The dataset was evaluated Table 3 and normalized to the number of reads. We found in total 2891 miRNAs and among those 313 putative and iso-miRs. 432 miRNAs with at least 5 TPMs in one sample were included into biostatistical analysis.

Results

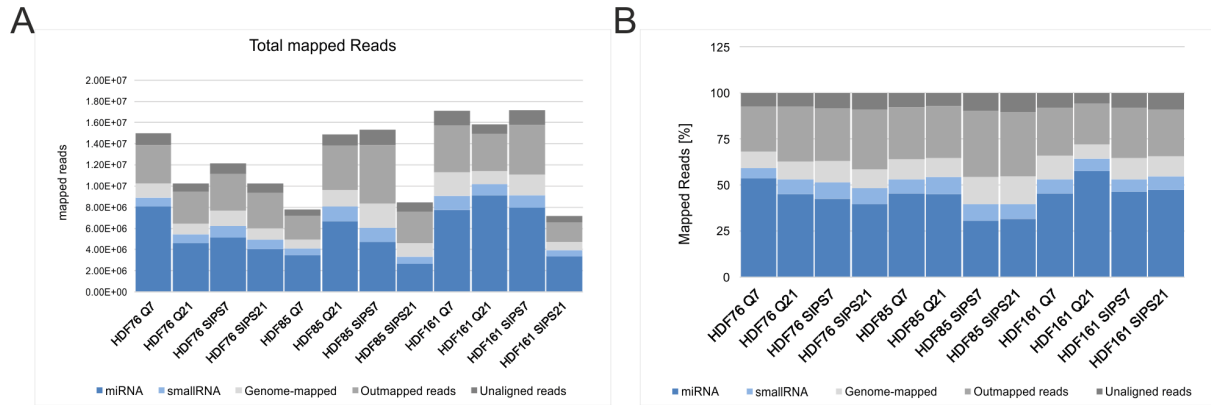


Figure 32 (A) Total mapped reads of sequencing. (B)% of total mapped reads. Reads were annotated to miRBase20 and classified according to the following categories: 'not aligned', 'outmapped', 'genome-mapped', 'smallRNA', 'miRNA'.

Table 3 Summary of miRNA next generation sequencing (NGS) and data quality control.

Experimental Design	
Instrument	NextSeq 500
Average number of reads (1 flowcell)	4.00E+08
Number of sequencing cycles	50 bp single-end read
Annotation reference	miRBase 20
Quality control	
Base call accuracy (Q-Score)	>30
Averaged Total reads	1.26E+07 ± 29.38%
miRNAs (44.2%)	5.64E+06 ± 38.39%
smallRNA (7.8%)	9.78E+05 ± 30.48
Genome-mapped (11.2%)	1.42E+06 ± 35.37%
outmapped (28.5%)	3.56E+06 ± 29.01%
unaligned reads (8.1%)	1.02E+06 ± 28.93%
Grouping Quantity (Number of Identified RNAs)	
< 10 rawcounts on average	2124
10 - 50 rawcounts on average	146
> 50 rawcounts on average	308
Number of analyzed miRNAs	
5 - 500 TPM	158
> 500 TPM	274

Exploratory analysis by PCA explains around 59% of total variability in component 1 and 2 and clusters samples derived from Q and SIPS cells in two different populations, as it is also visible after unsupervised hierarchical clustering by heatmap (Figure 33).

Differentially up- or downregulated miRNAs from both time points were identified, visualized by Volcano plot (Figure 34) and compared in Venn diagrams (Figure 35).

We confirmed several miRNAs that were previously reported to be differentially expressed in replicative or UVB induced senescent fibroblasts (Greussing et al. 2013; Napolitano et al. 2014; Marasa et al. 2010; Maes et al. 2009; Dhahbi et al. 2011; reviewed by Mancini et al. 2014) or in the dermis of elderly (Li et al. 2016). This pinpoints to a very robust miRNA-signature of senescent dermal cells, independent of the SIPS stimuli, time of recovery and miRNA-detection method.

Results

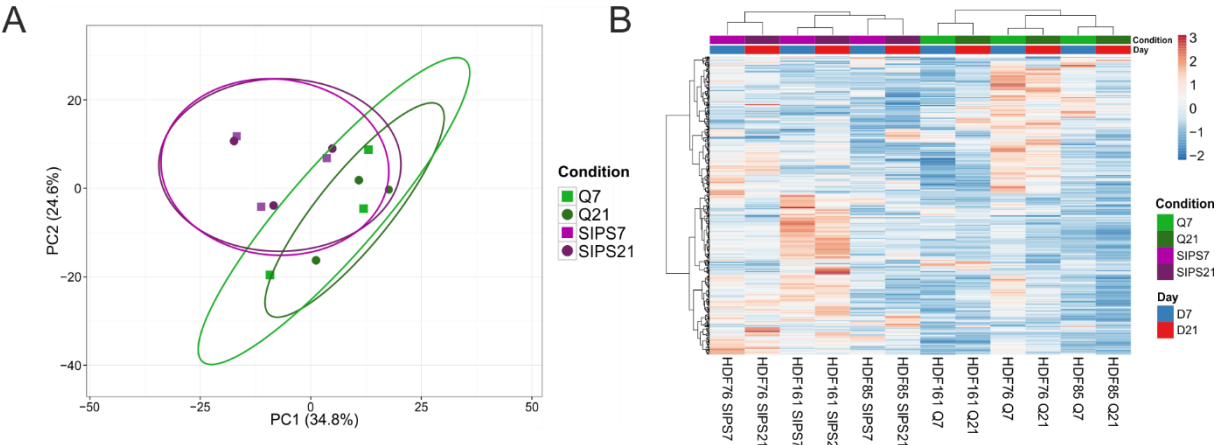


Figure 33 (B) Descriptive statics by Principal component analysis (B) and Hierarchical clustering (C) was performed on 432 miRNAs with normalized TPM > 5. The 2D plot shows the clustering of 12 samples and 432 miRNAs with normalized TPM signals >5 in all conditions in at least 1 donor. Principal components (PC) were calculated using SVD with imputation. Rows were scaled by applying unit variance scaling. Confidence level of 95% is indicated by ellipses assuming that a new observation from the same group will fall into it. Expression matrix of principal component 1 shows a variance of 37.4% and 25.4% in principal component 2. (C) Heatmap and hierarchical clustering of samples and miRNAs of SIPS versus quiescent HDFs. 432 miRNAs are clustered according to Euclidian distance and Ward linkage. Samples in columns (n = 12) are clustered using correlation distance and Ward linkage. (Colours in matrix: red = highly expressed = upregulated, blue = low expressed = downregulated). Each colour and symbol represents another annotation defined by data input file. Red Q21: quiescent HDF at day 21 recovery; blue Q7: quiescent HDF at day 7 recovery; green SIPSD21: SIPS HDF at day 21 recovery; purple SIPSD7: SIPS HDF at day 7 recovery. Circle: Day 21 recovery, rectangular: day 7 recovery.

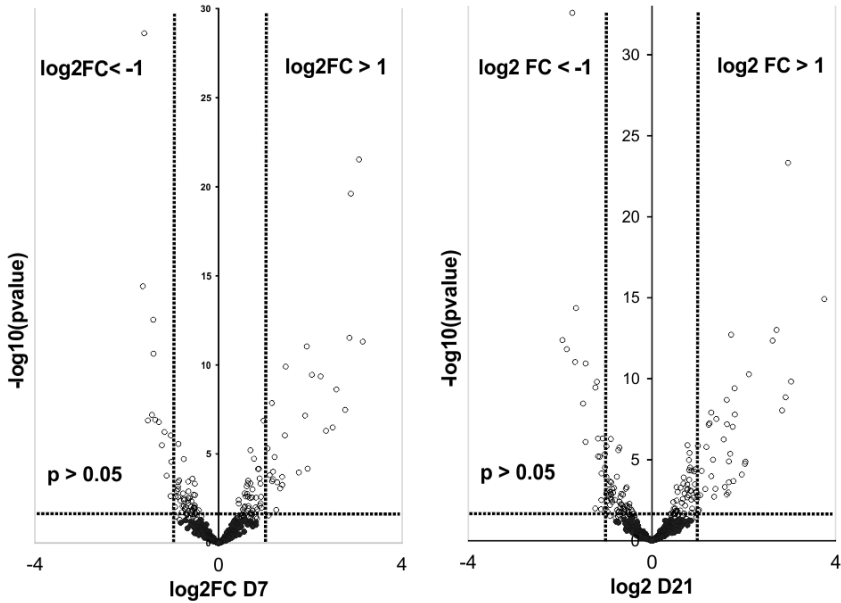


Figure 34 Volcano plot of differentially transcribed miRNAs after one (left D7) and three weeks (right D21) post stress treatment. Log2FC from 432 miRNAs with TPM > 5 at day 7 and day 21 are plotted on x-axis against their individual -log10 (p-value) on y-axis. Horizontal dotted lines indicate a separation between miRNA differences of a p-value higher or lower than 0.05. Vertical dotted lines separate transcribed miRNAs with log2FC > 1 or log2FC < -1. MiRNAs reaching a p-value < 0.05 are illustrated with white dots and miRNAs with a p-value > 0.05 are shown in black.

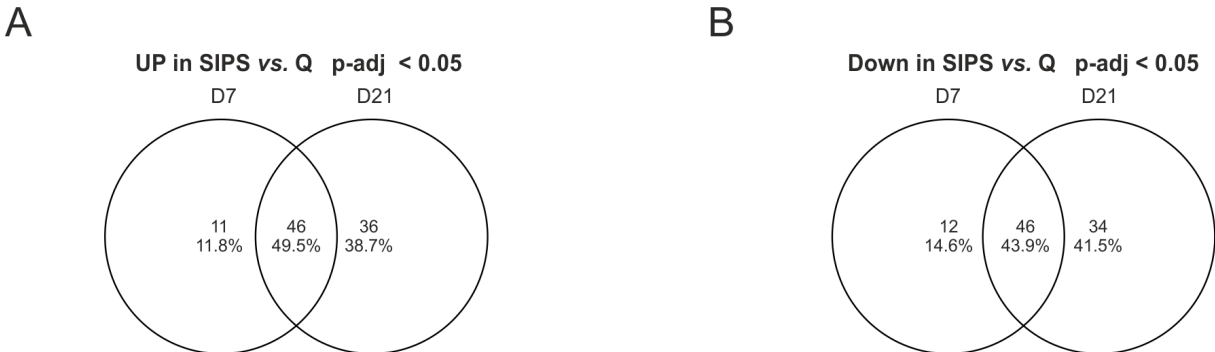


Figure 35 Venn diagram shows significant miRNAs (A) upregulated and (B) downregulated in SIPS cells from day 7 (D7) and day 21 (D21) post stress treatment. MiRNAs reaching an adjusted (adj.) -p-value < 0.05 were taken into account.

Results

Furthermore, in order to evaluate changes in miRNA transcription over time, we compared D21 relative to D7 and found only two miRNAs less transcribed but none were significantly up-regulated in both conditions (Figure 36). After elucidating differences between Q and SIPS cells and over time, we concluded that once senescence signaling induces a specific miRNA signature it does not change significantly over time. While, we observed significant changes in the miRNA composition of EV between the entry of cellular senescence and the fully established phenotype.

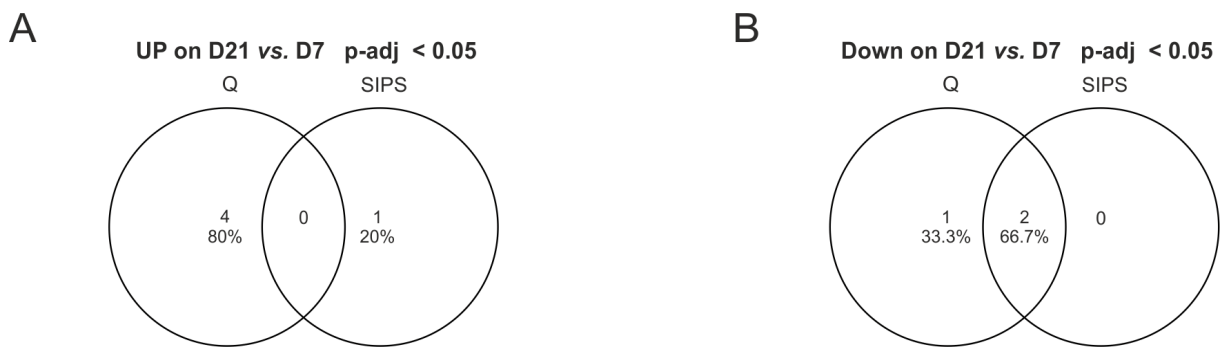


Figure 36 Venn diagram of significantly higher (A) and lower (B) transcribed miRNAs after 21 days relative to 7 days in Q compared to SIPS cells. miRNAs reaching an adj-p-value < 0.05 were taken into account.

3.3. Are specific EV-miRNAs selectively secreted or retained after entry into senescence?

We next addressed the question, if all miRNAs with high transcriptional levels would also be the ones most secreted, which would implicate a 'mirroring effect' between the cytoplasm and the extracellular environment. Similarly, we wanted to know, if physiological stimuli, such as cellular senescence, modulates the selective secretion or retaining of some miRNAs. Therefore, we correlated the intracellular NGS dataset with the extracellular qPCR data, by including only miRNAs with a complete dataset in both conditions and time points (228 miRNAs, Q = 6, SIPS = 6, see Material and Methods for filtering criteria). To detect the most abundant miRNAs present in EVs and in cells we ranked them from the lowest to the highest abundance. The top 20 most abundant each were then compared and visualized by Venn diagrams (Figure 37A,B). Consequently, by comparing these top intracellular versus EV-miRNAs with each other, we realized that indeed particular miRNAs are selectively secreted or retained in the two conditions (Figure 37C).

Results

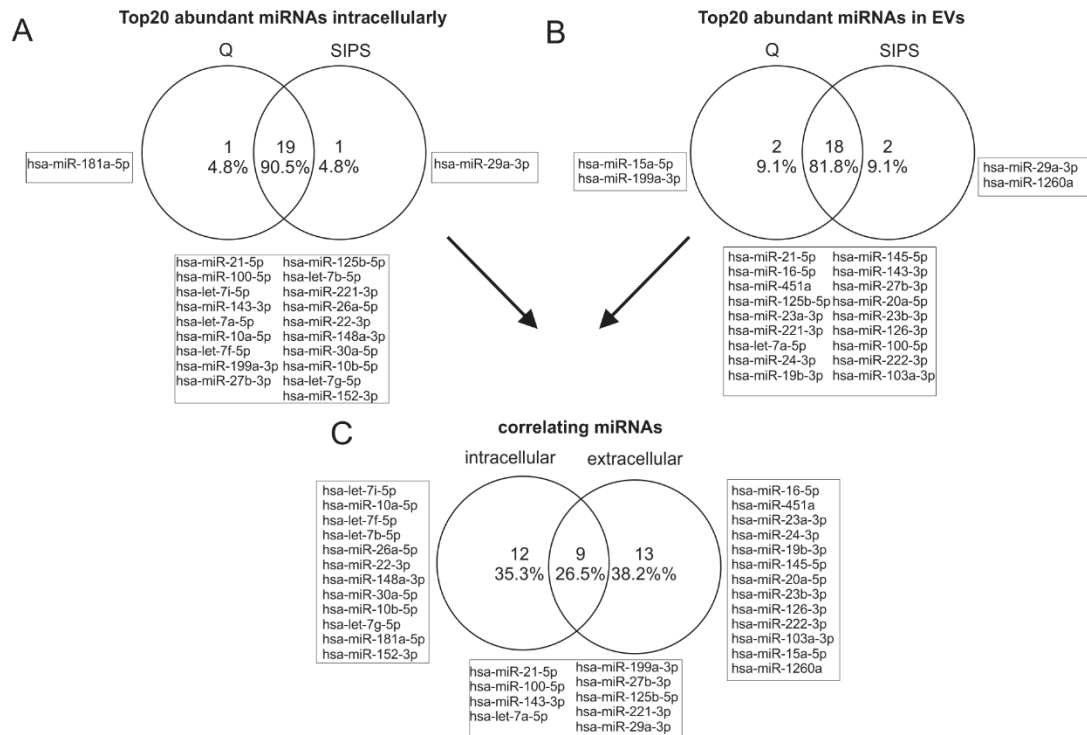


Figure 37 Correlation of intracellular and extracellular miRNAs by defining ranks. (A) Venn diagram of top 20 abundantly transcribed miRNAs in cells from Q and SIPS cells. (B) Venn diagram of top 20 abundant extracellular miRNAs in Q and SIPS cells. (C) positively and negatively correlating miRNAs are identified by combining results from A + B

3.3.1. Specific EV-packaging of miRNAs is directed by cellular senescence

In order to identify now those miRNAs that are preferentially sorted for secretion or retaining, we calculated the differences of ranks ($\Delta\text{rank} = \text{rank}_{\text{intra}} - \text{rank}_{\text{extra}}$) for Q and SIPS separately (Figure 38).

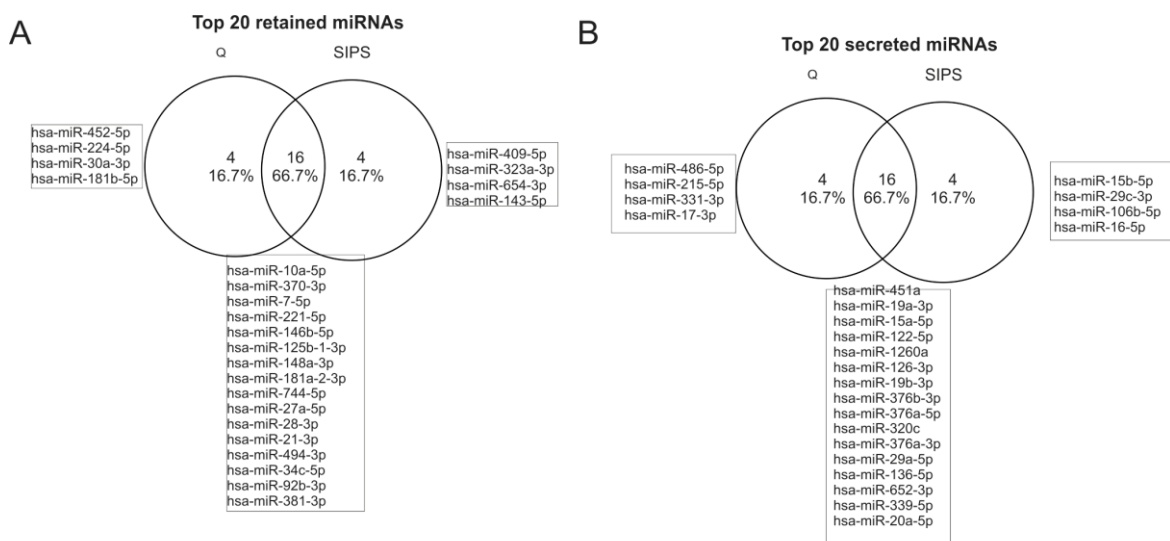


Figure 38 Venn diagram of top 16 retained (A) and secreted (B) miRNAs of fibroblasts, after calculating $\Delta\text{rank} = \text{rank}_{\text{intra}} - \text{rank}_{\text{extra}}$, from SIPS and Q separately.

Results

By further calculating the $\Delta\Delta\text{rank}(\Delta\text{rank}_{\text{SIPS}} - \Delta\text{rank}_{\text{Q}})$ of senescent versus quiescent we were then able to identify specifically sorted SA-EV-miRNAs after entry into cellular senescence. Whereby the higher the value, the higher is the selective secretion, and vice versa, the lower the value, the likelihood grows for retention (Figure 40).

In order to compare these results to a statistical analysis based on the quantitative content of qPCR and NGS and not on the rank, we also calculated ratios between extracellular and intracellular miRNA levels from quiescent ($\Delta\text{ratio}_{\text{Q}}$) and SIPS ($\Delta\text{ratio}_{\text{SIPS}}$) separately. Therefore, we transformed Ct-values to arbitrary units, by defining a Ct-value of 40 to 10 arbitrary units (AU). We then calculated $\Delta\Delta\text{ratios}(\Delta\text{ratio}_{\text{SIPS}}/\Delta\text{ratio}_{\text{Q}})$ and normalized obtained values to the global means and plotted the miRNAs in the same manner as it was sorted after determining the $\Delta\Delta\text{ranks}$ (Figure 39).

Thereby we observed the same trend as indicated by a similar shape and decided to correlate the $\Delta\Delta\text{ratios}$ with the $\Delta\Delta\text{rank}$ values and plotted a xy-diagram for Spearman correlation, which revealed $\sim 80\%$ of total variability (Spearman $R = 0.81$ 95% confidence interval 0.76 to 0.85 p-value (two-tailed) < 0.0001) (Figure 41).

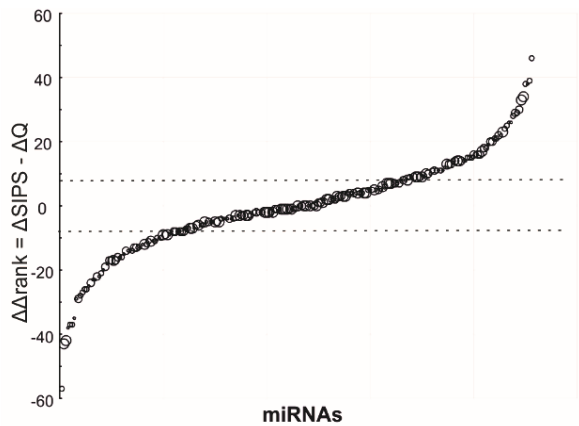


Figure 40 $\Delta\Delta\text{rank}$ values were calculate from Δrank values derived from Q and SIPS separately. Specifically SA- secreted (high values) or retained (low values) miRNAs were identified. Bubble size corresponds to average expression value from transformed Ct-values.

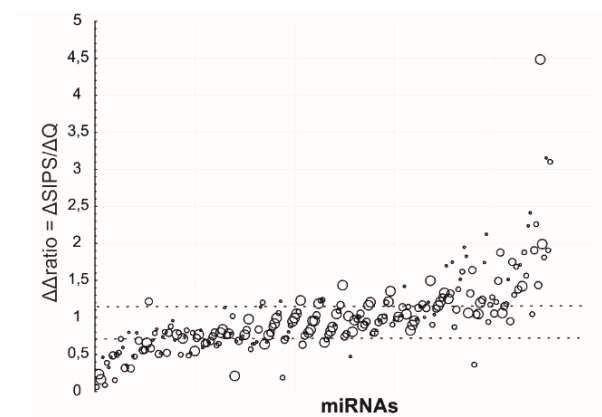


Figure 39 Specifically SA- secreted (high values) or retained (low values) miRNAs were identified. Due to differences in units, it is not possible to set the threshold to 1. Results are sorted from smallest to largest. They were plotted in the same manner as it resulted after sorting of $\Delta\Delta\text{ratios}$. Bubble size corresponds to average expression value from transformed Ct-values.

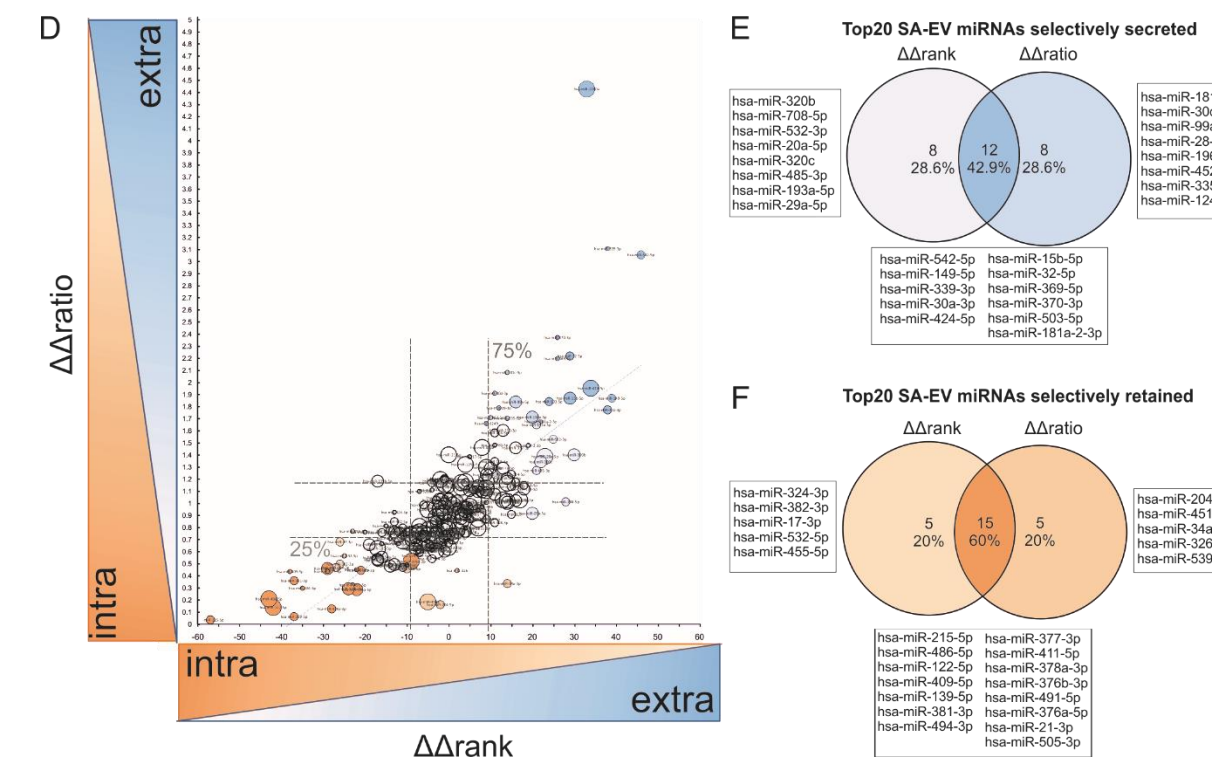
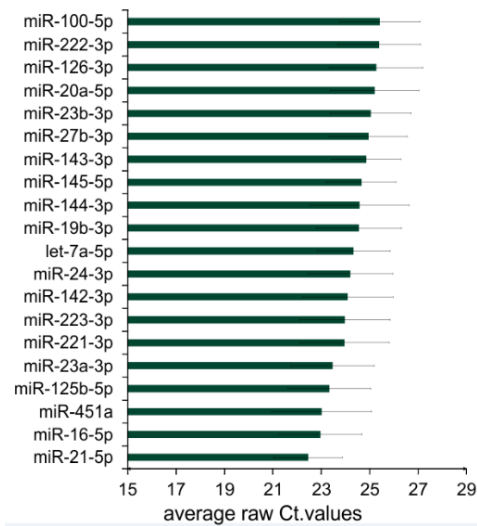


Figure 41 (D) $\Delta\Delta\text{rank}$ and $\Delta\Delta\text{ratio}$ were correlated and, specifically SA- secreted (high values) or retained (low values) miRNAs are identified. Spearman correlation shows a $R=0.8092$ with an 95% confidence interval 0.7574 to 0.8509 p-value (two-tailed) <0.0001 . (E) Venn diagram of the top specifically secreted (E) and retained (F) SA-miRNAs are identified by comparing the $\Delta\Delta\text{rank}$ and $\Delta\Delta\text{ratio}$ method.

Comparison of the top 20 from the $\Delta\Delta\text{rank}$ and the $\Delta\Delta\text{ratio}$ - approach indeed identified a similar set of selectively secreted (12 miRNAs) (Figure 41D) or retained (15 miRNAs) (Figure 41F) miRNAs after entry into cellular senescence, but also some that are only detected with one method. Finally, by defining a cut-off of the 25% and 75% percentiles from both approaches, we identified about 24% of the total EV contained miRNAs that are selectively packaged or retained responsive to senescence, while the remaining ones seem to be evenly distributed between cells and EVs.



To sum up, the 'ratio-' and 'rank-' approach allowed the correlation of extracellular and intracellular data independently and discovered a set of specific miRNAs associated for retention or secretion in response to SIPS. Whether the highly abundantly secreted miRNA (Figure 42 corresponds to Figure 24A) are the ones that confer a biological effect on recipient cells, or if the selectively secreted miRNAs are those to regulate the signaling during the miR-SASP, remains to be elucidated.

Figure 42 corresponds to Figure 24A. Bar chart of the top 20 abundant and highly secreted miRNAs. Normalized Ct-values, from Q and SIPS from two timepoints were averaged and are plotted \pm STD derived from all 12 samples.

Part B

3.4. EV mediated miRNAs crosstalk between fibroblasts and keratinocytes

3.4.1. EV-miRNA crosstalk in 2D monolayer cultures

In order to find out, if EV-miRNAs secreted from fibroblasts are taken up by keratinocytes, we overexpressed a C.elegans specific miRNA and its corresponding scrambled control in primary HDF. After 24 hours post transfection (hpt), FCS depleted secretion media was applied, and after 48h of secretion, the conditioned media was harvested. Small EVs were harvested by differential centrifugation and primary keratinocytes were incubated for 24 to 48 hours with EVs derived from 10 x to 20 x more fibroblasts and analysed by qPCR for the presence of cel-miR-39 transferred by vesicles (Figure 43).

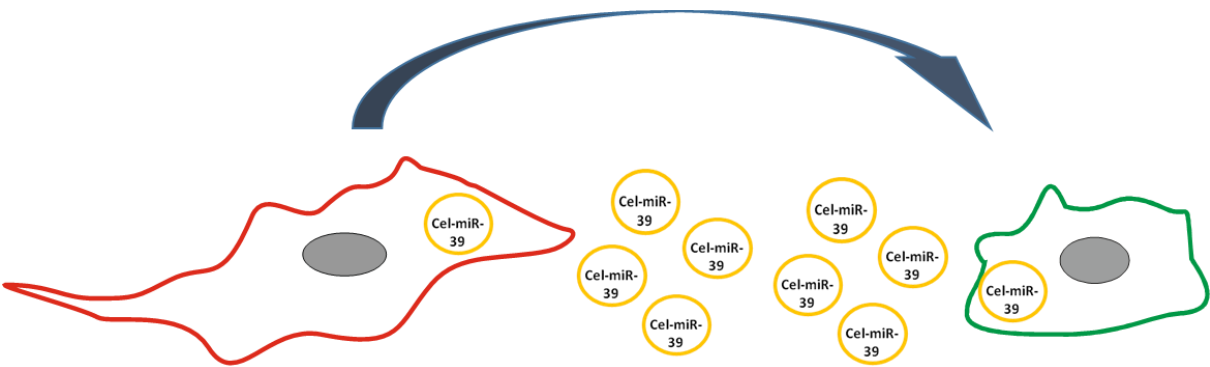
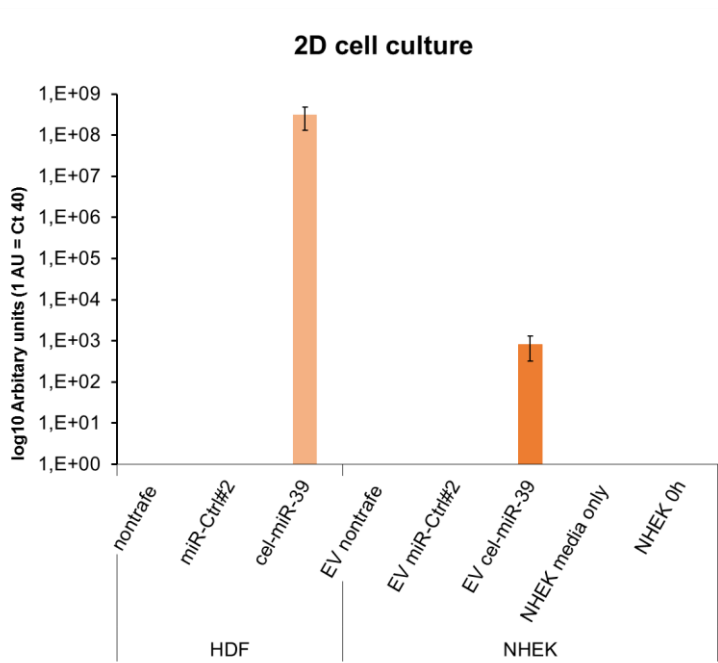


Figure 43 Experimental setup of the EV-miRNA crosstalk between HDF and keratinocytes (NHEK). Cel-miR-39 and corresponding miR-control was overexpressed in primary HDF. Secretion media was added after 24hpt and EVs were harvested after 48 hours secretion. NHEK were incubated with EVs derived from 10x to 20x more HDF for 36-48h.

Indeed, we found fibroblast derived vesicular cel-miR-39, in NHEK incubated with respective EVs, while we could



not detect any signal in control transfected HDF and corresponding NHEK, as quantitated by qPCR.

Figure 44 qPCR confirms transfer of cel-miR-39 enclosed in HDF derived EVs to NHEK after 36 to 48 hours post EV-incubation. Signal of negative controls were below detection limit of qPCR. Raw Ct-values were transformed to arbitrary units (AU) assuming a Ct-value of 40 to be 10.

Results

However, we could not detect any significant differences in cel-miR-39 expression levels of NHEK when varying either amount or incubation time of EVs (data not shown). This could indicate a saturation level, which might be reached after a specific amount of miRNA abundance in the microenvironment of keratinocytes.

3.4.2. EV-miRNA crosstalk in 3D human skin equivalents

We next tested if EV mediated miRNA crosstalk is also observed in 3D organotypic skin cultures that mimic many aspects of human skin. To our knowledge, it has not yet been shown, if EV-miRNAs are able to pass through ECM of dermal cells. Therefore, we overexpressed again cel-miR-39 in HDF, and after 24 hpt they were embedded into a collagen matrix. On the next day, NHEKs were seeded on the top to build up functional *in-vivo* mimicking 3D human skin equivalents (HSE). Differentiation was induced and after one week we harvested the supernatants, separated dermis and epidermis and extracted the RNA (Figure 45).

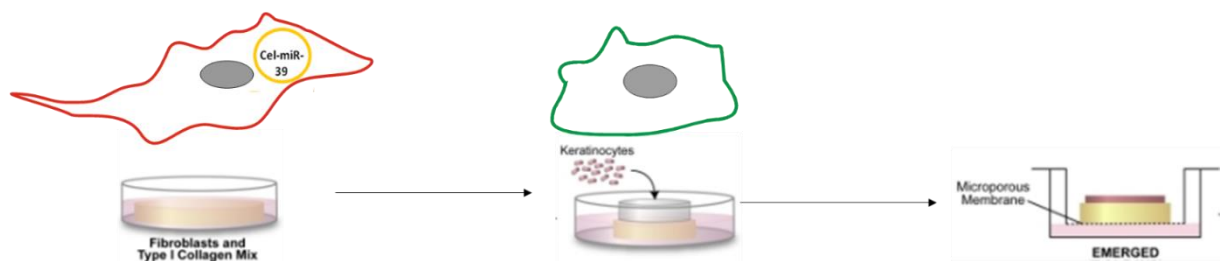


Figure 45 Cel-miR-39 and scrambled control overexpressing HDF were used to build *in-vivo* mimicking 3D skin equivalents (SE). 6 fold more NHEK were seeded on top and functional SE were formed. After 1 week, dermis, epidermis and supernatant was harvested for qPCR.

We first confirmed the overexpression of cel-miR-39 (24 hpt) prior embedding HSE and its preservation in the dermis of HSE after 8 days post transfection (day 7 of HSE) (Figure 46). Average Ct values were calculated to AU assuming a Ct-value of 40 to be 10 (Average Ct value of HDF intracellular ~13, average Ct value of dermis ~16).

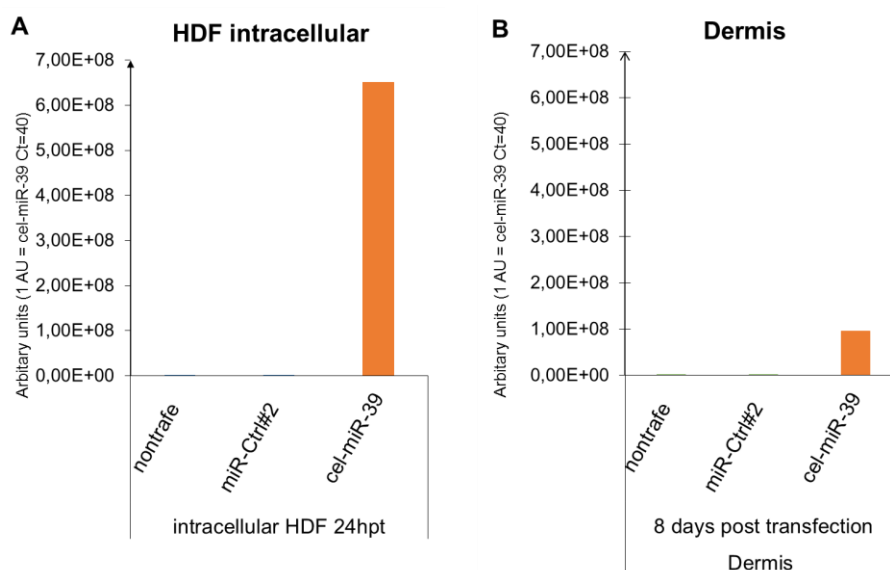


Figure 46 (A) qPCR confirms overexpression of cel-miR39 in HDF cells after 24 hpt prior of embedding the cells into the collagen matrix. Experiment was performed with 3 different donors of HDF and NHEK, one representative experiment is shown. Raw Ct-values were transformed to arbitrary units (AU) assuming a Ct-value of 40 to be 10.

Results

Finally, supernatants and epidermis harvested on day 7 of HSE, were analysed. QPCR confirmed the presence of cel-miR-39 in the total supernatant of HSE as well as the transfer of cel-miR-39 from dermis to epidermis, representative data from one experiment shown (Figure 47).

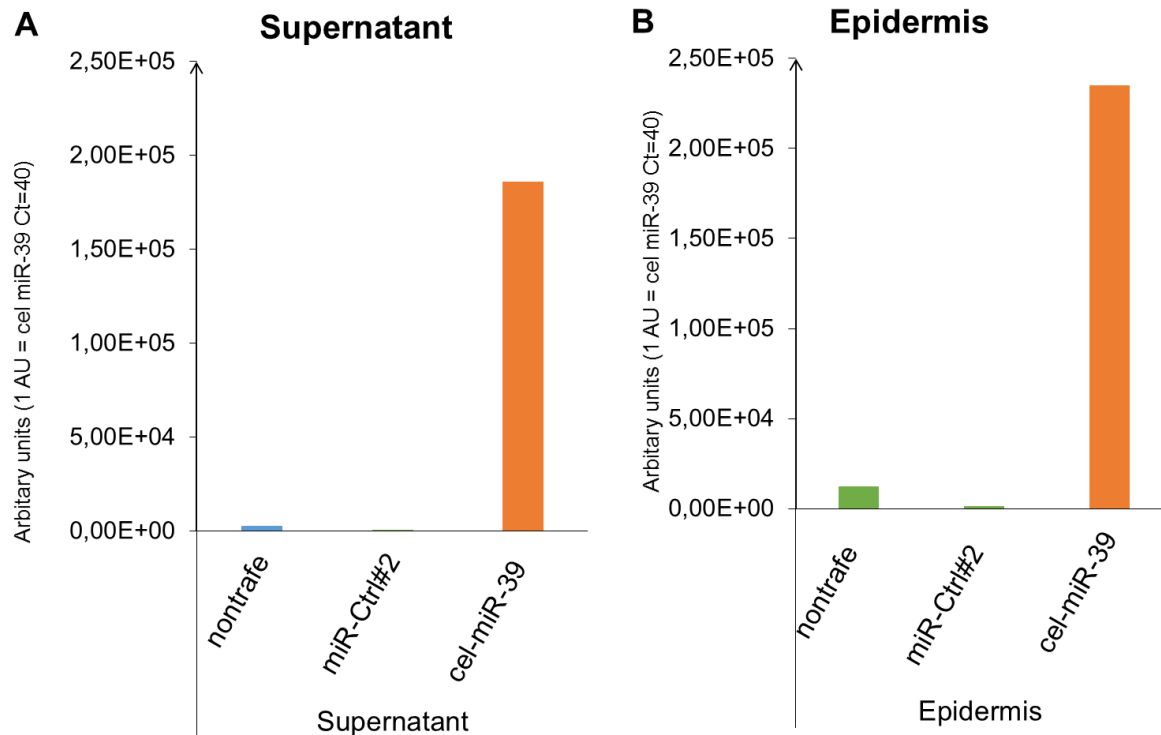


Figure 47 Samples from HSE were harvested after seven days of HSE (A) qPCR confirms the presence of cel-miR-39 in total supernatants from HSE, while it is absent in control and nontransfected HSE. (B) qPCR confirms the transfer of cel-miR-39 from the dermis to epidermis in HSE of HDF and NHEK (one representative experiment shown, three times repeated). Raw Ct-values were transformed to arbitrary units (AU) assuming a Ct-value of 40 to be 10.

Paradoxically, within the different repetitions of qPCR we observed a signal of cel-miR-39 in control samples, which never had contact with cel-miR-39 cells. Thus, we loaded the qPCR products on an agarose gel, and it clearly shows the presence of cel-miR-39 in the epidermis (Figure 48 lane 15 and 16). Counterintuitively, but in line with the results from qPCR, we also obtained an inconsistent signal of cel-miR-39 in control and non-transfected HDF cells embedded into the dermis (Figure 48 lane 4 to 9) and in miR-Ctrl transfected EV samples of the epidermis (Figure 48 lane 13 and 14). Given these results from qPCR and gel electrophoreses, we suspect an unspecific binding of the cel-miR-39 primer to components of the collagen matrix, since we (i) do not know the exact composition of the collagen matrix and (ii) the exact binding of the primers. Furthermore, (iii) this 'unspecific' signal in the negative controls appeared not in all experiments, while we were able to detect a consistent signal of cel-miR-39 in the epidermis within all repetitions.

Results

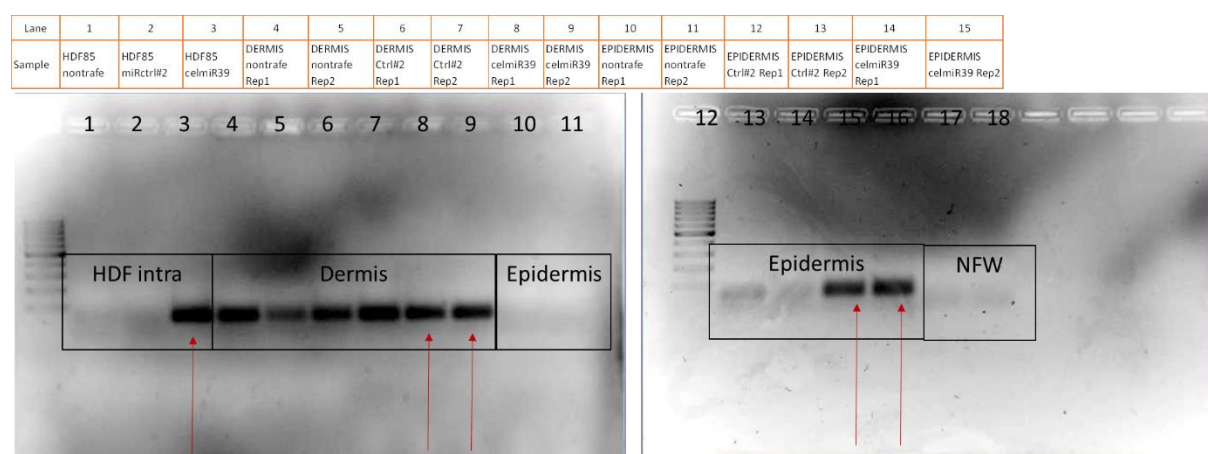


Figure 48 Agarose gel electrophoresis of qPCR products from cel-miR-39 transfection in HDF, dermis and epidermis. Red arrow indicates cel-miR-39 transfected samples or the incubation with them.

To summarize, we could show an EV-miRNA crosstalk between primary HDF and primary NHEK that is extended to a transfer through the collagen matrix in 3D skin equivalents. If the transfer in the 3D model is mediated by EVs or/and by miRNAs bound to protein complexes remains to be elucidated. In addition, we cannot rule out if the miRNA was taken up and/or if it is only attached onto the cell surface.

With the *in-vivo* mimicking proof of principle experiment of EV dependent miRNA communication between dermal and epidermal cells, we next aimed to detect EVs in different layers of human skin.

3.4.3. Implications for the presence of extracellular vesicles and multivesicular bodies in human skin

In order to find indications for the presence of EVs in human skin, we first aimed to isolate EVs from skin sections. The weight of both was measured before (62.77 g and 69.27 g) and after (20.1 g and 23.96 g) removal of the lipid layer. To separate the dermis from the epidermis, the skin sections were incubated with dispase overnight.



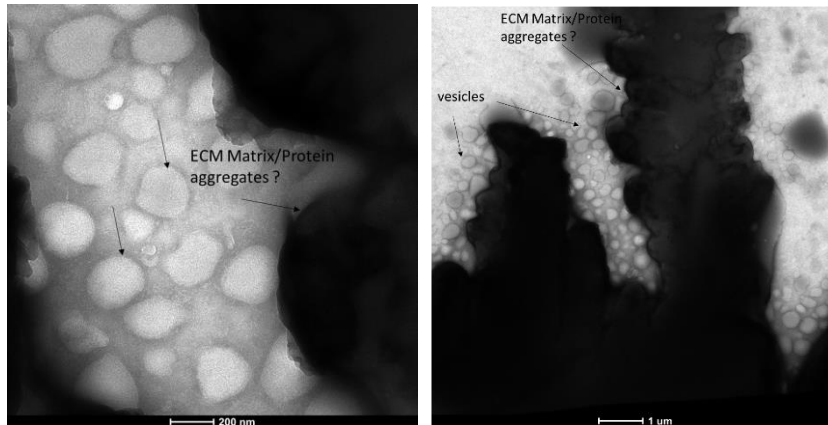
Figure 49 Washing and digestion solution from skin sections were used to harvest sEVs. Picture shows the pellet after two times 500xg and two times 14,000xg centrifugation.

Unfortunately, we were not able to separate the two distinct skin layers, which might be due to a low ratio of dispase concentration to skin volume and decided to isolate small EVs from the solvent used for digestion (dispase solution) and washing (PBS). Isolation was performed according to our standard protocol including four extra centrifugation steps prior ultracentrifugation showing a dark pellet, which we considered as residues from melanocytes (Figure 49). Protein determination after ultracentrifugation yielded in total ~4.45 mg protein and the sample was subsequently contrast stained for TEM. As far as we were able to interpret the electron microscopy images, we saw many 'particles', probably 'lipid-like- particles', distributed and attached to (extracellular matrix) fragments

(Figure 50). We thus decided to digest the sample with collagenase and added an additional ultracentrifugation

Results

step at 100.000 x g. Thereby, we were able to reduce the total protein content and stained again for electron microscopy.



This time we were able to see homogenously distributed vesicles in a size range between 50 - 100 nm. The aggregates, were absent in both cases either with or without collagenase treatment, suggesting that washing and an additional centrifugation step is already sufficient for pre-cleaning.

Figure 50 sEVs harvested from incubation solution of skin sections. We observed vesicle like structures attached and distributed next to tissue fragments.

Interestingly, without collagenase it seems that the lipid membrane is

more obscured than after digestion. Here we see round shaped vesicles that are probably surrounded by a lipid membrane (Figure 51), though the differences between plus or minus collagenase are not very pronounced.

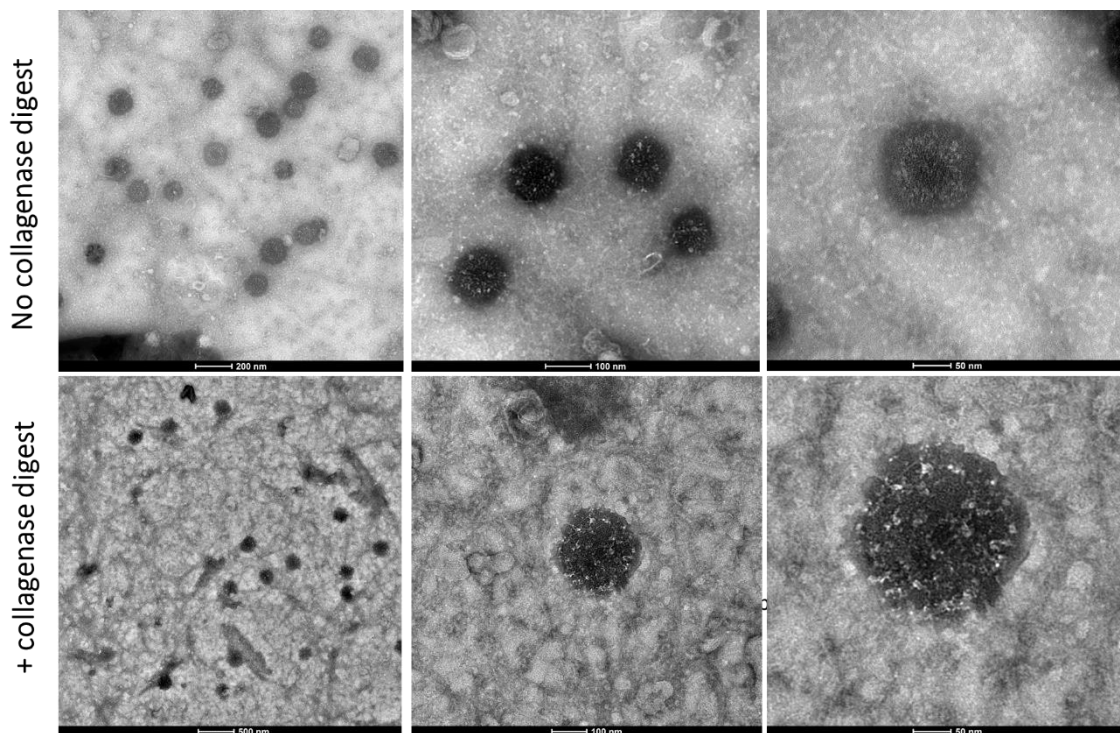


Figure 51 EVs from skin sections were digested with collagenase and after one centrifugation step at 100.000 x g the samples were contrast stained for TEM. EVs are homogenously distributed and after collagen digestion a surrounding membrane appears.

Since we were neither able to identify the cellular source of the small EVs derived from the entire skin sections, nor to detect any other EV marker, we decided to cooperate with Ida Perrotta from University of Calabria, Cosenza, Italy. In order to detect EVs in different skin layers, the samples were prepared for electron microscopy. Indeed, we found indications for the presence of EVs and multivesicular bodies (MVB) in the skin sections of all three donors. We were able to detect individual (not enclosed in MVB) vesicle-like structures in the extracellular space (Figure 52 right space right) and within the collagen matrix (Figure 52 left). In addition, keratinocytes show

Results

numerous irregularly arranged membrane protrusions that might point to the presence of EVs (Figure 52 right white arrow).

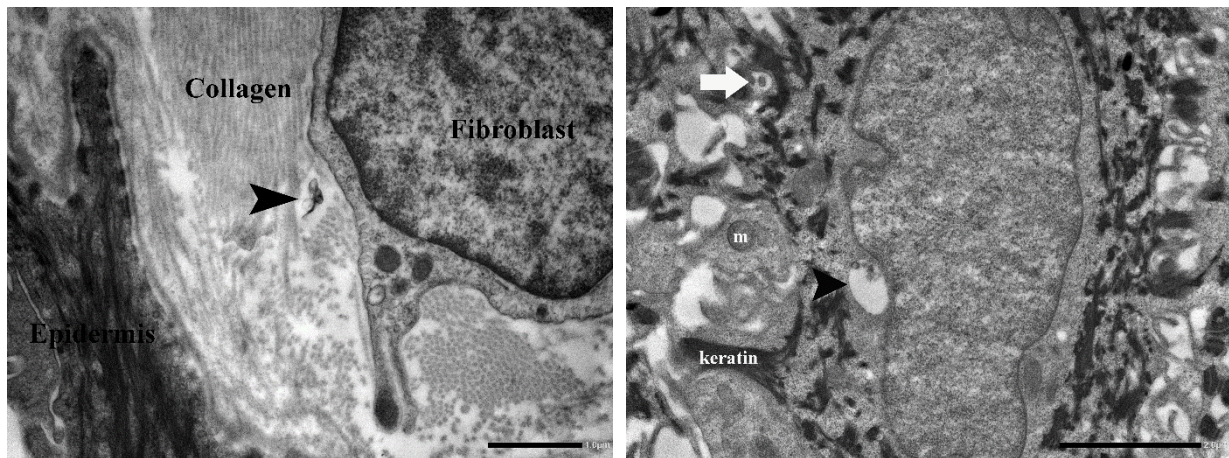


Figure 52 probably individual EVs between epidermis and dermal fibroblasts indicated by black arrows. Membrane protrusions from keratinocytes (white arrows)

Within the epidermal cells in the basal layer, we detected MVB containing intraluminal vesicles, which are known to be secreted as exosomes. They can be clearly recognized based on their peculiar ultrastructural features (shape, and a diameter of ~ 500 nm) (Figure 53).

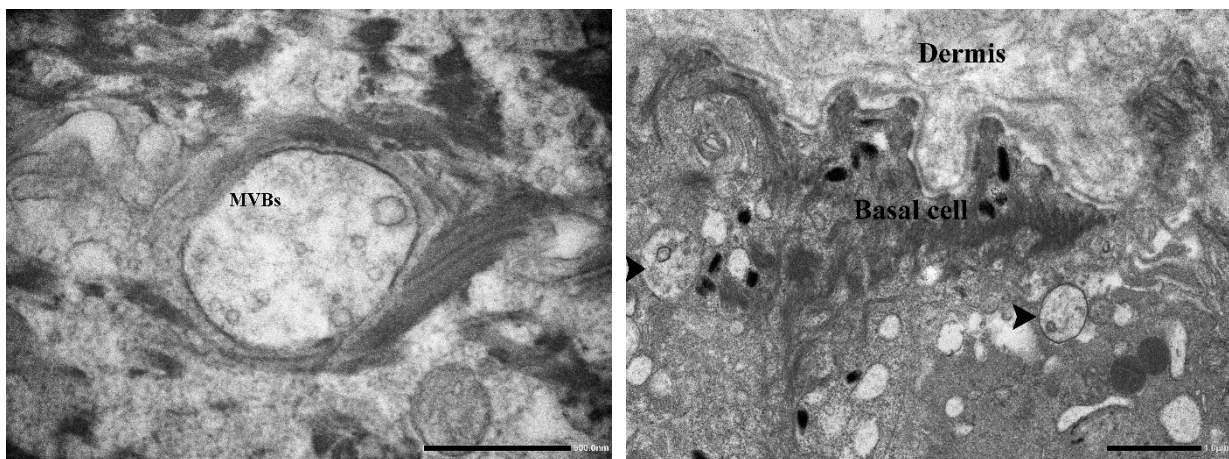


Figure 53 MVB in the basal layer of epidermal cells

Of particular interest are the pictures showing keratinocytes and fibroblasts side by side. It is here intriguing to speculate that they might interact with each other and communicate via EVs (Figure 55, Figure 54).

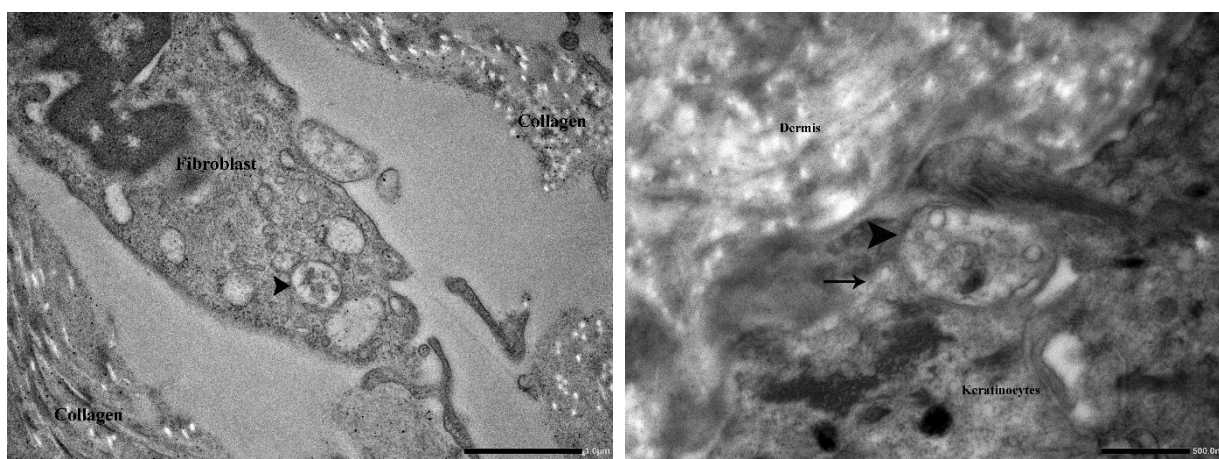


Figure 55 Left: MVB within fibroblasts that are secreted or taken up into/from the extracellular space. Right: keratinocytes next to the dermis contain MVB and release exosomes

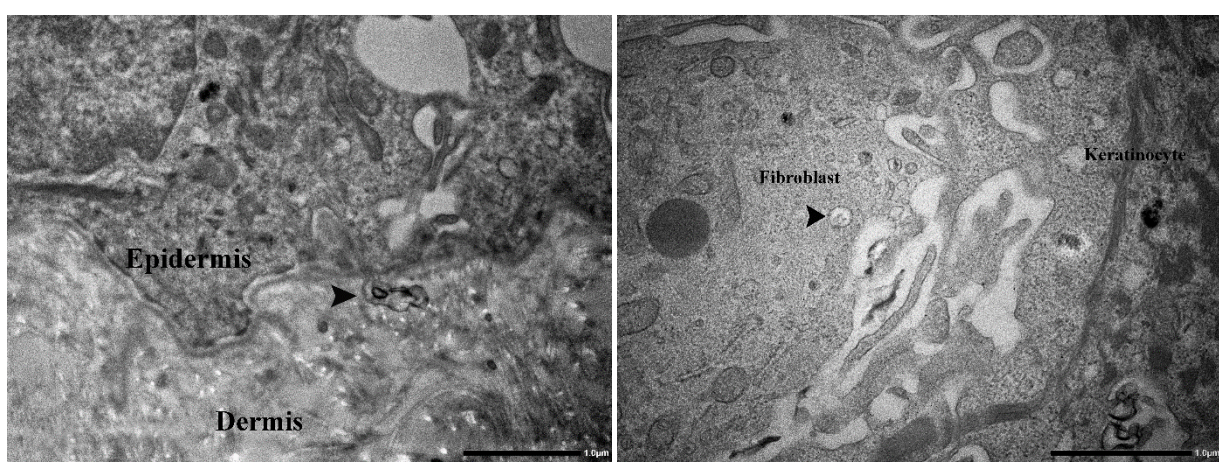


Figure 54 Fibroblasts in the dermal layer and keratinocytes in the epidermis side by side. Arrow indicates MVB and/or EVs in fibroblasts/dermis.

However, to reliably ascertain whether these vesicle-like structures are indeed extracellular vesicles, the detection of tetraspanins and other markers known to be specific for extracellular vesicles are necessary for classification. Accordingly, the presence of TSG101 by immunogold labelling was confirmed in EVs in MVB as well as in the extracellular space (Figure 56).

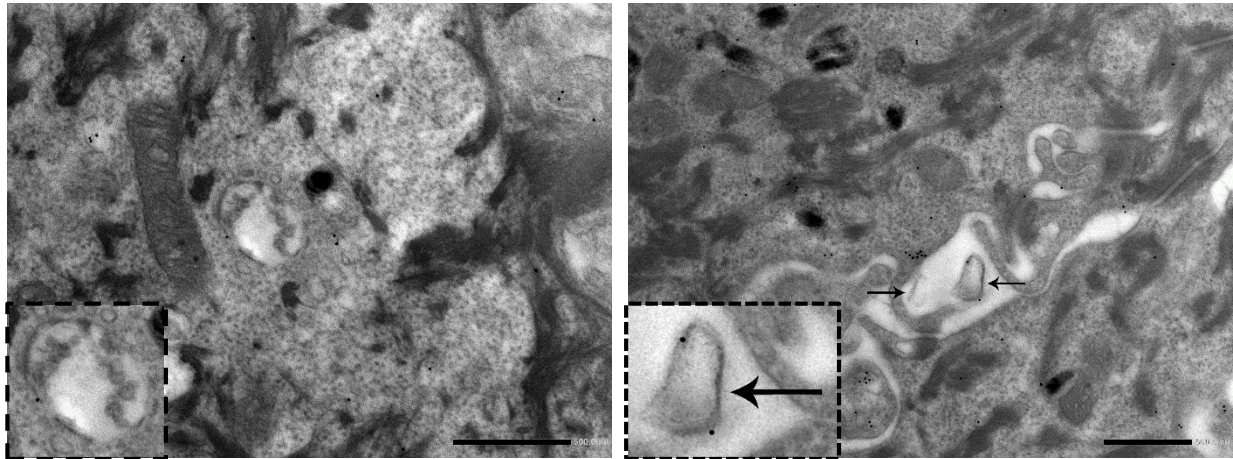


Figure 56 Immunogold labelling with TSG101 of skin sections. Left: MVB are positive for TSG101. Right: EVs positive for TSG in the extracellular space.

Summarizing so far, we collected pieces for a role of extracellular vesicles within human skin. Single EVs were detectable in the extracellular space, within collagen fibers as well as in the basal layer of epidermal cells. Based on these findings and the knowledge that EV containing miRNAs are able to transfer through an *in vivo* mimicking collagen matrix as tested in skin equivalents, we thus highly suspect an EV-miRNA crosstalk *in vivo*.

3.5. The EV-miR-SASP and its impact on keratinocyte's functionality

Keratinocyte functionality is highly dependent on the underlying dermis (Szabowski et al. 2000) and decreases as a consequence of ECM remodelling due to the presence of reticular fibroblasts (Mine et al. 2008). In addition, the presence of senescent fibroblast in skin equivalents, so-called 'aged-skin equivalents', decreased the epidermal thickness, impaired epidermal differentiation and consequently resulted in an intact barrier function (Weinmüller et al in preparation). It is considered that divergent secretory profiles obtained from aged, reticular and early passage papillary fibroblast are the driving forces for functional changes of the epidermis (Sorrell et al. 2004). This idea is supported by an increased proliferation of keratinocytes and by a pro-inflammatory effect on peripheral blood mononuclear cells after incubation with SIPS derived conditioned supernatants (Lämmermann et al in preparation). These observations led to the questions, whether the mere presence and uptake of specifically or highly secrete miRNAs enclosed in small EVs have the potential to modulate keratinocyte functionality and if an amelioration of keratinocyte functionality with age is connected to the miR-SASP?

3.5.1. The transient presence of the *in vitro* EV-miR-SASP increases wound healing of keratinocytes

A declined wound healing capacity is among many others an elementary sign of aging and is thought to be the consequence of a deprived immunosurveillance. Intriguingly, however, the transient presence of senescent cells and in particular their secretory compounds, enhanced the healing process and reduced fibrosis (J.-I. Jun & Lau 2010a; Krizhanovsky et al. 2008). Previous work already confirmed the contribution and the releases of EVs at sites

Results

of injuries (Moulin et al. 2010; reviewed by Rani & Ritter 2016) and emphasized their beneficial role within several stages of the wound healing process (Geiger et al. 2015; Leoni et al. 2015).

In order to analyse the physiological effect of senescence associated EVs on the wound healing rate of primary keratinocytes, we harvested EVs from different timepoints of HDF senescence and incubated NHEK for 24 to 48 hours with different ratios of EVs, meaning the amount of vesicles secreted from 'cell number' of fibroblasts, to 'number' of receiving keratinocytes. We selected the ratios of 1:1 and 5:1, to test their effect on the wound healing rate and selected two different experimental settings.

Initially, we seeded primary NHEK into ibidi® wound healing chambers, separated by an insert to prevent attachment of NHEK leaving a cell-free area. After 48 hours incubation with EVs in a ratio of 5:1 from SIPS and Q cells, we removed the insert and counted the number of NHEK growing into the cell-free area. We observed a clear improvement of wound closure and healing speed after incubation with SIPS derived vesicles. The exposure to SIPS derived vesicles even doubled the amount of cells within the 'wounded' area when compared to control treated cells (Figure 57).

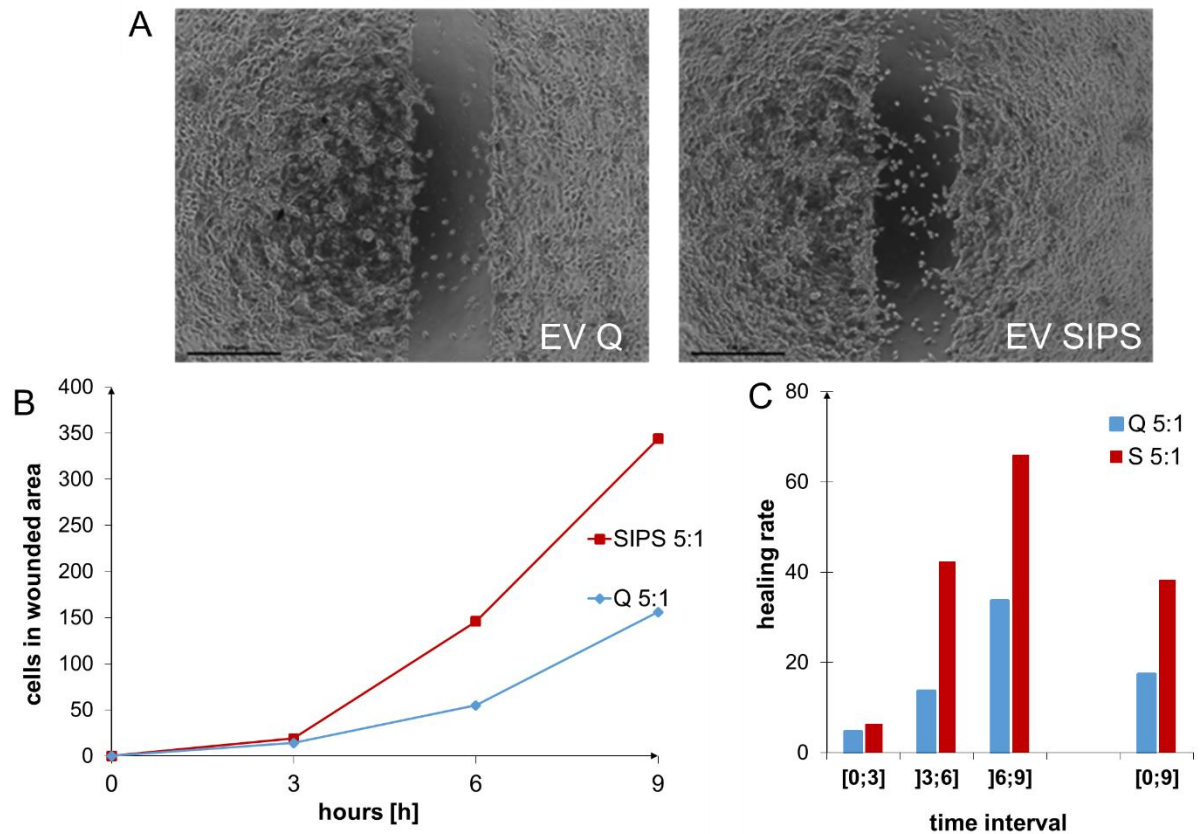


Figure 57 Enhanced wound healing capacity of primary NHEK after incubation with SIPS derived vesicles for 48 hours. Small EVs from HDF161 after 3 weeks recovery were harvested. NHEK were incubated for 48 hours with SIPS or Q derived vesicles with a ratio of 5:1. After removal of the ibidi® insert, cell movement was monitored and microscopic images were taken every 3 hours. (A) NHEK at the last time point (9 hours) of monitoring. (B) Number of keratinocytes within the cell-free area were counted after 3, 6 and 9 hours post removal of the ibidi® insert. (C) Healing rate was calculated from all timepoints as well as from the entire observation period. Scale bar = 400 μ m.

In addition, we tested the healing rate of NHEK after performing a scratch into a confluent cell layer. This 'classical' scratch assay allows the mimicking of an actual injury into a dense cell layer and provides a convenient and cheap assessment of the wound healing capacity.

Results

On day prior EV application, primary NHEK were seeded into 12 well plates and were pre-incubated for 24 to 48 hours with SIPS and Q derived EVs with the ratios 1:1 and 5:1. Wound closure was monitored and the cell free area was quantified with ImageJ. The healing rate between the first and last timepoint was calculated from the cell free areas at indicated timepoints.

As before, but with a different setup, we revealed again an accelerated wound healing rate of keratinocytes after the transient presence of senescence derived EVs from three different donors each (Figure 58). If the healing rates depend on migration or proliferation was not tested in these setups.

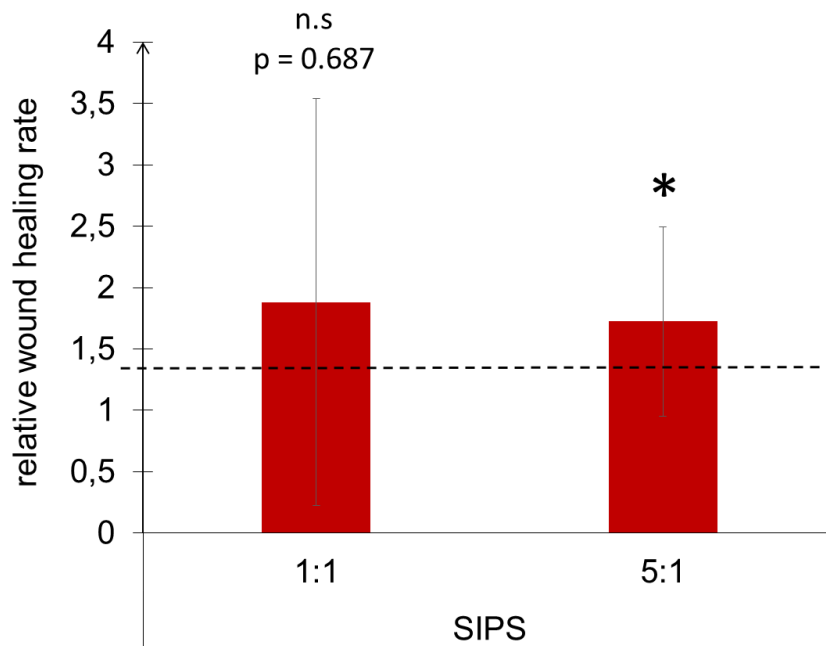


Figure 58 Enhanced wound healing capacity of primary NHEK after incubation with SIPS derived vesicles for 48 hours. Small EVs from three different donors between one to 5 weeks recovery were harvested. NHEK from three different donors were incubated for 48 hours with SIPS or Q derived vesicles with a ratio of 5:1 and 1:1 and a scratch was performed after 24 – 48 hours pre-incubation with EVs. Cell movement was monitored and microscopic images were. Cell free area was quantified with ImageJ. Healing rate was calculated with the areas obtained from the first and last timepoint. Results are averages from 6 independent experiments done with three different donor NHEK and HDF each. Averages were normalized to Q 1:1 or Q 5:1 +/- relative stdev derived from ratios. A Wilcoxon Signed Rank Test was performed: p-value * < 0.05, n.s non-significant > 0.05.

3.5.2. The chronic presence of the EV-miR-SASP impairs keratinocyte differentiation

Another major functionality of keratinocytes is their ability to differentiate and to form an intact and resilient epidermal layer. Age related skin atrophy is the consequence of impaired differentiation leading to an intact barrier function and to an increased vulnerability against exogenous harm. A similar effect of a reduced differentiation and an impaired barrier function was observed in aged skin model systems built with senescent fibroblasts (Weinmüller et al in progress).

In 2D monolayer cultures, keratinocyte differentiation is accompanied by changes in gene expression as well as by evident morphological changes. The cells cornify, shed anucleated mature/dead cells into cell culture media and form crosslinks between adjacent cells (Marcelo & Tong 1983). The late *in-vitro* differentiation marker involucrin

Results

(Poumay et al. 1999) is the principal initiator of the cornification process *in vivo* and provides a scaffold for the assembly of structural proteins (Robinson et al. 1996; Watt & Green 1981).

In order to address, whether the chronic presence of senescence-associated-EVs impacts on keratinocyte differentiation in monolayer cultures, they were incubated with Q and SIPS derived EVs for one week. We observed prominent changes in morphology, showing loss of nuclei and the formation of an interdigitated web after incubation with Q derived EVs, while less crosslinks were visible after incubation with SIPS vesicles. In order to manifest these changes in a quantitative manner, protein lysates were analysed for the expression of involucrin. We observed a reduced expression of involucrin in NHEK incubated with SIPS derived EVs in a ratio of 5:1, while we could not see an effect with a lower amount of EVs (1:1 ratio).

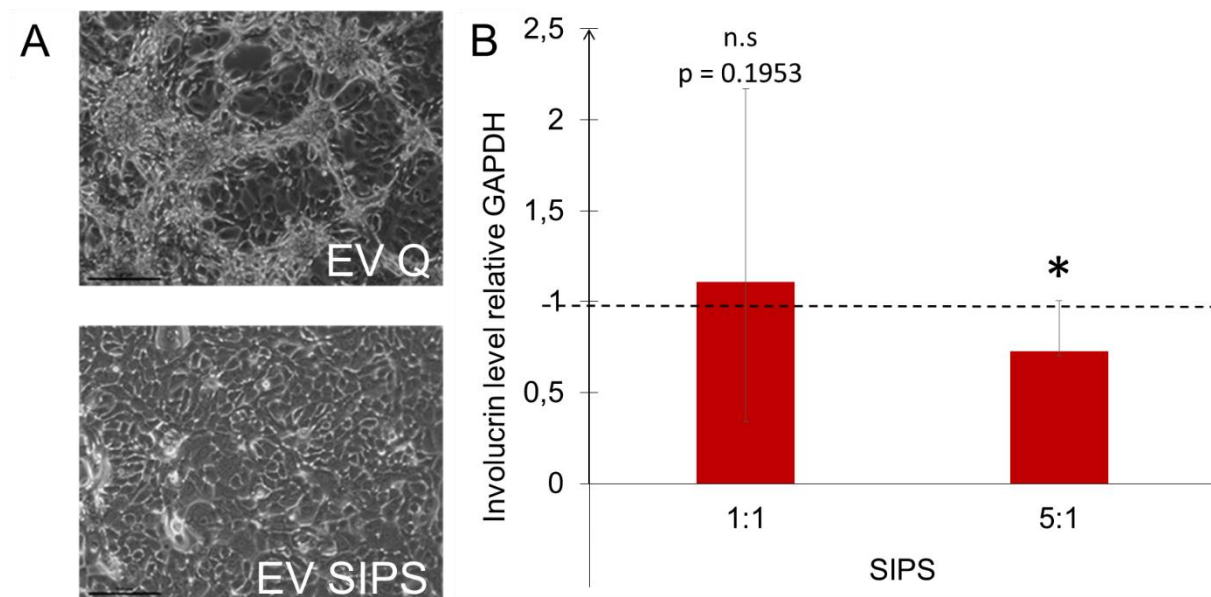


Figure 59 Expression of involucrin in primary keratinocytes after incubation with SIPS or Q derived EVs for one week. (A) morphological changes of keratinocytes after 1 week incubation with EVs from Q (top) and SIPS (bottom) fibroblasts (B) Involucrin levels were normalized to GAPDH and ratios relative to corresponding controls (either to 1:1 Q or 5:1 Q) were calculated Scale bar = 100 μ m. Results are averages from 8 independent experiments done with three different donor NHEK and HDF each. Averages were normalized to Q 1:1 or Q 5:1 +/- relative stdev derived from ratios. A Wilcoxon Signed Rank Test was performed: p-value * < 0.05, n.s non-significant > 0.05.

To summarize, our findings reinforce the current view of the transient and the chronic effects of the SASP as tested in monolayer cultures. The short term presence of pro-inflammatory SASP factors seem to be beneficial, while the long time exposure is thought to act detrimentally on its surrounding environment. However, contrary to other studies, we limited the SASP mediated effect to small EVs. We observed an enhanced wound healing capacity after the transient presence of SIPS derived EVs, while the chronic presence attenuated the differentiation of keratinocytes.

3.6. miR-23a-3p a skin aging associated 'miRdiator' of the miR-SASP

To discover mediators of the miR-SASP induced effects on keratinocytes, we considered to focus on the top highly abundantly secreted miRNAs identified earlier (Part A Figure 24).

We reviewed past literature and found miR-23a-3p to be modulated during keratinocyte and fibroblast senescence (Luo et al. 2015; J. Zhang et al. 2016) as well as in aged skin and fibroblasts by directly targeting HAS2 (Röck et al. 2014). In addition, the inhibition of its isoform miR-23b-3p in NHEK shows increased epidermal thickness and enhanced differentiation in 3D skin equivalent models (Barbollat-Boutrand et al. 2016).

Based on these implications from literature and on our observations on the wound healing capacity and differentiation, we analysed the expression of miR-23a-3p in NHEK after transient incubation with the EVs. Indeed, we were able to see an increase in miR-23a-3p upon incubation with SIPS derived vesicles, when using the ratio 1:1 and 5:1.

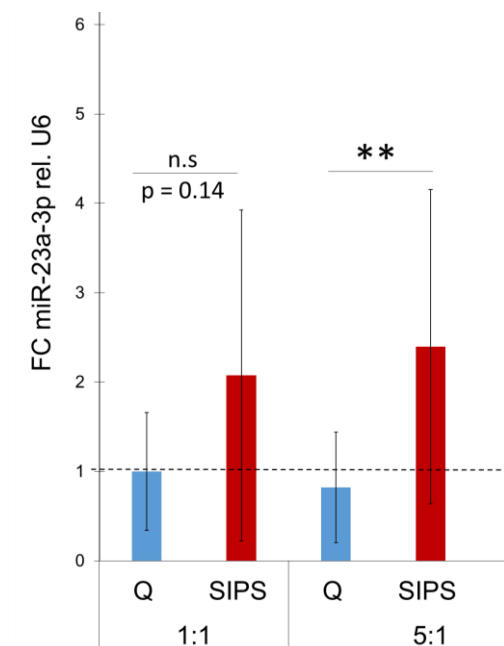


Figure 60 MiR-23a-3p levels in NHEK after incubation with SIPS derived EVs from different ratios. Keratinocytes were incubated with EVs in ratios of 1:1 and 5:1 for 48 h. miR-23a-3p levels were determined by qPCR and normalized to U6. ddCT method was used for quantification and results are averages from independent experiments done with three different donor NHEK and HDF each. Averages are from ddCT values \pm stdev were normalized to Q 1:1. Unpaired Students t-test was performed. 1:1 n = 8, 5:1 n = 11, p-value ** < 0.01 **, n.s. non-significant. > 0.05

In particular, since most prominent and significant effects on the wound healing capacity and on differentiation were achieved when using the 5:1 ratios, the data from qPCR point to an uptake of miR-23a-3p from keratinocytes, yielding again significant results with the 5:1 ratio.

3.6.1. miR-23a-3p mimics the wound healing mediated effects of SIPS EVs

To investigate, if miR-23a-3p is indeed a mediator of the EV-induced effect on the wound healing rate, we overexpressed pre-miR-23a-3p and its corresponding scrambled control miRNA (miR-Ctrl) in primary NHEK. Cells were seeded into ibidi® slides and after 48 to 72 hpt the insert was removed and the healing process was monitored.

QPCR confirmed the overexpression of miR-23a-3p in keratinocytes during the entire observation period from 24 hours until 72 hours post transfection (Figure 61).

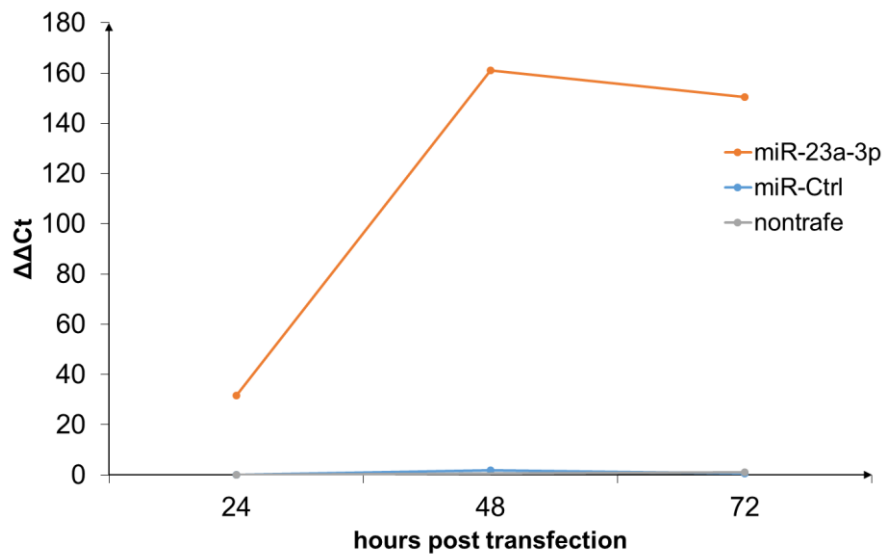


Figure 61 MiR-23a-3p overexpression in keratinocytes was confirmed after 24, 48 and 72 hours post transfection. miR-23a-3p and U6 as a housekeeper were measured in duplicates by qPCR. ΔCt values were calculated relative to U6 snRNA. $\Delta\Delta Ct$ values from one or two different NHEK donors and independent experiments are shown. 24 hpt n = 1, 48 hpt n = 2, 72 hpt n=2

Overexpression of miR-23a-3p significantly enhanced the wound healing process, in terms of wound closure (Figure 62B) and healing speed (Figure 62B), similar to the effect observed upon incubation with SIPS EVs (Figure 57).

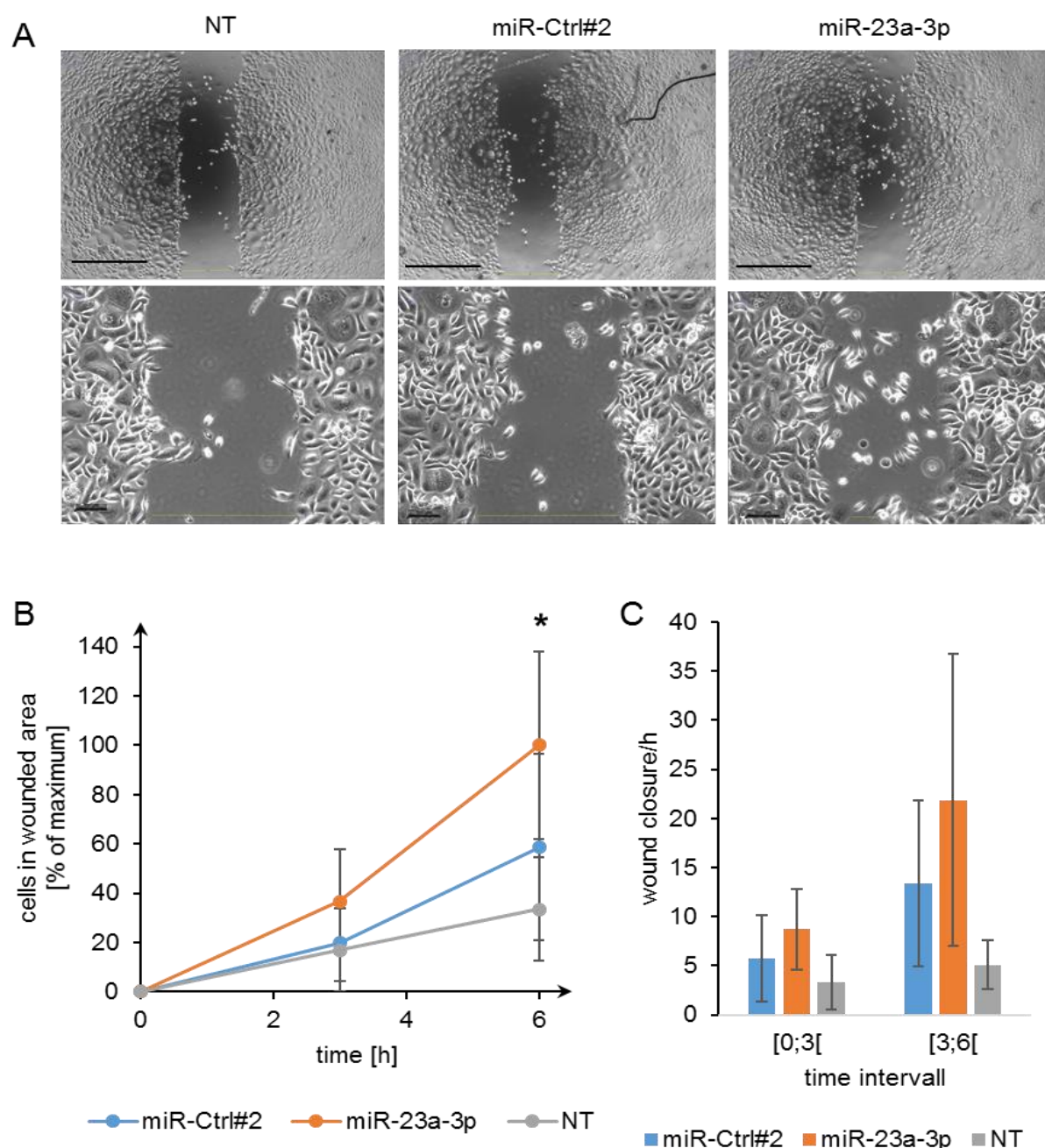


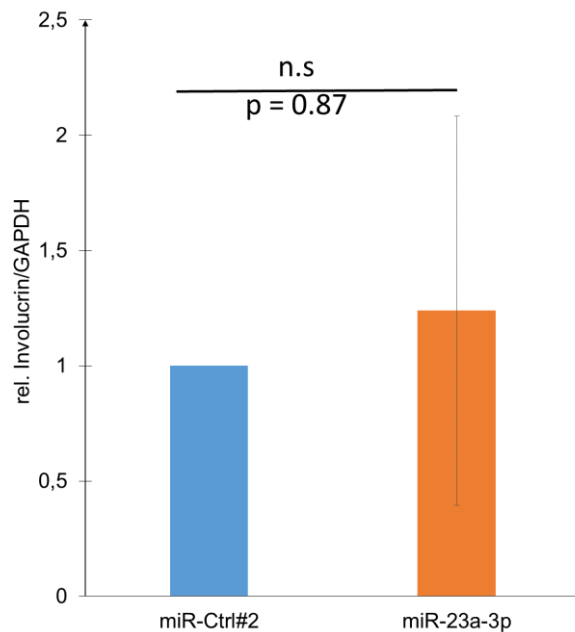
Figure 62 MiR-23a-3p overexpression accelerates wound closure in keratinocytes. NHEKs from two donors were transfected with miR-23a-3p or corresponding miR-Ctrl#2 and Non-transfected cells (NT) and were seeded into ibidi® slides. The ibidi® insert was removed after 48 hours post transfection (A) Wound healing was monitored over 6 hours. (B) Number of cells within the cell-free area were counted at three different timepoints and % of invading cells were calculated relative to the maximum. (C) Healing rate was calculated between different timepoints. Results are averages from normalized values of three independent experiments +/- stdev. Scale bar = 400 μ M (upper row) or 100 μ M (bottom row). * $p < 0.05$.

We concluded, that miR-23a-3p is indeed a modulator of the wound healing capacity of keratinocytes and endowed to mimic one perpetrator of the miR-SASP.

Results

3.6.2. miR-23a-3p and its effect on keratinocyte differentiation

To find out whether miR-23a-3p also modulates keratinocyte differentiation in the same manner as observed after incubation with SIPS derived EVs, we assessed involucrin levels after one week post transfection. However, we were not able to see a significant trend of differentiation as analysed by western blotting (Figure 63).



We concluded that miR-23a-3p is able to mimic the EV induced augmentation of keratinocyte's wound healing rate, but observed no significant effect on basal keratinocyte differentiation. We will next test, if miR-23a-3p is able to modulate keratinocyte differentiation capacity in 2D and 3D when triggering their differentiation with Ca^{2+} .

Figure 63 Involucrin expression after one week post miR-23a-3p overexpression. NHEK of one donor were either transfected with miR-23a-3p or a scrambled control miR. After one week samples were harvested for Western blot. Involucrin levels were normalized to GAPDH and miR-Ctrl#2 was set to one. Averages from four independent repetitions were derived from ratios. Wilcoxon signed rank test was performed (Rep) were performed.

3.7. miR-21-5p an 'oncomiR' as part of the SASP?

miR-21 is one of the most extensively studied miRNA and its upregulation has been commonly correlated with tumor progression and carcinogenesis, leading therefore to the term 'oncomiR-21' (Krichevsky & Gabriely 2009). However, counterintuitively to a plethora of pro-proliferative studies in cancerous cell lines and tissues, we recently confirmed its upregulation in senescent human endothelial cells (Hanna Dellago et al. 2013). MiR-21 directly targets two key cell cycle regulators and induces and maintains an irreversible growth arrest to abrogate uncontrolled proliferation. In addition, based on many miRNA-profiling studies, circulating miR-21 is indeed commonly found to be enriched in the extracellular environment and emerged to be the most abundant and highly secreted miRNA in fibroblast EVs (Terlecki-Zaniewicz in preparation, see also part A).

While EVs have already been reported to exert a protective (Eldh et al. 2010; reviewed by De Jong et al. 2014) and anti-apoptotic (Barile et al. 2014; Bruno et al. 2012) function on the surrounding tissues (Wen et al. 2016; Hergenreider et al. 2012) and cells (Jarmalaviciute et al. 2015), a recent report suggests that in particular the vesicular secretion of miR-21-5p mediates the protective function on recipient cells (Xiao et al. 2016). Prominent targets of miR-21 are a range of tumor suppressive and pro-proliferative candidates (reviewed by Buscaglia & Li 2011), and strikingly, also the top 20 highly secreted miRNAs of the miR-SASP, among those miR-21-5p, were

Results

identified to putatively suppress pro-proliferative downstream targets, such as PTEN (Terlecki-Zaniewicz in preparation, see also part A).

These findings from literature and our preliminary data may imply an anti-apoptotic, anti-proliferative and protective function of the miR-SASP, which until now was not tested yet. We therefore initially, addressed whether miR-21 knockout impacts on proliferation of primary keratinocyte's derived from transgenic miR-21 knockout mice.

The animals did not develop any apparent phenotype when comparing wildtype (wt, +/+) and knockout (KO, -/-) miR-21 mice and evaluation of the weight of six animals showed no significant differences (Figure 64).

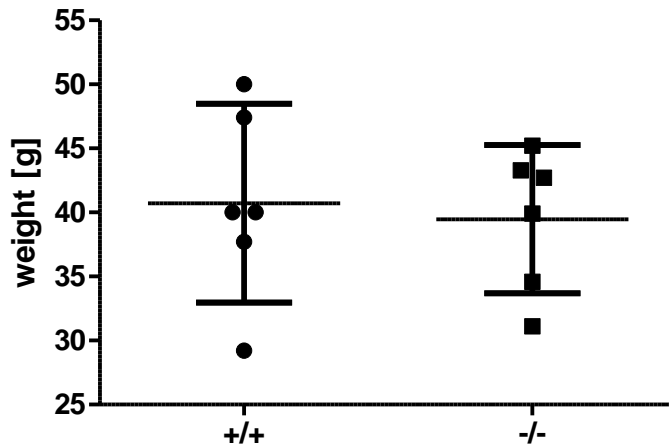


Figure 64 Differences in animal weight of wt (+/+) and knockout miR-21 mice are not significant (unpaired t-test $p < 0.05$). Dot plot shows 6 animals each and 95% of coefficient intervals are indicated

Tail keratinocytes from seven different mice pairs each wt (+/+) and knockout (-/-) were independently isolated on three different experimental days. The cells were isolated, and after 3 days in culture, equal cell densities were seeded into 96 well plates. 48h post seeding Resazurin, supplied as alamarBlue®, was added to the cells. It is a colorimetric and cell permeable dye, converted from metabolically active cells into a fluorescently detectable product. Monitoring of the growth behavior of wt versus KO keratinocytes revealed a significant growth advantage of KO cells compared to wt controls, that even increased after 2 days in culture (Figure 65).

Results

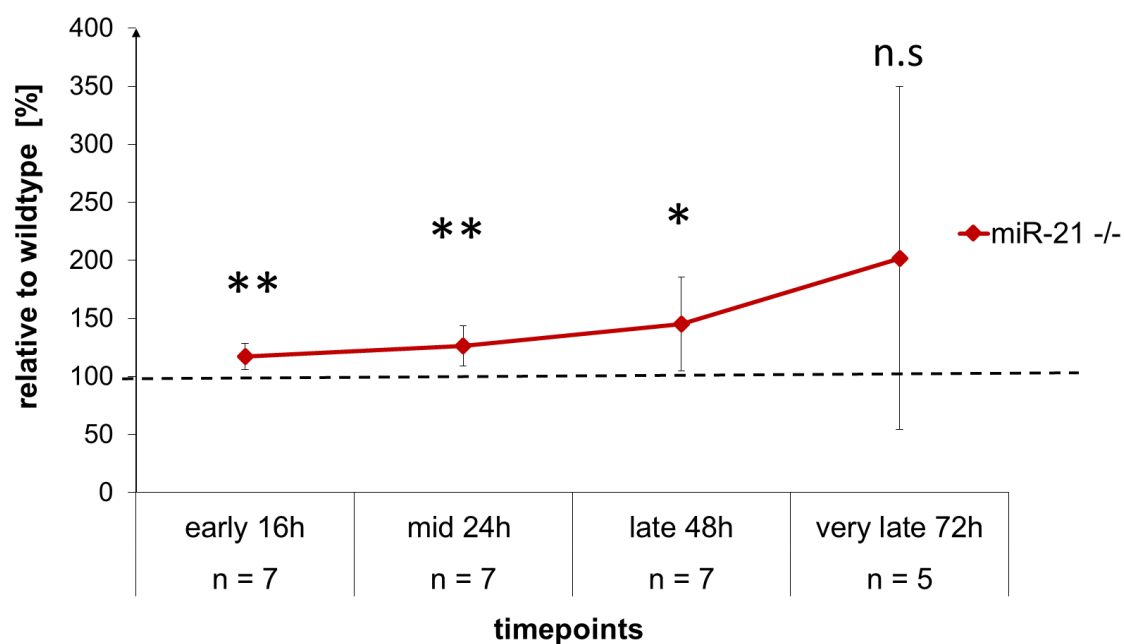


Figure 65 growth advantage of knockout (-/-) miR-21 keratinocytes compared to wt controls. Values were calculated relative wildtype controls and averages from 7 or 5 experiments were calculated. One sample t-test was performed. P -value ** < 0.01, * < 0.05 **, n.s. non-significant.> 0.05

3.7.1. Stress resistance of miR-21 knockout cells against various stress stimuli – pre-screening

In order to find out, if the growth advantage of the knockout cells sustain in response to different sources of stress stimuli, we first tested if either oxidative stress, induction of intrastrand DNA crosslinks or oxidized lipids affect the proliferation capacity of the cells.

Therefore, one day after seeding, the cells of two mice pairs (each wt and KO) were exposed to H₂O₂, paraquat, cisplatin and oxidized lipids (UV PAPC). Subsequently after the stress treatments their cellular activity was monitored.

Results

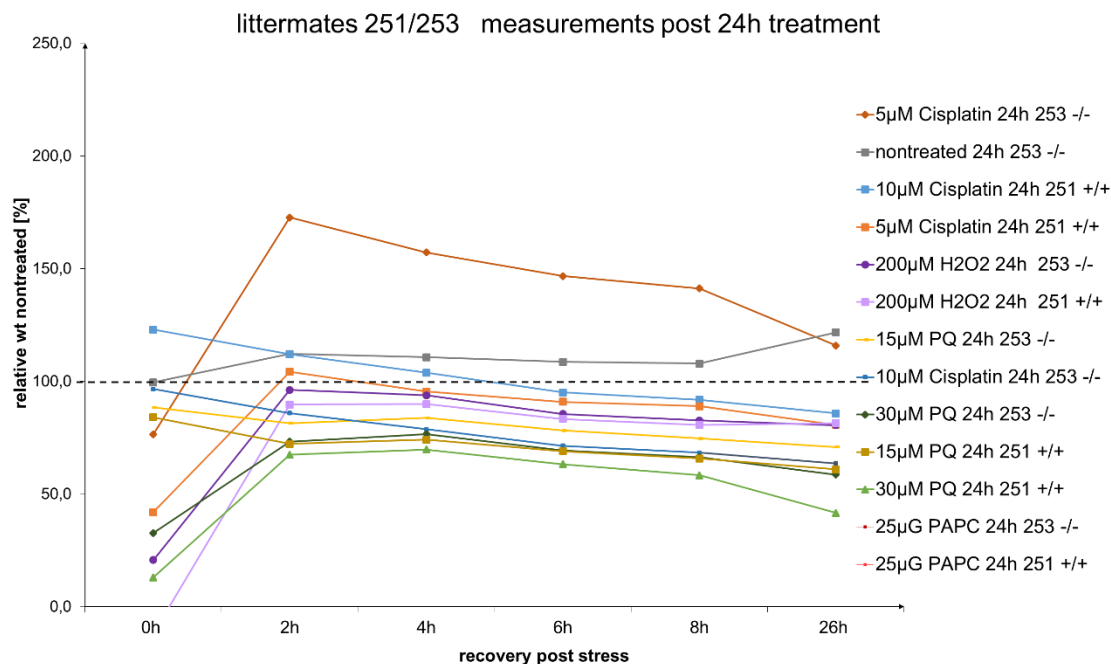


Figure 66 relative growth curves of littermates 251 and 253 after stress stimuli. Tail keratinocytes were treated for 24h with 5 µM and 10 µM cisplatin, 200 µM H₂O₂, 15 and 30 µM Paraquat and 25 µg UV-PAPC (cells stopped growing).

As observed earlier, we could confirm the growth advantage of the KO cells compared to wt keratinocytes under basal conditions and stressed conditions. However, comparing to nontreated cells, all stress stimuli attenuated the proliferation capacity, except 5 µM cisplatin, on knockout cells of one pair (253 -/- 5 µM Cisplatin, dark orange, Figure 66). Here, the proliferative activity even exceeded the one of nontreated KO (grey) and wt (252 +/+ , 100% dotted black line), while in the other littermates (85/86) (Figure 67) the cells grew almost comparable to nontreated KO (85 -/- nontreated grey) cells, but still faster than nontreated wt (86 +/+ , 100% dotted black line). In addition, even an increase of cisplatin concentration to 10 µM exhibited a substantial growth advantage of KO cells compared to wt (dark and light blue) in both littermate pairs.

Contrary, the exposure to oxidative stressors, such as paraquat and H₂O₂ revealed inconsistent results in the different pairs, showing in the littermates 251/253 only a minor to no effect, when comparing wt and KO, while in the littermates 85/86 the stress seems to confer a growth advantage to knockout cells.

Results

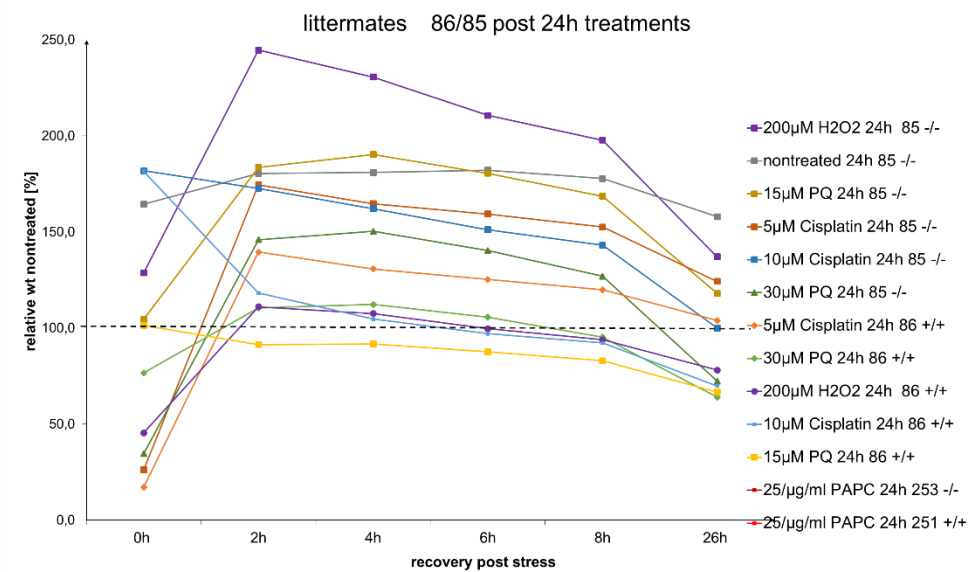


Figure 67 Relative growth curves of littermates 86 and 85 after stress stimuli. Tail keratinocytes were treated for 24h with 5 μ M and 10 μ M cisplatin, 200 μ M H₂O₂, 15 and 30 μ M paraquat and 25 μ g UV-PAPC (cells stopped growing).

Nonetheless, the impact of cisplatin, especially the differences between wt and KO, were more pivotal than the oxidative stress stimuli H₂O₂ and paraquat. In addition, independently of the stress stimuli, the relative signal of alamarBlue®, as an indicator of cellular health, decreased after one day recovery (26 hours post stress). However, based on microscopic examination, we concluded that growth arrest rather than apoptosis might be the reason for this decreased activity (pictures not shown).

Furthermore, we draw two other interesting conclusions from this experiment. After 24 hours exposure to 25 μ g/ml oxidized lipids we observed an immediate stop of proliferation in both littermates wt and KO (data not shown. Signals below detection limit). Consequently, we reduced the time of incubation to 6 hours and observed a remarkable growth advantage of the KO cells from both littermates compared to wt keratinocytes, though the absolute signals were still very low (Figure 68).

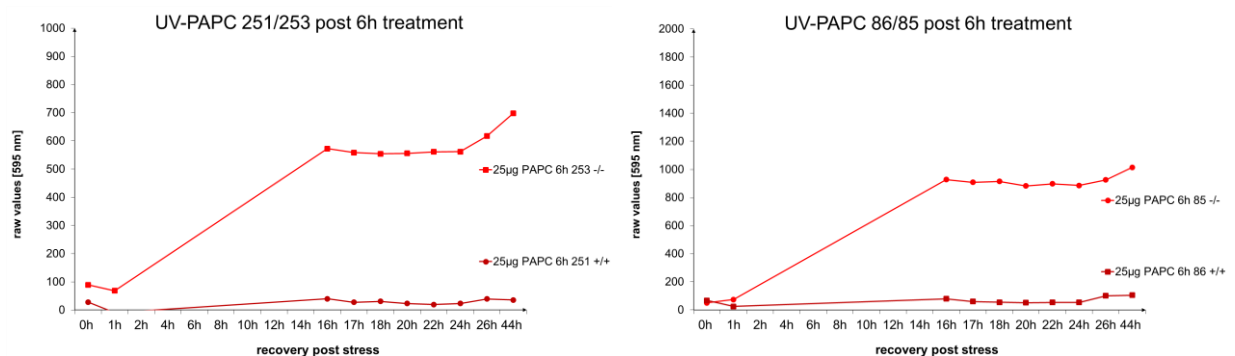


Figure 68 absolute growth curves of both littermates 251/253 and 86/85 after 6 hours 25 μ g/ml UV-PAPC.

Results

3.7.2. miR-21 knockout cells are stress resistant against Cisplatin

Finally, in order to assess the statistical impact of our preliminary data, we selected cisplatin and UV-PAPC to determine, if the growth advantage of miR-21 knockout cells compared to wildtype keratinocytes holds true, and whether the cisplatin induced amplification of proliferation did not occur by chance. In addition, since we observed a very potent effect of all stressors, we decided to start the treatments 2 days post seeding rather than one day to allow the cells prolonged reattachment.

Therefore, tail keratinocytes of five littermate control mice pairs each wt and KO were isolated on two independent experimental days. Three days after isolation, the cells were seeded in six technical replicates into 96 well plates to evaluate their stress resistance after exposure to oxidized lipids (UV PAPC) and cisplatin. To monitor their morphology during and after the stress stimuli, they were in addition seeded into 12 well plates. Two days post seeding we started to apply the stressors and to measure their metabolic activity using alamarBlue®. The averages of technical replicates from 5 biological replicates were averaged and normalized to the 'nontreated wt (+/+) group. Two way ANOVA was used to test whether the genotype and/or the treatment confers a significant effect on the growth behavior of the cells. One way ANOVA was used to compare different groups.

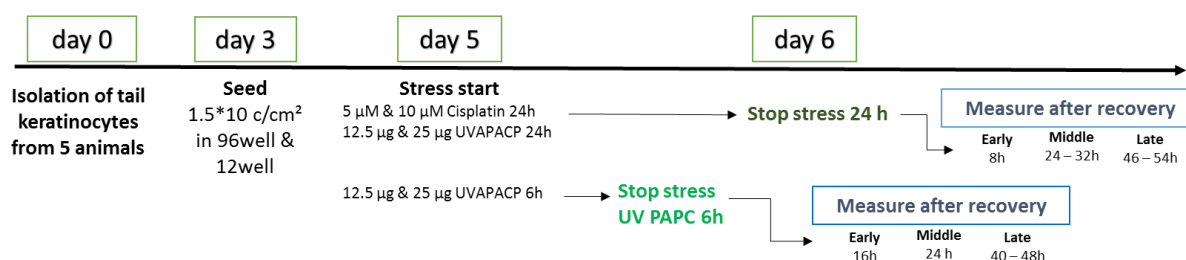


Figure 69 Experimental setup to assess the stress resistance of wt and KO miR-21 tail keratinocytes.

Indeed, after 24 hours treatment (Cisplatin, and UVPAPC) we observed a significant growth advantage of the genotype independently of the treatment and independently of the recovery phase, leading to an increased metabolic activity of miR-21 KO cells compared to wildtype (Table 4). It was even evident at the latest (48h recovery) timepoint, although we observed a confluent cell layer in several samples leading to higher standard deviation.

	Early		Mid		Late	
	Variance	p-value	Variance	p-value	Variance	p-value
Effect of Treatment	87,83%	< 0,0001	89,01%	< 0,0001	67,83%	< 0,0001
Effect of Genotype	1,80%	0,011	2,67%	0,0008	4,78%	0,0087

Table 4 Summary of 2 Way ANOVA after 24 hours stress treatments. The growth advantage of miR-21 knockout cells is considered very significant, independently ('factor genotype') or dependent (Factor 'treatment') of the treatment. The effect is sustained from early (16h) to late (40-48h) timepoints of recovery after the stress stimuli cisplatin and UVPAPC.

In addition, we experienced no significant difference of the growth behaviour of 5 μM cisplatin treated miR-21 knockout cells (dark purple), when compared to nontreated knockout cells (dark grey), after 24 (middle) to 48 hours (late) recovery. Intriguingly, after 48 hours post stress, even 10 μM treated miR-21 knockout cells amplified

Results

their proliferative capacity leading to a similar growth behaviour when compared to nontreated knockout cells. These findings indicate that 5 μ M cisplatin has no growth inhibiting effect on miR-21 knockout keratinocytes, they even show a similar growth behaviour as nontreated knockout cells (Figure 70).

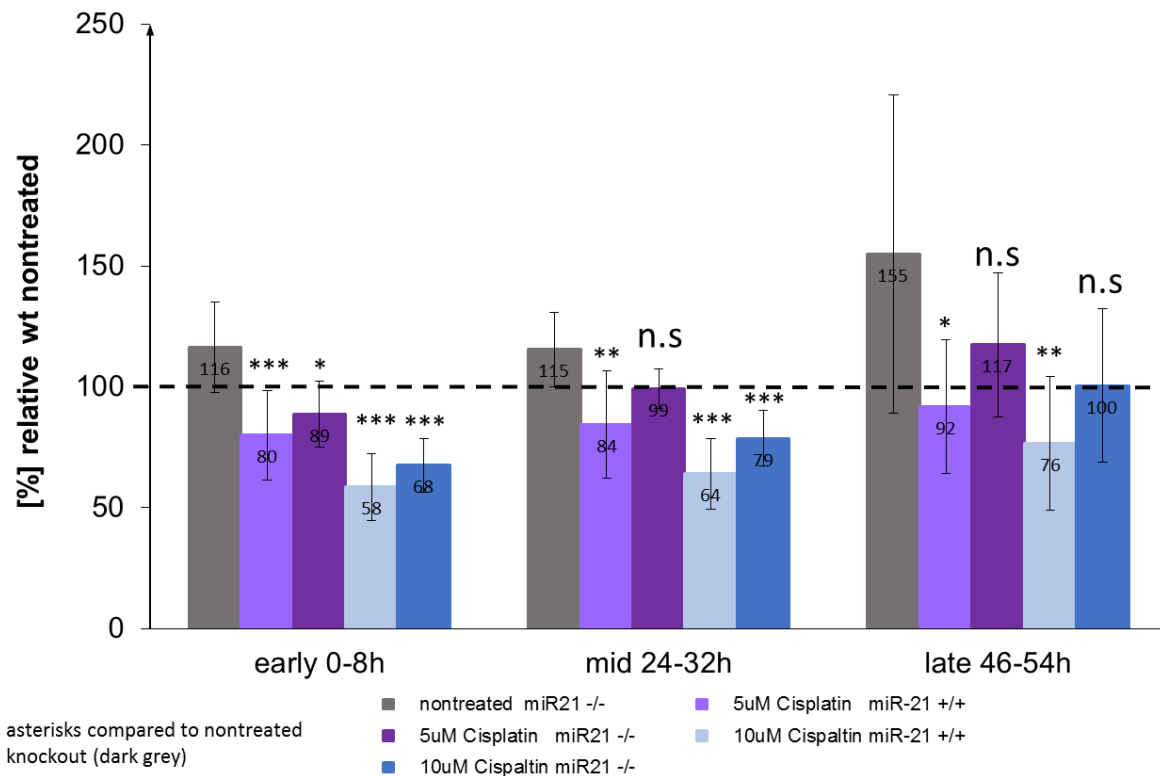


Figure 70 Growth advantage of miR-21 knockout cells under basal and after cisplatin induced stress. Metabolic activity of tail keratinocytes from miR-21 wt (+/+ light colours) and KO (-/- dark colours) mice, each nontreated and after 24 hours exposure to 5 μ M and 10 μ M cisplatin. Metabolic activity was measured at early (8 h recovery), middle (24 h – 36 h recovery) and late timepoints (46 h– 53 h) of recovery. Data from 5 biological replicates are shown. Averages \pm stdev are derived from ratios. 2way ANOVA with Bonferroni post-test was used to estimate the effect of the 'treatment' and 'genotype', respectively. For the presented statistics we used one way ANOVA for repeated measurements with turkey post hoc test comparing different groups with each other. Respective asterisk are shown from comparison to nontreated knockout (dark grey). nontreated wt (+/+) dotted line. P-value *** < 0.001, ** < 0.01, * < 0.05, > 0.05 n.s. non-significant. Light colours wt (+), dark colours KO (-/-), grey: nontreated, purple: 5 μ M Cisplatin, blue: 10 μ M Cisplatin.

3.7.3. Oxidized lipids impair the growth advantage of miR-21 knockout cells

Contrary, a very strong aggravation of metabolic activity when compared with nontreated cells, was observed after exposure to oxidized lipids for 24 hours. Although, the cells lost around 80 -70% of their growth capacity we compared only treated cells with each other (wt light red vs KO dark red, and wt light green vs KO dark green). We could detect a significant difference between wildtype and knockout cells after 12.5 μ g/ml at early and middle timepoints of recovery. However, we concluded that 25 μ g/ml is too potent leading to almost no growth. According to microscopy examination, it seems that the cells are rather arrested than apoptotic (Figure 71).

Results

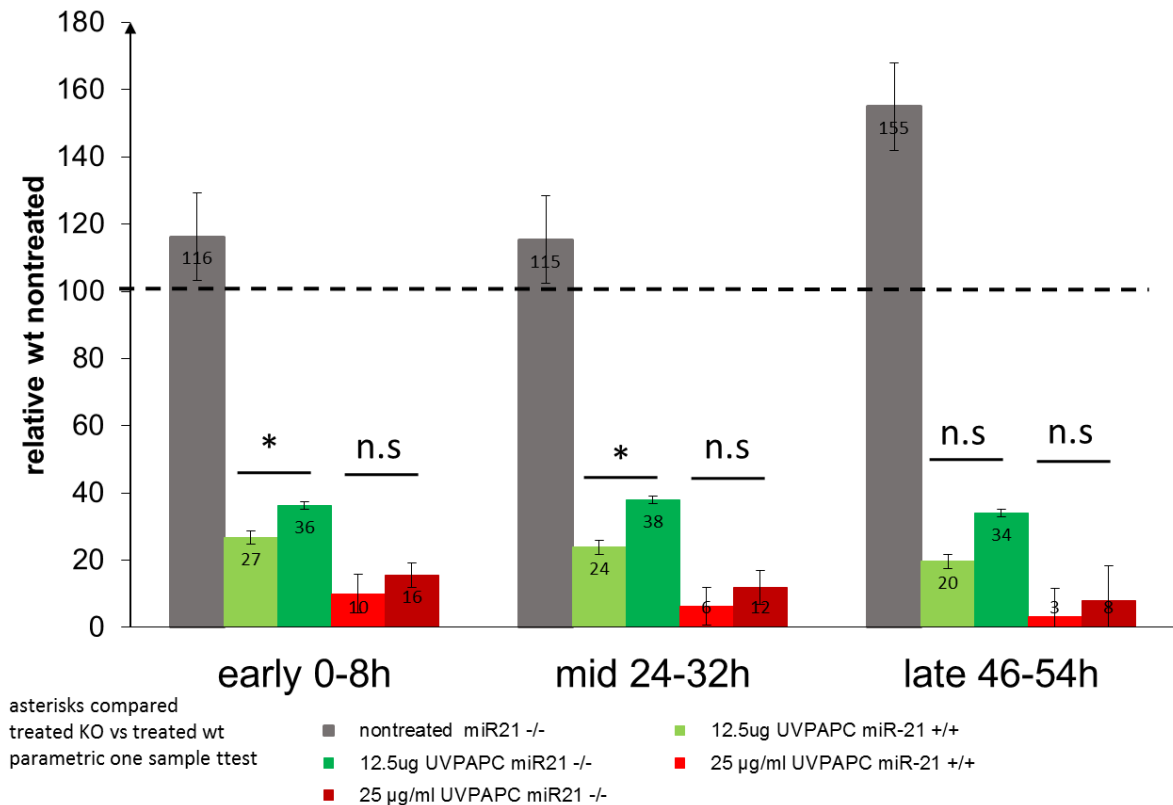


Figure 71 Growth advantage of miR-21 knockout cells under basal conditions and after exposure to oxidized lipids (UV PACP) for 24 hours. Metabolic activity of tail keratinocytes from miR-21 wt (+/+ light colours) and KO (-/- dark colours) mice, each nontreated and after 24 hours exposure to 12.5 µg/ml and 25 µg/ml UVPAPC. Metabolic activity was measured at early (8 h recovery), middle (24 h – 36 h recovery) and late timepoints (46 h– 53 h) of recovery. Data from 5 biological replicates are shown. Averages +/- stdev are derived from ratios. 2way ANOVA with Bonferroni post-test was used to estimate the effect of the 'treatment' and 'genotype', respectively. For the presented statistics we used one way ANOVA and tested 'treated +/+ vs 'treated -/-' nontreated wt (+/+) dotted line. P-value *** < 0.001, ** < 0.01, * < 0.05, > 0.05 n.s. non-significant. Light colours wt (+), colours KO (-/-), grey: nontreated, green: 12.5 µg/ml UVPAPC, blue: 25 µg/ml UVPAPC.

Due to the strong inhibitory effect of UVPAPC after 24 hours exposure, we reduced the treatment to a shorter period (6 h) of UVPACP incubation. With this strategy, we could not detect a significant difference between wt and KO cells (factor 'genotype'). Except after 48 hours (late) and 72 hours recovery (Table 5).

	Early		Mid		Late		Very Late	
	Variance	p-value	Variance	p-value	Variance	p-value	Variance	p-value
Effect of Treatment	33.54%	0,0035	37.63%	0,0018	46.32%	< 0,0001	29.36%	0,0053
Effect of Genotype	9.84%	0,0505	7.43%	0,0824	16.61%	0,0027	13.15%	0,0233

Table 5 Summary of 2 Way ANOVA after 6 hour stress treatment. A very significant effect of the treatment is apparent. There is no effect of the genotype at early and middle timepoints. A significant effect of the genotype is only after late (48h) and very late (72h) timepoints evident. The growth advantage of miR-21 knockout cells is considered very significant, independently ('factor genotype') or dependent (Factor 'treatment') of the treatment. The effect is sustained from early (16h) to late (40-48h) timepoints of recovery after the stress stimuli cisplatin and UVPAPC.

This finding might indicate that UVPAPC is potent and sensitive enough to impair the growth advantage of miR-21 knockout cells, while only a minor reduction of the average proliferative capacity is visible after comparing to nontreated cells (Figure 72). In addition, it points to a delayed response against short term incubation with UVPAPC and that miR-21 knockout cells develop their growth advantage over time.

Results

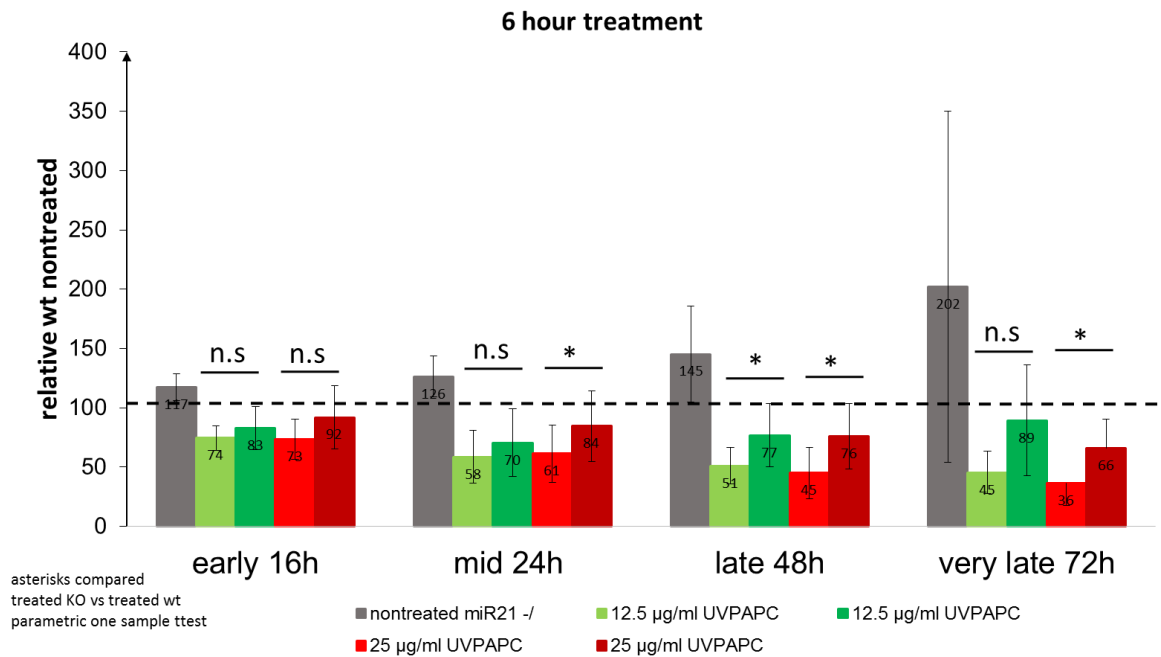


Figure 72 Proliferative capacity of miR-21 knockout cells under basal conditions and after exposure to oxidized lipids (UV PAPC) for 6 hours. Metabolic activity of tail keratinocytes from miR-21 wt (+/+ light colours) and KO (-/- dark colours) mice, each nontreated and after 6 hours exposure to 12.5 µg/ml and 25 µg/ml UVPAPC. Metabolic activity was measured at early (16 h recovery), middle (24 h recovery), late (48h) and very late (72h) timepoints of recovery. Data from 5 biological replicates are shown. Averages \pm stdev are derived from ratios. 2way ANOVA with Bonferroni post-test was used to estimate the effect of the 'treatment' and 'genotype, respectively. For the presented statistics we used one sample t-test to compare the pairs of 'treated +/+ vs 'treated -/-. P-value *** < 0.001, ** < 0.01, * < 0.05, > 0.05 n.s. non-significant nontreated wt (+/+) dotted line. Light colours wt (+), colours KO (-/-), grey: nontreated, green: 12.5 µg/ml UVPAPC, blue: 25 µg/ml UVPAPC.

To summarize, we detected a highly significant growth advantage of miR-21 KO cells compared to wt keratinocytes under basal conditions and after 24 hours of exposure to cisplatin. The exposure to 25 µg/ml UVPAPC for 24 hours turned out to impair the proliferative capacity of wt and knockout cells. Therefore, with a reduced incubation of 6 hours, we could not find a significant difference between wt and KO cells at an early timepoint of recovery, while it was evident at later timepoints.

The effect against 5 µM cisplatin was impressive. It seems that the miR-21 KO cells are indeed resistant against cisplatin showing no significant difference to nontreated cells while it reduced the activity of miR-21 wt cells significantly.

However, examination of the keratinocytes after the last timepoint of recovery, pointed to a growth arrested like phenotype in miR-21 wt cells. Contrary, we have the feeling that miR-21 KO cells are on the one hand resistant against stress stimuli, especially to 5 µM cisplatin, however, we observed more cell debris or apoptotic cells in the supernatants when comparing with wt cells (pictures not shown).

In order to find out whether miR-21 growth advantage and stress resistance is due to accumulating damage and whether the presence of miR-21 in normal proliferating cells confers protection, remains to be elucidated, in particular in terms of the miR-SASP.

4. Discussion

4.1. Why studying skin aging is important?

The skin, as the biggest organ of the human body is placed between in and outside and serve as a protective barrier against environmental hazards. Synergistic effects of intrinsic and extrinsic factors fastens the process of aging and act deleterious on skin homeostasis resulting in profound cellular, molecular and structural changes. The consequences and accumulations of those silent deteriorations coincided with impaired wound healing capacity, a declined regeneration potential leading to cutaneous irritations and potentially contribute to the development of systemic age-related diseases.

The main skin residents derive from two distinct germ layers, which makes this organ to an attractive model system to study intrinsic and extrinsic insults of age-related conditions. It was one of the first organs where senescent cells have been identified (Dimri, X. H. Lee, et al. 1995) and their increase in dermal as well as in epidermal layers of elderly (71 - 95 years) compared to young control group (below 20 years) underscores their accumulation with age (Ressler et al. 2006). The prevalence of senescent cells at sites of many age-related lesions and their health-promoting removal in transgenic mice (Baker et al. 2016) or by senolytics (Zhu et al. 2016; Wang et al. 2016; Chang et al. 2016; Eirin et al. 2014; Roos et al. 2016; Zhu et al. 2015; Yi Zhu et al. 2017) reflects their substantial influence on tissue homeostasis. It is in particular the acquiring of the SASP, a pro-inflammatory phenotype that is considered to contribute to signs of aging, frailty and to trigger the onset of several age-associated diseases.

Already several years ago, the idea came up whether secretory compounds present in the blood of young mice rejuvenate the skin of elderly (> 73 years) after xenografting. Gilhar and colleagues indeed observed an amelioration of age-related skin deteriorations and speculated that circulating factors derived from the young host mice favour the regeneration of aged tissue (Gilhar et al. 1991). Now 16 years later we can truly confirm this hypothesis, since myriad reports on secretory miRNAs describe their almost 'hormonal' action on recipient cells (Cortez et al. 2011) and their potential as therapeutic targets for age-associated diseases (reviewed by Jung & Suh 2014) or as easy accessible biomarkers (Cogswell et al. 2008).

The presence of senescence associated extracellular miRNAs in the circulation of several body fluids, enclosed in protective vesicles or protein complexes, makes them to small multifaceted paracrine communicators of age-related processes. However, while many protein factors were explained to be part of the senescent secretome, the question emanates whether secreted miRNAs, especially those enclosed in extracellular vesicles might also be part of the SASP from dermal fibroblasts.

4.2. Specifically packaged miRNAs in extracellular vesicles are novel members of the senescence-associated secretory phenotype

Mounting evidences directly link increased levels of secretory vesicles to ATP relying (Bianco et al. 2005) stress and inflammatory conditions. Either serum starvation (Wang et al. 2010), irradiation (Arscott et al. 2013) hypoxia (de Jong et al. 2012), oxidative burden (Eldh et al. 2010), diseases (Chistiakov et al. 2016) or normal physiological processes in terms of cellular aging (Lehmann et al. 2008; Joshi et al. 2014) triggered an augmented EV secretion in distinct cell types. In line with this observation, we also detected a 4-fold higher secretion of small EVs from senescent HDF compared to nontreated control cells. Such an increase is considered to be mediated by p53 activation in response to DNA damage (Yu et al. 2006), but also changes in membranous lipid compositions as a consequence of UVA irradiation (Wäster et al. 2016) stimulate a ceramide depended rise in EV shedding (Kosaka et al. 2010; Trajkovic et al. 2008; G. Wang et al. 2012; commented by Budnik et al. 2016). Recent implications propose a related increase of EVs in tissues of atherosclerotic aortas (Perrotta et al. 2016) where senescent endothelial and vascular smooth muscle cells are known to accumulate (Fenton et al. 2001; Baker et al. 2016). Similarly, EV increase in cerebrospinal fluid of Alzheimer's disease patients was found (Agosta et al. 2014), where also senescent astrocytes were reported to contribute to the SASP (Bhat et al. 2012). It is therefore intriguing to speculate that senescent cells might also secrete more EVs *in vivo*.

As a consequence of elevated small EV secretion, senescent fibroblasts showed an increased abundance of almost all EV-miRNAs compared to nontreated control cells. The most abundantly secreted miRNAs, seem to target pro-apoptotic mediators involved in longevity, nutrient sensing pathways and cancer signaling, thereby conferring protective functions on their environment, as it was already suggested by others (Cheng et al. 2014; Y. Zhou et al. 2013; Eldh et al. 2010; Livingston & Wei 2016). These findings in the context of cellular senescence are indeed conceivable, since secretory compounds of senescent cells have been shown to induce bystander senescence to abort uncontrolled proliferation as a way of tumor suppression (Acosta et al. 2013). Also EVs and irradiation induced changes of their miRNA composition mediated bystander effects on recipient cells (S. Xu et al. 2015).

Indeed, not only the entire abundance of EV secretion from HDF was altered, but also differences in miRNA composition of EVs from senescent versus control cells have been discovered. We found miR-23a-5p and miR-137 more abundant, while five miRNAs, including miR-17-3p and miR-199b-5p, were less abundant per vesicle from senescent cells. Several of these miRNAs were found to be regulated intracellularly in the same manner. While miR-23a-5p is also upregulated in senescence-induced by PUVA treatment (J. Zhang et al. 2016), miR-137 was induced in senescent fibroblasts (Neault et al. 2016) and keratinocytes (Shin et al. 2011). MiRNA-17-3p is also commonly downregulated in several models of replicative and organismal aging (Hackl et al. 2010, reviewed by Grillari et al. 2010), as well as miR-199b-5p in skin of elderly (Hackl et al. 2010) and in senescence of mesenchymal stem cells (Yoo et al. 2014).

Comparable differences in miRNA abundance of EVs have been detected over the timecourse of osteogenic differentiation (J.-F. Xu et al. 2014), as well as in proliferating versus differentiated keratinocytes (personal communication M. Mildner not published). Interestingly, even between Caucasian versus Black NHEK and after

their irradiation, differences in miRNA composition of EVs were uncovered (Cicero et al. 2015). Based on these phenomenon, the question arises whether change in EV composition relays on differences in transcriptional abundance, or if the mere introduction of physiological stimuli modulate the selective secretion or retention of specific miRNAs?

In order to pursue our ideas, we quantified intracellular miRNA transcription of senescent versus quiescent fibroblasts and could confirmed several miRNAs that were already reported to be differentially expressed in replicative or UVB induced senescence of fibroblasts (Greussing et al. 2013; Napolitano et al. 2014; Marasa et al. 2010; Maes et al. 2009; Dhahbi et al. 2011; Mancini et al. 2014). several of these were also found in the dermis of elderly (Li et al. 2016), where estimates from a non-human primate study (Herbig et al. 2006) and from human skin biopsies (Ressler et al. 2006) suggest an accumulation of senescent cells with donor age. In addition, several miRNAs were identified so far not yet described in fibroblast senescence, such as miR-1197 and miR-450-2-3p.

Finally, we wanted to find out whether specific EV-miRNA packaging is influenced by changes in cell physiology such as the induction of cellular senescence, or if high transcriptional abundance correlates with EV enrichment, occasionally referred as a sort of 'mirroring effect. With that question we have hit a highly discussed topic of the EV field, since it is still not universally supported if EV packaging is a directed mechanism or a passive form of garbage disposal as an alternative way of miRNA degradation, as we discussed it earlier in '1.4.3 The butterfly effect - RNA sorting and trafficking'. Although it is intriguing to assume that the many changes in recipient cell behaviour after EV mediated uptake of miRNAs (Cicero 2014; Weilner et al 2016; Valadi et al 2007; Mittelbrunn et al, and reviewed by (Zhang et al. 2015; Fritz et al. 2016) would not require specifically regulated packaging mechanism that are able to respond to environmental conditions or intracellular stimuli in terms of selecting the cargo of EVs. On the contrary, recent evidences abrogate a 'hormone' like effect of EV-containing miRNAs due to their low abundance in the circulation, when compared to other extracellular miRNA carrier (discussed by Turchinovich et al. 2016).

However, what is known so far? It is proposed that some miRNAs are indeed selectively packaged into EVs, when correlating to their intracellular miRNA abundance, either under basal, tumorigenic, or stress conditions (Eldh et al. 2014; Guduric-Fuchs et al. 2012; Ohshima et al. 2010; van Balkom et al. 2015; Pigati et al. 2010; Xiao et al. 2012; Fiskaa et al. 2016; Tosar et al. 2015; Kogure & Lin 2011; Baglio et al. 2015) such as serum starvation (Wang et al. 2010) and irradiation (Arscott et al. 2013). However, we found only few reports that cover changes in EV-miRNA packaging due to external stimuli including, differences in KRAS mutation status of isogenic cell lines (Cha et al. 2015) and changes in EV-miRNA composition of PBMCs (Yentrapalli et al. 2017) after irradiation, while no reports exist that compared changes in intracellular and vesicular miRNA abundance after induction of senescence.

Therefore, we correlated intra- versus extracellular miRNA levels. Overall, most miRNAs are as abundant intracellularly as extracellularly, suggesting that for the majority of miRNAs the extracellular environment seems to mirror the cytoplasm. However, we also provide evidence that around 24% of all miRNAs included in the correlation approaches, are selectively packaged into small EVs in response to cellular senescence, while the remaining ones are evenly distributed between cells and EVs. This finding supports the idea that some miRNAs are sorted into EVs in a selective and regulated manner and is in line with several reports showing an active mechanism of miRNA packaging into exosomes (Pigati et al. 2010; Ohshima et al. 2010; Guduric-Fuchs et al. 2012; Cha et al.

2015; Ji et al. 2014; Belleannée et al. 2013; Tosar et al. 2015; van Balkom et al. 2015; Mittelbrunn et al. 2011). several factors contributing to a selective packaging have been reported so far: (i) It can be orchestrated by sumoylation on ribonucleoproteins (Villarroya-Beltri et al. 2013) and their binding to specific sequence motifs (Villarroya-Beltri et al. 2013), often with non-template terminal nucleotide additions rich in 3' uridylation (Koppers-Lalic et al. 2014). (ii) It can be directed by Y-box proteins (Shurtleff et al. 2016), (iii) synaptotagmin-binding cytoplasmic RNA-interacting proteins (Santangelo et al. 2016) or (iv) the phosphorylation of Ago2, a component of the RNA-induced silencing complex (RISC) (McKenzie et al. 2016). Furthermore, (v) a miRNA sequence independent mechanism guided by distinct (vi) ribonucleoproteins relevant for RNA stability and transport (Collino et al. 2010; Wang et al. 2010) and (vii) accessory proteins involved in biogenesis of multivesicular bodies and membrane trafficking such as Alix (Iavello et al. 2016), TSG101 (Melo et al. 2014), the Rab proteins Rab7A and RAB27 and neural sphingomyelinase 2 (nSMase2) (Kosaka et al. 2010) have been described to be involved in specific miRNA loading. Finally, (viii) even miRNAs as endogenous stimuli can influence specific loading, as has been shown by overexpression of miR-146a-5p in HEK293 cells, which resulted in enrichment of several EV-miRNAs, while others remained constant (Guduric-Fuchs et al. 2012). However, if this mechanism is dependent and directed by downstream target regulations or on transcriptional level has not been addressed. Although the passive form of 'garbage disposal' as an alternative way of bulk miRNA degradation has also been suggested, our data in addition to the many changes in recipient cell behavior after EV mediated uptake of miRNAs (Valadi et al. 2007; Mittelbrunn et al. 2011; Skog et al. 2008 and many others) support the idea of a specifically regulated packaging mechanism as consequence of physiological and pathophysiological stimuli.

What effect on the microenvironment might such specifically packaged miRNAs have? And which miRNAs are now selectively secreted in cellular senescence and thus able to send distinct messages to their environment?

One prominent example to address these questions is miR-15b-5p, which we identified here to be selectively packaged and secreted by senescent cells. Intracellularly, we found miR-15b-5p to be downregulated in senescence as it was reported before (Lang et al. 2016). The fact that it is preferential packaged and secreted in senescence might be an additional mechanism to keep miR-15b-5p levels low within fibroblasts. Decrease of miR-15b-5p de-represses SIRT4, which has a regulatory role in stress-induced senescence-associated mitochondrial dysfunction (Lang et al. 2016) and in driving a NF- κ B mediated induction of the SASP (Kang et al. 2015). This is consistent with our data, where we see an induction of NF- κ B signaling in SIPS cells, as determined by biostatistical pathway analysis and in addition, the de-repression of known SASP components such as IL-8 (CXCL8), MCP-1 (CCL2), RANTES (CCL5), GRO α (CXCL1), INHBA (Lämmermann et al. in preparation). Specifically, miR-15b-5p seems to confer a crucial fine-tuning mechanism, similar to the 'inflammamiR' miR-146a/b (Taganov et al. 2006; Li et al. 2010), by dampening excessive secretion and transcription of SASP components (Bhaumik et al. 2009). In accordance to these *in vitro* data, miR-15b-5p was also found to be down-regulated *in vivo* in photo-aged and non-photoaged skin (Lang et al. 2016). Interestingly, it is lowly abundant in the dermis of skin biopsies derived from young individuals and elderly, while it appears highly enriched in the epidermis (Lang et al. 2016). Thus, it is tempting to speculate that the low dermal levels versus high epidermal levels are caused by an EV-miRNA crosstalk between fibroblast vesicles and keratinocytes. Such miRNA dependent crosstalk has already been described between senescent endothelial cells and mesenchymal stem cells (Weilner, Schraml, et al. 2016a). But also skin

cells communicated in a EV-miRNA dependent manner, between keratinocytes and melanocytes (Cicero et al. 2015) and thus strengthening our speculation.

Additionally, miR-17-3p, a member of the miR-17-92 cluster, described as oncogene as well as a factor modulating the life span of mice (reviewed by Dellago et al. 2016) is preferentially retained by senescent cells, but not in quiescent. The same is true for miR-199b-5p, which was also found significantly down regulated intracellularly in senescent cells (Favreau et al. 2015), less abundant per vesicle from senescent cells, and selectively retained in SIPS.

Interestingly, several miRNAs including miR-122-5p (P. Li et al. 2015b; Jiang et al. 2016), miR-21-3p (Ahmed et al. 2011), miR-376a-5p (Hildebrand et al. 2011), miR-378b which is highly similar to miR-378a-3p (Wang et al. 2015) and miR-17-3p (Wu et al. 2012) are connected to keratinocyte differentiation and/or proliferation, suggesting that senescent fibroblasts derived EV-miRNAs indeed communicated and impact on epidermal function.

Taken together, we conclude that miRNAs are specifically packaged depending on cellular conditions and/or external stimuli. The specific molecular mechanism of selective release and retention of senescence-associated EV-miRNAs and the miR-SASP crosstalk between different cell types and its consequences in the context of aging and age-associated diseases, however, remains largely to be discovered. Finally, we suggest that small EVs and EV-miRNAs are novel, *bona fide* members of the SASP, for which we suggest to use the term 'miR-SASP'.

4.3. Extracellular vesicles as paracrine communicators between skin residents

Considering that senescent cells secreted increasing amounts of EVs, and having identified differentially distributed and selectively secreted EV-miRNAs of senescent fibroblasts, it is tempting to speculate that they might interfere with neighboring cells to confer paracrine bystander effects on other skin residents. A growing body of literature already examined a cell-non autonomous skin communication via soluble factors (reviewed by Demaria et al. 2015) and their impact on skin functionality during wound healing, differentiation and malignancies. Whereas more detailed information to EV-mediated crosstalks, with a strong focus on keratinocyte EVs has only emerged within the last few years.

Under basal conditions keratinocyte derived EVs are able to attach to fibroblasts in 2D cultures and to regulate their gene and protein expression in a concentration depended manner (Huang et al. 2015). Consequently, initiation of an inflammatory cascade and an increased wound healing capacity was observed after co-incubation with keratinocyte EVs (Huang et al. 2015). Whether these effects are a result of EV uptake and subsequent post transcriptional regulations, or if the mere presence of EVs exerted this effect was not tested in this context. It is feasible to assume such a phenomena, since EVs per se are crucially involved in pro-inflammatory process and constituted with a huge regenerative potential. On the contrary, a direct uptake mechanism of fluorescently labelled melanocytic EVs from keratinocytes was confirmed by flow cytometry and after life cell imaging that was even amplified upon UVA stimulation of the donor cells (Wäster et al. 2016). In a similar study, but vice versa, EV secretion of keratinocytes was stimulated with UVB irradiation and their internalization from melanocytes triggered melanin synthesis (Cicero et al. 2015). The main mediator identified in this study, was a keratinocyte derived EV-miRNA, enriched after UVB stimulation and proficient to increase the melanin content in melanocytes,

while its inhibition alleviated pigmentation efficiency in keratinocytes (Cicero et al. 2015). However, to our knowledge no reports cover fibroblast derived EVs and their miRNA crosstalk with keratinocytes. In addition, we found only one study providing considerable indications for the *in vivo* presence and probably secretion of EVs in the dermis as visualized with a 3D electron microscopy technique in human skin sections (Cretoi et al. 2015). The reconstruction of the 3D structure of telocytes, embedded in the papillary dermis, revealed the surrounding of around 30 EVs per cell (Cretoi et al. 2015). Telocytes are interstitial cells, widely distributed and mainly detected adjacent to stem cell niches in distinct tissues and organs, among those also the skin (Ceafalan et al. 2012). They are considered to transfer EV-miRNAs to hematopoietic stem cells as it was tested in mouse and rat telocytes isolated from cardiac tissue (Cismasiu & Popescu 2015). It is thus very likely that EV containing miRNAs are similarly shuttled between dermal telocytes and skin stem cells and thus able to regulate skin homeostasis and regeneration in a post transcriptional manner.

Consequently, the question came up, if EVs in the skin are able to pass through the dense structure of the ECM? Previous studies mainly focused on the EV crosstalk between melanocytes and keratinocytes. Probably because they are both embedded in the epidermal layer, while a fibroblast to keratinocyte *in vivo* crosstalk would imply a transfer through the mesh-like collagen matrix. In order to validate an EV-miRNA crosstalk between fibroblasts and keratinocytes, we first established a 'traditional' co-culturing experiments using keratinocytes incubated with EVs derived from pre-transfected *C.elegans* (cel-miR-39) HDFs in 2D monolayer cultures. We indeed found cel-miR-39 in respective keratinocyte samples and adapted the current setup to 3D *in vivo* mimicking human skin equivalents (HES). Therefore, *C.elegans* transfected HDF were embedded into a collagen matrix. Six fold more keratinocytes were set on the top and incubation at an air-liquid interface allowed differentiation. After one week, the dermis and epidermis of functional HSE were separated and analysed by qPCR. To this end, we could detect cel-miR-39 in respective epidermal layers, pointing to an EV-miRNA crosstalk through the collagen matrix. In order to support our results ultrastructural analysis of human skin sections confirmed the presence of (i) MVB within keratinocytes and fibroblast, the occurrence of (ii) single EVs and (iii) TSG101 positive EVs within the extracellular space, in the collagen matrix as well as in the basal layer of keratinocytes.

These findings either in 2D, 3D HSE or in human skin sections, provide compelling evidences for an EV and/or EV-miRNA crosstalk between fibroblasts and keratinocytes through the ECM. However, we still cannot be sure if the EV cargo entered the keratinocytes *in vivo*. Therefore, to reliably ascertain that internalization of EV-miRNAs impact on transcriptional regulation rather than on uptake for lysosomal degradation or only attachment to the plasma membrane of recipient cells, the introduction of a Cre reporter system would elegantly confirm a functional transfer *in vivo* (Zomer et al. 2016; Zomer et al. 2015). The integration of Cre-lox recombinase in reporter cells (NHEK) and overexpression of fluorescently labelled Cre constructs in the donor cells (HDF), would allow the identification of functionally internalized EV-RNAs. We will then extend the system to an established mouse model and/or inject the Cre⁺ and Cre reporter⁺ cells, to investigate the crosstalk, specifically restricted between keratinocytes and fibroblasts *in vivo*. This system was established in a kind of 'milestone paper' of the EV field, showing EV enclosed RNAs to be functionally transferred through the blood brain barrier (Ridder et al. 2014).

To sum up, we have shed new light on cell non-autonomous communication between dermal and epidermal cells. We have confirmed an EV-miRNA crosstalk in 2D and 3D *in vivo* mimicking skin models and substantiated a miRNA

transfer through the collagen matrix. Supportive to that, we provide substantial indications for the presence of EVs in human skin, widely distributed between distinct skin residents as well as in the ECM. We are now excited to establish an *in vivo* model system to confirm a dermal fibroblast induced EV crosstalk with epidermal keratinocytes and their ability to interfere with the transcriptional machinery of the target cells.

4.4. The EV-miR SASP of fibroblasts modulates the wound healing capacity and differentiation of keratinocytes

The detrimental effect of the SASP is a pivotal and yet accepted characteristic of senescent cells and affects the entire systemic environment of elderly. Loss of regenerative potential and impaired tissue homeostasis triggers chronic wounds and delayed healing rates, still one of the most prevalent issue of geriatric patients. The reasons are manifold and each stage of the wound healing process is impaired by distinct age-related changes, which makes it still difficult to find proper therapies. However, it is obvious that the decline and weakening of the immunosurveillance with age is a fundamental driver of age-associated healing complications. In addition, ECM remodelling and re-epithelisation are elementary parts for tissue repair. An excess secretion of MMPs (Ashcroft et al. 1997) as part of the SASP, is thought to enhance collagen degradation leading to impaired contraction of wounds in fibroblasts from old rats, which delays wound closure (Ballas & Davidson 2001). On the contrary, the transient presence of MMPs facilitates collagen degradation, elementary for fibrosis free-healing processes. In particular, the transient presence of senescent cells and their secretory compounds limit fibrosis and promotes wound healing (Demaria et al. 2015; J.-I. Jun & Lau 2010b; J. II Jun & Lau 2010).

With the notion that most probably paracrine mediators regulate the crosstalk of numerous cell types at sides of wounds (Collino et al. 2010; Bruno et al. 2012; Lai et al. 2010; reviewed by Rani et al. 2015), the idea came up that EVs from skin cells might contribute to this processes. Especially, due to promising *in-vivo* indications, showing EV-like structures adjacent to wounds from human skin biopsies (Huang et al. 2015).

Based on those preliminary observations, we assessed if EVs from senescent fibroblasts modulate the wound healing kinetics of keratinocytes when comparing to non-senescent derived EVs. Intriguingly, we observed an amelioration of wound closure of keratinocytes after 48 hours exposure to EVs from senescent fibroblasts.

However, what are then underlying mechanism why elderlies are faced with delayed wound closure when the presence of senescent cells favours the healing process? The probably most important step in this scenario, is the removal of senescent cells by immune cells, which is disturbed in elderlies. Otherwise, the accumulation of senescent cells and the chronic presence of the SASP would initiate a vicious cycle of tissue derogatory effects leading to impaired differentiation, skin atrophy and loss of protective barrier function.

In order to test if the chronic presence of the EV-SASP governs such an impairment, keratinocytes were incubated with EVs from senescent and control cells for one week and their differentiation capacity was evaluated. An inhibitory effect of the differentiation potential was evident when exposed to EVs from senescent fibroblasts for an entire week. Concluding, we can substantiate the double edged role of the SASP by extending its culprits to EVs,

showing their beneficial effect after short term exposure, while its persistent presence affects the regeneration and differentiation capacity negatively.

Considering the fine-tuning ability of miRNAs during distinct wound healing phases and cellular senescence, their dynamic occurrence is probably regulated in an EV depended manner. In addition, based on recent studies, showing an impact of senescence-associated EV-miR-31 on osteogenic differentiation (Weilner, Schraml, et al. 2016b) and EV-miR-213 as a negative regulator of cellular senescence (Balkom et al. 2016), we hypothesize that the miR-SASP of fibroblasts identified in our previous study (Part A) might have a profound impact on neighbouring cells.

Within that miR-23a-3p turned out to be an interesting candidate, as it is one of the most highly secreted miRNA of fibroblasts. Interestingly, we also identified its 5p-fragment, differentially present in EVs of senescent fibroblasts (SIPS-EVs). Finding both miRNAs significantly secreted might be an indicator for their biological significance in the extracellular environment. In addition, miR-23a-3p was repeatedly connected with cellular senescence and skin aging (Dreesen, Chojnowski, et al. 2013; Röck et al. 2014; Z. Guo et al. 2013; Luo et al. 2015), strengthening our deliberation to further investigate its role in the crosstalk of fibroblasts and keratinocytes.

Therefore, miR-23a-3p levels of keratinocyte were determined after short term incubation with EVs and we detected a significant rise after incubation with SIPS-EVs, pointing to its internalization. Consequently, its overexpression mimicked the EV-SASP in terms of wound healing improvement, while we could not detect an effect on basal differentiation.

Although we see no effect of miR-23a-3p on keratinocytes differentiation, we still have to determine whether the lack of a differentiation phenotype is due to (i) loss of miR-23a-3p after one week post transfection, (ii) due to a missing exogenous stimulus of differentiation or if indeed a different mediator of the miR-SASP fulfils the modulatory role on differentiation. It remains to be elucidated, if another miRNA, or a combination of miRNAs, as part of the miR-SASP exert the inhibitory effect on differentiation.

To conclude, we speculate that an increased secretion of SIPS derived EVs and thus a concomitant amplification of miR-23a-3p levels present in the extracellular environment, allow its internalization to mediate an effect on wound healing, while the chronic presence of the miR-SASP impairs differentiation (Figure 73).

We therefore, suggest miR-23a-3p as a mediator or 'miRdiator' of the transient miR-SASP. Whether and how other mediators of the miR-SASP impact on keratinocyte functionality and if the miR-SASP or EV-miR-23a-3p interferes with the transcriptional machinery of keratinocytes is as yet not known.

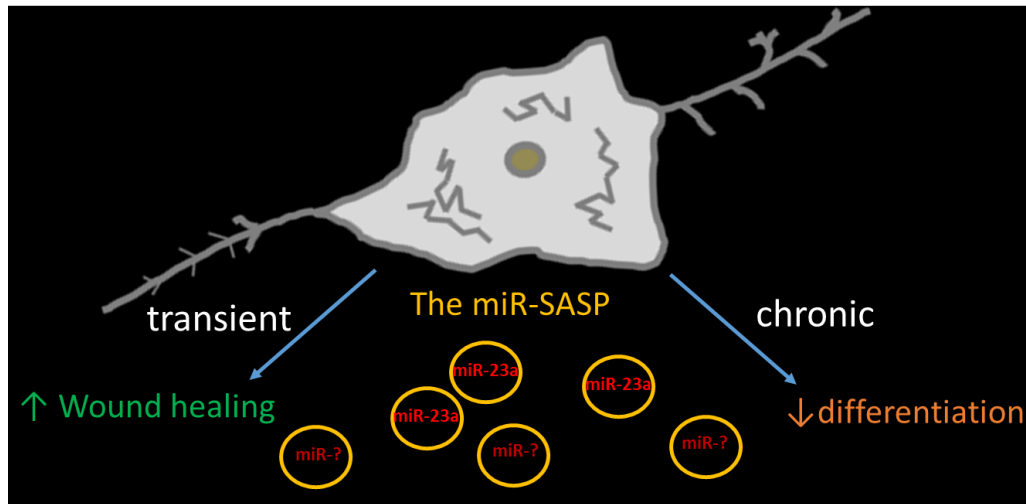


Figure 73 Hypothesis on the role of the miR-SASP. An increased secretion of EVs and their miRNA cargo elevates the levels of miR-23a-3p and many other. When taken up by keratinocytes their transient presence accelerated wound healing, while the chronic exposure results in an impaired differentiation. Whether miR-23a-3p is a mediator of the miR-SASP remains to be elucidated.

So what do we know about miR-23a-3p in the context of skin aging?

4.5. miR-23a-3p a mediator of the miR-SASP

miR-23a-3p was repeatedly reported to be intracellularly upregulated during cellular senescence of endothelial cells (H. Dellago et al. 2013) and dermal fibroblasts (Röck et al. 2014). Its direct interaction with telomeric repeat binding factor 2 (TRF 2) triggers telomere attrition, irreversible growth arrest and accumulation of SA- β -Gal positive cells (Luo et al. 2015). Its activity gradually increases with age as determined in skin sections of old mice and in fibroblasts derived from donors of various ages (Röck et al. 2014). miR-23a-3p was found to be upregulated in UVB (Z. Guo et al. 2013) and PUVA stimulated senescence of fibroblasts (J. Zhang et al. 2016) and accelerated the repair of cyclobutane pyrimidine dimer in a human keratinocyte cell line (Z. Guo et al. 2013). In addition, overexpression of miR-23a-3p induced cellular senescence and reduced hyaluronan (HA) secretion by directly targeting hyaluronan-synthase 2 (HAS2). Accordingly, age-associated reduction of HA and the induction of the senescence marker p16, p21 and SA- β -Gal were obvious in fibroblasts derived from elderly (> 60), when compared to cells from young individuals (< 35). This response was rescued upon HAS2 inhibition or silencing of miR-23a-3p. HA as an unbranched glycosaminoglycan polymer, is an essential component of the ECM and important for skin elasticity and for hydration. Chronic inhibition of its synthesis (HAS2) for two weeks caused reduced viscoelasticity, decreased skin moisture and a wrinkled skin phenotype. Finally, a strong induction of miR-23a-3p and a reduction of HA were evident after 48 weeks of chronic HAS2 inhibition (Röck et al. 2014).

Another target of miR-23a-3p, identified in senescent fibroblasts and aged human tissue is lamin B1 (LMNB1). LMNB1 deregulation lies on the crossroad between diseases and aging and causes progeroid diseases such as Hutchinson Gilford syndrome when downregulated, or ataxia telangiectasia upon gene duplication (reviewed by Dreesen, Ong, et al. 2013). It is highly involved in a plethora of essential cell cycle processes and its inhibition

triggers premature DNA damage-induced senescence and halts proliferation (Dreesen, Chojnowski, et al. 2013). Interestingly, miR-23b-3p, which differs only in 2 nucleotides, is induced upon keratinocyte differentiation, while its inhibition increased epidermal thickness, considered as a sign of hyperproliferation (Barbollat-Boutrand et al. 2016).

Based on literature and putative predictive algorithms (Agarwal et al. 2015) miR-23a-3p targets many EMT and wound healing related genes. Plakophilin 4 (PKP4/p0071), a putative target maintains the mechanical strength versus cell migration by interacting with the desmosomal plaques and the adherens junctions (Calkins et al. 2003). It inhibits wound closure, while preserving mechanical strength of epithelial cells (Setzer et al. 2004). HAS2, a validated target of miR-23a-3p, modulates terminal differentiation and stimulates wound healing capacity in a KGF depended manner (Karvinen et al. 2003). It facilitates embryonic EMT in cardiac development (Camenisch et al. 2001) and was shown to contribute to tumor invasiveness and progression (Bernert et al. 2011).

After reviewing our results, either after transient incubation with SIPS EVs and after OE of miR-23a-3p, we noticed such an evident epithelial to mesenchymal transition (EMT) phenotype. The migration of single cells with distinct fillopodien point to reduced cell-cell junctions after miR-23a OE that attracted our attention. Similar findings of an EMT phenotype in lung cancer cell strains have been observed after miR-23a OE by directly targeting E-cadherin (CDH1) (Cao et al. 2012).

Either way, it becomes evident that HAS2 as well as Plakophilin are in-between a dynamic network of migration and differentiation, while their balanced fine-tuning is essential for vital functions of epithelial tissue. Intriguingly, they are both significantly decreased in aged keratinocytes (Gruber, Narzt unpublished). Thus, it is tempting to speculate that secretory miR-23a-3p contributes to age related loss of the fine-tuning ability of keratinocytes to regulate functional wound healing and differentiation.

However, during our study, we were not able to see transcriptional changes of HAS2 either after overexpression of miR-23a-3p or after SIPS-EV incubation. Nonetheless, neither HAS2 protein levels nor Plakophilin 4 expression were determined until now.

Finally, to this end, we could identify one crucial mediator of the miR-SASP and its effects on keratinocyte functionality. We cannot rule out, and it is very likely that the complementary contribution of several miRNAs of the miR-SASP orchestrate paracrine EV mediated bystander effects on neighbouring cells.

4.6. Aging or dying? Is the miR- SASP a mediator of apoptosis resistance?

An important feature of senescent cells is their ability to activate pro-survival pathways and to resist apoptosis (reviewed by Childs et al. 2014; and Campisi 2003). Considering an increase of senescent cells with age, this could be an additional reason for their accumulation and their prolonged sustaining effects on gene expression and on the secretory behaviour. However, that is not universally supported.

Induction of apoptosis highly depends on concentration of the inducer, on the stimuli itself as well as on the cell type (reviewed by Childs et al. 2014). Fibroblasts and keratinocytes are highly resistant against genotoxic (Seluanov et al. 2001) and cytotoxic stimuli (Hampel et al. 2004) although their underlying pathways differ. Keratinocytes

activate NF- κ B signaling (Chaturvedi et al. 1999), which stimulates the expression of many apoptosis inhibitors (reviewed by Nakano 2004). Fibroblasts' resistance requires p53 destabilization and highly depends on the concentration of apoptotic stimuli. However, keratinocytes and fibroblasts are both supported by the protective activity of Bcl-2 (Wang 1995; Sanders et al. 2013; Takahashi et al. 2001) and are among the long lived senescent cell types that undergo necrosis (Seluanov et al. 2001) or autophagy (Gosselin et al. 2009) rather than apoptosis. On the contrary, endothelial cells, the main cell type lining the blood vessels of veins and arteries, are highly susceptible for apoptosis when turned into senescence (Zhang et al. 2002; Hampel et al. 2004).

But is the chronic pro-inflammatory signaling network of the SASP able to communicate protective, anti-apoptotic messages? This question sounds ambivalent, in particular because of its tumorigenic potential.

Apparently, however, the SASP and normal apoptosis use similar 'disposal' mechanisms. Natural killer cells (Krizhanovsky et al. 2008) and phagocytosis (Kang et al. 2011) direct 'normal' apoptosis or SASP-induced immunosurveillance to clear damaged and senescent cells (reviewed by Erwig & Henson 2007). However, bystander senescent macrophages (Hall et al. 2016) and a decline in the immune system impair proper removal and might reflect an increased probability for apoptosis resistance. Indeed, a recent study supports this idea and finds a prominent anti-apoptotic signature in the supernatants of senescent mesenchymal stem cells. Independently of the senescent stimuli, they detected five protective proteins that are reported to sit on the crossroad between apoptosis and survival (Özcan et al. 2016), which points to a pro-survival mechanism of the SASP.

Strikingly, our biostatistical pathway analysis of the most highly secreted miRNAs as part of the miR-SASP identified the collective targeting of five pro-apoptotic mediators suggesting again an anti-apoptotic activity of the SASP.

Dying or aging? Both protective measure with the same intrinsic objective, to abrogate further damage and malign transformations. Whether the SASP is a passive mediator or actively involved lacks functional evidences, but EV-miR-21-5p might be a prominent miR-SASP candidate in this context.

miR-21 was the most abundantly secreted miRNA of fibroblasts identified earlier (Part A) and directly targets components of the p53 signaling pathway (Hanna Dellago et al. 2013; Hammond 2006; He et al. 2005). Among those phosphatase tensin homologue (PTEN), which we unravelled as a target of the anti-apoptotic capacity of the miR-SASP (Part A).

Apparently, we are now dealing with a pleiotropic role of miR-21-5 and its target PTEN. Although miR-21 is one of the most published 'onco-miR', aberrantly expressed in many solid tumor types and cancerous cell lines, we found it upregulated in senescent endothelial cells and its overexpression induced a senescent-associated growth arrest. Similarly, PTEN, commonly found to be mutated or inactivated in malignant conditions, most probably as a consequence of miR-21-5p (reviewed by Ortega-Molina & Serrano 2013). Contrary, PTEN loss is also associated with the induction of senescence in prostate cells (Manda et al. 2016) and its downregulation in senescent fibroblasts is thought to contribute at least in part, to the secretion of the SASP components IL6 and MMP2 (Kabir et al. 2016). However, to disclose in a further step whether the miR-SASP and highly secreted EV-miR-21 confers

Discussion

an anti-proliferative and protective function on epidermal cells, we initially, tested whether miR-21 knockout keratinocytes are more susceptible to stress stimuli.

Similar to our previous findings after stable miR-21 inhibition using sponges in endothelial cells (Hanna Dellago et al. 2013). miR-21 knockout cells obtained a growth advantages compared to wildtype control cells. Even upon treatment with the interstrand crosslink inducer cisplatin and cells maintained their growth advantage that in the case of low doses of cisplatin, even exceed the proliferative capacity of nontreated knockout cells. However, exposure to oxidized lipids aggravated the growth advantage of miR-21 knockout cells. Although not quantitatively determine, we have the feeling that miR-21 inhibition increased not only the proliferative capacity, but also the amount of apoptotic cells in the supernatant, while the morphology of wildtype cells rendered a senescence-like growth arrested after exposure to stress stimuli.

Our hypothesis would make sense, since inhibition of miR-21 increased the sensitivity against cisplatin and therefore enhanced the success of chemotherapy in gastric- (S. Yang et al. 2013) and small cell carcinomas of the lung (L. Xu et al. 2014).

However, to this end, we could not determine whether normal proliferating miR-21 deficient keratinocytes increase their pro-apoptotic pathways in a similar apoptotic manner as reported from tumorigenic cell lines. In addition, the disclosure of the underlying mechanism of the increased stress resistance of miR-21 knockout cells will probably shed new light on miR-21 and its role in normal proliferating cells.

Finally, we are excited to determine if the miR-SASP confers protection on its environment and probably it turns out that the secretory EV-miR-21-5p is crucially involved in the maintenance of cellular senescence in order to abrogate malign transformations.

5. Material and Methods

Data and experimental procedures were recorded in registered lab journals following good laboratory practice (GLP). Property of University of Natural Resources and Life, Department for Biotechnology: Lab book 99/2013, Lab book 85/2014, Lab book 19/2016.

If not otherwise stated, all experiments were performed at room temperature

Cell Biology Methods

5.1. Primary cell culture

Antibiotic free cell culture experiments were performed under sterile working conditions in a laminar flow hood. Media and all reagents were warmed to room temperature (RT) before use. For routine culture, cells were cultivated in 25 cm² (T25), 75 cm² (T75) or 175 cm² (T175) Roux flasks (Corning) or in cell culture plates from under normoxic conditions at 37°C and 7% CO₂ in a HERAcell 150i incubator (Thermo Scientific). Centrifugation steps were conducted with sterile falcon tubes at RT. Before harvesting of cells, they were washed twice with Dulbecco's phosphate buffered saline (PBS) (L1820 Biochrom). Primary human dermal fibroblasts (HDF) and normal human epidermal keratinocytes (NHEK) were detached using 0.1% Trypsin/0.02% EDTA. Tail keratinocytes of mice were trypsinized with 0.25% Trypsin/0.02% EDTA

Human Dermal Fibroblasts

HDF were kindly provided by Evercyte GmbH. Cells were isolated from adult skin derived from abdominoplasty post liposuction of three healthy female donors between ages 49 and 65 (Donor: HDF76, HDF85, HDF161). They were routinely grown in DMEM/Ham's F-12 (1:1 mixture) (Biochrome GmbH, Berlin, Germany, F4815) supplemented with 10 % fetal calf serum (FCS) (Sigma Aldrich GmbH, St Louis, MO, USA, F7524) and 4 mM L-Glutamine (Sigma Aldrich GmbH St Louis, MO, USA, G7513). HDFs were routinely passaged twice a week with a split ratio of 1:3 to 1:2, dependent on replicative age.

For induction of stress-induced premature senescence (SIPS) (Toussaint et al. 2000; Fripiat et al. 2001) HDFs were used within the middle of their population doubling (PD). HDF85 and HDF161 were used between PD 12 to 14. HDF76 was used between PD 20 - and PD 26.

Normal Human Epidermal Keratinocytes (NHEK)

NHEK from were kindly provided by the Department of Dermatology (Medical University of Vienna, Austria). Cells were isolated from adult skin derived from abdominoplasty post liposuction from four healthy female donors. Cells were cultured under low levels of calcium ([Ca²⁺] = 0.06 mM using Dermalife® K media (LifeLine Cell Technology) supplemented with Dermalife® K LifeFactors® kit (LifeLine Cell Technology). Cells in PD3 were routinely thawed from working cell banks. They were passaged at a confluence of around 50% in split ratio of 1:3 or 1:4 depended on the donor. Trypsinization was stopped with trypsin inhibitor (T6416 Sigma Aldrich) in a ratio of 1:2 to the amount of trypsin. Cells were resuspended in PBS and centrifuged (5810 R Eppendorf) at 170 x g for 5 minutes

Material and Methods

(min) to get rid of trypsin inhibitor. The cell pellet was thoroughly resuspended in Dermalife® K media and cells were splitted into respective culture plates. Experiments with NHEK were routinely performed in PD5.

Isolation and cultivation of tail keratinocytes from mice

Tail keratinocytes were isolated from C57Bl/6J mice. See Table for overview of strains (Table 6). Mice were maintained according to the animal welfare guidelines of the Medical University of Vienna, und the Austrian laws.

Table 6 Background and details to miR-21 knockout and wildtype from C57Bl/6J mice.

ID	Sex	Line / Strain	Genotype	date of birth	date of sacrifice	Age (Weeks)	Weight [g]
GGRI-0085	m	MIR 21 ko m2 (B6) 1IC B	-/-	01.01.2015	28.09.2015	39	
GGRI-0086	m	MIR 21 ko m2 (B6) 1IC B	+/+			39	
GGRI-00251	m	MIR 21 ko m2 (B6) 1IC A	+/+	14.12.2014		41	
GGRI-00253	m	MIR 21 ko m2 (B6) 1IC A	-/-			41	
GGRI-00173	f	MIR 21 ko	+/+	27.10.2014	04.11.2015	53	40
GGRI-00174	f	MIR 21 ko	-/-				43.3
GGRI-00187	f	MIR 21 ko	-/-	29.12.2014		44	45.2
GGRI-00186	f	MIR 21 ko	+/+				40
GGRI-00097	f	MIR 21 ko m2 (B6) 1IC B	+/+	14.11.2014		63	47.4
GGRI-00098	f	MIR 21 ko m2 (B6) 1IC B	-/-			63	39.9
GGRI-00112	f	MIR 21 ko m2 (B6) 1IC A	-/-	26.10.2014	08.02.2016	66	34.6
GGRI-00113	f	MIR 21 ko m2 (B6) 1IC A	+/+			66	37.7
GGRI-00295	f	MIR 21 ko m2 (B6) 2IC A	-/-	20.04.2015		41	31.1
GGRI-00297	f	MIR 21 ko m2 (B6) 2IC A	+/+			41	29.2

Animals were sacrificed at animal facility. Tail was cut and put into 70% ethanol for 5 seconds and was transferred to falcon tube containing 10 ml sterile PBS. All steps were performed under quarantine conditions in a laminar flow hood.

At the thicker end of the tails a longitudinal cut was performed with a scalpel. The skin was stripped off from the tail using two tweezers. The tail skin was cut into 6 to 8 small pieces and put into a falcon tube containing 3 ml dispase solution/mouse in a 15ml tube and were incubated for one hour at 37 °C with rotation. Dermis and epidermis was separated. Dermis was discard and epidermis was incubated with 3 ml/per tail 0.025% trypsin/EDTA

Material and Methods

for 10 min at 37° with rotation. Cell suspension was then filtered through a cell strainer (70 micron) into 50 ml Falcon tubes. Trypsin was inhibited using 5 ml chelated FCS (generously provided by the Department for Dermatology) and 5 ml PBS and suspension was transferred into 15ml tubes for centrifugation at 1500 rpm for 5min. Cell pellet was resuspended in keratinocyte basal medium 2 (KBM-2) supplemented with KGM-2 singelquot kit (LONZA, CC-4152) and plated into pre-coated flasks (1 x T75/tail). Allow cells to attach for at least two days before subsequent experiments.

Pre-coating was performed with collagen solution containing 10 ml HBSS (Gibco), 200 µl HEPES, 100 µl Collagen (Invitrogen) for at least for 1 hour at 37°C. Afterwards plates were thoroughly washed twice with PBS.

Dispase (Roche, 04942078001 1.01 U/mg lyophilisate) 100 x Stock solution: 3.564 g/15ml KBM. Working 1 x Stock diluted in KBM (final 2.4U/ml).

For harvesting of tail keratinocytes 0.25% trypsin/EDTA was used. Enzyme reaction was stopped with 1:1 of chelated serum followed by centrifugation at 170 x g for 5 min.

Skin sections

Two human skin sections in a size of 10 x 10 (PT-0220257) were generously provided by Evercyte in cooperation with the Medical University Vienna.

Cell number determination, Cryopreservation

Calculation of population doublings (PD) was performed according to the following equation

$$PD_{n+1} = PD_n + \frac{\ln(\text{split ratio})}{\ln(2)}$$

Cryopreservation, Freezing and Thawing

Working and master cell banks were stored in liquid nitrogen (-196°C). For cryopreservation, cells were harvested, centrifugation (170 x g, 10 min) and resuspended in normal culture media, supplemented with 10% dimethylsulfoxid (cryomedia) (DMSO, ≥99.7%, Hybri-Max™, sterile-filtered and hybridoma tested) (D2650 Sigma Aldrich). For a final concentration of around 5·10⁵ to 1·10⁶ cells/vial we resuspended the cells of 1x T25 flask of HDF and NHEK in 1 ml cryomedia.

For thawing, DMSO was removed by centrifugation (170 x g 10 min) and the pellet was resuspended in respective culture media. NHEK from one cryotube were split into two T25; fibroblasts were transferred into one T25. 24 h post thawing, the media was changed.

Determination of Cell Concentration and Viability

Cell number and Viability was determined using a hemocytometer and/or the Vi-CELL™ XR Cell Counter (Beckman Coulter).

5.2. Induction of stress and stress-induced premature senescence

Fibroblasts

In order to establish a protocol of stress-induced premature senescence (SIPS) in HDF we tested the effectiveness and potency of paraquat and hydrogen peroxide in fibroblasts of all three donors HDF161, HDF85, HDF76, respectively.

Paraquat induced stress

Paraquat working solution was freshly prepared in PBS.

For optimization, several parameters were tested. Seeding before treatment: between 2000 – 5000 cells/cm² were seeded. Paraquat concentrations range from 40 µM – 100 µM. Treatment was conducted for 24 hours to 72 hours. We could not find a robust protocol to induce SIPS using paraquat.

H₂O₂ induced stress induced premature senescence

30% H₂O₂ stock solution was stored on -80°C. For a period of two weeks one aliquot, stored at 4°C, was used. Pre-dilution in PBS was performed freshly. Final dilution was performed in culture media.

On day 0, middle-aged HDFs (PD12-25) were seeded with 3500 cells/cm² into T75 flasks. On the following the cells were treated with 100 µM H₂O₂ (216763 Sigma Aldrich) for 1 h per day at 37°C over a period of four consecutive days. After 2 days of recovery, cells were stressed again for 5 days. After each treatment, media was exchanged to normal growth media. Media change of nontreated control cells was performed twice a week and cells reached quiescence (Q) by contact inhibition. Changes on cellular morphology were monitored and pictures were taken during the stress treatment and before subsequent experiments

After E7 (D7) and 21 days (D21) post last H₂O₂ application, major hallmarks of cellular senescence were confirmed. Irreversible growth arrest was tested with the ability to incorporate bromodeoxyuridine (BrdU). Accumulation of senescence-associated (SA)-β-Gal, detection of CDKN1A (p21) by qPCR and in order to exclude apoptosis Annexin-V staining were performed. At the same days, small extracellular vesicles (EV) below 220 nm were harvested by differential centrifugation (Théry et al. 2006; Cvjetkovic et al. 2014).

For miRNA profiling: Intracellular and corresponding EV-RNAs were isolated for small RNA next generation sequencing (NGS) and qPCR panels provided by Exiqon (Denmark) (FigS1A).

Stress treatment of tail keratinocytes from mice

Tail keratinocytes were stressed with distinct stress stimuli.

Oxidized lipids (UVPAPC) were freshly prepared and subsequently used. They were generously provided by the Gruber lab. The content of one vial was resuspended in media and vigorously vortex. Respective dilutions to 12.5 µg/ml and 25 µg/ml. Cells were exposed to UVPAPC for 6 or 24 hours.

Cisplatin was solved in DMSO and stored on -20°C. Pre-dilution were done in media to a concentration of 5 µM and 10 µM and cells were incubated for 24 hours.

H₂O₂ and Paraquat were prepared as mentioned above. Cells were stressed with 15 and 30 µM Paraquat overnight and with 100 µM H₂O₂ for 6 hours and overnight, respectively

5.3. Human Skin equivalents

The HSE were produced as recently published (Mildner et al. 2006). Briefly, 2.5×10^5 HDF were seeded in a collagen gel consisting of eight parts collagen G (Biochrome, Berlin, DE), one part 10 x HBSS (ThermoFisher Scientific, MA, USA) and one part FCS (Sigma-Aldrich, MO, USA). The gel was equilibrated overnight with KGM-2 supplemented with KGM-2 Bullet Kit (Lonza, Basel, CH) followed by a keratinocyte overlay of 1.5×10^6 cells on day 2. The so-formed early skin equivalents were then lifted to the air-liquid interface (ALI) to start differentiation on day 3. The differentiation media (KGM, Lonza, Basel, CH) was supplemented with all components of the KGM BulletKit (Lonza, Basel, CH) except for bovine pituitary extract. Additionally, 1.15 mM CaCl_2 (Sigma-Aldrich, MO, USA), 50 $\mu\text{g/ml}$ L-ascorbic acid (Sigma-Aldrich, MO, USA), 0.1 % bovine serum albumin (Sigma-Aldrich, MO, USA) and 10 $\mu\text{g/ml}$ transferrin (Sigma-Aldrich, MO, USA) were added. The differentiation media was refreshed every other day throughout the whole differentiation process (day 3-10). After 10 days, the skin equivalents were harvested, formalin-fixed, and paraffin-embedded for further histological analysis. Additionally, RNA and protein samples were taken to confirm the results of the histological analysis. All skin equivalent experiments were performed in duplicates.

5.4. Annexin-V-/PI staining

For staining of apoptotic cells, the Pacific Blue™ Annexin-V Kit (Biolegend, San Diego, CA, USA, 640918) was used. Cells and supernatants were harvested. Wells were rinsed with 1x PBS supplemented with Ca^{2+} and Mg^{2+} (Thermo Scientific, USA) added to cells and centrifuged at $200 \times g$ for 10 min. Pellets were washed twice with Annexin-V binding buffer (10 mM Hepes/NaOH pH 7.4, 140 mM NaCl, 5 mM CaCl_2). After centrifugation at $500 \times g$, the pellet was resuspended and incubated for 15 min in Annexin-V/PI staining solution (250 ng/mL propidium iodide PI, Sigma Aldrich GmbH, St Louis, MO, USA P4864, 200 ng/mL Pacific Blue, diluted in Annexin-V binding buffer) under light protection. The analysis was performed on a Gallios flow cytometer (Beckman coulter, Brea, CA, USA) using an excitation wavelength of 488 nm and a 600 nm emission filter for detection of PI (FL-3) and an excitation of 405 nm and a 450/50nm emission filter for Pacific-Blue-Annexin (FL-9). Cells treated with 300 nM Staurosporin for 24 hours were used as a positive control. Flow cytometry data were analysed with Kaluza software (Beckman Coulter, Brea, CA, USA, Version 1.2).

5.5. BrdU incorporation

In order to verify growth arrest, cells were incubated for 24 hours with 10 μM BrdU (Sigma Aldrich GmbH, St Louis, MO, USA, B5002). The cells were harvested by trypsinization, centrifuged at $170 \times g$ for 5 min and the pellet was fixed with ice cold 70% ethanol for at least one hour at 4°C. Cells were permeabilized for 30 min with 2 M HCl and 1% Triton X-100 (Sigma Aldrich GmbH, St Louis, MO, USA, X100), followed by neutralization with 0.1 M Na-Borat, pH 8.5. Pellets were resuspended in TBS (0.5% Tween20, 1% BSA in 1 x PBS) containing anti-BrdU antibody 1:50 (BD Biosciences, USA, 347580) and incubated for 30 min. After washing with TBS and counterstaining with anti-mouse FITC-conjugated antibody 1:100 (Sigma Aldrich GmbH, St Louis, MO, USA F8264) for 30 minutes, the pellet was washed with TBS and resuspended in 1 x PBS with 2.5 $\mu\text{g/ml}$ PI (Sigma Aldrich GmbH, St Louis, MO, USA, P4864).

Material and Methods

For compensation, cells were stained with either PI or BrdU alone. The analysis was performed by flow cytometry (Gallios Beckman coulter, Brea, CA, USA), using an excitation wavelength of 488 nm and a 600 nm emission filter for detection of PI (FL-3) and a 535 nm filter for BrdU-FITC (FL-1). Proliferating cells were used as positive controls. Flow cytometry data were analysed with Kaluza software (Beckman Coulter, Brea, CA, USA, Version 1.2).

5.6. Senescence associated β -Galactosidase staining

Senescent HDF and sub-confluent HDF at the middle of their replicative lifespan were stained according to the standard protocol described by Dimri et al. 1995 (Dimri, X. Lee, et al. 1995). 15 pictures per well were taken at 100 x magnification and after randomization and blinding, SA- β -Gal positive and negative cells were counted.

5.7. Isolation of small extracellular vesicles (EVs)

Isolation of EV by differential centrifugation was performed according to standards recommended from the international society for extracellular vesicles (IEV) and published by Hill et al. 2013 (Hill et al. 2013). Growth media containing FCS was depleted of EVs by ultracentrifugation at 100.000 x g overnight, followed by filtration with 0.22 μ m filter cups (Millipore, Germany, SCGPU05RE). The cells were allowed to secrete in EV depleted media for 48 hour and the supernatant was then centrifuged for 15 min at 500 x g (Eppendorf, 5804R) to remove cellular debris. By a second centrifugation with Corning® CentriStar™ tubes (430829 Corning) at 14,000 x g (Beckmann, Coulter, Brea, CA, USA, Avanti JXN-26) for 15 min, microvesicles were pelleted. Larger EVs were subsequently excluded by filtration using 0.22 μ m filter cups (Millipore, Germany, SCGPU05RE). Finally, the supernatants were filled into Quick-Seal, Polyallomer, 39ml, 25 x 89 mm tubes (Beckman, Brea, CA, USA, 342414) using a syringe and flat opening needle. Tubes need to be filled up to their maximal capacity to prevent deformation (either with supernatant or filtered PBS). Small EVs were enriched using a 70Ti Rotor Beckman coulter at 100.000 x g for 90 min (Beckman, Brea, CA, USA, I8-80M) and pellets in different tubes but from the same sample were pooled. Dependent on the subsequent analysis, the pellet was either resuspended in QIAzol reagent (Qiagen) or in filtered 1 x PBS. For TEM and keratinocyte treatment freezing and thawing was avoided.

For miRNA profiling, on average 92 ml supernatant from SIPS and 75 ml supernatant from Q (were harvested. For EV treatment of NHEK it was up-scaled to 24 x T75 flasks of SIPS cells and 12 x T75 flasks for Q cells, respectively. This allowed us to treat approximately $3.5\text{--}4.0 \times 10^6$ keratinocytes (in a ratio of 1:1 with secreting fibroblasts) with vesicles from SIPS cells and $8.5\text{--}10.0 \times 10^6$ keratinocytes with vesicles from Q cells (ratio of 1:1 with secreting fibroblasts). EVs were routinely harvested once per week within the first four weeks after the SIPS treatment.

5.8. EV Treatment of Keratinocytes

To evaluate the impact of fibroblast derived EVs on keratinocytes we assessed their wound healing capacity as well as their differentiation potential.

The amount of vesicles used for NHEK exposure was quantified by the 'number of secreting fibroblasts to number of receiving keratinocytes'. For functional studies, EVs were used in two different ratios, 1:1 and 5:1 (Fibroblasts:NHEK).

Material and Methods

One or two days before treatment (donor depended), NHEKs were seeded into 6-well plates, 12-well plates and/or ibidi® wound healing chambers (81176 ibidi®) with a cell number ranging from 1.5 to 3×10^4 cells/cm² depending on subsequent read out. EVs were prepared freshly, diluted in normal culture media and added to NHEK. Wound healing capacity and miRNA levels were monitored after short term treatment for 24 – 48 hours post EV addition. Differentiation potential of NHEK was assessed after one week EV treatment. Details of the different assays and sample preparations are indicated in respective chapters

5.9. Nanoparticle tracking analysis

In order to determine the size and amount of EVs, secreted from Q and SIPS cells, the Zetaview system (Particle Metrix, Meerbusch, Germany) was used. Calibration of the system was conducted with 110 nm polystyrene standard beads (Particle Metrix, Meerbusch, Germany). Vesicles were diluted in filtered 1 x PBS and each sample was measured in technical triplicates. For optimized performance, camera sensitivity was adjusted to fit the highest and lowest concentrated sample into the dynamic range and all samples were measured with the same dilution and settings. Settings: Gain 904, 98; Offset 0. Measurements were taken at two different camera positions. EVs secreted per cell were calculated using the cell number measured with Vi-CELL XR (Beckman Coulter, Brea, CA, USA). Categories of particle size were defined by the device. For Figure 16 categories below 15 nm, 15 nm, 45 nm, 105 nm, 135 nm, 165 nm, 195 nm and bigger than 225 nm are shown.

5.10. Electron microscopy

EVs for Transmission Electron microscopy (TEM) were freshly prepared. Solutions used for the staining procedure were pre-filtered using 0.22 µm filter units (Millipore, Germany, SCGPU05RE). EVs were adhered on Athene Old 300 mesh copper grids (Agar Scientific, Stansted, Essex, UK) and fixed with 1% glutaraldehyde. After washing three times with nuclease free water (NFW), vesicles were stained for 5 min with 2% phosphotungstic acid hydrate (Carl Roth, Karlsruhe, Germany). The grids were left to dry and the specimens were visualized using TEM (FEI Tecnai T20, FEI Eindhoven, Netherlands) operated at 160 kV.

Skin sections for ultrastructural analysis were generously provided by Michael Mildner from the Department of Dermatology, Medical University of Vienna, Vienna, Austria

5.11. miRNA transfections

In order to analyze the impact of miR-23a-3p overexpression on NHEK, they were transfected in $PD \leq 5$ using lipids from siPORT™ NeoFX™ transfection agent (AM4511 Thermo Scientific) according to the manufacturer's instructions. For 1 x 6 well, 5 µl lipids and 30 nM final concentration of respective pre-miRNAs was used. 2×10^4 to 3×10^4 cells/cm² cells were reverse transfected with pre-miR-23a-3p (AM17100 Ambion) and scrambled control pre-miR-Ctrl#2 (AM 17111 Thermo Scientific).

24 hours post transfection media changes was performed and wound healing capacity of miR-23a-3p overexpressing cells was monitored after 24 to 72 hours post transfection.

Material and Methods

To confirm the EV-miRNA crosstalk between HDF and NHEK, HDF were transfected using the C.elegans specific cel-miR-39 and corresponding miR-Ctrl#2. 24 hours post transfection. 24 hours post transfection, either secretion media was added or the cells were harvested for embedding into skin equivalents.

5.12. Wound Healing Assay

To determine the wound healing capacity of NHEK after EV incubation and after miR-23a-3p overexpression two different assays were performed.

ibidi® Wound Healing and Migration Assay

ibidi® wound healing and migration assay slides consist of two separated chambers of an area of 0.22 cm² and a maximum capacity of 120 µl.

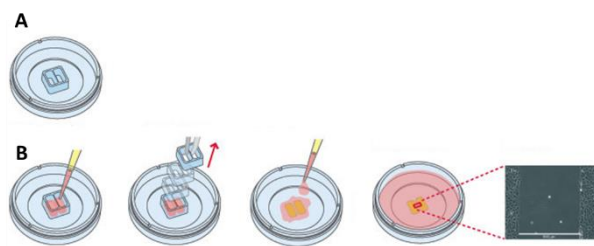


Figure 74 ibidi® wound healing and migration assay format (A) and work-flow (B). Adapted from ibidi®

NHEKs were either seeded 24-48 hours before EV-treatment or in the course of reverse transfection at seeding densities of 3×10^4 and $3.64-13.6 \times 10^4$ cells/cm², respectively. For the latter, cells were mixed with transfection agents in a 6 or 12-well and then transferred into ibidi® chambers.

Once keratinocytes reached confluence (48-72 h post seeding), the silicone insert was removed leaving behind a cell free area ('wounded area'). Fresh culture media (+/- EVs) was added and cells were incubated at 37°C at 7% CO₂. 'Wound' closure was monitored by taking non-overlapping pictures along the entirety of the gap every 3 h. Number of cells within the cell-free area were counted and quantified.

Traditional 'scratch' assay

NHEKs were seeded into 12-well plates. Upon confluence the monolayer was scratched using a 200 µl pipette tip. Wound healing capacity was monitored and every 3 hours the entire scratch was captured on pictures. Total area was quantified using ImageJ.

For both assays the wound closure per hour (/h) was calculated according to equation 2.

$$\text{wound healing rate} = \frac{(\text{area } t_{n+1} - \text{area } t_0)}{t_{n+1} - t_0}$$

5.13. Cellular proliferation and activity using AlamarBlue®

In order to investigate the impact of several stressors (according to chapter 5.2.) on miR-21 knockout cells and wt, the Resazurin based vitality assay (AlamarBlue®; ThermoFisher Scientific, MA, USA) was performed according to manufacturer's recommendations.

Three days after the isolation of primary tail keratinocytes they were seeded with 1.5×10^5 cells/cm² into 96 well plates (0.34cm² with 5100 cells per 100 µl). To allow proper cell attachment, the indicated stress treatments according to chapter 5.2, were started after 2 days post seeding. Immediately after the stress treatment the media

Material and Methods

was changed to normal culture media (KGM-2) supplemented with 1:10 Alamarblue® and subsequently measured using a Tecan M200 Reader at an excitation wavelength of 555nm, and an emission wavelength of 595 nm. Further measurements were performed according to each stress treatment and growth behavior of the cells.

Molecular Biology Methods

5.14. Protein quantification, western blot and antibodies

For protein isolation, a 2x TNE lysis buffer (2 x TNE: 100 mM Tris/HCl, pH 8.0, 300 mM NaCl, 1 mM EDTA, 2 % Triton X-100) was prepared and adjusted to pH 8.0 using HCl. Aliquots were stored at -20°C. Before use, the 1 x buffer in NFW was supplemented with 1x phosphatase inhibitor (PhosSTOP 4906837001 Roche) and 1x protease inhibitor (4693132001 Roche).

Cells were lysed using the freshly prepared 1 x TNE buffer plus supplements. Centrifugation steps were run at 4°C and samples were kept on ice for the entire procedure. Cells were pelleted at 600 x g for 10 min, washed with PBS once and resuspended in 1 x TNE buffer. Pellet was incubated for 10 min on ice (cell lysis), followed by vortexing and centrifuged at 6-000 x g for 10 min. The supernatant, containing the proteins, was transferred onto a QIAshredder spin column (79656 Qiagen) and centrifuged at 16.000 x g for 2 min to allow DNA fragmentation. The step was repeated with the flow-through. Finally, 90 µL of purified protein sample (1 x 6 well NHEK) were mixed with 30 µL 4x loading dye (LD) (dye (4 x SDS loading dye: 240 mM Tris/HCl, pH 6.8, 8% SDS, 40% glycerol, 0.05% bromophenolblue, 5% β-Mercaptoethanol) and incubated for 10 min at 95°C. Samples were stored at -20°C.

Vesicles were pelleted and resuspended and lysed in 1 x LD. The samples were then sonicated for 30 cycles à 30 sec with 30 sec breaks, at 4°C. Afterwards, they were incubated at 95°C for 10 min. Samples were stored at -20°C.

Protein content of lysates was quantified with the Pierce® BCA Protein Assay Kit (Thermo Scientific, USA, 23227) according to manufacturer's recommendations.

For SDS page samples were separated on a NuPAGE 4–12% Bis/Tris polyacrylamide gel (Invitrogen/Thermo Scientific, USA, 10472322) in 1x NuPAGE® MOPS SDS Running buffer (stock = 20x) at 200 V. 6 µL of marker PageRuler™ Plus Prestained Protein Ladder (26619 Thermo Scientific) and x µL of sample (depending on cell number and/or protein concentration) but at maximum 25 µL were pipetted into the slots. Subsequently, proteins were transferred to a PVDF membrane (Biorad, Hercules, CA, USA, 170-4156) in a BioRad SemiDry Blotting System at 1.3A 25V for 7 minutes.

Membranes were blocked for 1 h at room temperature or overnight (O/N) at 4°C in 3% milk in 1x PBS containing 0.01% Tween®20 (P4780 Sigma Aldrich). Membranes were then incubated with respective antibodies (Table 7). In-between incubation steps membrane was washed three times with PBS containing 0.01% Tween20. Proteins were detected using secondary antibodies for IRDye® 800CW Donkey anti-Rabbit IgG, 0.5 mg (LI-COR Biosciences, USA, 926-32213) and IRDye® 680RD Donkey anti-Mouse IgG, 0.5 mg (LI-COR Biosciences, USA, 926-68072) with a 1:10000 dilution using the Odyssey (LI-COR Biosciences, USA) infrared image system. All antibodies were diluted in

Material and Methods

3% milk-powder dissolved in 1x PBS with 0.1% Tween-20 (Sigma Aldrich GmbH, St Louis, MO, USA, P2287). For densitometric analysis, ImageJ was used for quantification.

Target	Company	Catalog Nr.	Source	dilution	incubation
TSG101	Abcam	ab125011	rabbit	1:200	Overnight 4°C
Involucrin	Thermo Scientific	MA5-11803	mouse	1:200	2 h RT or overnight 4°C
GAPDH	Santa Cruz	sc-25778	Rabbit	1:1000	1 h RT

Table 7 Primary antibodies used

5.15. RNA Isolation,

Working area, pipettes and hands were frequently wiped with RNaseZAP® (AM9780 Life Technologies) wipes and centrifugation steps using a micro-centrifuge (5415R Eppendorf) were performed at 4°C. Chemicals were diluted in nuclease-free water (NFW) (10977049 LifeTechnologies). RNA lysates were kept in nuclease-free tubes (72.692 Sarstedt).

For Routine RNA isolation

Before RNA extraction, cells were washed twice with PBS and harvested in 500 µL TRIzol® reagent (T9424 Sigma Aldrich). The lysates were vortexed for a few seconds and either immediately processed or frozen at -80°C after a short incubation at room temperature (5 min).

100 µL of chloroform (C2432 Sigma Aldrich) was added to fully thawed samples. After 30 sec vortexing, samples were incubated for 3-5 min at room temperature and then centrifuged at 12.000 x g for 15 min for phase separation. The aqueous phase was transferred into a fresh nuclease-free tube. 1 µL of GlycoBlue (AM9516 Life Technologies) as a carrier and 250 µL isopropanol (20922.394 VWR Chemicals Prolab) for precipitation were added.. Samples were gently and thoroughly mixed (not vortexed!). After 10 min incubation at RT, precipitated RNA was pelleted by centrifugation at 12.000g, 10 min. Supernatant was discarded and RNA pellet washed with 70% ethanol, followed by another centrifugation step (7,500g, 5 min). Finally, ethanol was removed and the RNA pellet was air-dried. Once completely dry, the pellet was resuspended in 20 µL of NFW and incubated at 55°C for 10 min. RNA was stored at -80°C.

Total RNA concentration and purity was measured with NanoDrop™ One spectrophotometer (Thermo Scientific).

For miRNA profiling

Cell pellets and EV were lysed in QIAzol Reagent (Qiagen). To monitor isolation efficiency of EV-RNA, spike -ins (UniSp2, UniSp4, UniSp5, Exiqon, Denmark, 203203) were added before RNA isolation. RNA was automatically extracted by miRNeasy Mini kit (Qiagen, 217004) based on QIAcube technology. Intracellular total RNA concentration and quality was controlled using Nanodrop spectrometer (ND-1000) and 2100 Bioanalyzer (Agilent) according to manufacturer's recommendations of the RNA-6000 Nano Kit. Average RNA concentration as determined by Nanodrop and Bioanalyzer revealed an average concentration (n = 6) of Q = 955 ng/µl SIPS = 234 ng/µl in a volume of 20 µl, and RIN of intracellular RNAs was determined with 2100 Bioanalyzer yielding for Q = 7.3 SIPS = 7.5.

From dermis and epidermis of human skin equivalents

Dermal and epidermal layer of skin equivalents was separated and resuspended in 500 µL TRIzol® reagent. Samples were homogenized for 30 seconds using pellet pestles (Sigma, Z359947) on ice. Followed by sonication for 30 cycles of 30 sec sonication and 30 sec hold. Subsequent RNA isolation was performed according to the standard protocol used for routine RNA isolation.

5.16. cDNA synthesis

RNAs were thawed and kept on ice. All dilutions were performed on ice as cDNA synthesis were performed in a thermocycler (T3 Biometra). For 'no reverse transcription' negative control, reaction mix was prepared without enzyme. For 'no template control', NFW was used instead of RNA.

cDNA for miRNA profiling

For cDNA synthesis of miRNA transcripts the Universal cDNA Synthesis Kit II (Exiqon, Denmark, 203301) according to the manufacturer's instruction was applied. Briefly, 5 ng of total RNA and equal volumes of 2 µl from EV-RNA diluted in NFW were mixed with 3 µL of master mix to achieve a total volume of 10 µL. EV-Samples were supplemented and spiked with UniSp6 and cel-miR-39 (Exiqon, Denmark) to control for enzyme activity. cDNA was synthesized by 42°C for 60 min, followed by heat inactivation of enzyme for 5 min at 95°C.

cDNA for mRNA

For determination of the senescence markers CDKN1A, cDNA was synthesized from 500 ng of total RNA with the High-Capacity cDNA Reverse Transcription Kit including RNase inhibitor (N2115 Promega), according to manual provided by the manufacturer (Applied Biosystems, USA, 10400745). Mastermix as listed in Table 8.

Component	Volume/Reaction [µL]
10x RT Buffer	2.0
25x dNTP Mix (100 mM)	0.8
10x RT Random Primers	2.0
MultiScript™ Reverse Transcriptase	1.0
RNase Inhibitor	1.0
Nuclease-free water	3.2
RNA template (500 ng)	10.0
Total	20.0

Table 8 Reaction mix of the High-Capacity cDNA Reverse Transcription kit.

Material and Methods

Reverse transcription was performed in a thermocycler according to Table 9.

	Step 1	Step 2	Step 3	Step 4
Temperature [°C]	25	37	85	15
Time [min]	10	120	5	∞

Table 9 Thermal cycler temperature profile for reverse transcription using the High-Capacity cDNA Reverse Transcription kit.

CDNAs were diluted up to 50 µl and were stored at -20°C in low DNA binding tubes (Eppendorf, 30108051).

5.17. Quantitative Real Time PCR (qPCR)

All steps were performed on ice. Negative controls tested as NFW only, and no template control derived from cDNA synthesis, were below detection limit of qPCR (> 40).

miRNA qPCR using ExiLENT SYBR® Green

MiRNA qPCR analyses were performed using ExiLENT SYBR® Green master mix (Exiqon, Denmark, 203403) and LNA-enhanced miRNA primer (Exiqon, Denmark). cDNA samples from total RNA and EV-RNAs were 1:40 freshly diluted in NFW and 4 µL of diluted template were used per reaction (50 pg final concentration).

Mastermix for routine qPCR and large scale miRNA profiling are presented in (Table 10)

Reagent	Volume per reaction [µl] for Routine	Volume per plate with 384 reactions per plate [µl]
ExiLENT SYBR® Green Master Mix	5.0	2100
LNA enhanced primer	1.0	lyophilized in qCPR plate
cDNA Template	4.0 (from 1:40 pre-dilution)	42.0 + 2079 NFW (1:50)

Table 10 ExiLENT SYBR® Green master mix for miRNA based qPCR analysis.

For the large scale miRNA profiling around 500 µl of mastermix were transferred into 8 separated tubes. They were put into the pipetting device kindly provided from TamiRNA and the 384 well plate was filled up. The qPCR was then performed on a LC 480 Real Time PCR system (Roche, Germany) according to Table 11.

The second derivative method was used to calculate the cycle of quantification values (Cq-values). A preliminary screening for secreted miRNAs was conducted using two 384-well plates covering 752 human miRNAs (microRNA, Ready-to-Use PCR, Human panel I+II, V3.R, Exiqon, Denmark, 203612), with samples derived from one HDF donor in two conditions (SIPS and Q). Based on that, a customized qPCR panel was designed comprising 375 miRNAs and internal and negative controls (Supplemental Table S2.). Experiments were performed in biological triplicates in two conditions (Q and SIPS) and two timepoints (D7 and D21). In total, 12 qPCR panels were set up on three consecutive days. MiRNA analysis was performed according to the ddCT method.

For routine miRNA quantification the reaction was performed in duplicates in a thermocycler Rotor-GenQ 6000 (Qiagen) according to Table 11. As a housekeeping miRNA, U6 snRNA (small non-coding RNA), were measured

Material and Methods

within each qPCR run of miRNA. Ct values were obtained by setting the threshold to 0.01. miRNA analysis was performed using the $\Delta\Delta C_t$ -method (comparative threshold method) (Arya et al. 2005).

	Cycles	Temp [°C]	Time [sec]	Ramp [°C/sec]	Acquisition Mode	Acquisition per °C
Activation	1	95	600	4.4		
Quantification	45	95	10	4.4	Single	
		60	60	1.6		
		95	10	4.4		
Melting Curve	1	55	60	2.2	Continuous	5
		99		0.11		

Table 11 Temperature profile for the use of ExiLENT SYBR® Green master mix in qPCR.

QPCR for mRNA levels with HOT FIREPol™ EvaGreen™

For the determination of CDKN1A and GAPDH was performed was performed in a thermocycler Rotor-GenQ 6000 (Qiagen) according to Table 13. Mastermix with 5x HOT FIREPol® EvaGreen® qPCR Mix Plus with ROX (Medibena, Austria, SB_08-25-00020) was mixed according to Table 12.

Component	Volume/Reaction [μL]
5x HOT FIREPol™ EvaGreen™ qPCR Mix Plus	2.00
Forward Primer	0.25
Reverse Primer	0.25
Nuclease-free water	6.50
cDNA Template (25 ng)	1.00
Total	10.00

Table 12 5x HOT FIREPol™ EvaGreen™ qPCR Mix Plus (ROX) reaction components and respective amounts per reaction.

	Cycles	Temp [°C]	Time [sec]	Acquisition Mode
Activation	1	95	600	
Quantification	45-55	95	15	Single
		60	30	
		72	15	
		80	2	
Melting Curve	1	65	10	continuous
		99	60	

Table 13 Temperature profile for 5x HOT FIREPol™ EvaGreen™ qPCR Mix Plus (ROX) qPCR.

Material and Methods

Standard curves for determination of copy numbers was done in duplicates. Average expression values from samples in quadruplicates were normalized to GAPDH as a reference gene and fold changes were

Primer used for qPCR:

Gene name	Sense primer	Anti-sense primer
GAPDH	CGACCACTTTGTCAAGCTCA	TGTGAGGAGGGGAGATTCAG
CDKN1A (p21)	GGCGGCAGACCAGCATGACAGATT	GCAGGGGGCGGCCAGGGTAT

5.18. Illumina small RNA cDNA library preparation

Intracellular small RNA cDNA library for Illumina Sequencing was synthesized according to the manual provided by NEBNext® Small RNA Library Prep Set for Illumina® (Multiplex Compatible) (NEB, E7330S). From initially 1 µg of total RNA, small RNA fragments from approximately 18 – 36 nucleotides were gel purified on a 10% TBE Gel (Invitrogen/ Thermo Scientific, EC62752), quantified by 2100 Bioanalyzer (Agilent, Santa Clara, CA, USA) and equimolar amounts were pooled and sent to Exiqon (Denmark) for Illumina RNA-Seq (Fig. S4).

To monitor isolation efficiency of EV-RNA, spike -ins (UniSp2, UniSp4, UniSp5, Exiqon, Denmark, 203203) were added before RNA isolation.

5.19. Illumina, miRNA next generation sequencing

The cDNA library pool was used to generate the clusters on the surface of a flowcell before sequencing with NextSeq 500 (Exiqon, Denmark). The collected reads were quality controlled, aligned and annotated to miRBase20 by Exiqon. Differential expression analysis was done using the R (version 3.2.2)/Bioconductor software package DESeq (Anders & Huber 2010). Low expressed miRNAs were first excluded from the analysis (Tags Per Million (TPM) < 5 for all the samples). Then, the raw read counts were normalized using the DESeq normalization and a model based on negative binomial distribution and local regression was fitted for each miRNA. In the model, 'fibroblast cell strains' (n = 3) were defined as a 'block effect' and 'day' and 'condition' as factor of 2 levels. The Benjamini and Hochberg (BH) procedure (Benjamini & Yekutieli 2001) was applied to adjust the raw p-values into false discovery rate (FDR). A FDR < 0.05 was chosen as the cut-off value.

qPCR panel, analysis of EVs- miRNAs

Spike-ins were detected in all 384-well plates to monitor purification efficiency of RNA Isolation (UniSp2, UniSp4, UniSp5), the presence of enzyme inhibitors during cDNA synthesis (Unisp6 and cel-miR-39–3p) and equal processing of RT-qPCR amplification (interplate calibrator IPC - UniSp3). Additionally, NFW was used to determine background levels of each miRNA. Constant expression of all spike-ins was evaluated with a range calculated by the difference of the highest and lowest and interplate calibration was performed with GenEX 6.0. Cq-values were either normalized to total number of cells used for secretion or by the mean-centering restricted (MCR) normalization (Deo et al. 2013; Mestdagh et al. 2009), also known as the global mean normalization. Thereby, the mean Ct-value across all detected miRNAs of a single sample was subtracted from each individual miRNA. Differences in global mean are presented in Fig. S3A.

Material and Methods

Both datasets were subjected to differential expression analysis with the R (version 3.2.2)/Bioconductor software package Limma (Smyth 2005). A linear model was applied for each miRNA and moderated t-tests were computed. In the model, fibroblast cell strains ($n = 3$) were defined as a 'block effect' and 'day' and 'condition' as factor of 2 levels. The raw p-values were corrected using BH method to control FDR.

5.20. Statistical analysis

Descriptive statistics

were performed using ClustVis, a web tool for the preparation of principal component 2D-biplots and heatmap analysis based on multivariate datasets using different R packages (Metsalu & Vilo 2015). For all exploratory analyses, normalized Ct-values and TPM values were used. Principal component analysis (PCA) of 371 extracellular miRNAs (out of 375) was calculated by iteration of missing values with Nipals PCA and unit variance scaling was applied to rows. Heatmap preparation and hierarchical clustering of secreted miRNAs was performed by applying correlation distance and Ward linkage. Samples in columns are clustered using Euclidean distance and Ward linkage method.

PCA for intracellular miRNAs was done for 432 miRNAs with TPM > 5 in at least one donor. We used Singular Value Decomposition (SVD) for imputation and unit variance scaling was applied on TPM values. Expression matrix and hierarchical clustering of 432 intracellularly transcribed miRNAs was done by applying unit variance scaling and rows were clustered using Euclidean distance and Ward linkage. Columns are clustered using correlation distance and Ward linkage.

Correlation of intracellular and extracellular miRNAs

Only miRNAs, included in the customized qPCR panels for determination of extracellular miRNA abundance (375) were selected. Prior correlation of intracellular and extracellular miRNAs, quartiles from Cq-values and TPM values were calculated and miRNAs being low expressed (quartile 1 corresponds to the lowest 25% of data) in NGS and qPCR were excluded from analysis (330 miRNAs). Then miRNAs giving no signal in NGS experiment (TPM = 0) were excluded (291 miRNAs), and finally all miRNAs not present in all three donors and conditions were excluded. Therefore, correlation was done on 228 miRNAs. Rank from averages were calculated from SIPS and Q separately. Rank order was done according to intracellular TPM values to identify most abundant miRNAs transcribed intracellularly, or according to extracellular Cq-values, to discover most abundantly present miRNAs in EVs. By calculating Δrank ($\text{rank}_{\text{intra}} - \text{rank}_{\text{extra}}$) from Q and SIPS separately, retained (negative value of Δrank) and secreted miRNAs (positive value of Δrank) were identified. By further calculating $\Delta\Delta\text{rank}$ ($\Delta\text{rank}_{\text{SIPS}} - \Delta\text{rank}_{\text{Q}}$) and the 25% and 75% percentiles, selectively higher secreted (high value of $\Delta\Delta\text{rank}$) or retained (low value of $\Delta\Delta\text{rank}$) miRNAs in SIPS were discovered. Next, we analyzed the same dataset with a different method to review our data, using the 'ratio-approach'. For a better visualization, Cq-values were transformed to arbitrary units, defining a Ct-value of 40 to '10' arbitrary units – assuming around 10 miRNA copies. Δratios were calculated from values $\text{intraSIPS}/\text{extraSIPS}$ and $\text{intraQ}/\text{extraQ}$ separately. Then $\Delta\Delta\text{ratios}$ from $\Delta\text{ratio}_{\text{SIPS}}/\Delta\text{ratio}_{\text{Q}}$ were calculated and normalized to the global mean of those ratios. Again, the 25% and 75% percentiles were calculated, and selectively higher secreted (high value of $\Delta\Delta\text{ratio}$) or retained (low value of $\Delta\Delta\text{ratio}$) miRNAs in SIPS were discovered. For Fig.

Material and Methods

6D miRNAs were sorted according to $\Delta\Delta$ ratio values from smallest to largest values and they were plotted on y-axis, $\Delta\Delta$ rank values were then plotted in another diagram in the same order as it was sorted before.

Pathway analysis of extracellular miRNAs

MiRWalk 'microRNA- gene target' tool (Dweep & Gretz 2015a) was used to find all validated targets for each of the 20 most highly abundantly secreted miRNAs. To evaluate the putative network on pathway level, enrichment analysis of pathway-based sets of the common regulated genes (targets) was performed using ConsensusPathDB (Kamburov et al. 2013) with the overrepresentation analysis tool. As input, HGNC symbol identifiers of our dataset were used and search was done against pathways with a minimal overlap of a p-value cutoff of 0.0001. Cytoscape (Smoot et al. 2011) and the BisoGenet plug-in (Martin et al. 2010a) was then used to generate a potential miRNA-regulated network using the list of validated targets and the modules obtained in the previous step. Crosstalk maps were created, linking curated pathways to metapathways where several pathways modules share a common set of genes.

Routine Statistics

Routine statistics were either calculated with Excel or Graph Pad Prism, and respective tests are indicated below figures in result sections. \pm Standard deviations were derived from at least 3 independent experiments. Two tailed tests were performed using an error probability of 0.05. If not indicated, the experiments were performed less than three times.

Data were tested for Gaussian distribution using D'Agostino & Pearson omnibus normality test. If normal distributed, two groups were compared using unpaired or paired student T-test using the raw values. One sample student's T-test was used to compare ratios to a hypothetical values of 1 or 100, respectively. For non parametric tests two groups were compared using the Mann Whitney test. For ratios compared to hypothetical value the Wilcoxon Signed Rank was used.

In order to analyse the impact of two independent factors ('treatment' and 'genotype') a two way ANOVA analysis was performed. For comparing more than 2 groups with each other one way ANOVA with turkey post hoc test was performed.

6. Supplementary Tables

6.1. Summary and evaluation of secreted miRNAs by qPCR panel

Summary and evaluation of secreted miRNAs by qPCR panel. Preliminary screening of secreted miRNAs to determine detectable miRNAs in small EVs derived from HDFs, was performed using one HDF strain in both conditions, stress-induced premature senescent (SIPS) and nontreated quiescent control (Q), from one timepoint (D21). 375 miRNAs out of 752 screened were selected for the screening with three different HDF cell strains derived from healthy donors, in 2 conditions (SIPS and Q) and at 7 (D7) and 21 days (D21) after treatment.

Table 14 Summary and evaluation of secreted miRNAs by qPCR panel.

conditions	Preliminary screening		Screening	
	Q control	SIPS	Q control	SIPS
biological replicates (HDF)	n=1	n=1	n=3	n=3
timepoints (days post treatment)	D21	D21	D7; D21	D7; D21
number of cells used for exRNA (average)	1,27E+07	9,13E+05	1,50E+07 ± 33%	1,65E+06 ± 30%
screened miRNAs (Exiqon)	752		375	
detected miRNAs in 2 conditions (average)	386		371	
detected miRNAs in 1 condition (average)	156		0	
not detected (average)	210		4	
raw Ct-values normalized to number of cells used for EV-miRNA				
detected miRNAs Ct(Average) ≤ 31	101	187	112	220
detected miRNAs Ct(Average) 31 - 35	197	142	138	132
detected miRNAs Ct(Average) 35 - 38	459	313	121	19
detected miRNAs Ct(Average) > 38	366	235	0	0
Dataset of miRNAs for statistic quantification (Ct(Average) < 38)			352	
miRNAs with complete dataset for 3 Donor D7/D21			280/290	
miRNAs with complete dataset for 2 Donor D7/D21			36/38	
miRNAs with complete dataset for 1 Donor D7/D21			36/24	

6.2. miRNAs from customized qPCR panel.

Table 15 Customized qPCR panel for the screening of secretory miRNAs

microRNA Name	Order in 384 (for sorting by row)	Order in 384 (for sorting by column)	Panel plate position	Target sequence
hsa-miR-1	1	1	A01	UGGAAUGUAAAGAAGUAUGUAU
hsa-let-7g-3p	2	17	A02	CUGUACAGGCCACUGCCUUGC
hsa-miR-18a-3p	3	33	A03	ACUGCCCUAAGUGCUCCUUCUGG
hsa-miR-24-3p	4	49	A04	UGGCUCAGUUCAGCAGGAACAG
hsa-miR-29c-3p	5	65	A05	UAGCACCAUUUGAAAUCGGUUA
hsa-miR-34b-3p	6	81	A06	CAAUCACUAACUCCACUGCCAU
hsa-miR-106b-5p	7	97	A07	UAAAGUGCUGACAGUGCAGAU
hsa-miR-132-3p	8	113	A08	UACAGUCUACAGCCAUGGUCG
hsa-miR-143-3p	9	129	A09	UGAGAUGAAGCACUGUAGCUC
hsa-miR-152-3p	10	145	A10	UCAGUGCAUGACAGAACUUGG
hsa-miR-192-5p	11	161	A11	CUGACCUAUGAAUUGACAGCC
hsa-miR-199b-5p	12	177	A12	CCCAGUGUUUAGACUAUCUGUUC
hsa-miR-221-3p	13	193	A13	AGCUACAUUGUCUGCUGGGUUUC
hsa-miR-323a-3p	14	209	A14	CACAUUACACGGUCGACCUCU
hsa-miR-340-3p	15	225	A15	UCCGUCUCAGUUACUUUAUAGC
hsa-miR-376b-3p	16	241	A16	AUCAUAGAGGAAAUCCAUGUU
hsa-miR-411-5p	17	257	A17	UAGUAGACCGUAUAGCGUACG
hsa-miR-450b-5p	18	273	A18	UUUUGCAUAUGUUCUGAAUA
hsa-miR-493-3p	19	289	A19	UGAAGGUCUACUGUGGCCAGG
hsa-miR-514a-3p	20	305	A20	AUUGACACUUCUGUGAGUAGA
hsa-miR-590-5p	21	321	A21	GAGCUUAUUCAUAAAAGUGCAG
hsa-miR-660-5p	22	337	A22	UACCAUUGCAUACGGAGUUG
hsa-miR-940	23	353	A23	AAGGCAGGCCCCCGCUCUCCC
hsa-miR-95-3p	24	369	A24	UUCAACGGUAUUUUUUGAGCA
U6 snRNA	25	2	B01	
hsa-let-7g-5p	26	18	B02	UGAGGUAGUAGUUUGUACAGUU
hsa-miR-18a-5p	27	34	B03	UAAGGUGCAUCUAGUGCAGAUAG
hsa-miR-25-3p	28	50	B04	CAUUGCACUUGUCUCGGUCUGA
hsa-miR-29c-5p	29	66	B05	UGACCGAUUUCUCCUGGUGUUC
hsa-miR-34b-5p	30	82	B06	UAGGCAGUGUCAUAGCUGAUUG
hsa-miR-107	31	98	B07	AGCAGCAUUGUACAGGGCUAUC
hsa-miR-133a-3p	32	114	B08	UUUGGUCCCCUUAACACAGCUG
hsa-miR-143-5p	33	130	B09	GGUGCAGUGCUGCAUCUCUGGU
hsa-miR-154-3p	34	146	B10	AAUCAUACACGGUUGACCUAUU
hsa-miR-193a-3p	35	162	B11	AACUGGCCUACAAGUCCCAGU
hsa-miR-200a-3p	36	178	B12	UAACACUGUCUGGUUACGAUGU
hsa-miR-221-5p	37	194	B13	ACCUGGCAUACAAGUAGAUUU
hsa-miR-324-3p	38	210	B14	ACUGCCCCAGGUGCUGCUGG
hsa-miR-342-3p	39	226	B15	UCUCACACAGAAAUCGCACCCGU
hsa-miR-376c-3p	40	242	B16	AACAUAGAGGAAAUCCACGU
hsa-miR-412-3p	41	258	B17	ACUUCACCUUGGUCCACUAGCCGU
hsa-miR-451a	42	274	B18	AAACCGUUACCAUACUGAGUU
hsa-miR-493-5p	43	290	B19	UUGUACAUGGUAGGCUUUCAUU
hsa-miR-520h	44	306	B20	ACAAAGUGCUUCCUUUAGAGU
hsa-miR-595	45	322	B21	GAAGUGUGCCGUGGUGUGUCU
hsa-miR-663a	46	338	B22	AGGCGGGGCGCCGCGGGACCGC
hsa-miR-941	47	354	B23	CACCCGGCUGUGUGCACAUGUGC
hsa-miR-98-5p	48	370	B24	UGAGGUAGUAAGUUGUAUUGUU

Supplementary Tables

hsa-miR-7-5p	49	3	C01	UGGAAGACUAGUGAUUUUGUUGU
hsa-let-7i-3p	50	19	C02	CUGCGCAAGCUACUGCCUUGCU
hsa-miR-18b-5p	51	35	C03	UAAGGUGCAUCUAGUGCAGUUAG
hsa-miR-26a-5p	52	51	C04	UUCAAGUAAUCCAGGAUAGGCU
hsa-miR-30a-3p	53	67	C05	CUUUCAGUCGGAUGUUUGCAGC
hsa-miR-34c-3p	54	83	C06	AAUCACUAACCACACGGCCAGG
hsa-miR-125a-3p	55	99	C07	ACAGGUGAGGUUCUUGGGAGCC
hsa-miR-133b	56	115	C08	UUUGGUCCCCUUAACCAGCUA
hsa-miR-144-3p	57	131	C09	UACAGUAUAGAUGAUUACU
hsa-miR-154-5p	58	147	C10	UAGGUUAUCCGUGUUGCCUUCG
hsa-miR-193a-5p	59	163	C11	UGGGUCUUUGCGGGCGAGAUGA
hsa-miR-200b-3p	60	179	C12	UAAUACUGCCUGGUAAUGAUGA
hsa-miR-222-3p	61	195	C13	AGCUACAUCUGGCUACUGGGU
hsa-miR-324-5p	62	211	C14	CGCAUCCCCUAGGGCAUUGGUGU
hsa-miR-346	63	227	C15	UGUCUGCCCGCAUGCCUGCCUCU
hsa-miR-377-3p	64	243	C16	AUCACACAAAGGCAACUUUUGU
hsa-miR-421	65	259	C17	AUCAACAGACAUUAAUUGGGCGC
hsa-miR-452-5p	66	275	C18	AACUGUUUGCAGAGGAAACUGA
hsa-miR-494-3p	67	291	C19	UGAAACAUACACGGGAAACCUC
hsa-miR-532-3p	68	307	C20	CCUCCACACCCAAGGCUUGCA
hsa-miR-604	69	323	C21	AGGCUGCGGAUUUCAGGAC
hsa-miR-663b	70	339	C22	GGUGGCCCGGCCUGCCUGAGG
hsa-miR-1185-5p	71	355	C23	AGAGGAUACCCUUUGUAUGUU
hsa-miR-99a-3p	72	371	C24	CAAGCUCGCUUCUAGGGUCUG
hsa-let-7a-2-3p	73	4	D01	CUGUACAGCCUCCUAGCUUUC
hsa-let-7i-5p	74	20	D02	UGAGGUAGUAGUUUGUGCUGUU
hsa-miR-19a-3p	75	36	D03	UGUGCAAUCUAUGCAAAACUGA
hsa-miR-26b-3p	76	52	D04	CCUGUUCUCAAUACUUGGCUC
hsa-miR-30a-5p	77	68	D05	UGUAAACAUCUCGACUGGAAG
hsa-miR-34c-5p	78	84	D06	AGGCAGUGUAGUUAGCUGAUUGC
hsa-miR-122-5p	79	100	D07	UGGAGUGUGACAAUGGUGUUUG
hsa-miR-136-3p	80	116	D08	CAUCAUCGUCUCAAUGAGUCU
hsa-miR-144-5p	81	132	D09	GGAUUAUCAUAUACUGUAAG
hsa-miR-181a-2-3p	82	148	D10	ACCACUGACCGUUGACUGUACC
hsa-miR-193b-3p	83	164	D11	AACUGGCCCUCAAAGUCCCGCU
hsa-miR-200c-3p	84	180	D12	UAAUACUGCCGGGUAAUGAUGA
hsa-miR-222-5p	85	196	D13	CUCAGUAGCCAGUGUAGAUCU
UniSp2 CP	86	212	D14	
hsa-miR-361-3p	87	228	D15	UCCCCAGGUGUGAUUCUGAUUU
hsa-miR-377-5p	88	244	D16	AGAGGUUGCCCUUGGUGAAUUC
hsa-miR-423-3p	89	260	D17	AGCUCGGUCUGAGGCCCCUCAGU
hsa-miR-454-3p	90	276	D18	UAGUGCAAUUAUGCUUAUAGGGU
hsa-miR-495-3p	91	292	D19	AAACAAACAUGGUGCACUUCU
hsa-miR-532-5p	92	308	D20	CAUGCCUUGAGUGUAGGACCGU
hsa-miR-615-3p	93	324	D21	UCCGAGCCUGGGUCUCCUCU
hsa-miR-664a-3p	94	340	D22	UAUUCAUUUAUCCCCAGCCUACA
hsa-miR-1207-5p	95	356	D23	UGGCAGGGAGGCUGGGAGGGG
hsa-miR-99a-5p	96	372	D24	AACCCGUAGAUCGACUUGUG
hsa-let-7a-3p	97	5	E01	CUAUACAUCUACUGUCUUUC
hsa-miR-9-3p	98	21	E02	AUAAAGCUAGAUAAACCGAAAGU
hsa-miR-19b-3p	99	37	E03	UGUGCAAUCCAUGCAAAACUGA
hsa-miR-26b-5p	100	53	E04	UUCAAGUAAUUCAGGAUAGGU
hsa-miR-30b-5p	101	69	E05	UGUAAACAUCUACACUCAGCU
hsa-miR-92a-3p	102	85	E06	UAUUGCACUUGUCCCGGCCUGU
hsa-miR-125a-5p	103	101	E07	UCCUGAGACCCUUUAACUGUGA

Supplementary Tables

hsa-miR-134-5p	104	117	E08	UGUGACUGGUUGACCAGAGGGG
hsa-miR-145-3p	105	133	E09	GGAUUCCUGGAAUACUGUUCU
hsa-miR-181a-3p	106	149	E10	ACCAUCGACCGUUGAUUGUACC
hsa-miR-193b-5p	107	165	E11	CGGGGUUUUGAGGGCGAGAUGA
hsa-miR-200b-5p	108	181	E12	CAUCUUACUGGGCAGCAUUGGA
hsa-miR-223-3p	109	197	E13	UGUCAGUUUGUCAAAUACCCCA
hsa-miR-328-3p	110	213	E14	CUGGCCUCUCUGCCCUUCCGU
hsa-miR-361-5p	111	229	E15	UUAUCAGAAUCUCAGGGGUAC
hsa-miR-378a-3p	112	245	E16	ACUGGACUUGGAGUCAGAAGGC
hsa-miR-423-5p	113	261	E17	UGAGGGGCAGAGAGCGAGACUUU
hsa-miR-455-3p	114	277	E18	GCAGUCCAUGGGCAUUAACAC
hsa-miR-496	115	293	E19	UGAGUAUUACAUGGCCAAUCUC
hsa-miR-539-5p	116	309	E20	GGAGAAUUUAUCCUUGGUGUGU
hsa-miR-625-3p	117	325	E21	GACUAUAGAACUUUCCCCUCA
hsa-miR-665	118	341	E22	ACCAGGAGGCUGAGGCCCU
hsa-miR-1247-5p	119	357	E23	ACCCGUCCGUUCGUCCCCGGA
hsa-miR-99b-3p	120	373	E24	CAAGCUCGUGUCUGUGGGUCCG
hsa-let-7a-5p	121	6	F01	UGAGGUAGUAGGUUGUAUAGUU
hsa-miR-10a-3p	122	22	F02	CAAAUUCGUUUAUAGGGGAUA
hsa-miR-20a-3p	123	38	F03	ACUGCAUUAUGAGCACUUAAG
hsa-miR-27a-3p	124	54	F04	UUCACAGUGGCUAAGUUCGCG
hsa-miR-30c-2-3p	125	70	F05	CUGGGAGAAGGCUUUUACUCU
hsa-miR-92b-3p	126	86	F06	UAUUGCACUCGUCCCGGCCUCC
hsa-miR-125b-1-3p	127	102	F07	ACGGGUUAGGCUCUUGGGAGCU
hsa-miR-136-5p	128	118	F08	ACUCCAUUUGUUUUGAUGAUGGA
hsa-miR-145-5p	129	134	F09	GUCCAGUUUCCAGGAUCCCU
hsa-miR-181a-5p	130	150	F10	AACAUUCAACGCUGUCGGUGAGU
hsa-miR-194-3p	131	166	F11	CCAGUGGGGCGUCUGUUUUCUG
hsa-miR-203a	132	182	F12	GUGAAUGUUUAGGACCACUAG
hsa-miR-224-3p	133	198	F13	AAAAUGGUGCCCUAGUGACUACA
hsa-miR-329-3p	134	214	F14	AACACACCUGUUUAAACCUCUUU
hsa-miR-362-3p	135	230	F15	AACACACCUAUUCAAGGAUUCA
hsa-miR-378a-5p	136	246	F16	CUCCUGACUCCAGGUCCUGUGU
hsa-miR-424-3p	137	262	F17	CAAAACGUGAGGCGCUGCUAU
hsa-miR-455-5p	138	278	F18	UAUGUGCCUUUGGACUACAUCG
hsa-miR-497-5p	139	294	F19	CAGCAGCACACUGUGGUUUUGU
hsa-miR-542-5p	140	310	F20	UCGGGGAUCAUUAUGUCACGAGA
hsa-miR-628-3p	141	326	F21	UCUAGUAAGAGUGGCAGUCGA
hsa-miR-671-5p	142	342	F22	AGGAAGCCCUUGAGGGGCGUGAG
hsa-miR-1249	143	358	F23	ACGCCCCUCCCCCUUCUUCA
hsa-miR-99b-5p	144	374	F24	CACCCGUAGAACCACCUUGCG
hsa-let-7b-3p	145	7	G01	CUAUACAACCUACUGCCUCCCC
hsa-miR-10a-5p	146	23	G02	UACCCUGUAGAUCCGAUUUGUG
hsa-miR-20a-5p	147	39	G03	UAAAGUGCUUUAUGUCAGGUAG
hsa-miR-27a-5p	148	55	G04	AGGGCUUAGCUGCUUGUGAGCA
hsa-miR-30c-5p	149	71	G05	UGUAAACAUCUACACUCUCAGC
hsa-miR-93-3p	150	87	G06	ACUGCUGAGCUAGCACUUCGCG
hsa-miR-125b-5p	151	103	G07	UCCUGAGACCCUAAUUGUGA
hsa-miR-137	152	119	G08	UUAUUGCUUUAAGAAUACGCGUAG
hsa-miR-146a-5p	153	135	G09	UGAGAACUGAAUUAUUGGGUU
hsa-miR-181b-5p	154	151	G10	AACAUUCAUUGCUGUCGGUGGGU
hsa-miR-195-5p	155	167	G11	UAGCAGCACAGAAAUUUGGC
hsa-miR-204-5p	156	183	G12	UUCCUUUGUCAUCCUAUGCCU
hsa-miR-224-5p	157	199	G13	CAAGUCACUAGUGGUUCCGUU
hsa-miR-330-3p	158	215	G14	GCAAAGCACACGGCCUGCAGAGA

Supplementary Tables

hsa-miR-362-5p	159	231	G15	AAUCCUUGGAACCUAGGUGUGAGU
hsa-miR-379-3p	160	247	G16	UAUGUAAACUGGUCCACUAAACU
hsa-miR-424-5p	161	263	G17	CAGCAGCAAUUAUGUUUUGAA
hsa-miR-483-3p	162	279	G18	UCACUCCUCUCCUCCGUCUU
hsa-miR-499a-5p	163	295	G19	UUAAGACUUGCAGUGAUGUUU
hsa-miR-543	164	311	G20	AAACAUUCGCGGUGCACUUCUU
hsa-miR-629-5p	165	327	G21	UGGGUUUACGUUGGGAGAACU
hsa-miR-675-3p	166	343	G22	CUGUAUGCCCUACCCGCUCA
hsa-miR-1256	167	359	G23	AGGCAUUGACUUCUCACUAGCU
hsa-miR-155-5p	168	375	G24	UUAUUGCUAAUCGUAUAGGGGU
hsa-let-7b-5p	169	8	H01	UGAGGUAGUAGGUUGUGUGUU
hsa-miR-10b-5p	170	24	H02	UACCCUGUAGAACCAGAAUUUGUG
hsa-miR-21-3p	171	40	H03	CAACACCAGUCGUAUGGGCUGU
hsa-miR-27b-3p	172	56	H04	UUCACAGUGGCUAAGUUCUGC
hsa-miR-30d-3p	173	72	H05	CUUUCAGUCAGAUUUUUGCUGC
hsa-miR-93-5p	174	88	H06	CAAAGUCGUGUUCGUGCAGGUAG
hsa-miR-126-3p	175	104	H07	UCGUACCGUGAGUAAUUAUGCG
hsa-miR-138-1-3p	176	120	H08	GCUACUUCACAACACCAGGGCC
hsa-miR-146b-5p	177	136	H09	UGAGAACUGAAUUCUAGGCU
hsa-miR-181c-3p	178	152	H10	AACCAUCGACCGUUGAGUGGAC
Cel-miR-39-3p CP	179	168	H11	
hsa-miR-205-5p	180	184	H12	UCCUUCAUUCCACCGGAGUCUG
hsa-miR-296-3p	181	200	H13	GAGGGUUGGGUGGAGGCUCUCC
hsa-miR-331-3p	182	216	H14	GCCCCUGGGCCUAUCCUAGAA
hsa-miR-365a-3p	183	232	H15	UAAUGCCCCUAAAAUCCUUUAU
hsa-miR-379-5p	184	248	H16	UGGUAGACUAUGGAACGUAGG
hsa-miR-425-3p	185	264	H17	AUCGGGAUGUCGUGUCCGCC
hsa-miR-483-5p	186	280	H18	AAGACGGGAGGAAAGAAGGGAG
hsa-miR-500a-5p	187	296	H19	UAAUCCUUGCUACCUGGGUGAGA
hsa-miR-548c-5p	188	312	H20	AAAAGUAAUUGCGGUUUUUGCC
hsa-miR-632	189	328	H21	GUGUCUGCUUCCUGUGGA
hsa-miR-708-3p	190	344	H22	CAACUAGACUGUGAGCUUCUAG
hsa-miR-1260a	191	360	H23	AUCCCACCUCUGCCACCA
hsa-miR-487a-3p	192	376	H24	AAUCAUACAGGGACAUCAGUU
hsa-let-7c-5p	193	9	I01	UGAGGUAGUAGGUUGUAUGUU
hsa-miR-15a-3p	194	25	I02	CAGGCCAUUUGUGCUGCCUCA
hsa-miR-21-5p	195	41	I03	UAGCUUAUCAGACUGAUGUUGA
hsa-miR-27b-5p	196	57	I04	AGAGCUUAGCUGAUUGGUGAAC
hsa-miR-30d-5p	197	73	I05	UGUAAACAUCCCCGACUGGAAG
hsa-miR-100-5p	198	89	I06	AACCCGUAUAUCCGAACUUGUG
hsa-miR-126-5p	199	105	I07	CAUUAAUACUUUUGGUACGCG
hsa-miR-138-5p	200	121	I08	AGCUGGUGUUGUGAAUCAGGCCG
hsa-miR-148a-3p	201	137	I09	UCAGUGCACUACAGAACUUUGU
hsa-miR-181c-5p	202	153	I10	AACAUUCAACCUUGCGGUGAGU
hsa-miR-194-5p	203	169	I11	UGUAACAGCAACUCCAUGUGGA
hsa-miR-206	204	185	I12	UGGAAUGUAAGGAAGUGUGUGG
hsa-miR-296-5p	205	201	I13	AGGGCCCCCCCCUAAUCCUGU
hsa-miR-331-5p	206	217	I14	CUAGGUUAGGUUCCAGGGUAUCC
hsa-miR-365b-5p	207	233	I15	AGGGACUUUCAGGGGACGUGU
hsa-miR-381-3p	208	249	I16	UAUACAAGGGCAAGCUCUCUGU
hsa-miR-425-5p	209	265	I17	AAUGACACGAUCACUCCGUUGA
hsa-miR-484	210	281	I18	UCAGGCUCAGUCCCCUCCGAU
hsa-miR-501-3p	211	297	I19	AAUGCACCCGGGCAAGGAUUCU
hsa-miR-548k	212	313	I20	AAAAGUACUUGCGGAUUUUGCU
hsa-miR-638	213	329	I21	AGGGAUCGCGGGCGGGUGGCGGCCU

Supplementary Tables

hsa-miR-708-5p	214	345	I22	AAGGAGCUUACAAUCUAGCUGGG
hsa-miR-1271-5p	215	361	I23	CUUGGCACCUAGCAAGCACUCA
	216	377	I24	
hsa-let-7d-3p	217	10	J01	CUAUACGACCUGCUGCCUUUCU
hsa-miR-15a-5p	218	26	J02	UAGCAGCACAUAAUGGUUUGUG
hsa-miR-22-3p	219	42	J03	AAGCUGCCAGUUGAAGAACUGU
hsa-miR-28-3p	220	58	J04	CACUAGAUUGUGAGCUCUGGA
hsa-miR-30e-3p	221	74	J05	CUUUCAGUCGGAUGUUUACAGC
hsa-miR-101-3p	222	90	J06	UACAGUACUGUGAUAAACUGAA
hsa-miR-127-3p	223	106	J07	UCGGAUCCGUCUGAGCUUGGCU
hsa-miR-139-3p	224	122	J08	UGGAGACGCGGCCUGUUGGAGU
hsa-miR-147b	225	138	J09	GUGUGCGAAUUGCUUCUGCUA
hsa-miR-185-5p	226	154	J10	UGGAGAGAAAGGCAGUUCUGA
hsa-miR-196a-5p	227	170	J11	UAGGUAGUUUCAUGUUUGGG
hsa-miR-212-3p	228	186	J12	UACAGUCUCCAGUCACGGCC
hsa-miR-299-5p	229	202	J13	UGGUUUACCGUCCACAUACAU
hsa-miR-335-3p	230	218	J14	UUUUUCAUUUUGCUCCUGACC
hsa-miR-369-3p	231	234	J15	AAUAAUACAUGGUUGAUCUUU
hsa-miR-382-3p	232	250	J16	AAUCAUUCACGGACAACACUU
hsa-miR-431-3p	233	266	J17	CAGGUCGUCUUGCAGGGCUUCU
hsa-miR-485-3p	234	282	J18	GUCAUACACGGCUCUCCUCUCU
hsa-miR-502-3p	235	298	J19	AAUGCACCUUGGCAAGGAUUCA
hsa-miR-550a-3p	236	314	J20	UGUCUUACUCCUCACGGCACAU
hsa-miR-642a-5p	237	330	J21	GUCCCUCUCCAAUUGUGUCUUG
hsa-miR-744-5p	238	346	J22	UGC GG GCUAGGGCUAACAGCA
hsa-miR-1296-5p	239	362	J23	UUAGGGCCUGGCUCUCCUCC
hsa-miR-382-5p	240	378	J24	GAAGUUGUUGGUGGUAUUCG
hsa-let-7d-5p	241	11	K01	AGAGGUAGUAGGUUGCAUAGUU
hsa-miR-15b-3p	242	27	K02	CGAAUCAUUUUUGCUGCUCUA
hsa-miR-22-5p	243	43	K03	AGUUCUUCAGUGGCAAGCUUUA
hsa-miR-28-5p	244	59	K04	AAGGAGCUCACAGUCUAUUGAG
hsa-miR-30e-5p	245	75	K05	UGUAAACAUCUUGACUGGAAG
hsa-miR-101-5p	246	91	K06	CAGUUAUCACAGUCUGAUGCU
hsa-miR-127-5p	247	107	K07	CUGAAGCUCAGAGGGCUCUGAU
hsa-miR-139-5p	248	123	K08	UCUACAGUGCACGUGUCUCCAGU
hsa-miR-148b-3p	249	139	K09	UCAGUGCAUCACAGAACUUUGU
hsa-miR-326	250	155	K10	CCUCUGGGCCUUCUCCAG
hsa-miR-196b-3p	251	171	K11	UCGACAGCACGACACUGCCUUC
hsa-miR-214-3p	252	187	K12	ACAGCAGGCACAGACAGGCAGU
hsa-miR-301a-3p	253	203	K13	CAGUGCAAUAGUAUUGUCAAGC
hsa-miR-335-5p	254	219	K14	UCAAGAGCAAUACGAAAAAUGU
hsa-miR-370-3p	255	235	K15	GCCUCUGGGGUGGAACCUUGU
UniSp3 IPC	256	251	K16	
hsa-miR-431-5p	257	267	K17	UGUCUUGCAGGCGUCAUGCA
hsa-miR-486-5p	258	283	K18	UCCUGUACUGAGCUGCCCCGAG
hsa-miR-502-5p	259	299	K19	AUCCUUGCUAUCUGGGUGCUA
hsa-miR-551a	260	315	K20	GCGACCCACUCUUGGUUCCA
hsa-miR-643	261	331	K21	ACUUGUAUGCUAGCUCAGGUAG
hsa-miR-758-3p	262	347	K22	UUUGUGACCUUGGUCCACUAACC
hsa-miR-1468-5p	263	363	K23	CUCCGUUUGCCUGUUUCGUG
hsa-miR-585-3p	264	379	K24	UGGCGUAUCUGUAUGCUA
hsa-let-7e-3p	265	12	L01	CUAUACGGCCUCCUAGCUUUC
hsa-miR-15b-5p	266	28	L02	UAGCAGCACAUCAUGGUUUAACA
hsa-miR-23a-3p	267	44	L03	AUCACAUUGCCAGGGAUUUC
hsa-miR-29a-3p	268	60	L04	UAGCACCAUCUGAAUCCGUUA

Supplementary Tables

hsa-miR-31-3p	269	76	L05	UGCUAUGCCAACAUAUUGCCAU
hsa-miR-103a-3p	270	92	L06	AGCAGCAUUGUACAGGGCUAUGA
hsa-miR-128-3p	271	108	L07	UCACAGUGAACCGGUCUCUUU
hsa-miR-140-3p	272	124	L08	UACCACAGGGUAGAACCACGG
hsa-miR-148b-5p	273	140	L09	AAGUUCUGUUUAUACACUCAGGC
hsa-miR-186-5p	274	156	L10	CAAAGAAUUCUCCUUUUGGGCU
hsa-miR-197-3p	275	172	L11	UUCACCACCUUCUCCACCCAGC
hsa-miR-214-5p	276	188	L12	UGCCUGUCUACACUUGCUGUGC
hsa-miR-301b	277	204	L13	CAGUGCAAUGAUUUGUCAAAAGC
hsa-miR-337-3p	278	220	L14	CUCCUAUAUGAUGCCUUUCUUC
hsa-miR-373-5p	279	236	L15	ACUCAAAAUGGGGGCGCUUUC
hsa-miR-383-5p	280	252	L16	AGAUCAGAAGGUGAUUUGGGCU
hsa-miR-432-3p	281	268	L17	CUGGAUGGCUCUCCAUUGUCU
hsa-miR-487b-3p	282	284	L18	AAUCGUACAGGGUCAUCCACUU
hsa-miR-503-5p	283	300	L19	UAGCAGCGGGAACAGUUCUGCAG
hsa-miR-570-3p	284	316	L20	CGAAAACAGCAAUACCUUUGC
hsa-miR-649	285	332	L21	AAACUGUGUUGUUAAGAGUC
hsa-miR-766-3p	286	348	L22	ACUCCAGCCCCACAGCCUCAGC
hsa-miR-1913	287	364	L23	UCUGCCCCCUCGCGUCUGCCA
UniSp3 IPC	288	380	L24	
hsa-let-7e-5p	289	13	M01	UGAGGUAGGAGGUUGUAUAGUU
hsa-miR-16-1-3p	290	29	M02	CCAGUAUUAAACUGUGCUGCUGA
hsa-miR-23a-5p	291	45	M03	GGGGUUCUGGGGAUGGGAUUU
hsa-miR-29a-5p	292	61	M04	ACUGAUUUUUUUGGUGUUCAG
hsa-miR-31-5p	293	77	M05	AGGCAAGAUUGCUGGCAUAGCU
hsa-miR-106a-5p	294	93	M06	AAAAGUGCUUACAGUGCAGGUAG
hsa-miR-129-2-3p	295	109	M07	AAGCCCUUACCCCAAAAGCAU
hsa-miR-140-5p	296	125	M08	CAGUGGUUUUACCCUAUGGUAG
UniSp6 CP	297	141	M09	
hsa-miR-188-3p	298	157	M10	CUCCCACAUGCAGGGUUUGCA
hsa-miR-196b-5p	299	173	M11	UAGGUAGUUUCCUGUUGUUGGG
hsa-miR-215-5p	300	189	M12	AUGACCUAUGAAUUGACAGAC
hsa-miR-320a	301	205	M13	AAAAGCUGGGUUGAGAGGGCGA
hsa-miR-337-5p	302	221	M14	GAACGGCUUCAUACAGGAGUU
hsa-miR-374a-5p	303	237	M15	UUUAUAUACAACCUGAUUAGUG
hsa-miR-409-3p	304	253	M16	GAAUGUUGCUCGGUGAACCCCU
hsa-miR-432-5p	305	269	M17	UCUUGGAGUAGGUCAUUGGGUGG
hsa-miR-489-3p	306	285	M18	GUGACAUCACAUUACGGCAGC
hsa-miR-504-5p	307	301	M19	AGACCCUGGUCUGCACUCUAUC
hsa-miR-572	308	317	M20	GUCCGUCGCGCGUGGCCCA
hsa-miR-652-3p	309	333	M21	AAUGGCGCCACUAGGGUUGUG
hsa-miR-769-5p	310	349	M22	UGAGACCUCUGGGUUCUGAGCU
hsa-miR-1972	311	365	M23	UCAGGCCAGGCACAGUGGCUCA
hsa-miR-369-5p	312	381	M24	AGAUCGACCGUGUUUAUUCGC
hsa-let-7f-1-3p	313	14	N01	CUAUACAAUCUAUUGCCUCCCC
hsa-miR-16-5p	314	30	N02	UAGCAGCACGUAAAUAUUGGCG
hsa-miR-23b-3p	315	46	N03	AUCACAUUGCCAGGGAUUACC
UniSp5 CP	316	62	N04	
hsa-miR-32-5p	317	78	N05	UAUUGCACAUAUUAAGUUGCA
UniSp4 CP	318	94	N06	
hsa-miR-130a-3p	319	110	N07	CAGUGCAAUGUUAAAAGGGCAU
hsa-miR-141-3p	320	126	N08	UAACACUGUCUGGUAAAGAUGG
hsa-miR-150-5p	321	142	N09	UCUCCCAACCCUUGUACCAGUG
hsa-miR-188-5p	322	158	N10	CAUCCCUUGCAUGGUGGAGGG
hsa-miR-210-3p	323	174	N11	CUGUGCGUGUGACAGCGGCUGA

Supplementary Tables

hsa-miR-218-5p	324	190	N12	UUGUGCUUGAUCUAACCAUGU
hsa-miR-320b	325	206	N13	AAAAGCUGGGUUGAGAGGGCAA
hsa-miR-338-3p	326	222	N14	UCCAGCAUCAGUGAUUUUGUUG
hsa-miR-374b-5p	327	238	N15	AUAUAUAACAACCUGCUAAGUG
hsa-miR-409-5p	328	254	N16	AGGUUACCCGAGCAACUUUGCAU
hsa-miR-433-3p	329	270	N17	AUCAUGAUGGGCUCUCGGUGU
hsa-miR-490-3p	330	286	N18	CAACCUGGAGGACUCCAUGCUG
hsa-miR-505-3p	331	302	N19	CGUCAACACUUGCUGGUUCCU
hsa-miR-574-3p	332	318	N20	CACGCUCAUGCACACACCCACA
hsa-miR-654-3p	333	334	N21	UAUGUCUGCUGACCAUACCCUU
hsa-miR-874-3p	334	350	N22	CUGCCCUGGCCGAGGGACCGA
hsa-miR-2110	335	366	N23	UUGGGGAAACGGCCGCUGAGUG
hsa-miR-450a-5p	336	382	N24	UUUUGCGAUGUGUCCUAAUUAU
hsa-let-7f-2-3p	337	15	O01	CUAUACAGUCUACUGUCUUUCC
hsa-miR-17-3p	338	31	O02	ACUGCAGUGAAGGCACUUGUAG
hsa-miR-24-1-5p	339	47	O03	UGCCUACUGAGCUGAUUACAGU
hsa-miR-29b-2-5p	340	63	O04	CUGGUUUCACAUGGUGGCUUAG
hsa-miR-34a-3p	341	79	O05	CAAUCAGCAAGUAUACUGCCCU
hsa-miR-106b-3p	342	95	O06	CCGCACUGUGGGUACUUGCUGC
hsa-miR-130b-3p	343	111	O07	CAGUGCAAUGAUGAAAGGGCAU
hsa-miR-142-3p	344	127	O08	UGUAGUGUUUCCUACUUUAUGGA
hsa-miR-151a-3p	345	143	O09	CUAGACUGAAGCUCUUGAGG
hsa-miR-191-3p	346	159	O10	GCUGCGCUUGGAUUUCGUCCCC
hsa-miR-199a-3p	347	175	O11	ACAGUAGUCUGCACAUGGUUA
hsa-miR-219a-1-3p	348	191	O12	AGAGUUGAGUCUGGACGUCCCCG
hsa-miR-320c	349	207	O13	AAAAGCUGGGUUGAGAGGGU
hsa-miR-339-3p	350	223	O14	UGAGCGCCUCGACGACAGAGCCG
hsa-miR-376a-3p	351	239	O15	AUCAUAGAGGAAAAUCCACGU
hsa-miR-410-3p	352	255	O16	AAUUAACACAGAUGGCCUGU
hsa-miR-449a	353	271	O17	UGGCAGUGUAUUGUUAGCUGGU
hsa-miR-490-5p	354	287	O18	CCAUGGAUCUCCAGGUGGGU
hsa-miR-505-5p	355	303	O19	GGGAGCCAGGAAGUAUUGAUGU
hsa-miR-582-5p	356	319	O20	UUACAGUUGUUAACCCAGUUACU
hsa-miR-654-5p	357	335	O21	UGGUGGGCCGCGAGAACUUGUC
hsa-miR-885-5p	358	351	O22	UCCAUUACACUACCCUGCCUCU
hsa-miR-33a-5p	359	367	O23	GUGCAUUGUAGUUGCAUUGCA
hsa-miR-582-3p	360	383	O24	UAACUGGUUGAACAACUGAACC
hsa-let-7f-5p	361	16	P01	UGAGGUAGUAGAUUGUAUAGUU
hsa-miR-17-5p	362	32	P02	CAAAGUGCUUACAGUGCAGGUAG
hsa-miR-24-2-5p	363	48	P03	UGCCUACUGAGCUGAAACACAG
hsa-miR-29b-3p	364	64	P04	UAGCACCAUUUGAAUACAGUUU
hsa-miR-34a-5p	365	80	P05	UGGCAGUGUCUAGCUGGUUGU
hsa-miR-149-5p	366	96	P06	UCUGGCUCGGUGUCUUCACUCCC
hsa-miR-130b-5p	367	112	P07	ACUCUUUCCUGUUGCACUAC
hsa-miR-142-5p	368	128	P08	CAUAAAGUAGAAAGCACUACU
hsa-miR-151a-5p	369	144	P09	UCGAGGAGCUCACAGUCUAGU
hsa-miR-191-5p	370	160	P10	CAACGGAAUCCAAAAGCAGCUG
hsa-miR-199a-5p	371	176	P11	CCCAGUGUUCAGACUACCUGUUC
hsa-miR-219a-5p	372	192	P12	UGAUUGUCCAAACGCAAUUCU
hsa-miR-320d	373	208	P13	AAAAGCUGGGUUGAGAGGA
hsa-miR-339-5p	374	224	P14	UCCUGUCCUCCAGGAGCUCACG
hsa-miR-376a-5p	375	240	P15	GUAGAUUCUCCUUCUUAUGAGUA
hsa-miR-411-3p	376	256	P16	UAUGUAACACGGUCCACUAACC
hsa-miR-450b-3p	377	272	P17	UUGGGAUCAUUUUGCAUCCAUA
hsa-miR-491-5p	378	288	P18	AGUGGGGAACCCUCCAUGAGG

Supplementary Tables

hsa-miR-509-3-5p	379	304	P19	UACUGCAGACGUGGCAAUCAUG
hsa-miR-590-3p	380	320	P20	UAAUUUUUAUGUAUAAGCUAGU
hsa-miR-655-3p	381	336	P21	AUAAUACAUGGUUAACCUCUUU
hsa-miR-889-3p	382	352	P22	UUAAUAUCGGACAACCAUUGU
hsa-miR-7-1-3p	383	368	P23	CAACAAAUACAGUCUGCCAUA
hsa-miR-877-5p	384	384	P24	GUAGAGGAGAUGGCGCAGGG

6.3. Significantly differentially secrete miRNAs from SIPS cells from two timepoints D7 and D21 after the SIPS treatment

Top differentially secrete miRNAs from D7 and D21 separately, normalized to total cell number used for secretion.

Table 16 Significantly higher secrete miRNAs per cell from D7

miRNA	log2FC D7	AveExpr	p-value	adj. p-value
hsa-miR-196b-3p	7,5759	35,3239	2,25E-08	2,65E-06
hsa-miR-200c-3p	7,4822	31,9010	6,13E-08	5,41E-06
hsa-miR-378a-5p	7,2012	32,6093	7,36E-07	4,33E-05
hsa-miR-181a-3p	7,0348	32,9760	1,27E-06	6,39E-05
hsa-miR-582-5p	6,9512	33,5326	1,76E-06	7,75E-05
hsa-miR-582-3p	6,9012	32,4576	2,00E-06	7,86E-05
hsa-miR-129-2-3p	6,6912	32,4760	5,27E-06	1,86E-04
hsa-miR-26b-3p	6,4512	34,5351	6,34E-06	2,03E-04
hsa-miR-377-5p	6,3412	34,4326	1,09E-05	3,20E-04
hsa-miR-212-3p	6,2412	36,4110	1,41E-05	3,83E-04
hsa-miR-191-3p	6,1012	35,4676	1,61E-05	4,07E-04
hsa-miR-149-5p	5,9855	33,2360	1,87E-05	4,40E-04
hsa-miR-550a-3p	5,8212	34,6001	2,06E-05	4,54E-04
hsa-miR-361-3p	5,7380	33,9276	3,05E-05	6,31E-04
hsa-miR-642a-5p	5,5609	32,1576	3,22E-05	6,31E-04
hsa-miR-339-3p	5,4822	35,2514	3,64E-05	6,56E-04
hsa-miR-532-3p	5,4622	34,8593	3,72E-05	6,56E-04
hsa-miR-369-5p	5,3422	29,8293	4,81E-05	8,08E-04
hsa-miR-431-3p	5,3112	33,8160	5,19E-05	8,23E-04
hsa-miR-335-3p	5,2689	34,9951	5,36E-05	8,23E-04
hsa-miR-542-5p	5,2389	35,1251	9,44E-05	1,39E-03
hsa-let-7a-3p	5,1212	35,3126	1,34E-04	1,89E-03
hsa-miR-632	5,0609	35,2401	1,54E-04	2,09E-03
hsa-miR-30a-3p	5,0155	35,0364	1,68E-04	2,20E-03
hsa-miR-203a	4,9906	30,6543	1,77E-04	2,23E-03
hsa-miR-200b-5p	4,9706	36,0760	1,83E-04	2,23E-03
hsa-miR-1185-5p	4,9480	30,0610	1,94E-04	2,29E-03
hsa-miR-10a-3p	4,8859	35,6601	2,17E-04	2,47E-03
hsa-miR-24-1-5p	4,8422	33,3101	2,34E-04	2,58E-03
hsa-miR-23a-5p	4,7789	35,3651	2,57E-04	2,75E-03
hsa-miR-638	4,7455	36,6689	2,79E-04	2,84E-03
hsa-let-7a-2-3p	4,7109	35,3901	2,84E-04	2,84E-03
hsa-miR-370-3p	4,7089	32,5676	2,90E-04	2,84E-03
hsa-miR-154-3p	4,6709	34,8593	3,53E-04	3,37E-03
hsa-miR-758-3p	4,5855	35,4951	4,32E-04	3,85E-03
hsa-miR-425-3p	4,5722	31,2026	4,53E-04	3,85E-03
hsa-miR-181c-5p	4,5355	34,0464	4,57E-04	3,85E-03
hsa-miR-205-5p	4,4712	27,0776	4,58E-04	3,85E-03
hsa-miR-138-5p	4,4689	26,0643	4,58E-04	3,85E-03

Supplementary Tables

hsa-miR-769-5p	4,4489	33,0360	5,07E-04	4,02E-03
hsa-miR-93-3p	4,2259	34,2964	5,10E-04	4,02E-03
hsa-miR-125b-1-3p	4,1955	31,5643	5,13E-04	4,02E-03
hsa-miR-29b-2-5p	4,1509	32,3176	5,73E-04	4,40E-03
hsa-miR-134-5p	4,1189	33,5210	6,13E-04	4,60E-03
hsa-miR-595	4,1089	32,3410	6,41E-04	4,71E-03
hsa-miR-196a-5p	4,0922	35,6151	6,87E-04	4,95E-03
hsa-miR-224-3p	4,0709	31,3626	7,07E-04	4,99E-03
hsa-miR-940	3,9789	31,5326	7,23E-04	5,00E-03
hsa-miR-9-3p	3,9512	30,4560	7,39E-04	5,02E-03
hsa-miR-138-1-3p	3,9277	35,9543	7,81E-04	5,20E-03
hsa-miR-1207-5p	3,9222	35,6701	8,45E-04	5,53E-03
hsa-miR-660-5p	3,8489	36,4960	9,18E-04	5,89E-03
hsa-miR-31-5p	3,8455	33,6643	9,90E-04	6,24E-03
hsa-miR-1260a	3,8455	35,7201	1,02E-03	6,31E-03
hsa-miR-483-3p	3,8155	33,2843	1,06E-03	6,42E-03
hsa-miR-32-5p	3,8122	29,5743	1,13E-03	6,73E-03
hsa-miR-34b-5p	3,8080	26,1543	1,15E-03	6,76E-03
hsa-miR-34a-3p	3,7789	35,8726	1,19E-03	6,86E-03
hsa-miR-337-5p	3,7589	30,3710	1,22E-03	6,86E-03
hsa-let-7f-2-3p	3,7455	29,1343	1,22E-03	6,86E-03
hsa-miR-137	3,7155	35,7901	1,32E-03	7,23E-03
hsa-miR-708-5p	3,7089	31,1643	1,33E-03	7,23E-03
hsa-miR-485-3p	3,7022	35,2443	1,42E-03	7,59E-03
hsa-miR-139-3p	3,6855	33,1039	1,65E-03	8,69E-03
hsa-miR-675-3p	3,6355	33,2643	1,67E-03	8,69E-03
hsa-miR-496	3,6122	36,4576	1,71E-03	8,71E-03
hsa-miR-502-3p	3,5980	31,9693	1,73E-03	8,71E-03
hsa-miR-28-3p	3,5922	28,1210	1,85E-03	9,22E-03
hsa-miR-132-3p	3,5722	34,9664	1,99E-03	9,73E-03
hsa-miR-29a-3p	3,5655	33,0643	2,01E-03	9,73E-03
hsa-miR-483-5p	3,5555	35,9226	2,07E-03	9,90E-03
hsa-miR-337-3p	3,5455	35,9301	2,17E-03	1,02E-02
hsa-miR-31-3p	3,5455	27,6143	2,27E-03	1,06E-02
hsa-miR-362-3p	3,5189	33,0514	2,42E-03	1,10E-02
hsa-miR-548c-5p	3,4989	32,5693	2,44E-03	1,10E-02
hsa-miR-323a-3p	3,4455	33,8160	2,59E-03	1,13E-02
hsa-miR-663b	3,4389	33,5660	2,59E-03	1,13E-02
hsa-miR-885-5p	3,4355	35,1860	2,59E-03	1,13E-02
hsa-miR-34a-5p	3,4122	30,9860	2,69E-03	1,16E-02
hsa-miR-193a-3p	3,3855	36,3676	2,77E-03	1,18E-02
hsa-miR-2110	3,3755	31,7493	3,34E-03	1,40E-02
hsa-miR-193b-3p	3,3455	33,9414	3,43E-03	1,42E-02
hsa-miR-219a-5p	3,3222	31,9093	3,61E-03	1,48E-02
hsa-miR-663a	3,3022	31,7610	3,79E-03	1,53E-02
hsa-miR-664a-3p	3,3022	30,2660	3,83E-03	1,53E-02
hsa-miR-744-5p	3,3022	32,0043	4,09E-03	1,62E-02
hsa-miR-505-5p	3,2930	27,8110	4,25E-03	1,66E-02
hsa-miR-133a-3p	3,2889	31,5426	4,29E-03	1,66E-02
hsa-miR-590-3p	3,2789	35,8076	4,33E-03	1,66E-02
hsa-miR-432-5p	3,2155	24,4710	4,50E-03	1,70E-02
hsa-miR-1271-5p	3,1948	34,5351	4,54E-03	1,70E-02
hsa-miR-196b-5p	3,1889	28,7493	4,63E-03	1,72E-02
hsa-miR-219a-1-3p	3,1812	29,5126	4,90E-03	1,80E-02
hsa-miR-346	3,1812	34,8876	5,04E-03	1,82E-02
hsa-miR-34b-3p	3,1812	30,9910	5,04E-03	1,82E-02
hsa-miR-504-5p	3,1812	35,1851	5,12E-03	1,83E-02
hsa-miR-324-5p	3,1722	31,9876	5,33E-03	1,88E-02

Supplementary Tables

hsa-miR-195-5p	3,1689	29,4843	5,74E-03	1,99E-02
hsa-miR-1249	3,1455	23,7410	5,74E-03	1,99E-02
hsa-miR-499a-5p	3,1430	27,1343	5,85E-03	2,00E-02
hsa-miR-152-3p	3,1322	28,1243	6,07E-03	2,04E-02
hsa-miR-590-5p	3,1289	27,6460	6,12E-03	2,04E-02
hsa-miR-30d-3p	3,1255	31,2960	6,12E-03	2,04E-02
hsa-miR-24-3p	3,1122	26,2476	6,30E-03	2,08E-02
hsa-miR-320b	3,1022	31,2943	6,41E-03	2,10E-02
hsa-miR-133b	3,0822	23,6610	6,77E-03	2,18E-02
hsa-miR-148b-5p	3,0722	34,5893	6,84E-03	2,18E-02
hsa-miR-218-5p	3,0722	35,2810	6,90E-03	2,18E-02
hsa-miR-141-3p	3,0630	36,2801	6,94E-03	2,18E-02
hsa-miR-99a-3p	3,0580	29,7176	7,02E-03	2,18E-02
hsa-miR-329-3p	3,0522	29,9776	7,02E-03	2,18E-02
hsa-miR-29b-3p	3,0255	30,2193	7,09E-03	2,18E-02
hsa-miR-23a-3p	3,0255	30,8826	7,22E-03	2,20E-02
hsa-miR-125a-5p	3,0189	34,7851	7,31E-03	2,20E-02
hsa-miR-365a-3p	3,0055	32,8543	7,42E-03	2,20E-02
hsa-miR-376c-3p	3,0022	32,7076	7,42E-03	2,20E-02
hsa-miR-193a-5p	3,0022	25,2776	7,69E-03	2,26E-02
hsa-miR-27a-3p	2,9922	33,2576	7,97E-03	2,33E-02
hsa-miR-224-5p	2,9855	31,3860	8,19E-03	2,37E-02
hsa-miR-206	2,9777	30,1926	8,34E-03	2,39E-02
hsa-miR-125b-5p	2,9655	31,7278	8,50E-03	2,39E-02
hsa-miR-101-5p	2,9622	34,2293	8,64E-03	2,39E-02
hsa-miR-222-5p	2,9589	30,2126	8,64E-03	2,39E-02
hsa-miR-543	2,9522	31,9560	8,64E-03	2,39E-02
hsa-miR-128-3p	2,9522	29,3343	8,71E-03	2,39E-02
hsa-miR-214-5p	2,9489	36,8978	8,77E-03	2,39E-02
hsa-miR-328-3p	2,9422	29,2226	8,79E-03	2,39E-02
hsa-miR-452-5p	2,9322	27,3143	8,87E-03	2,39E-02
hsa-let-7i-3p	2,9322	32,6143	9,19E-03	2,44E-02
hsa-miR-23b-3p	2,9189	24,2876	9,19E-03	2,44E-02
hsa-miR-7-1-3p	2,9055	36,5160	9,44E-03	2,49E-02
hsa-miR-204-5p	2,8955	30,2393	9,60E-03	2,51E-02
hsa-miR-154-5p	2,8889	30,0243	9,69E-03	2,51E-02
hsa-miR-502-5p	2,8755	29,7293	9,77E-03	2,52E-02
hsa-miR-493-5p	2,8755	27,2710	9,86E-03	2,52E-02
hsa-miR-17-5p	2,8755	28,9143	1,00E-02	2,53E-02
hsa-miR-192-5p	2,8722	25,7760	1,01E-02	2,53E-02
hsa-miR-197-3p	2,8689	26,4860	1,01E-02	2,53E-02
hsa-miR-22-3p	2,8655	31,6460	1,03E-02	2,56E-02
hsa-miR-331-5p	2,8630	25,2360	1,05E-02	2,59E-02
hsa-miR-10a-5p	2,8522	28,9560	1,07E-02	2,61E-02
hsa-miR-221-3p	2,8522	32,8443	1,11E-02	2,71E-02
hsa-miR-643	2,8422	33,9760	1,14E-02	2,76E-02
hsa-let-7b-3p	2,8355	28,6143	1,15E-02	2,77E-02
hsa-miR-410-3p	2,8322	30,3143	1,17E-02	2,80E-02
hsa-miR-130a-3p	2,8289	29,1343	1,26E-02	2,98E-02
hsa-miR-423-5p	2,8255	29,9960	1,29E-02	3,01E-02
hsa-miR-29a-5p	2,8189	31,7743	1,30E-02	3,01E-02
hsa-miR-222-3p	2,8155	30,9526	1,31E-02	3,01E-02
hsa-miR-320a	2,8155	26,3893	1,31E-02	3,01E-02
hsa-miR-145-3p	2,8089	37,4443	1,32E-02	3,01E-02
hsa-miR-27b-3p	2,8022	29,2426	1,33E-02	3,01E-02
hsa-miR-99b-5p	2,7955	30,7526	1,36E-02	3,01E-02
hsa-miR-335-5p	2,7789	28,4926	1,36E-02	3,01E-02
hsa-miR-221-5p	2,7689	31,2793	1,36E-02	3,01E-02

Supplementary Tables

hsa-miR-136-3p	2,7655	27,6793	1,36E-02	3,01E-02
hsa-miR-126-5p	2,7589	27,2043	1,37E-02	3,02E-02
hsa-miR-409-3p	2,7322	34,3626	1,40E-02	3,08E-02
hsa-miR-30a-5p	2,7222	30,3010	1,44E-02	3,14E-02
hsa-miR-326	2,7189	34,1960	1,45E-02	3,14E-02
hsa-miR-342-3p	2,7155	32,9126	1,53E-02	3,28E-02
hsa-let-7b-5p	2,7155	32,2826	1,55E-02	3,30E-02
hsa-miR-1256	2,7122	25,0793	1,55E-02	3,30E-02
hsa-miR-29c-3p	2,7089	33,3843	1,59E-02	3,36E-02
hsa-miR-503-5p	2,7022	27,9526	1,60E-02	3,37E-02
hsa-let-7e-5p	2,7022	25,6976	1,62E-02	3,38E-02
hsa-miR-421	2,7022	27,2543	1,64E-02	3,41E-02
hsa-miR-127-3p	2,7022	29,3510	1,67E-02	3,45E-02
hsa-miR-136-5p	2,6989	25,7510	1,70E-02	3,48E-02
hsa-miR-194-5p	2,6789	31,5010	1,73E-02	3,48E-02
hsa-miR-1468-5p	2,6755	27,4443	1,73E-02	3,48E-02
hsa-miR-92b-3p	2,6555	31,6560	1,74E-02	3,48E-02
hsa-miR-186-5p	2,6489	28,1710	1,76E-02	3,48E-02
hsa-miR-126-3p	2,6489	32,4410	1,76E-02	3,48E-02
hsa-miR-125a-3p	2,6389	32,4810	1,76E-02	3,48E-02
hsa-miR-361-5p	2,6355	30,6576	1,84E-02	3,62E-02
hsa-miR-92a-3p	2,6322	29,4510	1,84E-02	3,62E-02
hsa-let-7i-5p	2,6255	28,3843	1,88E-02	3,66E-02
hsa-miR-140-5p	2,6189	33,2326	1,90E-02	3,69E-02
hsa-miR-100-5p	2,6122	30,8960	1,92E-02	3,71E-02
hsa-miR-338-3p	2,6055	30,8210	1,94E-02	3,72E-02
hsa-miR-376a-3p	2,6055	33,8476	1,97E-02	3,76E-02
hsa-miR-148a-3p	2,6022	28,6793	1,98E-02	3,77E-02
hsa-miR-18b-5p	2,5989	27,8676	2,00E-02	3,78E-02
hsa-miR-1296-5p	2,5989	30,1576	2,03E-02	3,82E-02
hsa-miR-143-5p	2,5989	31,3076	2,07E-02	3,84E-02
hsa-miR-188-3p	2,5906	28,7143	2,07E-02	3,84E-02
hsa-miR-497-5p	2,5789	27,9760	2,08E-02	3,85E-02
hsa-miR-10b-5p	2,5789	32,7343	2,17E-02	3,99E-02
hsa-miR-495-3p	2,5722	31,5426	2,22E-02	4,05E-02
hsa-miR-374a-5p	2,5622	32,8526	2,23E-02	4,05E-02
hsa-miR-454-3p	2,5589	32,3851	2,25E-02	4,07E-02
hsa-miR-491-5p	2,5522	30,9943	2,27E-02	4,08E-02
hsa-let-7c-5p	2,5489	31,6643	2,27E-02	4,08E-02
hsa-miR-199a-5p	2,5455	32,1893	2,29E-02	4,09E-02
hsa-miR-378a-3p	2,5389	34,1393	2,33E-02	4,13E-02
hsa-miR-30e-3p	2,5322	24,7510	2,39E-02	4,19E-02
hsa-miR-320c	2,5322	29,6226	2,40E-02	4,19E-02
hsa-miR-411-3p	2,5312	32,2926	2,40E-02	4,19E-02
hsa-miR-574-3p	2,5289	27,9410	2,42E-02	4,19E-02
hsa-miR-431-5p	2,5122	28,0143	2,42E-02	4,19E-02
hsa-miR-493-3p	2,5022	27,3426	2,44E-02	4,21E-02
hsa-miR-628-3p	2,5009	32,3193	2,52E-02	4,32E-02
hsa-miR-20a-3p	2,4922	32,0293	2,56E-02	4,35E-02
hsa-miR-24-2-5p	2,4922	22,7560	2,56E-02	4,35E-02
hsa-miR-320d	2,4889	37,7914	2,63E-02	4,44E-02
hsa-miR-7-5p	2,4822	27,7976	2,66E-02	4,47E-02
hsa-miR-145-5p	2,4722	31,5893	2,68E-02	4,47E-02
hsa-miR-22-5p	2,4689	24,5926	2,68E-02	4,47E-02
hsa-miR-654-3p	2,4689	28,4826	2,73E-02	4,50E-02
hsa-miR-107	2,4655	32,1326	2,73E-02	4,50E-02
hsa-miR-369-3p	2,4655	26,7043	2,88E-02	4,72E-02
hsa-miR-185-5p	2,4622	27,4543	2,97E-02	4,85E-02

Supplementary Tables

hsa-miR-130b-5p	2,4489	28,2443	3,01E-02	4,89E-02
hsa-miR-379-3p	2,4422	34,5360	3,04E-02	4,89E-02
hsa-miR-21-5p	2,4422	26,6526	3,04E-02	4,89E-02
hsa-miR-296-5p	2,4259	30,7376	3,06E-02	4,91E-02
hsa-miR-30d-5p	2,4255	30,6343	3,11E-02	4,94E-02
hsa-miR-539-5p	2,4222	30,4310	3,11E-02	4,94E-02
hsa-let-7a-5p	2,4222	30,9843	3,15E-02	4,97E-02
hsa-miR-99a-5p	2,4155	32,0610	3,15E-02	4,97E-02

Table 17 Significantly higher secrete miRNAs per cell from D21

miRNA	log2FC D21	AveExpr	p-value	adj. p-value
hsa-miR-23a-5p	7,0445	35,9347	4,05E-03	5,76E-03
hsa-miR-138-1-3p	6,5539	34,7384	3,10E-03	4,64E-03
hsa-miR-450b-5p	5,9789	34,3509	1,29E-02	1,59E-02
hsa-miR-1	5,8591	35,0748	1,25E-04	1,25E-03
hsa-miR-212-3p	5,7258	34,2482	1,14E-02	1,43E-02
hsa-miR-490-3p	5,4333	33,3071	7,57E-03	9,79E-03
hsa-miR-483-5p	5,1691	36,0598	8,72E-04	1,69E-03
hsa-miR-370-3p	4,9491	33,0798	1,00E-02	1,27E-02
hsa-miR-1256	4,9391	36,7548	7,35E-04	1,56E-03
hsa-miR-34c-3p	4,9058	35,0115	2,51E-03	3,89E-03
hsa-miR-129-2-3p	4,9039	35,5284	7,65E-03	9,86E-03
hsa-miR-432-3p	4,8645	36,1447	9,86E-03	1,26E-02
hsa-miR-708-5p	4,8491	31,2732	1,37E-04	1,25E-03
hsa-miR-29c-5p	4,7515	35,1024	4,49E-03	6,26E-03
hsa-miR-487a-3p	4,7425	33,5565	2,54E-04	1,25E-03
hsa-miR-632	4,6939	35,5834	1,14E-03	2,10E-03
hsa-miR-551a	4,5525	37,3582	6,23E-04	1,46E-03
hsa-miR-502-3p	4,5439	33,6484	1,33E-03	2,32E-03
hsa-miR-27b-5p	4,5433	35,6121	1,16E-02	1,45E-02
hsa-miR-200a-3p	4,4733	34,9171	1,20E-02	1,49E-02
hsa-miR-138-5p	4,4725	29,5882	6,36E-04	1,47E-03
hsa-miR-206	4,4589	37,7109	3,42E-03	4,99E-03
hsa-miR-550a-3p	4,3839	36,0734	1,13E-02	1,42E-02
hsa-miR-29b-3p	4,3791	29,0682	9,65E-05	1,25E-03
hsa-miR-570-3p	4,3345	33,8197	1,30E-02	1,59E-02
hsa-miR-34b-5p	4,2939	32,7884	1,79E-03	2,98E-03
hsa-miR-485-3p	4,2391	30,5048	5,67E-04	1,43E-03
hsa-miR-889-3p	4,2091	34,3198	7,58E-05	1,25E-03
hsa-miR-663a	4,1925	33,7382	8,22E-05	1,25E-03
hsa-miR-141-3p	4,1691	33,5098	3,08E-03	4,63E-03
hsa-miR-940	4,1691	32,2765	7,08E-03	9,23E-03
hsa-miR-191-3p	4,1233	37,9021	1,46E-02	1,78E-02
hsa-miR-671-5p	4,1191	33,0915	3,85E-03	5,53E-03
hsa-miR-323a-3p	4,0658	32,0348	3,08E-04	1,25E-03
hsa-miR-496	4,0591	33,4815	4,59E-03	6,37E-03
hsa-miR-29a-3p	4,0458	25,5648	3,76E-04	1,25E-03
hsa-miR-142-5p	4,0133	28,7171	1,55E-02	1,88E-02
hsa-miR-134-5p	4,0125	30,0782	1,23E-04	1,25E-03
hsa-miR-642a-5p	3,9933	35,7971	1,57E-02	1,90E-02
hsa-miR-137	3,9825	30,3198	1,90E-04	1,25E-03
hsa-miR-194-3p	3,9789	37,4509	4,96E-03	6,84E-03
hsa-miR-200b-3p	3,9496	32,3477	1,61E-02	1,94E-02
hsa-miR-1260a	3,9491	25,8532	1,12E-03	2,08E-03
hsa-miR-483-3p	3,9358	34,0332	7,40E-03	9,61E-03
hsa-miR-543	3,9358	29,4498	9,95E-05	1,25E-03

Supplementary Tables

hsa-miR-373-5p	3,9258	33,5515	5,73E-03	7,69E-03
hsa-miR-30d-3p	3,9225	33,6998	3,87E-04	1,25E-03
hsa-miR-24-2-5p	3,9158	31,7465	8,64E-04	1,69E-03
hsa-miR-1296-5p	3,9025	32,1698	5,32E-03	7,19E-03
hsa-miR-29c-3p	3,8891	28,4032	2,67E-04	1,25E-03
hsa-miR-590-3p	3,8889	33,6959	1,96E-03	3,19E-03
hsa-let-7a-2-3p	3,8825	32,8298	2,64E-04	1,25E-03
hsa-miR-339-3p	3,8558	32,3465	9,73E-05	1,25E-03
hsa-miR-500a-5p	3,8525	34,0548	2,80E-04	1,25E-03
hsa-miR-200c-3p	3,8370	33,0612	3,23E-03	4,79E-03
hsa-miR-1207-5p	3,8291	34,1765	2,69E-02	2,99E-02
hsa-miR-337-3p	3,8158	29,2965	2,44E-04	1,25E-03
hsa-miR-133b	3,7958	30,2665	3,25E-04	1,25E-03
hsa-miR-330-3p	3,7958	33,5565	3,19E-04	1,25E-03
hsa-miR-101-5p	3,7891	34,3698	8,44E-04	1,67E-03
hsa-miR-221-5p	3,7825	33,0432	6,25E-03	8,29E-03
hsa-miR-638	3,7725	33,8248	6,38E-04	1,47E-03
hsa-miR-30a-5p	3,7691	29,2098	1,45E-04	1,25E-03
hsa-miR-196a-5p	3,7625	29,4098	1,46E-04	1,25E-03
hsa-miR-505-5p	3,7525	32,9748	2,93E-03	4,46E-03
hsa-miR-221-3p	3,7458	23,6415	1,56E-04	1,25E-03
hsa-miR-31-3p	3,7458	28,8648	1,79E-04	1,25E-03
hsa-miR-769-5p	3,7158	33,0932	7,50E-04	1,58E-03
hsa-miR-181c-5p	3,7125	34,9182	6,58E-03	8,70E-03
hsa-miR-654-5p	3,6958	32,9132	1,57E-04	1,25E-03
hsa-miR-409-3p	3,6958	28,8932	7,56E-04	1,58E-03
hsa-miR-378a-3p	3,6758	31,1798	4,27E-04	1,29E-03
hsa-miR-1468-5p	3,6558	32,9765	2,83E-04	1,25E-03
hsa-miR-411-3p	3,6458	34,6615	3,79E-04	1,25E-03
hsa-miR-218-5p	3,6158	30,8765	2,19E-04	1,25E-03
hsa-miR-361-3p	3,6125	33,8582	1,36E-03	2,36E-03
hsa-miR-31-5p	3,5958	27,1298	2,85E-04	1,25E-03
hsa-miR-29a-5p	3,5925	28,4448	2,22E-04	1,25E-03
hsa-let-7a-3p	3,5633	38,1821	2,05E-02	2,37E-02
hsa-miR-99b-3p	3,5591	33,5648	4,68E-03	6,48E-03
hsa-miR-132-3p	3,5558	28,8965	1,70E-04	1,25E-03
hsa-miR-154-5p	3,5558	29,1098	2,20E-04	1,25E-03
hsa-miR-410-3p	3,5558	29,8665	4,89E-04	1,35E-03
hsa-miR-329-3p	3,5391	30,8082	2,55E-04	1,25E-03
hsa-miR-665	3,5358	32,8498	2,31E-04	1,25E-03
hsa-miR-539-5p	3,5325	30,8948	2,92E-04	1,25E-03
hsa-miR-30a-3p	3,5258	30,5048	1,40E-04	1,25E-03
hsa-let-7e-5p	3,5191	28,1315	8,17E-04	1,65E-03
hsa-miR-193a-3p	3,5191	32,2615	1,75E-03	2,95E-03
hsa-miR-337-5p	3,5158	32,8532	5,13E-03	6,99E-03
hsa-miR-10a-5p	3,5125	32,0548	1,48E-04	1,25E-03
hsa-miR-502-5p	3,5058	34,5348	5,81E-03	7,77E-03
hsa-miR-32-5p	3,4991	31,4182	2,32E-04	1,25E-03
hsa-miR-379-3p	3,4958	32,0132	3,51E-04	1,25E-03
hsa-miR-128-3p	3,4825	30,3165	1,06E-03	2,00E-03
hsa-miR-29b-2-5p	3,4815	33,8424	1,92E-02	2,26E-02
hsa-miR-193b-3p	3,4791	27,1348	5,30E-04	1,41E-03
hsa-miR-150-5p	3,4758	27,4432	3,63E-04	1,25E-03
hsa-miR-326	3,4758	32,1365	3,57E-04	1,25E-03
hsa-miR-151a-3p	3,4725	30,5815	4,19E-04	1,29E-03
hsa-miR-197-3p	3,4458	29,3148	3,70E-04	1,25E-03
hsa-miR-296-5p	3,4391	32,4248	1,62E-04	1,25E-03
hsa-miR-382-3p	3,4358	31,0765	1,38E-03	2,38E-03

Supplementary Tables

hsa-miR-377-3p	3,4325	31,8415	4,46E-04	1,31E-03
hsa-miR-204-5p	3,4258	32,0715	1,65E-02	1,98E-02
hsa-miR-127-3p	3,4125	27,3382	1,60E-04	1,25E-03
hsa-miR-22-3p	3,3991	26,5748	1,71E-04	1,25E-03
hsa-miR-186-5p	3,3991	31,5748	4,00E-04	1,27E-03
hsa-miR-376a-3p	3,3958	27,0732	2,03E-04	1,25E-03
hsa-miR-643	3,3891	37,9398	1,65E-04	1,25E-03
hsa-miR-495-3p	3,3858	28,1348	6,96E-04	1,53E-03
hsa-miR-361-5p	3,3825	27,8265	1,99E-04	1,25E-03
hsa-miR-652-3p	3,3691	29,0965	1,79E-04	1,25E-03
hsa-miR-497-5p	3,3591	30,1948	2,62E-04	1,25E-03
hsa-miR-92b-3p	3,3591	32,1682	1,68E-04	1,25E-03
hsa-miR-152-3p	3,3525	27,1515	2,34E-04	1,25E-03
hsa-miR-376a-5p	3,3325	29,4782	2,50E-04	1,25E-03
hsa-miR-885-5p	3,3291	31,8398	3,61E-04	1,25E-03
hsa-miR-365b-5p	3,3245	34,1547	2,40E-02	2,74E-02
hsa-miR-130b-3p	3,3191	31,0748	4,03E-04	1,27E-03
hsa-miR-654-3p	3,3158	31,6698	1,81E-04	1,25E-03
hsa-miR-320b	3,3158	28,2998	2,14E-04	1,25E-03
hsa-miR-487b-3p	3,3091	30,2665	2,50E-04	1,25E-03
hsa-miR-7-5p	3,2991	34,3182	3,84E-04	1,25E-03
hsa-miR-18b-5p	3,2991	28,3448	1,77E-04	1,25E-03
hsa-miR-433-3p	3,2925	32,1482	1,09E-03	2,03E-03
hsa-miR-369-3p	3,2858	28,3182	3,84E-04	1,25E-03
hsa-miR-24-1-5p	3,2833	33,5021	2,47E-02	2,81E-02
hsa-miR-30c-2-3p	3,2789	34,6409	3,25E-03	4,80E-03
hsa-miR-125b-5p	3,2725	23,0048	2,02E-04	1,25E-03
hsa-miR-383-5p	3,2696	33,2177	2,50E-02	2,82E-02
hsa-miR-24-3p	3,2691	23,9232	2,47E-04	1,25E-03
hsa-miR-20a-3p	3,2691	31,3298	1,87E-03	3,10E-03
hsa-miR-432-5p	3,2625	31,8398	5,41E-04	1,42E-03
hsa-miR-223-3p	3,2625	24,2265	1,93E-04	1,25E-03
hsa-miR-127-5p	3,2591	33,2348	6,23E-04	1,46E-03
hsa-miR-34a-3p	3,2591	31,1115	3,27E-03	4,81E-03
hsa-miR-874-3p	3,2591	32,3048	1,24E-03	2,22E-03
hsa-miR-23a-3p	3,2558	23,1932	3,53E-04	1,25E-03
hsa-let-7f-2-3p	3,2558	32,0298	1,00E-03	1,90E-03
hsa-miR-192-5p	3,2525	29,5315	1,90E-04	1,25E-03
hsa-miR-542-5p	3,2525	30,7848	2,04E-04	1,25E-03
hsa-miR-514a-3p	3,2396	37,4027	2,55E-02	2,85E-02
hsa-miR-708-3p	3,2396	37,4027	2,55E-02	2,85E-02
hsa-miR-346	3,2396	37,4027	2,55E-02	2,85E-02
hsa-miR-133a-3p	3,2391	31,2015	4,61E-04	1,33E-03
hsa-miR-320a	3,2391	26,2382	3,02E-04	1,25E-03
hsa-miR-320c	3,2391	28,4882	2,60E-04	1,25E-03
hsa-miR-877-5p	3,2389	33,1309	1,99E-02	2,32E-02
hsa-miR-1271-5p	3,2339	34,6334	7,04E-03	9,20E-03
hsa-miR-34a-5p	3,2325	27,5782	2,68E-04	1,25E-03
hsa-miR-301b	3,2325	31,0882	9,37E-04	1,80E-03
hsa-let-7b-3p	3,2291	29,6765	2,61E-03	4,02E-03
hsa-miR-362-3p	3,2225	31,0665	6,10E-04	1,46E-03
hsa-miR-16-1-3p	3,2158	31,1198	2,50E-03	3,89E-03
hsa-miR-28-3p	3,2125	31,8148	3,07E-04	1,25E-03
hsa-miR-139-5p	3,2091	30,9132	3,74E-04	1,25E-03
hsa-miR-532-5p	3,2025	31,9398	2,17E-02	2,51E-02
hsa-miR-193a-5p	3,1991	30,5215	4,93E-04	1,35E-03
hsa-miR-376b-3p	3,1891	28,9198	3,35E-04	1,25E-03
hsa-miR-185-5p	3,1891	27,4032	4,53E-04	1,32E-03

Supplementary Tables

hsa-miR-362-5p	3,1870	34,1062	2,44E-03	3,82E-03
hsa-miR-27a-5p	3,1858	32,8348	5,07E-03	6,96E-03
hsa-miR-376c-3p	3,1825	27,1398	3,43E-04	1,25E-03
hsa-miR-30e-3p	3,1758	30,3798	1,15E-03	2,10E-03
hsa-miR-423-5p	3,1758	27,3032	2,46E-04	1,25E-03
hsa-miR-23b-3p	3,1725	24,8148	3,17E-04	1,25E-03
hsa-miR-126-3p	3,1725	25,4582	3,06E-04	1,25E-03
hsa-miR-27a-3p	3,1658	25,7182	8,06E-04	1,64E-03
hsa-miR-379-5p	3,1491	28,9465	2,82E-04	1,25E-03
hsa-miR-224-3p	3,1491	31,9332	4,11E-03	5,82E-03
hsa-miR-28-5p	3,1391	29,7482	2,70E-04	1,25E-03
hsa-miR-100-5p	3,1325	25,0848	2,64E-04	1,25E-03
hsa-miR-328-3p	3,1225	30,6665	2,96E-03	4,49E-03
hsa-miR-222-3p	3,1125	25,0082	5,60E-04	1,43E-03
hsa-miR-203a	3,1120	33,3887	1,72E-02	2,06E-02
hsa-miR-147b	3,1096	34,1277	2,80E-02	3,10E-02
hsa-miR-33a-5p	3,1091	30,5265	6,17E-04	1,46E-03
hsa-let-7b-5p	3,0991	25,9048	2,53E-04	1,25E-03
hsa-miR-125b-1-3p	3,0958	32,2298	3,58E-04	1,25E-03
hsa-miR-140-5p	3,0891	29,4332	7,22E-04	1,56E-03
hsa-miR-365a-3p	3,0858	27,6548	4,69E-04	1,35E-03
hsa-miR-382-5p	3,0758	29,0932	4,87E-04	1,35E-03
hsa-miR-122-5p	3,0725	27,3215	3,48E-04	1,25E-03
hsa-miR-95-3p	3,0715	33,4474	4,41E-03	6,18E-03
hsa-miR-10b-5p	3,0625	29,1632	2,80E-04	1,25E-03
hsa-miR-374b-5p	3,0625	30,1265	2,74E-04	1,25E-03
hsa-miR-30e-5p	3,0591	28,1048	2,33E-04	1,25E-03
hsa-miR-146b-5p	3,0525	34,1415	7,93E-04	1,63E-03
hsa-miR-409-5p	3,0525	32,0282	1,93E-03	3,15E-03
hsa-miR-136-5p	3,0525	26,7382	7,32E-04	1,56E-03
hsa-miR-590-5p	3,0458	31,1382	7,64E-04	1,59E-03
hsa-miR-136-3p	3,0391	28,6182	6,12E-04	1,46E-03
hsa-miR-744-5p	3,0391	35,1482	5,40E-03	7,27E-03
hsa-miR-22-5p	3,0225	29,3198	2,66E-04	1,25E-03
hsa-miR-324-5p	3,0225	31,2532	3,14E-04	1,25E-03
hsa-miR-130a-3p	3,0191	29,4315	5,70E-04	1,43E-03
hsa-miR-493-3p	3,0091	31,2265	8,72E-03	1,12E-02
hsa-miR-27b-3p	3,0025	24,6665	3,55E-04	1,25E-03
hsa-let-7g-5p	2,9991	26,1115	2,74E-04	1,25E-03
hsa-miR-664a-3p	2,9991	32,4282	6,03E-04	1,46E-03
hsa-miR-26b-5p	2,9891	28,8198	3,11E-04	1,25E-03
hsa-miR-30b-5p	2,9858	26,7515	3,78E-04	1,25E-03
hsa-miR-431-5p	2,9825	32,7832	3,04E-03	4,58E-03
hsa-miR-103a-3p	2,9791	25,5448	2,89E-04	1,25E-03
hsa-miR-423-3p	2,9791	27,5082	3,30E-04	1,25E-03
hsa-miR-301a-3p	2,9758	28,1232	4,28E-04	1,29E-03
hsa-miR-451a	2,9725	23,1582	4,40E-04	1,31E-03
hsa-miR-194-5p	2,9725	30,8748	6,66E-04	1,53E-03
hsa-miR-493-5p	2,9725	29,8082	6,77E-04	1,53E-03
hsa-miR-25-3p	2,9691	26,4898	3,70E-04	1,25E-03
hsa-miR-148a-3p	2,9691	31,2965	1,29E-03	2,27E-03
hsa-miR-196b-3p	2,9689	33,4609	3,91E-03	5,59E-03
hsa-miR-299-5p	2,9625	29,7498	1,77E-03	2,96E-03
hsa-miR-30c-5p	2,9625	26,5532	3,48E-04	1,25E-03
hsa-miR-15a-5p	2,9591	25,7682	2,91E-04	1,25E-03
hsa-miR-15b-5p	2,9525	28,3282	8,63E-04	1,69E-03
hsa-miR-615-3p	2,9491	31,0832	3,55E-04	1,25E-03
hsa-miR-149-5p	2,9458	31,5448	5,89E-03	7,85E-03

Supplementary Tables

hsa-miR-484	2,9391	29,1315	1,76E-03	2,95E-03
hsa-miR-142-3p	2,9258	24,1615	3,26E-04	1,25E-03
hsa-miR-18a-3p	2,9191	32,5982	5,13E-03	6,99E-03
hsa-let-7d-5p	2,9158	28,3698	3,63E-04	1,25E-03
hsa-miR-92a-3p	2,9158	25,9098	5,70E-04	1,43E-03
hsa-miR-339-5p	2,9158	27,5332	4,40E-03	6,18E-03
hsa-miR-1972	2,9125	31,8648	6,95E-04	1,53E-03
hsa-miR-148b-3p	2,9125	28,5748	8,44E-04	1,67E-03
hsa-miR-20a-5p	2,9091	25,3232	3,07E-04	1,25E-03
hsa-miR-1249	2,9091	32,0165	7,38E-04	1,56E-03
hsa-let-7a-5p	2,8925	24,0782	3,67E-04	1,25E-03
hsa-miR-144-3p	2,8925	24,6115	4,11E-04	1,28E-03
hsa-miR-125a-5p	2,8925	26,7748	1,08E-03	2,02E-03
hsa-miR-106a-5p	2,8858	25,8982	3,41E-04	1,25E-03
hsa-miR-107	2,8825	27,7998	3,69E-04	1,25E-03
hsa-miR-145-3p	2,8791	31,4348	1,00E-03	1,90E-03
hsa-miR-101-3p	2,8791	26,9882	3,06E-04	1,25E-03
hsa-miR-505-3p	2,8725	30,4948	5,02E-04	1,36E-03
hsa-miR-574-3p	2,8658	27,2948	3,93E-04	1,26E-03
hsa-miR-18a-5p	2,8625	28,4032	7,70E-04	1,59E-03
hsa-miR-34c-5p	2,8625	32,2565	2,38E-02	2,72E-02
hsa-miR-425-5p	2,8458	28,4848	3,26E-04	1,25E-03
hsa-miR-19a-3p	2,8425	26,2565	3,45E-04	1,25E-03
hsa-let-7c-5p	2,8325	28,4782	4,15E-04	1,29E-03
hsa-miR-30d-5p	2,8291	27,6632	8,38E-04	1,67E-03
hsa-miR-224-5p	2,8291	30,5365	2,04E-03	3,28E-03
hsa-miR-126-5p	2,8291	30,8065	6,22E-04	1,46E-03
hsa-miR-21-3p	2,8225	33,5765	4,18E-03	5,91E-03
hsa-miR-19b-3p	2,8191	24,6348	3,34E-04	1,25E-03
hsa-miR-93-5p	2,8191	25,8415	3,46E-04	1,25E-03
hsa-miR-331-3p	2,8158	28,8965	5,11E-04	1,38E-03
hsa-miR-452-5p	2,8025	31,9732	8,17E-04	1,65E-03
hsa-let-7d-3p	2,7991	28,5415	4,77E-04	1,35E-03
hsa-miR-335-5p	2,7991	32,8782	4,95E-04	1,35E-03
hsa-miR-421	2,7925	31,6115	6,75E-04	1,53E-03
hsa-miR-140-3p	2,7891	28,1098	3,52E-04	1,25E-03
hsa-miR-98-5p	2,7725	30,4148	1,66E-03	2,81E-03
hsa-miR-145-5p	2,7658	24,5715	5,75E-04	1,43E-03
hsa-miR-338-3p	2,7625	32,4665	1,27E-03	2,26E-03
hsa-miR-16-5p	2,7491	22,9598	3,71E-04	1,25E-03
hsa-miR-181b-5p	2,7458	31,2082	5,56E-04	1,43E-03
hsa-miR-99a-5p	2,7291	28,6132	4,33E-04	1,30E-03
hsa-miR-106b-3p	2,7158	30,6632	5,69E-04	1,43E-03
hsa-miR-369-5p	2,7091	32,6232	2,31E-02	2,65E-02
hsa-miR-486-5p	2,7058	27,1415	6,10E-04	1,46E-03
hsa-miR-374a-5p	2,7058	30,6248	5,90E-04	1,46E-03
hsa-miR-660-5p	2,6958	31,0665	1,81E-02	2,15E-02
hsa-miR-106b-5p	2,6925	27,2348	4,82E-04	1,35E-03
hsa-miR-188-5p	2,6791	34,2482	1,93E-03	3,15E-03
hsa-miR-572	2,6689	36,9509	1,50E-02	1,83E-02
hsa-miR-490-5p	2,6633	33,5121	3,96E-02	4,35E-02
hsa-miR-324-3p	2,6591	31,1215	7,04E-04	1,54E-03
hsa-miR-196b-5p	2,6525	31,2815	8,57E-04	1,69E-03
hsa-miR-143-3p	2,6525	24,6648	2,12E-03	3,39E-03
hsa-miR-15b-3p	2,6425	31,0865	6,83E-04	1,53E-03
hsa-miR-26a-5p	2,6391	27,1548	6,90E-04	1,53E-03
hsa-miR-181a-5p	2,6091	26,8498	5,39E-04	1,42E-03
hsa-let-7f-1-3p	2,6025	33,1465	1,23E-03	2,21E-03

Supplementary Tables

hsa-miR-331-5p	2,5870	33,6412	1,88E-02	2,22E-02
hsa-miR-99b-5p	2,5825	28,5132	6,98E-04	1,53E-03
hsa-let-7e-3p	2,5791	32,6682	3,46E-03	5,02E-03
hsa-let-7f-5p	2,5758	27,2698	1,30E-03	2,27E-03
hsa-miR-454-3p	2,5691	30,6165	1,23E-03	2,21E-03
hsa-miR-210-3p	2,5525	28,1315	2,04E-03	3,28E-03
hsa-miR-219a-5p	2,5525	33,3582	1,16E-02	1,45E-02
hsa-miR-21-5p	2,5391	22,1648	5,24E-04	1,40E-03
hsa-miR-154-3p	2,5391	33,8915	2,45E-03	3,82E-03
hsa-miR-144-5p	2,5391	28,4048	1,41E-03	2,43E-03
hsa-miR-532-3p	2,5191	31,8282	3,14E-03	4,68E-03
hsa-miR-195-5p	2,5158	29,7032	1,56E-03	2,66E-03
hsa-miR-655-3p	2,5158	35,0165	1,02E-02	1,30E-02
hsa-miR-1185-5p	2,5070	31,8312	3,64E-02	4,02E-02
hsa-let-7i-5p	2,5058	26,9115	1,16E-03	2,12E-03
hsa-miR-378a-5p	2,5020	34,5587	6,83E-03	8,99E-03
hsa-miR-455-3p	2,4991	28,7548	7,32E-04	1,56E-03
hsa-miR-425-3p	2,4958	31,6498	2,26E-03	3,60E-03
hsa-miR-199a-3p	2,4525	25,4815	9,96E-04	1,90E-03
hsa-miR-503-5p	2,4425	30,7565	3,76E-03	5,44E-03
hsa-miR-450a-5p	2,4391	29,1748	1,22E-03	2,20E-03
hsa-miR-424-5p	2,4225	26,7232	9,03E-04	1,74E-03
hsa-miR-215-5p	2,3858	30,8248	3,29E-03	4,81E-03
hsa-miR-17-5p	2,3825	32,2098	1,80E-02	2,14E-02
hsa-miR-151a-5p	2,3789	26,9609	1,41E-02	1,73E-02
hsa-miR-181a-2-3p	2,3758	31,8632	2,31E-03	3,66E-03
hsa-miR-411-5p	2,3758	28,6632	1,14E-02	1,43E-02
hsa-miR-93-3p	2,3558	31,9898	1,09E-02	1,39E-02
hsa-miR-675-3p	2,3425	35,9065	1,97E-02	2,30E-02
hsa-miR-214-3p	2,2858	28,4915	1,50E-03	2,57E-03
hsa-miR-455-5p	2,2791	31,8548	2,83E-03	4,35E-03
hsa-miR-143-5p	2,2458	32,1982	7,04E-03	9,20E-03
hsa-miR-381-3p	2,2391	31,0515	1,97E-03	3,20E-03
hsa-miR-494-3p	2,1491	34,1798	1,91E-03	3,15E-03
hsa-miR-155-5p	2,0891	30,8065	2,90E-03	4,44E-03
hsa-miR-139-3p	2,0870	34,2062	1,94E-02	2,28E-02
hsa-miR-17-3p	1,9891	30,7465	2,33E-03	3,68E-03
hsa-miR-214-5p	1,9258	30,0915	1,89E-02	2,23E-02
hsa-miR-7-1-3p	1,8691	32,4532	2,04E-02	2,37E-02
hsa-miR-342-3p	1,8025	29,9932	5,26E-03	7,14E-03
hsa-miR-125a-3p	1,7491	35,3332	2,36E-02	2,71E-02
hsa-let-7i-3p	1,6191	32,5182	3,78E-03	5,45E-03
hsa-miR-491-5p	1,5225	33,0898	4,08E-02	4,47E-02
hsa-miR-199a-5p	1,4589	27,4759	2,72E-02	3,02E-02
hsa-miR-424-3p	1,2791	31,2315	2,53E-02	2,85E-02

6.4. Table to different composition of miRNAs per vesicle between Q and SIPS cells from two timepoints

Secretory miRNAs normalized to the global mean using the MCR method. From SIPS, Q, D7 and D21

Changes of miRNA composition of SIPS EVs

miRNAs presented are either more or less abundant per vesicle of SIPS cells

Table 18 miRNAs significantly more abundant in SIPS on D7 rel. Q

miRNA	log2FC D7	AveExpr	p-value	adj. p-value
hsa-miR-181a-3p	5,4552	6,1767	0,0359	0,4859
hsa-miR-200c-3p	4,8127	5,6368	0,0239	0,4859
hsa-miR-196b-3p	4,3615	4,9841	0,0108	0,4859
hsa-miR-149-5p	3,3161	4,3139	0,0234	0,4859
hsa-miR-361-3p	2,9777	4,5610	0,0315	0,4859
hsa-miR-339-3p	2,8127	2,8017	0,0308	0,4859
hsa-miR-369-5p	2,6727	4,6014	0,0077	0,4859
hsa-miR-335-3p	2,5994	3,2984	0,0199	0,4859
hsa-miR-642a-5p	2,3465	1,6667	0,0477	0,4859
hsa-miR-24-1-5p	2,1727	4,1984	0,0234	0,4859
hsa-miR-23a-5p	2,1094	1,6450	0,0307	0,4859
hsa-miR-638	2,0761	4,1317	0,0012	0,4277
hsa-miR-181c-5p	1,8661	5,0210	0,0464	0,4859
hsa-miR-138-5p	1,7994	3,2867	0,0416	0,4859
hsa-miR-196a-5p	1,4227	2,7417	0,0156	0,4859
hsa-miR-660-5p	1,1794	5,2334	0,0039	0,4859
hsa-miR-483-3p	1,1461	0,9684	0,0244	0,4859
hsa-miR-337-5p	1,0894	-5,6683	0,0268	0,4859
hsa-miR-137	1,0461	4,9170	0,0468	0,4859

Table 19 miRNAs significantly more abundant in SIPS on D21 rel. Q

miRNA	log2FC D21	AveExpr	p-value	adj. p-value
hsa-miR-23a-5p	3,6508	5,7770	0,0266	0,3918
hsa-miR-138-1-3p	3,4334	4,3623	0,0236	0,3918
hsa-miR-1	2,7450	5,1140	0,0028	0,3918
hsa-miR-490-3p	2,5861	2,7127	0,0495	0,5116
hsa-miR-483-5p	2,0550	6,0990	0,0233	0,3918
hsa-miR-708-5p	1,7350	1,3123	0,0108	0,3918
hsa-miR-487a-3p	1,6284	3,5957	0,0325	0,4419
hsa-miR-29b-3p	1,2650	-0,8927	0,0065	0,3918
hsa-miR-485-3p	1,1250	0,5440	0,0452	0,5116
hsa-miR-889-3p	1,0950	4,3590	0,0131	0,3918
hsa-miR-663a	1,0784	3,7773	0,0235	0,3918
hsa-miR-137	0,8684	0,3590	0,0278	0,3925
hsa-miR-543	0,8217	-0,5110	0,0247	0,3918

Table 20 miRNAs significantly less abundant in SIPS on D7 rel. Q

miRNA	log2FC D7	AveExpr	p-value	adj. p-value
hsa-miR-654-5p	-4,2448	1,2550	0,0335	0,4859
hsa-miR-625-3p	-3,5623	3,5317	0,0319	0,4859
hsa-let-7g-3p	-2,9406	-0,4050	0,0327	0,4859
hsa-miR-766-3p	-2,7473	4,9116	0,0156	0,4859
hsa-miR-95-3p	-2,0123	3,8284	0,0303	0,4859

Supplementary Tables

hsa-miR-655-3p	-1,4860	0,5434	0,0477	0,4859
hsa-miR-17-3p	-1,3906	2,7964	0,0496	0,4859
hsa-miR-144-3p	-1,3206	4,6250	0,0135	0,4859
hsa-miR-486-5p	-1,2506	-0,9133	0,0404	0,4859
hsa-miR-199b-5p	-1,1773	-3,2600	0,0386	0,4859
hsa-miR-381-3p	-1,1206	1,1284	0,0469	0,4859
hsa-miR-615-3p	-1,0739	-0,1733	0,0194	0,4859

Table 21 miRNAs significantly less abundant in SIPS on D21 rel. Q

miRNA	log2FC D21	AveExpr	p-value	adj. p-value
hsa-miR-766-3p	-4,2692	5,9570	0,0200	0,3918
hsa-miR-595	-3,6255	6,3346	0,0037	0,3918
hsa-miR-222-5p	-2,4766	4,5773	0,0055	0,3918
hsa-miR-340-3p	-2,0778	5,7275	0,0089	0,3918
hsa-miR-199b-5p	-1,9983	-1,5610	0,0183	0,3918
hsa-miR-625-3p	-1,8816	5,0798	0,0111	0,3918
hsa-miR-424-3p	-1,8350	1,2707	0,0130	0,3918
hsa-miR-199a-5p	-1,6616	-2,9002	0,0185	0,3918
hsa-miR-491-5p	-1,5916	3,1290	0,0230	0,3918
hsa-let-7i-3p	-1,4950	2,5573	0,0058	0,3918
hsa-miR-342-3p	-1,3116	0,0323	0,0232	0,3918
hsa-miR-7-1-3p	-1,2450	2,4923	0,0465	0,5116
hsa-miR-17-3p	-1,1250	0,7857	0,0104	0,3918
hsa-miR-155-5p	-1,0250	0,8457	0,0184	0,3918
hsa-miR-494-3p	-0,9650	4,2190	0,0260	0,3918
hsa-miR-381-3p	-0,8750	1,0907	0,0256	0,3918
hsa-miR-455-5p	-0,8350	1,8940	0,0465	0,5116
hsa-miR-214-3p	-0,8283	-1,4693	0,0385	0,5039
hsa-miR-424-5p	-0,6916	-3,2377	0,0419	0,5116

Changes of miRNA composition per vesicle over time MCR

Table 22 more abundant on D21 in Q rel. D7

miRNA	log2FC Q	AveExpr	p-value	adj. p-value
hsa-miR-1185-5p	5,6747	4,0588	0,0124	0,9529
hsa-miR-590-3p	4,1950	5,8015	0,0048	0,9529
hsa-miR-125b-1-3p	3,5815	4,0506	0,0244	0,9529
hsa-miR-663b	2,8649	5,1756	0,0175	0,9529
hsa-miR-30a-3p	2,6649	2,0823	0,0140	0,9529
hsa-miR-181a-2-3p	2,6015	2,8340	0,0135	0,9529
hsa-miR-339-3p	2,1815	3,8473	0,0126	0,9529

Table 23 less abundant on D21 in Q rel. D7

miRNA	log2FC Q	AveExpr	p-value	adj. p-value
hsa-miR-378a-3p	-1,6418	0,6790	0,0447	0,9529
hsa-miR-500a-5p	-2,0951	3,4156	0,0329	0,9529
hsa-miR-142-5p	-3,6813	-3,1349	0,0482	0,9529

Supplementary Tables

Table 24 more abundant on D21 in SIPS rel. D7

miRNA	log2FC SIPS	AveExpr	p-value	adj. p-value
hsa-miR-450b-5p	4,9996	5,1494	0,0128	0,6267
hsa-miR-654-5p	4,5794	4,6653	0,0038	0,4615
hsa-miR-34c-3p	3,0339	5,6717	0,0102	0,6267
hsa-miR-1972	2,0739	3,0417	0,0121	0,6267
hsa-miR-30d-3p	2,0105	4,3401	0,0237	0,6486
hsa-miR-1	1,5572	4,5201	0,0333	0,6486

Table 25 less abundant on D21 in SIPS rel. D7

miRNA	log2FC SIPS	AveExpr	p-value	adj. p-value
hsa-miR-548c-5p	-1,4795	5,3351	0,0412	0,7095
hsa-miR-149-5p	-1,6595	0,8384	0,0496	0,8072
hsa-miR-219a-5p	-1,6695	2,8434	0,0241	0,6486
hsa-miR-125a-3p	-2,8895	4,6101	0,0338	0,6486
hsa-miR-130b-5p	-2,9428	3,6667	0,0209	0,6486
hsa-miR-99a-3p	-3,3089	3,8920	0,0381	0,6900
hsa-miR-431-3p	-3,6773	6,3645	0,0339	0,6486
hsa-miR-377-5p	-3,7073	6,3495	0,0331	0,6486
hsa-miR-203a	-3,9607	1,7512	0,0271	0,6486
hsa-miR-595	-4,2890	6,0029	0,0030	0,4615
hsa-miR-181a-3p	-4,3204	5,0694	0,0206	0,6486
hsa-miR-188-3p	-5,7307	5,2262	0,0080	0,6267
hsa-miR-205-5p	-6,2540	3,3304	0,0252	0,6486
hsa-miR-766-3p	-6,9607	4,6112	0,0040	0,4615

6.5. Differentially transcribed miRNAs (intracellular)

Changes in miRNA transcription between SIPS and Q

Table 26 Differentially higher transcribed miRNAs of SIPS cells after 7 days post treatment (upregulated in SIPS)

miRNA	log2FC SIPS	baseMean	p-value	adj. p-value
hsa-miR-509-3-5p	3,14	17,5731	4,94E-12	3,05E-10
hsa-miR-215-5p	3,06	69,7848	2,95E-22	6,37E-20
hsa-miR-9-5p	2,88	72,7301	2,45E-20	3,53E-18
hsa-miR-139-5p	2,85	31,0924	3,05E-12	2,20E-10
hsa-miR-1298-5p	2,76	5,9741	3,35E-08	9,64E-07
hsa-miR-3591-5p	2,57	14,2920	2,40E-09	7,98E-08
hsa-miR-514a-3p	2,49	14,9530	3,23E-07	6,34E-06
hsa-miR-190b	2,34	12,4560	5,04E-07	9,47E-06
hsa-miR-182-5p	2,22	114,6053	4,41E-10	1,59E-08
hsa-miR-200c-3p	2,03	75,4084	3,61E-10	1,42E-08
hsa-miR-891a-5p	1,94	9,1409	6,71E-05	8,17E-04
hsa-miR-378a-3p	1,92	110,4422	9,21E-12	4,97E-10
hsa-miR-183-5p	1,88	63,9769	7,03E-08	1,79E-06
hsa-miR-375	1,75	12,8724	1,10E-04	1,22E-03
hsa-miR-29b-3p	1,46	763,7999	1,25E-10	5,41E-09
hsa-miR-138-5p	1,44	249,5759	9,08E-07	1,52E-05
hsa-miR-380-3p	1,39	21,2302	5,39E-04	4,16E-03
hsa-miR-3117-3p	1,38	79,3119	1,93E-04	1,99E-03
hsa-miR-2682-3p	1,34	13,8248	8,58E-04	6,28E-03
hsa-miR-200a-3p	1,27	35,3187	3,90E-04	3,31E-03

Supplementary Tables

hsa-miR-129-2-3p	1,22	174,6052	1,49E-05	2,08E-04
hsa-miR-7706	1,19	102,6088	2,64E-04	2,53E-03
hsa-miR-412-5p	1,19	125,9522	9,98E-05	1,14E-03
hsa-miR-708-3p	1,17	264,9692	3,37E-04	3,03E-03
hsa-miR-2682-5p	1,16	294,9364	1,38E-08	4,24E-07
hsa-miR-708-5p	1,11	392,6600	1,54E-04	1,66E-03
hsa-miR-129-5p	1,06	1261,5547	4,93E-06	7,35E-05
hsa-miR-192-5p	0,98	248,8229	1,35E-07	2,93E-06
hsa-miR-129-1-3p	0,93	33,1034	1,07E-02	4,53E-02
hsa-miR-1197	0,92	38,8819	2,54E-03	1,50E-02
hsa-miR-194-5p	0,91	78,7754	5,92E-03	2,94E-02
hsa-miR-137	0,91	656,3629	4,61E-04	3,67E-03
hsa-miR-4775	0,89	28,2180	8,10E-03	3,88E-02
hsa-miR-34a-5p	0,89	2016,2421	2,36E-04	2,37E-03
hsa-miR-584-5p	0,87	139,4513	6,88E-05	8,17E-04
hsa-miR-29a-3p	0,86	42516,6962	6,99E-05	8,17E-04
hsa-miR-486-5p	0,82	245,1750	2,85E-03	1,62E-02
hsa-miR-31-3p	0,80	273,5708	9,94E-03	4,36E-02
hsa-miR-30a-5p	0,77	79196,0252	1,84E-05	2,49E-04
hsa-miR-376a-3p	0,74	258,2234	9,69E-04	6,86E-03
hsa-miR-377-3p	0,73	236,0858	2,75E-03	1,59E-02
hsa-miR-494-3p	0,69	2276,2744	4,48E-04	3,67E-03
hsa-miR-10a-3p	0,69	1146,4830	6,21E-06	8,94E-05
hsa-miR-323a-3p	0,68	1713,3771	3,01E-03	1,65E-02
hsa-miR-324-5p	0,65	60,9490	1,14E-02	4,75E-02
hsa-miR-487a-3p	0,65	148,5998	8,27E-03	3,88E-02
hsa-miR-221-3p	0,64	126786,6781	3,17E-04	2,91E-03
hsa-miR-1185-1-3p	0,64	1128,7339	2,48E-03	1,49E-02
hsa-miR-539-3p	0,63	395,7349	4,52E-04	3,67E-03
hsa-miR-487b-3p	0,62	420,0111	1,77E-03	1,16E-02
hsa-miR-30e-5p	0,61	4838,9346	6,54E-04	4,95E-03
hsa-miR-196a-3p	0,59	903,3676	2,43E-03	1,48E-02
hsa-miR-655-3p	0,57	204,9754	8,80E-03	4,05E-02
hsa-miR-221-5p	0,57	6870,7115	1,62E-03	1,09E-02
hsa-miR-758-3p	0,56	292,8704	1,02E-02	4,36E-02
hsa-miR-31-5p	0,44	6324,9727	3,85E-03	2,05E-02
hsa-miR-409-5p	0,44	1428,0695	6,07E-03	2,98E-02

Table 27 Differentially higher transcribed miRNAs after 21 days post stress treatment (upregulated in SIPS D21)

miRNA	log2FC SIPS	baseMean	p-value	adj. p-value
hsa-miR-509-3-5p	3,75	17,5731	1,22E-15	1,75E-13
hsa-miR-375	3,03	12,8724	1,49E-10	4,78E-09
hsa-miR-378a-3p	2,97	110,4422	4,77E-24	1,03E-21
hsa-miR-514a-3p	2,91	14,9530	1,40E-09	3,56E-08
hsa-miR-891a-5p	2,83	9,1409	9,09E-09	1,96E-07
hsa-miR-183-5p	2,71	63,9769	9,73E-14	8,41E-12
hsa-miR-182-5p	2,63	114,6053	4,45E-13	2,40E-11
hsa-miR-215-5p	2,11	69,7848	5,37E-11	1,93E-09
hsa-miR-122-5p	2,04	225,5032	1,33E-05	1,22E-04
hsa-miR-190b	2,03	12,4560	1,82E-05	1,63E-04
hsa-miR-124-3p	1,96	9,8164	8,26E-05	6,26E-04
hsa-miR-9-5p	1,81	72,7301	1,63E-08	3,21E-07
hsa-miR-129-2-3p	1,80	174,6052	3,92E-10	1,06E-08
hsa-miR-451a	1,77	14,7579	2,07E-04	1,42E-03
hsa-miR-200c-3p	1,76	75,4084	9,33E-08	1,49E-06
hsa-miR-129-5p	1,73	1261,5547	1,89E-13	1,36E-11

Supplementary Tables

hsa-miR-3117-3p	1,70	79,3119	4,35E-06	4,69E-05
hsa-miR-1	1,68	17,6675	2,48E-04	1,62E-03
hsa-miR-129-1-3p	1,67	33,1034	1,28E-05	1,20E-04
hsa-miR-1298-5p	1,66	5,9741	1,06E-03	5,14E-03
hsa-miR-138-5p	1,63	249,5759	6,39E-08	1,10E-06
hsa-miR-486-5p	1,63	245,1750	2,05E-09	4,92E-08
hsa-miR-184	1,63	32,4530	1,42E-03	6,47E-03
hsa-miR-3591-5p	1,59	14,2920	4,85E-04	2,95E-03
hsa-miR-412-5p	1,56	125,9522	5,58E-07	7,78E-06
hsa-miR-323b-3p	1,40	474,4384	3,05E-08	5,73E-07
hsa-miR-380-3p	1,38	21,2302	6,29E-04	3,47E-03
hsa-miR-2682-3p	1,35	13,8248	1,96E-03	8,31E-03
hsa-miR-212-3p	1,33	43,0961	1,00E-05	9,85E-05
hsa-miR-1197	1,29	38,8819	1,04E-04	7,74E-04
hsa-miR-584-5p	1,29	139,4513	1,23E-08	2,53E-07
hsa-miR-323a-3p	1,26	1713,3771	5,63E-08	1,01E-06
hsa-miR-29b-3p	1,24	763,7999	6,99E-08	1,16E-06
hsa-miR-212-5p	1,19	142,6153	1,64E-06	1,96E-05
hsa-miR-4775	1,16	28,2180	6,45E-04	3,48E-03
hsa-miR-543	1,08	1123,6227	4,97E-05	3,98E-04
hsa-miR-496	1,05	39,9449	1,57E-03	6,77E-03
hsa-miR-139-5p	1,02	31,0924	1,29E-02	4,05E-02
hsa-miR-3177-3p	1,01	16,3643	1,45E-02	4,37E-02
hsa-miR-2682-5p	1,00	294,9364	1,41E-06	1,79E-05
hsa-miR-185-3p	0,99	113,4370	1,67E-03	7,12E-03
hsa-miR-708-3p	0,98	264,9692	2,92E-03	1,16E-02
hsa-miR-708-5p	0,97	392,6600	1,02E-03	5,01E-03
hsa-miR-539-5p	0,96	85,1155	9,68E-04	4,88E-03
hsa-miR-134-5p	0,95	4082,5485	3,89E-05	3,29E-04
hsa-miR-137	0,94	656,3629	3,30E-04	2,10E-03
hsa-miR-127-3p	0,92	19769,4877	5,28E-05	4,14E-04
hsa-miR-30c-2-3p	0,92	324,7992	2,19E-03	9,03E-03
hsa-miR-380-5p	0,88	41,2851	1,05E-02	3,45E-02
hsa-miR-1185-1-3p	0,86	1128,7339	4,66E-05	3,80E-04
hsa-miR-154-3p	0,86	68,3736	2,97E-03	1,17E-02
hsa-miR-409-3p	0,85	8305,8420	8,33E-04	4,34E-03
hsa-miR-485-3p	0,84	738,5513	8,18E-04	4,31E-03
hsa-miR-487b-3p	0,83	420,0111	3,07E-05	2,65E-04
hsa-miR-221-3p	0,82	126786,6781	3,88E-06	4,29E-05
hsa-miR-29a-3p	0,81	42516,6962	1,76E-04	1,23E-03
hsa-miR-494-3p	0,81	2276,2744	4,44E-05	3,69E-04
hsa-miR-539-3p	0,81	395,7349	1,07E-05	1,02E-04
hsa-miR-370-3p	0,80	6494,5715	1,57E-03	6,77E-03
hsa-miR-376a-3p	0,78	258,2234	6,19E-04	3,47E-03
hsa-miR-409-5p	0,78	1428,0695	1,26E-06	1,66E-05
hsa-miR-487a-3p	0,77	148,5998	2,12E-03	8,81E-03
hsa-miR-329-3p	0,77	530,4236	3,51E-04	2,17E-03
hsa-miR-410-3p	0,76	381,7867	7,26E-04	3,87E-03
hsa-miR-377-5p	0,72	85,1199	6,82E-03	2,37E-02
hsa-miR-758-3p	0,71	292,8704	1,20E-03	5,72E-03
hsa-miR-30a-5p	0,69	79196,0252	1,26E-04	8,94E-04
hsa-miR-654-5p	0,69	1390,5760	2,96E-04	1,91E-03
hsa-miR-127-5p	0,67	1386,0253	2,66E-03	1,07E-02
hsa-miR-1185-2-3p	0,65	193,2367	4,68E-03	1,71E-02
hsa-miR-221-5p	0,62	6870,7115	5,42E-04	3,16E-03
hsa-miR-501-3p	0,62	116,5625	1,37E-02	4,23E-02
hsa-miR-369-3p	0,56	509,4265	9,84E-04	4,88E-03
hsa-miR-222-3p	0,56	11304,9566	1,56E-02	4,57E-02

Supplementary Tables

hsa-miR-493-5p	0,54	10599,2688	1,42E-02	4,34E-02
hsa-miR-10a-3p	0,54	1146,4830	4,97E-04	2,98E-03
hsa-miR-889-3p	0,54	1236,6988	3,33E-03	1,27E-02
hsa-miR-30a-3p	0,53	3361,3082	1,56E-02	4,57E-02
hsa-miR-432-5p	0,51	1621,8408	1,43E-02	4,36E-02
hsa-miR-196a-3p	0,50	903,3676	1,02E-02	3,40E-02
hsa-miR-299-3p	0,47	902,2963	1,05E-02	3,45E-02
hsa-miR-654-3p	0,47	3395,1048	4,12E-03	1,52E-02

Table 28 Differentially lower transcribed miRNAs after 7 days post stress treatment (downregulated in SIPS D7)

miRNA	log2FC SIPS	baseMean	p-value	adj. p-value
hsa-miR-181a-2-3p	-1,65	2762,2122	3,87E-15	4,18E-13
hsa-miR-199a-5p	-1,62	62878,4037	2,40E-29	1,04E-26
hsa-miR-424-3p	-1,54	2532,4047	1,32E-07	2,93E-06
hsa-miR-199b-5p	-1,45	16565,5675	6,38E-08	1,72E-06
hsa-miR-503-5p	-1,42	1748,1315	2,90E-13	2,51E-11
hsa-miR-210-3p	-1,42	7704,0476	2,37E-11	1,14E-09
hsa-miR-424-5p	-1,38	1982,3524	1,22E-07	2,93E-06
hsa-miR-15b-5p	-1,30	165,5028	1,61E-07	3,30E-06
hsa-miR-1260a	-1,24	85,4972	3,22E-06	4,97E-05
hsa-miR-16-2-3p	-1,18	161,1700	5,86E-07	1,06E-05
hsa-miR-210-5p	-1,13	68,4823	1,66E-04	1,75E-03
hsa-miR-585-3p	-1,05	32,1699	2,33E-03	1,46E-02
hsa-miR-155-5p	-1,04	2702,8938	9,13E-07	1,52E-05
hsa-miR-99a-5p	-1,03	9275,0914	2,79E-05	3,55E-04
hsa-miR-93-3p	-0,95	19,1327	9,62E-03	4,33E-02
hsa-miR-15b-3p	-0,93	34,9752	2,42E-03	1,48E-02
hsa-miR-1304-3p	-0,91	56,8304	1,17E-03	8,13E-03
hsa-miR-4521	-0,89	54,8928	9,49E-04	6,83E-03
hsa-miR-21-5p	-0,88	1270429,0687	6,74E-04	5,02E-03
hsa-miR-450a-2-3p	-0,88	91,7813	2,59E-03	1,51E-02
hsa-miR-1271-5p	-0,88	108,4761	3,83E-04	3,31E-03
hsa-miR-214-3p	-0,88	3283,5447	2,72E-06	4,35E-05
hsa-let-7c-5p	-0,86	3656,4911	3,10E-04	2,91E-03
hsa-miR-3158-3p	-0,83	44,1653	4,30E-03	2,21E-02
hsa-miR-17-5p	-0,79	434,7572	8,80E-03	4,05E-02
hsa-miR-342-3p	-0,78	671,0716	1,64E-03	1,09E-02
hsa-miR-25-3p	-0,76	6407,5008	1,93E-05	2,52E-04
hsa-miR-181b-5p	-0,76	8527,5680	3,35E-03	1,81E-02
hsa-miR-92b-5p	-0,76	109,0557	8,21E-03	3,88E-02
hsa-miR-20a-5p	-0,76	885,0178	3,99E-03	2,10E-02
hsa-miR-1260b	-0,72	199,9894	9,80E-03	4,36E-02
hsa-miR-195-3p	-0,67	154,1246	4,12E-03	2,14E-02
hsa-miR-193a-5p	-0,66	2064,3928	3,53E-04	3,12E-03
hsa-miR-452-5p	-0,66	2126,9590	3,01E-03	1,65E-02
hsa-miR-224-5p	-0,66	11553,6778	1,28E-03	8,74E-03
hsa-miR-143-3p	-0,66	315234,8109	5,60E-03	2,81E-02
hsa-miR-484	-0,63	901,0962	3,01E-03	1,65E-02
hsa-miR-214-5p	-0,60	208,4409	9,26E-03	4,21E-02
hsa-miR-148a-3p	-0,59	51926,9777	4,50E-03	2,29E-02
hsa-miR-199a-3p	-0,57	114971,0249	2,44E-04	2,39E-03
hsa-miR-140-3p	-0,55	5230,7870	1,09E-02	4,59E-02
hsa-miR-28-3p	-0,54	2810,3819	1,97E-03	1,27E-02
hsa-miR-125a-5p	-0,54	13555,5625	1,00E-02	4,36E-02
hsa-miR-143-5p	-0,53	1996,8482	1,17E-02	4,82E-02
hsa-miR-93-5p	-0,52	1404,8806	7,85E-03	3,81E-02

Supplementary Tables

hsa-miR-199b-3p	-0,52	86177,4985	4,67E-04	3,67E-03
hsa-miR-106b-3p	-0,52	1284,8050	1,01E-02	4,36E-02
hsa-miR-99b-5p	-0,51	24798,8214	2,04E-03	1,29E-02

Table 29 Differentially lower transcribed miRNAs after 21 days post stress treatment (downregulated in SIPS D21)

miRNA	log2FC SIPS	baseMean	p-value	adj. p-value
hsa-miR-199b-5p	-1,95	16565,5675	4,13E-13	2,40E-11
hsa-miR-424-5p	-1,85	1982,3524	1,51E-12	7,23E-11
hsa-miR-199a-5p	-1,73	62878,4037	2,60E-33	1,12E-30
hsa-miR-99a-5p	-1,67	9275,0914	9,34E-12	4,03E-10
hsa-miR-181a-2-3p	-1,65	2762,2122	4,39E-15	4,74E-13
hsa-miR-15b-5p	-1,50	165,5028	3,43E-09	7,81E-08
hsa-miR-424-3p	-1,45	2532,4047	8,00E-07	1,08E-05
hsa-miR-210-3p	-1,44	7704,0476	1,15E-11	4,51E-10
hsa-miR-18a-5p	-1,23	11,0554	1,02E-02	3,40E-02
hsa-miR-503-5p	-1,23	1748,1315	3,50E-10	1,01E-08
hsa-miR-214-3p	-1,20	3283,5447	1,55E-10	4,78E-09
hsa-miR-21-5p	-1,17	1270429,0687	6,34E-06	6,52E-05
hsa-miR-214-5p	-1,17	208,4409	4,96E-07	7,39E-06
hsa-miR-16-5p	-1,14	1648,1096	6,52E-06	6,55E-05
hsa-miR-342-5p	-1,11	15,5377	1,13E-02	3,65E-02
hsa-miR-335-3p	-1,10	189,1582	3,08E-03	1,19E-02
hsa-miR-542-3p	-1,10	2262,3299	7,04E-05	5,43E-04
hsa-miR-155-5p	-1,07	2702,8938	4,85E-07	7,39E-06
hsa-miR-452-5p	-1,03	2126,9590	4,50E-06	4,74E-05
hsa-miR-16-2-3p	-1,02	161,1700	3,00E-05	2,65E-04
hsa-miR-4791	-1,01	23,5211	1,09E-02	3,56E-02
hsa-miR-3158-3p	-0,99	44,1653	1,28E-03	5,94E-03
hsa-miR-1271-5p	-0,99	108,4761	1,14E-04	8,21E-04
hsa-miR-224-5p	-0,99	11553,6778	1,49E-06	1,84E-05
hsa-miR-19b-3p	-0,98	254,8194	8,91E-04	4,58E-03
hsa-miR-548o-3p	-0,97	31,2191	3,51E-03	1,33E-02
hsa-miR-335-5p	-0,97	55,2587	1,57E-02	4,57E-02
hsa-miR-450a-2-3p	-0,95	91,7813	1,53E-03	6,73E-03
hsa-miR-20a-5p	-0,95	885,0178	3,41E-04	2,14E-03
hsa-miR-17-3p	-0,91	32,5509	6,23E-03	2,21E-02
hsa-miR-342-3p	-0,91	671,0716	2,25E-04	1,52E-03
hsa-miR-1260a	-0,91	85,4972	9,78E-04	4,88E-03
hsa-miR-1304-3p	-0,91	56,8304	2,50E-03	1,02E-02
hsa-miR-224-3p	-0,90	69,7334	1,35E-03	6,21E-03
hsa-miR-25-3p	-0,89	6407,5008	5,21E-07	7,50E-06
hsa-miR-450a-5p	-0,89	956,5081	2,47E-04	1,62E-03
hsa-miR-106b-5p	-0,88	374,0921	1,48E-03	6,59E-03
hsa-miR-3613-5p	-0,87	43,2078	2,90E-03	1,16E-02
hsa-miR-19a-3p	-0,87	51,7469	3,97E-03	1,49E-02
hsa-miR-195-5p	-0,86	372,2200	6,26E-04	3,47E-03
hsa-miR-181b-5p	-0,85	8527,5680	1,08E-03	5,17E-03
hsa-miR-455-3p	-0,82	583,4553	5,57E-04	3,21E-03
hsa-miR-625-3p	-0,81	84,6545	3,06E-03	1,19E-02
hsa-miR-30d-3p	-0,76	43,1975	1,31E-02	4,07E-02
hsa-miR-455-5p	-0,76	1677,3546	1,11E-04	8,16E-04
hsa-miR-199a-3p	-0,73	114971,0249	2,61E-06	2,97E-05
hsa-miR-17-5p	-0,73	434,7572	1,56E-02	4,57E-02

Supplementary Tables

hsa-miR-125b-2-3p	-0,72	125,8325	1,71E-02	4,90E-02
hsa-miR-199b-3p	-0,71	86177,4985	1,79E-06	2,10E-05
hsa-miR-1180-3p	-0,71	224,9858	4,01E-03	1,49E-02
hsa-miR-450b-5p	-0,69	1400,4838	9,36E-03	3,16E-02
hsa-miR-28-5p	-0,68	920,5871	1,98E-03	8,31E-03
hsa-miR-181a-5p	-0,68	37064,9611	5,61E-03	2,02E-02
hsa-miR-101-3p	-0,66	12733,5317	1,27E-03	5,94E-03
hsa-let-7f-2-3p	-0,66	74,6773	1,75E-02	4,98E-02
hsa-let-7c-5p	-0,66	3656,4911	5,84E-03	2,09E-02
hsa-miR-320a	-0,63	9761,5148	1,44E-03	6,50E-03
hsa-let-7i-5p	-0,62	366740,4960	8,33E-03	2,83E-02
hsa-miR-193b-5p	-0,62	190,2705	1,16E-02	3,70E-02
hsa-miR-140-5p	-0,59	568,0289	1,68E-02	4,83E-02
hsa-miR-195-3p	-0,58	154,1246	1,30E-02	4,07E-02
hsa-miR-99b-5p	-0,57	24798,8214	6,35E-04	3,47E-03
hsa-miR-106b-3p	-0,55	1284,8050	6,54E-03	2,30E-02
hsa-miR-30d-5p	-0,55	23701,8412	5,09E-04	3,01E-03
hsa-miR-93-5p	-0,53	1404,8806	7,36E-03	2,54E-02
hsa-miR-148a-3p	-0,50	51926,9777	1,62E-02	4,70E-02
hsa-miR-193a-5p	-0,49	2064,3928	8,16E-03	2,80E-02
hsa-miR-28-3p	-0,49	2810,3819	5,32E-03	1,93E-02
hsa-miR-98-5p	-0,45	2212,8196	1,23E-02	3,92E-02
hsa-miR-145-3p	-0,43	1516,9500	1,57E-02	4,57E-02

Changes in miRNA transcription over time

Table 30 Differentially higher transcribed miRNAs in **SIPS** on day 21 post stress treatment rel. D7 (Up on D21 in SIPS rel. D7)

miRNA	log2FC D21	baseMean	p-value	p.adj
hsa-miR-122-5p	2,50	225,5032	8,79E-08	3,60E-05

Table 31 Differentially lower transcribed miRNAs in **SIPS** on day 21 post stress treatment rel. D7 (Down on D21 in SIPS rel. D7)

miRNA	log2FC D21	baseMean	p-value	p.adj
hsa-miR-27a-5p	-1,29	1888,5905	2,27E-04	3,59E-02
hsa-miR-365a-5p	-0,82	336,7168	2,63E-04	3,59E-02

Table 32 Differentially higher transcribed miRNAs in **Q** on day 21 post stress treatment rel. D7 (Up on D21 in Q rel. D7)

miRNA	log2FC D21	baseMean	p-value	p.adj
hsa-miR-664a-5p	0,92	165,3610	7,39E-05	8,49E-03
hsa-miR-199b-5p	0,89	16565,5675	9,53E-04	4,70E-02
hsa-miR-101-3p	0,70	12733,5317	7,32E-04	4,21E-02
hsa-miR-199a-5p	0,59	62878,4037	4,77E-05	8,24E-03

Table 33 Differentially lower transcribed miRNAs in **Q** on day 21 post stress treatment rel. D7 (Down on D21 in Q rel. D7)

miRNA	log2FC D21	baseMean	p-value	p.adj
hsa-miR-27a-5p	-1,77	1888,5905	3,94E-07	1,36E-04
hsa-miR-365a-5p	-0,80	336,7168	2,81E-04	2,36E-02
hsa-miR-299-3p	-0,66	902,2963	3,43E-04	2,36E-02

6.6. Correlation of intracellular to extracellular miRNAs

Top 20 miRNAs in cells

Table 34 Top 20 most abundant miRNAs in cells of Q and SIPS

Top 20 miRNAs in cells					
Quiescent (n=6)			SIPS (n=6)		
miRNA	Rank in cells	Rank in EV	miRNA	Rank in cells	Rank in EV
hsa-miR-21-5p	1	1	hsa-miR-21-5p	1	1
hsa-miR-100-5p	2	16	hsa-miR-100-5p	2	18
hsa-let-7i-5p	3	38	hsa-let-7i-5p	3	43
hsa-miR-143-3p	4	11	hsa-miR-10a-5p	4	184
hsa-let-7a-5p	5	7	hsa-miR-143-3p	5	13
hsa-miR-10a-5p	6	185	hsa-let-7a-5p	6	8
hsa-let-7f-5p	7	43	hsa-miR-221-3p	7	6
hsa-miR-199a-3p	8	20	hsa-let-7f-5p	8	50
hsa-miR-27b-3p	9	12	hsa-let-7b-5p	9	25
hsa-miR-125b-5p	10	4	hsa-miR-30a-5p	10	101
hsa-let-7b-5p	11	25	hsa-miR-27b-3p	11	11
hsa-miR-221-3p	12	6	hsa-miR-125b-5p	12	2
hsa-miR-26a-5p	13	41	hsa-miR-22-3p	13	34
hsa-miR-22-3p	14	42	hsa-miR-199a-3p	14	24
hsa-miR-148a-3p	15	156	hsa-miR-26a-5p	15	54
hsa-miR-30a-5p	16	105	hsa-miR-29a-3p	16	17
hsa-miR-10b-5p	17	94	hsa-miR-10b-5p	17	97
hsa-let-7g-5p	18	26	hsa-miR-148a-3p	18	160
hsa-miR-181a-5p	19	35	hsa-miR-152-3p	19	46
hsa-miR-152-3p	20	56	hsa-let-7g-5p	20	29

Top 20 miRNAs in EVs

Table 35 Top 20 most abundant miRNAs in EVs of Q and SIPS

Top 20 miRNAs in EVs					
Quiescent (n=6)			SIPS (n=6)		
miRNA	Rank in cells	Rank in EV	miRNA	Rank in cells	Rank in EV
hsa-miR-21-5p	1	1	hsa-miR-21-5p	1	1
hsa-miR-16-5p	87	2	hsa-miR-125b-5p	12	2
hsa-miR-451a	226	3	hsa-miR-16-5p	102	3
hsa-miR-125b-5p	10	4	hsa-miR-451a	221	3
hsa-miR-23a-3p	25	5	hsa-miR-23a-3p	22	5
hsa-miR-221-3p	12	6	hsa-miR-221-3p	7	6
hsa-let-7a-5p	5	7	hsa-miR-24-3p	25	7
hsa-miR-24-3p	28	8	hsa-let-7a-5p	6	8
hsa-miR-19b-3p	149	9	hsa-miR-19b-3p	166	9
hsa-miR-145-5p	30	10	hsa-miR-145-5p	29	10
hsa-miR-143-3p	4	11	hsa-miR-27b-3p	11	11
hsa-miR-27b-3p	9	12	hsa-miR-23b-3p	51	12
hsa-miR-20a-5p	105	13	hsa-miR-143-3p	5	13
hsa-miR-23b-3p	49	14	hsa-miR-126-3p	158	14
hsa-miR-126-3p	157	15	hsa-miR-222-3p	31	15
hsa-miR-100-5p	2	16	hsa-miR-20a-5p	131	16
hsa-miR-222-3p	42	17	hsa-miR-29a-3p	16	17
hsa-miR-103a-3p	27	18	hsa-miR-100-5p	2	18
hsa-miR-15a-5p	181	19	hsa-miR-1260a	201	19
hsa-miR-199a-3p	8	0	hsa-miR-103a-3p	28	20

Top 20 retained miRNAs

Table 36 Top 20 retained miRNAs in Q and SIPS as determined after calculating the differences of ranks (Δ rank) from intra – extra for SIPS and Q separated

Top 20 retained miRNAs

Quiescent (n=6)		SIPS (n=6)	
miRNA	Δ rank(I-E)	miRNA	Δ rank(I-E)
hsa-miR-10a-5p	-179	hsa-miR-10a-5p	-180
hsa-miR-370-3p	-166	hsa-miR-7-5p	-167
hsa-miR-7-5p	-165	hsa-miR-221-5p	-165
hsa-miR-221-5p	-159	hsa-miR-146b-5p	-161
hsa-miR-146b-5p	-157	hsa-miR-494-3p	-154
hsa-miR-125b-1-3p	-156	hsa-miR-125b-1-3p	-148
hsa-miR-148a-3p	-141	hsa-miR-381-3p	-145
hsa-miR-181a-2-3p	-134	hsa-miR-21-3p	-144
hsa-miR-744-5p	-132	hsa-miR-148a-3p	-142
hsa-miR-27a-5p	-130	hsa-miR-370-3p	-140
hsa-miR-28-3p	-126	hsa-miR-744-5p	-136
hsa-miR-21-3p	-122	hsa-miR-34c-5p	-135
hsa-miR-494-3p	-119	hsa-miR-27a-5p	-123
hsa-miR-34c-5p	-119	hsa-miR-409-5p	-120
hsa-miR-92b-3p	-113	hsa-miR-92b-3p	-116
hsa-miR-452-5p	-110	hsa-miR-28-3p	-114
hsa-miR-381-3p	-108	hsa-miR-181a-2-3p	-112
hsa-miR-224-5p	-107	hsa-miR-323a-3p	-111
hsa-miR-30a-3p	-104	hsa-miR-654-3p	-110
hsa-miR-181b-5p	-100	hsa-miR-143-5p	-110

Top 20 secreted miRNAs

Table 37 Top 20 secreted miRNAs in Q and SIPS as determined after calculating the differences (Δ rank) of ranks from intra – extra for SIPS and Q separated

Top 20 secreted miRNAs

Quiescent (n=6)		SIPS (n=6)	
miRNA	Δ rank(I-E)	miRNA	Δ rank(I-E)
hsa-miR-451a	223	hsa-miR-451a	218
hsa-miR-19a-3p	172	hsa-miR-1260a	182
hsa-miR-15a-5p	162	hsa-miR-19a-3p	176
hsa-miR-122-5p	153	hsa-miR-15a-5p	165
hsa-miR-1260a	149	hsa-miR-19b-3p	157
hsa-miR-126-3p	142	hsa-miR-126-3p	144
hsa-miR-19b-3p	140	hsa-miR-320c	141
hsa-miR-376b-3p	137	hsa-miR-29a-5p	136
hsa-miR-486-5p	136	hsa-miR-136-5p	123
hsa-miR-376a-5p	131	hsa-miR-15b-5p	119
hsa-miR-320c	119	hsa-miR-20a-5p	115
hsa-miR-376a-3p	117	hsa-miR-376b-3p	113
hsa-miR-29a-5p	116	hsa-miR-122-5p	111
hsa-miR-136-5p	110	hsa-miR-376a-5p	109
hsa-miR-652-3p	103	hsa-miR-376a-3p	108
hsa-miR-339-5p	102	hsa-miR-29c-3p	104
hsa-miR-215-5p	94	hsa-miR-106b-5p	104
hsa-miR-20a-5p	92	hsa-miR-339-5p	102
hsa-miR-331-3p	92	hsa-miR-652-3p	102
hsa-miR-17-3p	91	hsa-miR-16-5p	99

Top 20 selectively secreted miRNAs in SIPS – rank based method

Table 38 Top selectively secreted miRNAs from SIPS cells after calculating the differences of the Δ ranks

miRNA	$\Delta\Delta\text{rank} (\Delta\text{SIPS}-\Delta\text{Q})$
hsa-miR-542-5p	46
hsa-miR-149-5p	39
hsa-miR-339-3p	38
hsa-miR-30a-3p	38
hsa-miR-424-5p	34
hsa-miR-1260a	33
hsa-miR-320b	30
hsa-miR-15b-5p	29
hsa-miR-32-5p	29
hsa-miR-708-5p	28
hsa-miR-369-5p	26
hsa-miR-370-3p	26
hsa-miR-532-3p	25
hsa-miR-503-5p	24
hsa-miR-20a-5p	23
hsa-miR-320c	22
hsa-miR-181a-2-3p	22
hsa-miR-485-3p	21
hsa-miR-193a-5p	21
hsa-miR-29a-5p	20

Top 20 selectively secreted miRNAs in SIPS –from the ratio based method in comparison to rank method

Table 39 Top 20 selectively secreted miRNAs from SIPS cells as determined with the 'ratio method' in comparison to rank method

miRNA	norm. To GM	$\Delta\Delta\text{rank} (\Delta\text{SIPS}-\Delta\text{Q})$
hsa-miR-1260a	4,484	33
hsa-miR-339-3p	3,154	38
hsa-miR-542-5p	3,102	46
hsa-miR-370-3p	2,413	26
hsa-miR-32-5p	2,259	29
hsa-miR-369-5p	2,237	26
hsa-miR-181c-5p	2,122	14
hsa-miR-424-5p	1,991	34
hsa-miR-30d-3p	1,949	11
hsa-miR-15b-5p	1,907	29
hsa-miR-149-5p	1,907	39
hsa-miR-503-5p	1,879	24
hsa-miR-99a-5p	1,876	16
hsa-miR-28-3p	1,826	12
hsa-miR-30a-3p	1,810	38
hsa-miR-196a-5p	1,749	20
hsa-miR-452-5p	1,746	10
hsa-miR-335-5p	1,740	14
hsa-miR-181a-2-3p	1,712	22
hsa-miR-1249	1,697	9

selectively secreted miRNAs in SIPS – Found with both methods

Table 40 selectively secreted miRNAs out of the top20 from SIPS cells determined with ratio and rank method

miRNA
hsa-miR-542-5p
hsa-miR-149-5p
hsa-miR-30a-3p
hsa-miR-339-3p
hsa-miR-424-5p
hsa-miR-1260a
hsa-miR-15b-5p
hsa-miR-32-5p
hsa-miR-369-5p
hsa-miR-370-3p
hsa-miR-503-5p
hsa-miR-181a-2-3p

Top 20 selectively retained miRNAs in SIPS with the rank based method

Table 41 Top selectively retained miRNAs from SIPS cells after calculating the differences of the Δ ranks

miRNA	$\Delta\Delta\text{rank } (\Delta\text{SIPS}-\Delta\text{Q})$
hsa-miR-215-5p	-57
hsa-miR-486-5p	-43
hsa-miR-122-5p	-42
hsa-miR-409-5p	-38
hsa-miR-139-5p	-37
hsa-miR-381-3p	-37
hsa-miR-494-3p	-35
hsa-miR-411-5p	-29
hsa-miR-377-3p	-29
hsa-miR-378a-3p	-28
hsa-miR-324-3p	-27
hsa-miR-17-3p	-26
hsa-miR-382-3p	-26
hsa-miR-532-5p	-25
hsa-miR-376b-3p	-24
hsa-miR-491-5p	-23
hsa-miR-455-5p	-23
hsa-miR-376a-5p	-22
hsa-miR-21-3p	-22
hsa-miR-505-3p	-21

Top 20 selectively retained miRNAs in SIPS –from the ratio based method in comparison to rank method

Table 42 Top 20 selectively retained miRNAs from SIPS cells as determined with the 'ratio method' in comparison to rank method

miRNA	norm. To GM	$\Delta\Delta\text{rank} (\Delta\text{SIPS}-\Delta\text{Q})$
hsa-miR-215-5p	0,060	-57
hsa-miR-139-5p	0,087	-37
hsa-miR-378a-3p	0,152	-28
hsa-miR-122-5p	0,164	-42
hsa-miR-204-5p	0,187	-2
hsa-miR-451a	0,211	-5
hsa-miR-486-5p	0,235	-43
hsa-miR-376a-5p	0,312	-22
hsa-miR-376b-3p	0,318	-24
hsa-miR-494-3p	0,324	-35
hsa-miR-491-5p	0,351	-23
hsa-miR-34a-3p	0,363	14
hsa-miR-381-3p	0,386	-37
hsa-miR-409-5p	0,462	-38
hsa-miR-377-3p	0,464	-29
hsa-miR-326	0,471	2
hsa-miR-505-3p	0,473	-21
hsa-miR-21-3p	0,478	-22
hsa-miR-539-5p	0,486	-10
hsa-miR-411-5p	0,488	-29

selectively retained miRNAs in SIPS – Found with both methods

Table 43 selectively retained miRNAs out of the top 20 from SIPS cells determined with ratio and rank method

miRNA
hsa-miR-215-5p
hsa-miR-486-5p
hsa-miR-122-5p
hsa-miR-409-5p
hsa-miR-139-5p
hsa-miR-381-3p
hsa-miR-494-3p
hsa-miR-411-5p
hsa-miR-377-3p
hsa-miR-378a-3p
hsa-miR-376b-3p
hsa-miR-491-5p
hsa-miR-376a-5p
hsa-miR-21-3p
hsa-miR-505-3p

6.7. miRNA - gene interaction from pathways analysis

Dataset is too big. Can be found in 2017_Terlecki_HDF_H2O2_SIPS_Supplementary_Lists.xlsx
 /Arbeitsbereiche/Netzwerkordner/DATAH79000/H791/ZK/ZK/projekte/AGING/Projects/19_CD-LAB/01_Projects/05_secreting_miRNAs/04_paper_poster_talks/Papers/miR_SASP/04_Lists

7. References

- Aatonen, M.T. et al., 2014. Isolation and characterization of platelet-derived extracellular vesicles. *Journal of extracellular vesicles*, 3.
- Acosta, J.C. et al., 2013. A complex secretory program orchestrated by the inflammasome controls paracrine senescence. *Nature cell biology*, 15(8), pp.978–90.
- Agarwal, V. et al., 2015. Predicting effective microRNA target sites in mammalian mRNAs E. Izaurralde, ed. *eLife*, 4, p.e05005. Available at: <https://dx.doi.org/10.7554/eLife.05005>.
- Agosta, F. et al., 2014. Myeloid microvesicles in cerebrospinal fluid are associated with myelin damage and neuronal loss in mild cognitive impairment and Alzheimer disease. *Annals of neurology*, 76(6), pp.813–825.
- Ahmed, M.I. et al., 2011. MicroRNA-21 is an important downstream component of BMP signalling in epidermal keratinocytes. *Journal of cell science*, 124(Pt 20), pp.3399–404. Available at: <http://www.pubmedcentral.nih.gov/articlerender.fcgi?artid=3196856&tool=pmcentrez&rendertype=abstract> [Accessed March 22, 2015].
- Alberts, B., 2008. Molecular Biology of the Cell, 5th edition. *Garland Science*.
- Alexander, M. et al., 2015. Exosome-delivered microRNAs modulate the inflammatory response to endotoxin. 1. Alexander, M., Hu, R., Runtzsch, M.C., Kagele, D.A., Mosbruger, T.L., Tolmachova, T., Seabra, M.C., Round, J.L., Ward, D.M. and O'Connell, R.M. (2015) Exosome-delivered microRNAs modulate. *Nat. Commun.*, 6, p.7321. Available at: <http://www.ncbi.nlm.nih.gov/pubmed/26084661>.
- Alvarez-Erviti, L. et al., 2011. Delivery of siRNA to the mouse brain by systemic injection of targeted exosomes. *Nature biotechnology*, 29(4), pp.341–345.
- El Andaloussi, S. et al., 2013. Extracellular vesicles: biology and emerging therapeutic opportunities. *Nature reviews. Drug discovery*, 12(5), pp.347–57. Available at: <http://www.ncbi.nlm.nih.gov/pubmed/23584393>.
- Anders, S. & Huber, W., 2010. Differential expression analysis for sequence count data. *Genome Biology*, 11(10), p.R106. Available at: <http://dx.doi.org/10.1186/gb-2010-11-10-r106>.
- Anderson, H.C., 1969. Vesicles associated with calcification in the matrix of epiphyseal cartilage. *The Journal of cell biology*, 41(1), pp.59–72.
- Andl, T. et al., 2006. The miRNA-processing enzyme dicer is essential for the morphogenesis and maintenance of hair follicles. *Current biology : CB*, 16(10), pp.1041–1049.
- Andreou, I. et al., 2015. miRNAs in atherosclerotic plaque initiation, progression, and rupture. *Trends in molecular medicine*, 21(5), pp.307–318. Available at: <http://www.ncbi.nlm.nih.gov/pmc/articles/PMC4424146/>.
- Angel, P., Szabowski, a & Schorpp-Kistner, M., 2001. Function and regulation of AP-1 subunits in skin physiology and pathology. *Oncogene*, 20(19), pp.2413–2423.
- Arroyo, J.D. et al., 2011. Argonaute2 complexes carry a population of circulating microRNAs independent of vesicles in human plasma. *Proceedings of the National Academy of Sciences of the United States of America*, 108(12), pp.5003–8. Available at: <http://www.pubmedcentral.nih.gov/articlerender.fcgi?artid=3064324&tool=pmcentrez&rendertype=abstract> [Accessed November 11, 2013].
- Arcsott, W.T. et al., 2013. Ionizing radiation and glioblastoma exosomes: implications in tumor biology and cell migration. *Translational Oncology*, 6(6), pp.638–48. Available at: <http://www.pubmedcentral.nih.gov/articlerender.fcgi?artid=3890698&tool=pmcentrez&rendertype=abstract>.
- Arya, M. et al., 2005. Basic principles of real-time quantitative PCR. *Expert review of molecular diagnostics*, 5(2), pp.209–19. Available at: <http://www.ncbi.nlm.nih.gov/pubmed/15833050>.
- Ashcroft, G.S. et al., 1997. Age-related differences in the temporal and spatial regulation of matrix metalloproteinases (MMPs)

References

- in normal skin and acute cutaneous wounds of healthy humans. *Cell and tissue research*, 290(3), pp.581–591.
- Aw, S. & Cohen, S.M., 2012. Time is of the essence: microRNAs and age-associated neurodegeneration. *Cell Research*, 22(8), pp.1218–1220. Available at: <http://www.ncbi.nlm.nih.gov/pmc/articles/PMC3411169/>.
- Babst, M., 2005. A Protein 's Final ESCRT. *Traffic*, pp.2–9.
- Baglio, S.R. et al., 2015. Human bone marrow- and adipose-mesenchymal stem cells secrete exosomes enriched in distinctive miRNA and tRNA species. *Stem Cell Research & Therapy*, 6(1), p.127. Available at: <http://www.pubmedcentral.nih.gov/articlerender.fcgi?artid=4529699&tool=pmcentrez&rendertype=abstract>.
- Bak, M. et al., 2008. MicroRNA expression in the adult mouse central nervous system. *RNA*, 14(3), pp.432–444. Available at: <http://www.ncbi.nlm.nih.gov/pmc/articles/PMC2248253/>.
- Baker, D.J. et al., 2011. Clearance of p16Ink4a-positive senescent cells delays ageing-associated disorders. *Nature*, 479(7372), pp.232–236.
- Baker, D.J. et al., 2016. Naturally occurring p16 Ink4a -positive cells shorten healthy lifespan. *Nature*, pp.1–5. Available at: <http://dx.doi.org/10.1038/nature16932>.
- van Balkom, B.W., Bervoets, S. & Verhaar, M.C., 2015. Quantitative and qualitative analysis of small RNAs in human endothelial cells and exosomes provides insights into localized RNA processing, degradation and sorting. *Journal of extracellular vesicles*, 1, pp.1–14.
- Balkom, B.W.M. Van et al., 2016. Endothelial cells require miR-214 to secrete exosomes that suppress senescence and induce angiogenesis. , 121(19), pp.3997–4007.
- Ballas, C.B. & Davidson, J.M., 2001. Delayed wound healing in aged rats is associated with increased collagen gel remodeling and contraction by skin fibroblasts, not with differences in apoptotic or myofibroblast cell populations. *Wound Repair and Regeneration*, 9(3), pp.223–237.
- Banerjee, J., 2015. microRNA and wound healing. *Adv Exp Med Biol*, 888, pp.291–305. Available at: <http://link.springer.com/10.1007/978-3-319-22671-2>.
- Barbollat-Boutrand, L. et al., 2016. microRNA-23b-3p regulates human keratinocyte differentiation through repression of TGF1 and activation of the TGF- β -SMAD2 signaling pathway. *Experimental Dermatology*, (June 2016), pp.51–57. Available at: <http://doi.wiley.com/10.1111/exd.13119>.
- Barile, L. et al., 2014. Extracellular vesicles from human cardiac progenitor cells inhibit cardiomyocyte apoptosis and improve cardiac function after myocardial infarction. *Cardiovascular research*, 103(4), pp.530–541.
- Bartel, D.P., 2009. MicroRNA Target Recognition and Regulatory Functions. *Cell*, 136(2), pp.215–233.
- Beattie, J. et al., 2006. Insulin-like growth factor-binding protein-5 (IGFBP-5): a critical member of the IGF axis. *The Biochemical journal*, 395(1), pp.1–19.
- Beauséjour, C.M. et al., 2003. Reversal of human cellular senescence: roles of the p53 and p16 pathways. *The EMBO journal*, 22(16), pp.4212–22. Available at: <http://www.pubmedcentral.nih.gov/articlerender.fcgi?artid=175806&tool=pmcentrez&rendertype=abstract>.
- Beer, L. et al., 2015. Analysis of the Secretome of Apoptotic Peripheral Blood Mononuclear Cells: Impact of Released Proteins and Exosomes for Tissue Regeneration. *Scientific Reports*, 5(October), p.16662. Available at: <http://www.nature.com/articles/srep16662>.
- Belleannée, C. et al., 2013. Epididymosomes convey different repertoires of microRNAs throughout the bovine epididymis. *Biology of reproduction*, 89(2), p.30. Available at: <http://www.ncbi.nlm.nih.gov/pubmed/23803555>.
- Ben-Porath, I. & Weinberg, R.A., 2005. The signals and pathways activating cellular senescence. *The international journal of biochemistry cell biology*, 37(5), pp.961–976. Available at: <http://www.ncbi.nlm.nih.gov/pubmed/15743671>.
- Benjamini, Y. & Yekutieli, D., 2001. The Control of the False Discovery Rate in Multiple Testing under Dependency. *The Annals*

References

- of Statistics*, 29(4), pp.1165–1188. Available at: <http://www.jstor.org/stable/2674075>.
- Vande Berg, J.S. et al., 2005. Cultured pressure ulcer fibroblasts show replicative senescence with elevated production of plasmin, plasminogen activator inhibitor-1, and transforming growth factor- β 1. *Wound Repair and Regeneration*, 13(1), pp.76–83. Available at: <http://dx.doi.org/10.1111/j.1067-1927.2005.130110.x>.
- Berika, M. & Garrod, D., 2014. Desmosomal adhesion in vivo. *Cell communication & adhesion*, 21(1), pp.65–75. Available at: <http://www.ncbi.nlm.nih.gov/pubmed/24460202>.
- Bernert, B., Porsch, H. & Heldin, P., 2011. Hyaluronan synthase 2 (HAS2) promotes breast cancer cell invasion by suppression of tissue metalloproteinase inhibitor 1 (TIMP-1). *The Journal of biological chemistry*, 286(49), pp.42349–42359.
- Bernstein, E.F. et al., 1994. Enhanced elastin and fibrillin gene expression in chronically photodamaged skin. *The Journal of investigative dermatology*, 103(2), pp.182–186.
- Bhat, R. et al., 2012. Astrocyte Senescence as a Component of Alzheimer's Disease. *PLoS ONE*, 7(9), pp.1–10.
- Bhaumik, D. et al., 2009. MicroRNAs miR-146a/b negatively modulate the senescence-associated inflammatory mediators IL-6 and IL-8. *Aging*, 1(4), pp.402–411.
- Bianco, F. et al., 2009. Acid sphingomyelinase activity triggers microparticle release from glial cells. *The EMBO Journal*, 28(8), p.1043 LP-1054. Available at: <http://emboj.embopress.org/content/28/8/1043.abstract>.
- Bianco, F. et al., 2005. Astrocyte-derived ATP induces vesicle shedding and IL-1 beta release from microglia. *Journal of immunology (Baltimore, Md. : 1950)*, 174(11), pp.7268–7277.
- Bittles, A.H. & Harper, N., 1984. Increased glycolysis in ageing cultured human diploid fibroblasts. *Bioscience reports*, 4(9), pp.751–756.
- Le Blanc, K. et al., 2004. Treatment of severe acute graft-versus-host disease with third party haploidentical mesenchymal stem cells. *Lancet (London, England)*, 363(9419), pp.1439–1441.
- Bobrie, A. et al., 2012. Diverse subpopulations of vesicles secreted by different intracellular mechanisms are present in exosome preparations obtained by differential ultracentrifugation. *Journal of extracellular vesicles*, 1.
- Boehm, M. & Slack, F., 2005. A developmental timing microRNA and its target regulate life span in *C. elegans*. *Science*, 310(5756), pp.1954–7. Available at: <http://www.ncbi.nlm.nih.gov/pubmed/16373574>.
- Bonafè, M. & Olivieri, F., 2015. Circulating microRNAs in aging. *Oncotarget*, 6(3), pp.1340–1341.
- Borysenko, J.Z. & Revel, J.P., 1973. Experimental manipulation of desmosome structure. *American Journal of Anatomy*, 137(4), pp.403–421. Available at: <http://dx.doi.org/10.1002/aja.1001370404>.
- Botchkareva, N. V., 2012. MicroRNA/mRNA regulatory networks in the control of skin development and regeneration. *Cell Cycle*, 11(3), pp.468–474.
- Bremnes, R.M. et al., 2011. The role of tumor stroma in cancer progression and prognosis: emphasis on carcinoma-associated fibroblasts and non-small cell lung cancer. *Journal of thoracic oncology : official publication of the International Association for the Study of Lung Cancer*, 6(1), pp.209–217. Available at: <http://dx.doi.org/10.1097/JTO.0b013e3181f8a1bd>.
- De Broe, M., Wieme, R. & Roels, F., 1975. Membrane fragments with koinozymic properties released from villous adenoma of the rectum. *The Lancet*, 306(7946), pp.1214–1215. Available at: [http://dx.doi.org/10.1016/S0140-6736\(75\)92709-9](http://dx.doi.org/10.1016/S0140-6736(75)92709-9).
- Brouwers, J.F. et al., 2013. Distinct lipid compositions of two types of human prostasomes. *PROTEOMICS*, 13(10–11), pp.1660–1666. Available at: <http://www.ncbi.nlm.nih.gov/pubmed/23404715> [Accessed March 6, 2017].
- Brown, B.D. et al., 2007. Endogenous microRNA can be broadly exploited to regulate transgene expression according to tissue, lineage and differentiation state. *Nature Biotechnology*, 25(12), pp.1457–1467. Available at: <http://www.nature.com/doifinder/10.1038/nbt1372>.

References

- Bruno, S. et al., 2012. Microvesicles Derived from Mesenchymal Stem Cells Enhance Survival in a Lethal Model of Acute Kidney Injury. *PLOS ONE*, 7(3), p.e33115. Available at: <http://dx.doi.org/10.1371/journal.pone.0033115>.
- Budnik, V., Ruiz-Cañada, C. & Wendler, F., 2016. Extracellular vesicles round off communication in the nervous system. *Nature reviews. Neuroscience*, 17(3), pp.160–72. Available at: <http://www.nature.com/doi/10.1038/nrn.2015.29>
<http://www.ncbi.nlm.nih.gov/pubmed/26891626>.
- Bus, J.S. & Gibson, J.E., 1984. Paraquat: Model for Oxidant-Initiated Toxicity. *Environmental Health Perspectives*, 55, pp.37–46. Available at: <http://www.jstor.org/stable/3429690>.
- Buscaglia, L.E.B. & Li, Y., 2011. Apoptosis and the target genes of microRNA-21. *Chinese Journal of Cancer*, 30(6), pp.371–380.
- Buschow, S.I. et al., 2009. MHC II in dendritic cells is targeted to lysosomes or T cell-induced exosomes via distinct multivesicular body pathways. *Traffic (Copenhagen, Denmark)*, 10(10), pp.1528–42. Available at: <http://doi.wiley.com/10.1111/j.1600-0854.2009.00963.x> [Accessed March 6, 2017].
- Calkins, C.C. et al., 2003. The Armadillo family protein p0071 is a VE-cadherin- and desmoplakin-binding protein. *The Journal of biological chemistry*, 278(3), pp.1774–1783.
- Camenisch, T.D. et al., 2001. Regulation of cardiac cushion development by hyaluronan. *Experimental & Clinical Cardiology*, 6(1), pp.4–10. Available at: <http://www.ncbi.nlm.nih.gov/pmc/articles/PMC2858958/>.
- Campisi, J., 2013. Aging, Cellular Senescence, and Cancer Judith. *Annu Rev Physiol*, 75, pp.685–705.
- Campisi, J., 2003. Cellular senescence and apoptosis: how cellular responses might influence aging phenotypes. *Experimental gerontology*, 38(1–2), pp.5–11. Available at: <http://www.ncbi.nlm.nih.gov/pubmed/12543256>.
- Campisi, J., 2001. From cells to organisms: can we learn about aging from cells in culture? *Experimental Gerontology*, 36(4–6), pp.607–618. Available at: <http://www.ncbi.nlm.nih.gov/pubmed/11295503>.
- Camussi, G. et al., 2011. Exosome/microvesicle-mediated epigenetic reprogramming of cells. *American journal of cancer research*, 1(1), pp.98–110.
- Candi, E. et al., 2001. Transglutaminase 5 cross-links loricrin, involucrin, and small proline-rich proteins in vitro. *The Journal of biological chemistry*, 276(37), pp.35014–35023.
- Candi, E., Schmidt, R. & Melino, G., 2005. The cornified envelope: a model of cell death in the skin. *Nature reviews. Molecular cell biology*, 6(4), pp.328–40. Available at: <http://dx.doi.org/10.1038/nrm1619>.
- Cao, M. et al., 2012. MiR-23a regulates TGF- β -induced epithelial-mesenchymal transition by targeting E-cadherin in lung cancer cells. *International Journal of Oncology*, 41(3), pp.869–875.
- Castellana, D. et al., 2009. Membrane microvesicles as actors in the establishment of a favorable prostatic tumoral niche: a role for activated fibroblasts and CX3CL1-CX3CR1 axis. *Cancer research*, 69(3), pp.785–793.
- Ceafalan, L. et al., 2012. Telocytes in human skin - are they involved in skin regeneration? *Journal of Cellular and Molecular Medicine*, 16(7), pp.1405–1420.
- Cha, D.J. et al., 2015. KRAS-dependent sorting of miRNA to exosomes. *eLife*, 4(JULY 2015), pp.1–22.
- Chairoungdua, A. et al., 2010. Exosome release of β -catenin: a novel mechanism that antagonizes Wnt signaling. *The Journal of Cell Biology*, 190(6), pp.1079–1091. Available at: <http://www.ncbi.nlm.nih.gov/pmc/articles/PMC3101591/>.
- Chang, J. et al., 2016. Clearance of senescent cells by ABT263 rejuvenates aged hematopoietic stem cells in mice. *Nat Med*, 22(1), pp.78–83. Available at: <http://www.ncbi.nlm.nih.gov/pubmed/26657143>.
- Chaturvedi, V. et al., 1999. Apoptosis in proliferating, senescent, and immortalized keratinocytes. *The Journal of biological chemistry*, 274(33), pp.23358–23367.
- Chen, Q. & Ames, B.N., 1994. Senescence-like growth arrest induced by hydrogen peroxide in human diploid fibroblast F65 cells. *Proceedings of the National Academy of Sciences of the United States of America*, 91(10), pp.4130–4. Available at:

References

- <http://www.pubmedcentral.nih.gov/articlerender.fcgi?artid=43738&tool=pmcentrez&rendertype=abstract>.
- Chen, X. et al., 2008. Characterization of microRNAs in serum: a novel class of biomarkers for diagnosis of cancer and other diseases. *Cell research*, 18(10), pp.997–1006. Available at: <http://eutils.ncbi.nlm.nih.gov/entrez/eutils/elink.fcgi?dbfrom=pubmed&id=18766170&retmode=ref&cmd=prlinks%5Cnpapers3://publication/doi/10.1038/cr.2008.282>.
- Chen, X. et al., 2012a. Horizontal transfer of microRNAs: molecular mechanisms and clinical applications. *Protein & cell*, 3(1), pp.28–37. Available at: <http://www.ncbi.nlm.nih.gov/pubmed/22314808> [Accessed November 10, 2013].
- Chen, X. et al., 2012b. Secreted microRNAs: a new form of intercellular communication. *Trends in cell biology*, 22(3), pp.125–32. Available at: <http://www.ncbi.nlm.nih.gov/pubmed/22260888> [Accessed November 11, 2013].
- Cheng, L. et al., 2014. Exosomes provide a protective and enriched source of miRNA for biomarker profiling compared to intracellular and cell-free blood. , 1, pp.1–14.
- Chevillet, J.R. et al., 2014. Quantitative and stoichiometric analysis of the microRNA content of exosomes. *Proceedings of the National Academy of Sciences of the United States of America*, 111(41), pp.14888–93. Available at: <http://www.pubmedcentral.nih.gov/articlerender.fcgi?artid=4205618&tool=pmcentrez&rendertype=abstract>.
- Chidgey, M. et al., 2001. Mice lacking desmocollin 1 show epidermal fragility accompanied by barrier defects and abnormal differentiation. *The Journal of cell biology*, 155(5), pp.821–832.
- Childs, B.G. et al., 2015. Cellular senescence in aging and age-related disease: from mechanisms to therapy. *Nature medicine*, 21(12), pp.1424–35. Available at: <http://dx.doi.org/10.1038/nm.4000>.
- Childs, B.G. et al., 2014. Senescence and apoptosis: dueling or complementary cell fates? *EMBO reports*, 15(11), pp.1139–53. Available at: <http://www.pubmedcentral.nih.gov/articlerender.fcgi?artid=4253488&tool=pmcentrez&rendertype=abstract>.
- Chistiakov, D., Orekhov, A. & Bobryshev, Y., 2016. Cardiac Extracellular Vesicles in Normal and Infarcted Heart. *International Journal of Molecular Sciences*, 17(1), p.63. Available at: <http://www.mdpi.com/1422-0067/17/1/63/htm>.
- Cicero, A. Lo et al., 2015. Exosomes released by keratinocytes modulate melanocyte pigmentation. *Nature Communications*, 6(May), p.7506. Available at: <http://www.nature.com/doifinder/10.1038/ncomms8506>.
- Cismasiu, V.B. & Popescu, L.M., 2015. Telocytes transfer extracellular vesicles loaded with microRNAs to stem cells. *Journal of Cellular and Molecular Medicine*, 19(2), pp.351–358.
- Cock, P.J.A. et al., 2010. The Sanger FASTQ file format for sequences with quality scores, and the Solexa/Illumina FASTQ variants. *Nucleic Acids Research*, 38(6), pp.1767–1771. Available at: <http://www.ncbi.nlm.nih.gov/pmc/articles/PMC2847217/>.
- Cocucci, E. & Meldolesi, J., 2015. Ectosomes and exosomes: Shedding the confusion between extracellular vesicles. *Trends in Cell Biology*, 25(6), pp.364–372. Available at: <http://dx.doi.org/10.1016/j.tcb.2015.01.004>.
- Cocucci, E., Racchetti, G. & Meldolesi, J., 2009. Shedding microvesicles: artefacts no more. *Trends in Cell Biology*, 19(2), pp.43–51.
- Cogswell, J.P. et al., 2008. Identification of miRNA changes in Alzheimer's disease brain and CSF yields putative biomarkers and insights into disease pathways. *Journal of Alzheimer's disease : JAD*, 14(1), pp.27–41.
- Collino, F. et al., 2010. Microvesicles derived from adult human bone marrow and tissue specific mesenchymal stem cells shuttle selected pattern of miRNAs. *PLoS ONE*, 5(7).
- Colombo, M. et al., 2013. Analysis of ESCRT functions in exosome biogenesis, composition and secretion highlights the heterogeneity of extracellular vesicles. *Journal of Cell Science*, 126(24), p.5553 LP-5565. Available at: <http://jcs.biologists.org/content/126/24/5553.abstract>.
- Colombo, M., Raposo, G. & Théry, C., 2014. Biogenesis, Secretion, and Intercellular Interactions of Exosomes and Other Extracellular Vesicles. *Annu. Rev. Cell Dev. Biol*, 30(August), pp.255–89.

References

- Coppé, J.-P. et al., 2008. Senescence-associated secretory phenotypes reveal cell-nonautonomous functions of oncogenic RAS and the p53 tumor suppressor. *PLoS biology*, 6(12), pp.2853–68. Available at: <http://www.pubmedcentral.nih.gov/articlerender.fcgi?artid=2592359&tool=pmcentrez&rendertype=abstract>.
- Coppé, J.-P., Desprez, P.Y. & Campisi, J., 2010. The Senescence-Associated Secretory Phenotype: The Dark Side of Tumor Suppression. *Annu Rev Pathol*, 5, pp.99–118.
- Cortez, M.A. et al., 2011. MicroRNAs in body fluids—the mix of hormones and biomarkers. *Nature reviews. Clinical oncology*, 8(8), pp.467–477. Available at: <http://www.ncbi.nlm.nih.gov/pmc/articles/PMC3423224/>.
- Cretoi, D. et al., 2015. FIB-SEM tomography of human skin telocytes and their extracellular vesicles. *Journal of Cellular and Molecular Medicine*, 19(4), pp.714–722.
- Cristofalo, V.J. et al., 1998. Relationship between donor age and the replicative lifespan of human cells in culture: a reevaluation. *Proceedings of the National Academy of Sciences of the United States of America*, 95(18), pp.10614–10619.
- Curtis, A.M. et al., 2009. p38 mitogen-activated protein kinase targets the production of proinflammatory endothelial microparticles. *Journal of Thrombosis and Haemostasis*, 7(4), pp.701–709. Available at: <http://doi.wiley.com/10.1111/j.1538-7836.2009.03304.x> [Accessed March 6, 2017].
- Cvijetkovic, A., Lötvall, J. & Lässer, C., 2014. The influence of rotor type and centrifugation time on the yield and purity of extracellular vesicles. *Journal of extracellular vesicles*, 3, pp.3–4. Available at: <http://www.ncbi.nlm.nih.gov/pmc/articles/PMC3760649/%5Cnhttp://www.pubmedcentral.nih.gov/articlerender.fcgi?artid=3760649&tool=pmcentrez&rendertype=abstract%5Cnhttp://www.pubmedcentral.nih.gov/articlerender.fcgi?artid=3967015&tool=pmcentrez&rendertype=abstract>.
- d'Adda di Fagagna, F. et al., 2003. A DNA damage checkpoint response in telomere-initiated senescence. *Nature*, 426(6963), pp.194–8. Available at: <http://www.ncbi.nlm.nih.gov/pubmed/14608368>.
- Dai, G. et al., 2007. Chronic ultraviolet B irradiation causes loss of hyaluronic acid from mouse dermis because of down-regulation of hyaluronic acid synthases. *The American journal of pathology*, 171(5), pp.1451–1461.
- Darby, I.A. & Hewitson, T.D., 2007. Fibroblast differentiation in wound healing and fibrosis. *International review of cytology*, 257, pp.143–179.
- Davalos, A.R. et al., 2010. Senescent cells as a source of inflammatory factors for tumor progression. *Cancer metastasis reviews*, 29(2), pp.273–283. Available at: <http://www.pubmedcentral.nih.gov/articlerender.fcgi?artid=2865636&tool=pmcentrez&rendertype=abstract>.
- Dayan, N., 2008. *SKIN AGING HANDBOOK An Integrated Approach to Biochemistry and Product Development*, Available at: <http://www.knovel.com>.
- Deatherage, B.L. & Cookson, B.T., 2012. Membrane Vesicle Release in Bacteria, Eukaryotes, and Archaea: a Conserved yet Underappreciated Aspect of Microbial Life. *Infection and Immunity*, 80(6), pp.1948–1957. Available at: <http://iai.asm.org/content/80/6/1948.abstract>.
- Dellago, H. et al., 2013. High levels of oncomiR-21 contribute to the senescence-induced growth arrest in normal human cells and its knock-down increases the replicative lifespan. *Aging Cell*, 12(3).
- Dellago, H. et al., 2013. High levels of oncomiR-21 contribute to the senescence induced growth arrest in normal human cells and its knock-down increases the replicative life span. *Aging cell*, pp.1–13. Available at: <http://www.ncbi.nlm.nih.gov/pubmed/23496142> [Accessed March 27, 2013].
- Dellago, H., Bobbili, M.R. & Grillari, J., 2016. MicroRNA-17-5p: At the Crossroads of Cancer and Aging - A Mini-Review. *Gerontology*. Available at: <http://www.ncbi.nlm.nih.gov/pubmed/27577994>.
- Demaria, M. et al., 2014. An Essential Role for Senescent Cells in Optimal Wound Healing through Secretion of PDGF-AA. *Developmental Cell*, 31(6), pp.722–733. Available at: <http://linkinghub.elsevier.com/retrieve/pii/S1534580714007291>.
- Demaria, M. et al., 2015. Cell Autonomous and Non-Autonomous Effects of Senescent Cells in the Skin. *Journal of Investigative Dermatology*, pp.1–5. Available at: <http://www.nature.com/doifinder/10.1038/jid.2015.108>.

References

- Denchi, E.L. et al., 2005. Deregulated E2F Activity Induces Hyperplasia and Senescence-Like Features in the Mouse Pituitary Gland. *Molecular and Cellular Biology*, 25(7), pp.2660–2672. Available at: <http://mcb.asm.org/content/25/7/2660.abstract>.
- Denda, M. et al., 2003. Altered distribution of calcium in facial epidermis of aged adults. *The Journal of investigative dermatology*, 121(6), pp.1557–1558.
- Deo, A., Carlsson Jessica & Lindlöf, A., 2013. How to choose a normalization strategy for miRNA quantitative. *Journal of Chemical Information and Modeling*, 53(9), pp.1689–1699.
- Dhahbi, J.M. et al., 2011. Deep Sequencing Reveals Novel MicroRNAs and Regulation of MicroRNA Expression during Cell Senescence. *PLoS ONE*, 6(5), p.e20509. Available at: <http://dx.plos.org/10.1371/journal.pone.0020509>.
- Dhar, A., Young, M.R. & Colburn, N.H., 2002. The role of AP-1, NF-kappaB and ROS/NOS in skin carcinogenesis: the JB6 model is predictive. *Molecular and cellular biochemistry*, 234–235(1–2), pp.185–193.
- Dimri, G.P., Lee, X.H., et al., 1995. A Biomarker That Identifies Senescent Human-Cells in Culture and in Aging Skin in-Vivo. *Proceedings of the National Academy of Sciences of the United States of America*, 92(20), pp.9363–9367.
- Dimri, G.P., Lee, X., et al., 1995. A biomarker that identifies senescent human cells in culture and in aging skin in vivo. *Proceedings of the National Academy of Sciences of the United States of America*, 92(20), pp.9363–9367. Available at: <http://www.pubmedcentral.nih.gov/articlerender.fcgi?artid=40985&tool=pmcentrez&rendertype=abstract>.
- Dreesen, O., Chojnowski, A., et al., 2013. Lamin B1 fluctuations have differential effects on cellular proliferation and senescence. *The Journal of cell biology*, 200(5), pp.605–17. Available at: <http://www.pubmedcentral.nih.gov/articlerender.fcgi?artid=3587829&tool=pmcentrez&rendertype=abstract> [Accessed March 14, 2015].
- Dreesen, O., Ong, P.F., et al., 2013. The contrasting roles of lamin B1 in cellular aging and human disease. *Nucleus*, 4(4), pp.283–290. Available at: <http://www.ncbi.nlm.nih.gov/pmc/articles/PMC3810336/>.
- Driskell, R. et al., 2014. Defining dermal adipose tissue. *Experimental dermatology*, 23(9), pp.629–631. Available at: <http://www.ncbi.nlm.nih.gov/pmc/articles/PMC4282701/>.
- Du, W.W. et al., 2014. miR-17 extends mouse lifespan by inhibiting senescence signaling mediated by MKP7. *Cell death & disease*, 5, p.1355. Available at: <http://www.ncbi.nlm.nih.gov/pubmed/25077541> [Accessed August 5, 2014].
- Dweep, H. & Gretz, N., 2015a. miRWalk2.0: a comprehensive atlas of microRNA-target interactions. *Nat Meth*, 12(8), p.697.
- Dweep, H. & Gretz, N., 2015b. miRWalk2.0: a comprehensive atlas of microRNA-target interactions. *Nat Meth*, 12(8), p.697. Available at: <http://dx.doi.org/10.1038/nmeth.3485>.
- Eckert, R.L. et al., 2005. Transglutaminase function in epidermis. *Journal of Investigative Dermatology*, 124(3), pp.481–492. Available at: <http://dx.doi.org/10.1111/j.0022-202X.2005.23627.x>.
- Eckhart, L. et al., 2013. Cell death by cornification. *Biochimica et Biophysica Acta - Molecular Cell Research*, 1833(12), pp.3471–3480.
- Effenberger, T. et al., 2014. Senescence-associated release of transmembrane proteins involves proteolytic processing by ADAM17 and microvesicle shedding. *FASEB Journal*, 28(11), pp.4847–4856.
- Eirin, A. et al., 2014. MicroRNA and mRNA cargo of extracellular vesicles from porcine adipose tissue-derived mesenchymal stem cells. *Gene*, 551(1), pp.55–64. Available at: <http://www.ncbi.nlm.nih.gov/pubmed/25158130> [Accessed October 23, 2014].
- Elder, J.T. et al., 2010. Molecular dissection of psoriasis: integrating genetics and biology. *The Journal of investigative dermatology*, 130(5), pp.1213–1226.
- Eldh, M. et al., 2010. Exosomes Communicate Protective Messages during Oxidative Stress; Possible Role of Exosomal Shuttle RNA. *PLoS ONE*, 5(12), pp.1–8.

References

- Eldh, M. et al., 2014. MicroRNA in exosomes isolated directly from the liver circulation in patients with metastatic uveal melanoma. *BMC cancer*, 14(962), pp.1–10.
- Elias, P. et al., 2002. Origin of the epidermal calcium gradient: regulation by barrier status and role of active vs passive mechanisms. *The Journal of investigative dermatology*, 119(6), pp.1269–1274.
- ElSharawy, A. et al., 2012. Genome-wide miRNA signatures of human longevity. *Aging Cell*, 11(4), pp.607–616.
- Elzi, D.J. et al., 2012. Plasminogen activator inhibitor 1 - insulin-like growth factor binding protein 3 cascade regulates stress-induced senescence. *Proceedings of the National Academy of Sciences of the United States of America*, 109(30), pp.12052–12057. Available at: <http://www.ncbi.nlm.nih.gov/pmc/articles/PMC3409757/>.
- Erusalimsky, J.D. et al., 2015. In Search of “Omics”-Based Biomarkers to Predict Risk of Frailty and Its Consequences in Older Individuals: The FRAILOMIC Initiative. *Gerontology*. Available at: <http://www.karger.com/?doi=10.1159/000435853>.
- Erusalimsky, J.D. & Kurz, D.J., 2005. Cellular senescence in vivo: its relevance in ageing and cardiovascular disease. *Experimental gerontology*, 40(8–9), pp.634–42. Available at: <http://www.ncbi.nlm.nih.gov/pubmed/15970413> [Accessed March 14, 2013].
- Erwig, L.-P. & Henson, P.M., 2007. Clearance of apoptotic cells by phagocytes. *Cell Death Differ*, 15(2), pp.243–250. Available at: <http://dx.doi.org/10.1038/sj.cdd.4402184>.
- Fabbri, M. et al., 2012. MicroRNAs bind to Toll-like receptors to induce prometastatic inflammatory response. *Proceedings of the National Academy of Sciences of the United States of America*, 109(31), pp.E2110-6.
- Farage, M.A. et al., 2008. Intrinsic and extrinsic factors in skin ageing: A review. *International Journal of Cosmetic Science*, 30(2), pp.87–95.
- Farage, M.A., Miller, K.W. & Maibach, H.I., 2009. *Textbook of Aging Skin*, Available at: <https://books.google.at/books?id=9-ALWZhXomAC&pg=PA29&lpg=PA29&dq=transepidermal+water+loss+and+dermal+epidermal+junctions&source=bl&ots=t1IB7IQEL4&sig=nXBTlj8RT-wVCmRgzBYvZoirSfE&hl=de&sa=X&ved=0ahUKEwjdsomp1vnSAhVDWywKHXYmDhkQ6AEIQjAE#v=onepage&q=transe>.
- Faraonio, R. et al., 2011. A set of miRNAs participates in the cellular senescence program in human diploid fibroblasts. *Cell Death and Differentiation*, 19(10), pp.713–721. Available at: <http://dx.doi.org/10.1038/cdd.2011.143>.
- Favreau, A.J. et al., 2015. miR-199b, a novel tumor suppressor miRNA in acute c with prognostic implications. *Experimental Hematology & Oncology*, 5, p.4. Available at: <http://www.ncbi.nlm.nih.gov/pmc/articles/PMC4740997/>.
- Fenton, M. et al., 2001. Cellular senescence after single and repeated balloon catheter denudations of rabbit carotid arteries. *Arteriosclerosis, thrombosis, and vascular biology*, 21(2), pp.220–226.
- Fertig, E.J. et al., 2013. Preferential activation of the hedgehog pathway by epigenetic modulations in HPV negative HNSCC identified with meta-pathway analysis. *PloS one*, 8(11), p.e78127.
- Filipowicz, W., Bhattacharyya, S.N. & Sonenberg, N., 2008. Mechanisms of post-transcriptional regulation by microRNAs: are the answers in sight? *Nature reviews. Genetics*, 9(2), pp.102–14. Available at: <http://www.ncbi.nlm.nih.gov/pubmed/18197166> [Accessed February 28, 2013].
- Firth, S.M. & Baxter, R.C., 2002. Cellular Actions of the Insulin-Like Growth Factor Binding Proteins. *Endocrine Reviews*, 23(6), pp.824–854. Available at: <http://dx.doi.org/10.1210/er.2001-0033>.
- Fisher, G.J. et al., 1996. Molecular basis of sun-induced premature skin ageing and retinoid antagonism. *Nature*, 379(6563), pp.335–339.
- Fiskaa, T. et al., 2016. Distinct small RNA signatures in extracellular vesicles derived from breast cancer cell lines. *PLoS ONE*, 11(8).
- Foster, B.P. et al., 2016. Extracellular vesicles in blood, milk and body fluids of the female and male urogenital tract and with special regard to reproduction. *Critical reviews in clinical laboratory sciences*, 53(6), pp.379–395.

References

- Franceschi, C. et al., 2000. Inflamm-aging. An evolutionary perspective on immunosenescence. *Annals of the New York Academy of Sciences*, 908, pp.244–254.
- Fransen, M. et al., 2012. Role of peroxisomes in ROS/RNS-metabolism: Implications for human disease. *Biochimica et Biophysica Acta (BBA) - Molecular Basis of Disease*, 1822(9), pp.1363–1373.
- Freund, A. et al., 2010. Inflammatory Networks during Cellular Senescence: Causes and Consequences. *Trends Mol Med.*, 16(5), pp.238–246.
- Freund, A. et al., 2012. Lamin B1 loss is a senescence-associated biomarker. *Molecular biology of the cell*, 23(11), pp.2066–2075.
- Frippiat, C. et al., 2001. Subcytotoxic H₂O₂ Stress Triggers a Release of Transforming Growth Factor- β 1, Which Induces Biomarkers of Cellular Senescence of Human Diploid Fibroblasts. *Journal of Biological Chemistry*, 276(4), pp.2531–2537.
- Fritz, J. V et al., 2016. Sources and Functions of Extracellular Small RNAs in Human Circulation. *Annual Review of Nutrition*, (May), pp.1–36. Available at: <http://www.annualreviews.org/doi/abs/10.1146/annurev-nutr-071715-050711>.
- Gangadaran, P., Hong, C.M. & Ahn, B., 2017. Current Perspectives on In Vivo Noninvasive Tracking of Extracellular Vesicles with Molecular Imaging. , 2017.
- Garrod, D. & Kimura, T.E., 2008. Hyper-adhesion: a new concept in cell–cell adhesion. *Biochemical Society Transactions*, 36(2), pp.195–201. Available at: <http://www.ncbi.nlm.nih.gov/pubmed/18363561> <http://biochemsoctrans.org/lookup/doi/10.1042/BST0360195>.
- Garrod, D. & Tabernero, L., 2014. Hyper-adhesion: A Unique Property of Desmosomes. *Cell communication & adhesion*, (June 2014), pp.1–8. Available at: <http://www.ncbi.nlm.nih.gov/pubmed/24978153>.
- Garrod, D.R., 2013. The assay that defines desmosome hyper-adhesion. , 133(2), pp.576–577.
- Gascard, P. & Tlsty, T.D., 2016. Carcinoma-associated fibroblasts: Orchestrating the composition of malignancy. *Genes and Development*, 30(9), pp.1002–1019.
- Geiger, A., Walker, A. & Nissen, E., 2015. Human fibrocyte-derived exosomes accelerate wound healing in genetically diabetic mice. *Biochemical and Biophysical Research Communications*, 467(2), pp.303–309. Available at: <http://linkinghub.elsevier.com/retrieve/pii/S0006291X15306963>.
- Gibbins, D.J. et al., 2009. Multivesicular bodies associate with components of miRNA effector complexes and modulate miRNA activity. *Nat Cell Biol*, 11(9), pp.1143–1149. Available at: <http://dx.doi.org/10.1038/ncb1929>.
- Gilchrest, B.A. et al., 2015. Skin Aging: Molecular Mechanisms and Tissue Consequences. *The Journal of investigative dermatology*, 135(4), pp.950–953. Available at: <http://www.ncbi.nlm.nih.gov/pmc/articles/PMC4367196/>.
- Gilhar, A. et al., 1991. Melanocytes and Langerhans Cells in Aged Versus Young Skin Before and After Transplantation onto Nude Mice. *Journal of Investigative Dermatology*, 96(2), pp.210–214. Available at: <http://linkinghub.elsevier.com/retrieve/pii/S0022202X91903843>.
- Goldstein, S. et al., 1982. Energy metabolism in cultured human fibroblasts during aging in vitro. *Journal of cellular physiology*, 112(3), pp.419–424.
- Gordon-Alonso, M. et al., 2012. EWI-2 association with alpha-actinin regulates T cell immune synapses and HIV viral infection. *Journal of immunology (Baltimore, Md. : 1950)*, 189(2), pp.689–700.
- Gosselin, K. et al., 2009. Senescent Keratinocytes Die by Autophagic Programmed Cell Death. *The American Journal of Pathology*, 174(2), pp.423–435. Available at: <http://www.ncbi.nlm.nih.gov/pmc/articles/PMC2630552/>.
- Gould, S.J. & Raposo, G., 2013. As we wait: coping with an imperfect nomenclature for extracellular vesicles. *Journal of Extracellular Vesicles*, 2, p.10.3402/jev.v2i0.20389. Available at: <http://www.ncbi.nlm.nih.gov/pmc/articles/PMC3760635/>.
- Greussing, R. et al., 2013. Identification of microRNA-mRNA functional interactions in UVB-induced senescence of human

References

- diploid fibroblasts. *BMC genomics*, 14, p.224. Available at: <http://www.pubmedcentral.nih.gov/articlerender.fcgi?artid=4008267&tool=pmcentrez&rendertype=abstract>.
- Grillari, J. & Grillari-Voglauer, R., 2010. Novel modulators of senescence, aging, and longevity: Small non-coding RNAs enter the stage. *Experimental gerontology*, 45(4), pp.302–11. Available at: <http://www.ncbi.nlm.nih.gov/pubmed/20080172> [Accessed March 8, 2013].
- Grillari, J., Hackl, M. & Grillari-Voglauer, R., 2010. miR-17-92 cluster: ups and downs in cancer and aging. *Biogerontology*, 11(4), pp.501–6. Available at: <http://www.pubmedcentral.nih.gov/articlerender.fcgi?artid=2899009&tool=pmcentrez&rendertype=abstract> [Accessed August 29, 2014].
- Grillari, J., Katinger, H. & Voglauer, R., 2007. Contributions of DNA interstrand cross-links to aging of cells and organisms. *Nucleic Acids Research*, 35(22), pp.7566–7576.
- Guay, C. & Regazzi, R., 2013. Circulating microRNAs as novel biomarkers for diabetes mellitus. *Nat Rev Endocrinol*, 9(9), pp.513–521. Available at: <http://dx.doi.org/10.1038/nrendo.2013.86>.
- Guduric-Fuchs, J. et al., 2012. Selective extracellular vesicle-mediated export of an overlapping set of microRNAs from multiple cell types. *BMC Genomics*, 13(1), p.357. Available at: BMC Genomics.
- Guinea-Viniegra, J. et al., 2014. Targeting miR-21 to treat psoriasis. *Science translational medicine*, 6(225), p.225re1. Available at: <http://www.ncbi.nlm.nih.gov/pubmed/24574341>.
- Guo, J., Hanawalt, P.C. & Spivak, G., 2013. Comet-FISH with strand-specific probes reveals transcription-coupled repair of 8-oxoGuanine in human cells. *Nucleic acids research*, 41(16), pp.7700–12. Available at: <http://www.pubmedcentral.nih.gov/articlerender.fcgi?artid=3763531&tool=pmcentrez&rendertype=abstract> [Accessed September 19, 2013].
- Guo, Z. et al., 2013. MiR-23a regulates DNA damage repair and apoptosis in UVB-irradiated HaCaT cells. *Journal of Dermatological Science*, 69(1), pp.68–76.
- Hackl, M. et al., 2016. Circulating microRNAs as novel biomarkers for bone diseases – Complex signatures for multifactorial diseases? *Molecular and Cellular Endocrinology*, 432, pp.83–95. Available at: <http://dx.doi.org/10.1016/j.mce.2015.10.015>.
- Hackl, M. et al., 2010. miR-17, miR-19b, miR-20a, and miR-106a are down-regulated in human aging. *Aging cell*, 9(2), pp.291–6. Available at: <http://www.pubmedcentral.nih.gov/articlerender.fcgi?artid=2848978&tool=pmcentrez&rendertype=abstract> [Accessed October 7, 2014].
- Hall, B.M. et al., 2016. Aging of mice is associated with p16(Ink4a)- and β -galactosidase-positive macrophage accumulation that can be induced in young mice by senescent cells. *Aging*, 8(7), pp.1294–315. Available at: <http://www.ncbi.nlm.nih.gov/pubmed/27391570> <http://www.pubmedcentral.nih.gov/articlerender.fcgi?artid=P> MC4993332.
- Hammond, S.M., 2006. MicroRNAs as oncogenes. *Current opinion in genetics development*, 16(1), pp.4–9. Available at: <http://www.ncbi.nlm.nih.gov/pubmed/16361094>.
- Hampel, B. et al., 2005. Apoptosis resistance of senescent human fibroblasts is correlated with the absence of nuclear IGFBP-3. *Aging cell*, 4(6), pp.325–330.
- Hampel, B. et al., 2004. Differential regulation of apoptotic cell death in senescent human cells. *Experimental Gerontology*, 39(11–12), pp.1713–1721. Available at: <http://www.sciencedirect.com/science/article/pii/S0531556504002864>.
- Hampel, B. et al., 2006. Increased expression of extracellular proteins as a hallmark of human endothelial cell in vitro senescence. *Experimental Gerontology*, 41(5), pp.474–481. Available at: <http://www.ncbi.nlm.nih.gov/pubmed/16626901>.
- Harding, C., Heuser, J. & Stahl, P., 1984. Endocytosis and intracellular processing of transferrin and colloidal gold-transferrin in rat reticulocytes: demonstration of a pathway for receptor shedding. *European journal of cell biology*, 35(2), pp.256–

References

- 263.
- Harding, C., Heuser, J. & Stahl, P., 1983. Receptor-mediated endocytosis of transferrin and recycling of the transferrin receptor in rat reticulocytes. *Journal of Cell Biology*, 97(2), pp.329–339.
- Hardman, M.J. et al., 2005. Desmosomal Cadherin Misexpression Alters β -Catenin Stability and Epidermal Differentiation. *Molecular and Cellular Biology*, 25(3), pp.969–978. Available at: <http://www.ncbi.nlm.nih.gov/pmc/articles/PMC544013/>.
- Harley, C.B., Futcher, A.B. & Greider, C.W., 1990. Telomeres shorten during ageing of human fibroblasts. *Nature*, 345(6274), pp.458–460. Available at: <http://dx.doi.org/10.1038/345458a0>.
- Harper, R.A. & Grove, G., 1979. Human skin fibroblasts derived from papillary and reticular dermis: differences in growth potential in vitro. *Science (New York, N.Y.)*, 204(4392), pp.526–527.
- Hatse, S. et al., 2014. Circulating MicroRNAs as Easy-to-Measure Aging Biomarkers in Older Breast Cancer Patients: Correlation with Chronological Age but Not with Fitness/Frailty Status. *PLoS ONE*, 9(10), p.e110644. Available at: <http://dx.plos.org/10.1371/journal.pone.0110644>.
- Hawkes, J.E. et al., 2016. microRNAs in Psoriasis. *The Journal of investigative dermatology*, 136(2), pp.365–71. Available at: <http://www.jidonline.org/article/S0022202X15000445/fulltext>.
- Hayflick, L. & Moorhead, P.S., 1961. The serial cultivation of human diploid cell strains. *Experimental Cell Research*, 25(3), pp.585–621. Available at: <http://linkinghub.elsevier.com/retrieve/pii/0014482761901926>.
- He, L. et al., 2005. A microRNA polycistron as a potential human oncogene. *Nature*, 435(7043), pp.828–833. Available at: <http://www.ncbi.nlm.nih.gov/pubmed/15944707>.
- Heath, W.R. & Carbone, F.R., 2013. The skin-resident and migratory immune system in steady state and memory: innate lymphocytes, dendritic cells and T cells. *Nature immunology*, 14(10), pp.978–85. Available at: <http://www.ncbi.nlm.nih.gov/pubmed/24048119>.
- Henry, F. et al., 1997. Age-related changes in facial skin contours and rheology. *Journal of the American Geriatrics Society*, 45(2), pp.220–222.
- Herbig, U. et al., 2006. Cellular senescence in aging primates. *Science*, 311(5765), p.1257. Available at: http://www.ncbi.nlm.nih.gov/entrez/query.fcgi?cmd=Retrieve&db=PubMed&dopt=Citation&list_uids=16456035.
- Hergenreider, E. et al., 2012. Atheroprotective communication between endothelial cells and smooth muscle cells through miRNAs. *Nature Cell Biology*, 14(3), pp.249–256. Available at: <http://dx.doi.org/10.1038/ncb2441>.
- Higareda-Almaraz, J.C. et al., 2013. Analysis and prediction of pathways in HeLa cells by integrating biological levels of organization with systems-biology approaches. *PloS one*, 8(6), p.e65433.
- Higareda-Almaraz, J.C. et al., 2016. Systems-level effects of ectopic galectin-7 reconstitution in cervical cancer and its microenvironment. *BMC cancer*, 16, p.680.
- Hildebrand, J. et al., 2011. A comprehensive analysis of microRNA expression during human keratinocyte differentiation in vitro and in vivo. *The Journal of investigative dermatology*, 131(1), pp.20–29.
- Hill, A.F. et al., 2013. ISEV position paper: extracellular vesicle RNA analysis and bioinformatics. , 1, pp.1–8.
- Hoare, M. & Narita, M., 2013. Transmitting senescence to the cell neighbourhood. *Nature cell biology*, 15(8), pp.887–889. Available at: <http://www.ncbi.nlm.nih.gov/pubmed/23907191>.
- Holly, A.C. et al., 2015. Comparison of senescence-associated miRNAs in primary skin and lung fibroblasts. *Biogerontology*. Available at: <http://link.springer.com/10.1007/s10522-015-9560-5>.
- Hsu, Y.-C., Li, L. & Fuchs, E., 2014. Emerging interactions between skin stem cells and their niches. *Nature Medicine*, 20(8), pp.847–856. Available at: <http://www.nature.com/doi/10.1038/nm.3643%5Cnpapers3://publication/doi/10.1038/nm.3643>.

References

- Huang, P. et al., 2015. Keratinocyte Microvesicles Regulate the Expression of Multiple Genes in Dermal Fibroblasts. *The Journal of investigative dermatology*, pp.1–9. Available at: <http://dx.doi.org/10.1038/jid.2015.320>.
- Huang, X. et al., 2013. Characterization of human plasma-derived exosomal RNAs by deep sequencing. , pp.1–14.
- Hubackova, S. et al., 2012. IL1 - and TGF β - Nox4 signaling , oxidative stress and DNA damage response are shared features of replicative , oncogene - induced , and drug - induced paracrine “ Bystander senescence .” *Aging*, 4(12), pp.932–951.
- Hunter, M.P. et al., 2008. Detection of microRNA expression in human peripheral blood microvesicles. *PLoS one*, 3(11), p.e3694.
- Hwa, V., Oh, Y. & Rosenfeld, R.G., 1999. The Insulin-Like Growth Factor-Binding Protein (IGFBP) Superfamily*. *Endocrine Reviews*, 20(6), pp.761–787. Available at: <http://dx.doi.org/10.1210/edrv.20.6.0382>.
- Hwang, I., 2013. Cell-cell communication via extracellular membrane vesicles and its role in the immune response. *Molecules and Cells*, 36(2), pp.105–111.
- Iavello, A. et al., 2016. Role of Alix in miRNA packaging during extracellular vesicle biogenesis. *International Journal of Molecular Medicine*, 37(4), pp.958–966.
- Ibanez-Ventoso, C. et al., 2006. Modulated microRNA expression during adult lifespan in *Caenorhabditis elegans*. *Aging cell*, 5(3), pp.235–246.
- Jaé, N. et al., 2015. Rab7a and Rab27b control secretion of endothelial microRNA through extracellular vesicles. *FEBS Letters*, 589(20), pp.3182–3188.
- James, E.L. et al., 2015. Senescent Human Fibroblasts Show Increased Glycolysis and Redox Homeostasis with Extracellular Metabolomes That Overlap with Those of Irreparable DNA Damage, Aging, and Disease. *Journal of Proteome Research*, 14(4), pp.1854–1871. Available at: <http://dx.doi.org/10.1021/pr501221g>.
- Janson, D. et al., 2013. Papillary fibroblasts differentiate into reticular fibroblasts after prolonged in vitro culture. *Experimental dermatology*, 22(1), pp.48–53. Available at: <http://www.ncbi.nlm.nih.gov/pubmed/23278894> [Accessed November 14, 2014].
- Janson, D.G. et al., 2012. Different gene expression patterns in human papillary and reticular fibroblasts. *The Journal of investigative dermatology*, 132(11), pp.2565–72. Available at: <http://www.ncbi.nlm.nih.gov/pubmed/22696053> [Accessed November 14, 2014].
- Jarmalaviciute, A. et al., 2015. Exosomes from dental pulp stem cells rescue human dopaminergic neurons from 6-hydroxy-dopamine-induced apoptosis. *Cytotherapy*, 17(7), pp.932–939.
- Jeyapalan, J.C. et al., 2012. Accumulation of Senescent Cells in Mitotic Tissue of Aging Primates. , 100(2), pp.130–134.
- Ji, H. et al., 2014. Deep Sequencing of RNA from Three Different Extracellular Vesicle (EV) Subtypes Released from the Human LIM1863 Colon Cancer Cell Line Uncovers Distinct Mirna-Enrichment Signatures. *PLoS one*, 9(10), p.e110314. Available at: <http://www.ncbi.nlm.nih.gov/pubmed/25330373> [Accessed October 21, 2014].
- Jiang, M. et al., 2016. IL-22 induced miR-122-5p promotes keratinocyte proliferation by targeting Sprouty2. *Experimental dermatology*.
- de Jong, O.G. et al., 2012. Cellular stress conditions are reflected in the protein and RNA content of endothelial cell-derived exosomes. *Journal of Extracellular Vesicles*, 1(4), pp.1–12.
- De Jong, O.G. et al., 2014. Extracellular vesicles: potential roles in regenerative medicine. *Frontiers in immunology*, 5, p.608.
- Joshi, P. et al., 2014. Microglia convert aggregated amyloid-beta into neurotoxic forms through the shedding of microvesicles. *Cell death and differentiation*, 21(4), pp.582–593.
- Jun, J.-I. & Lau, L.F., 2010a. The matricellular protein CCN1 induces fibroblast senescence and restricts fibrosis in cutaneous wound healing. *Nature cell biology*, 12(7), pp.676–685.
- Jun, J.-I. & Lau, L.F., 2010b. The matricellular protein CCN1 induces fibroblast senescence and restricts fibrosis in cutaneous

References

- wound healing. *Nature cell biology*, 12(7), pp.676–85. Available at: <http://www.pubmedcentral.nih.gov/articlerender.fcgi?artid=2919364&tool=pmcentrez&rendertype=abstract>.
- Jun, J. II & Lau, L.F., 2010. Cellular senescence controls fibrosis in wound healing. *Aging*, 2(9), pp.627–631.
- Jung, H.J. & Suh, Y., 2014. Circulating miRNAs in Ageing and Ageing-Related Diseases. *Journal of genetics and genomics = Yi chuan xue bao*, 41(9), pp.465–472. Available at: <http://www.ncbi.nlm.nih.gov/pmc/articles/PMC4354804/>.
- Jung, T. et al., 2009. Age-related differences in oxidative protein-damage in young and senescent fibroblasts. *Archives of Biochemistry and Biophysics*, 483(1), pp.127–135. Available at: <http://www.sciencedirect.com/science/article/pii/S0003986108005742>.
- Kabir, D. et al., 2016. A miR-335/COX-2/PTEN axis regulates the secretory phenotype of senescent cancer-associated fibroblasts. *Journal of Cellular Biochemistry*, 121(8), pp.1608–1624. Available at: <https://www.ncbi.nlm.nih.gov/pmc/articles/PMC5032686/>.
- Kalinin, A., Marekov, L.N. & Steinert, P.M., 2001. Assembly of the epidermal cornified cell envelope. *Journal of cell science*, 114(Pt 17), pp.3069–70.
- Kalra, H. et al., 2012. Vesiclepedia: A Compendium for Extracellular Vesicles with Continuous Community Annotation. *PLoS Biology*, 10(12), pp.8–12.
- Kalra, H., Drummen, G.P.C. & Mathivanan, S., 2016. Focus on extracellular vesicles: Introducing the next small big thing. *International Journal of Molecular Sciences*, 17(2).
- Kamburov, A. et al., 2013. The ConsensusPathDB interaction database: 2013 update. *Nucleic acids research*, 41(Database issue), pp.D793–800.
- Kang, C. et al., 2015. The DNA damage response induces inflammation and senescence by inhibiting autophagy of GATA4. *Science (New York, N.Y.)*, 349(6255), p.aaa5612.
- Kang, T.-W. et al., 2011. Senescence surveillance of pre-malignant hepatocytes limits liver cancer development. *Nature*, 479(7374), pp.547–551. Available at: <http://dx.doi.org/10.1038/nature10599>.
- Kapsogeorgou, E.K. et al., 2005. Salivary gland epithelial cell exosomes: A source of autoantigenic ribonucleoproteins. *Arthritis and rheumatism*, 52(5), pp.1517–1521.
- Karvinen, S. et al., 2003. Keratinocyte growth factor stimulates migration and hyaluronan synthesis in the epidermis by activation of keratinocyte hyaluronan synthases 2 and 3. *The Journal of biological chemistry*, 278(49), pp.49495–49504.
- Kent, O.A. & Mendell, J.T., 2006. A small piece in the cancer puzzle: microRNAs as tumor suppressors and oncogenes. *Oncogene*, 25(46), pp.6188–6196. Available at: <http://dx.doi.org/10.1038/sj.onc.1209913>.
- Kim, D.-K. et al., 2015. EVpedia: A community web resource for prokaryotic and eukaryotic extracellular vesicles research. *Seminars in Cell & Developmental Biology*, pp.2–5. Available at: <http://linkinghub.elsevier.com/retrieve/pii/S1084952115000324>.
- Kim, K.S. et al., 2007. Induction of Cellular Senescence by Insulin-like Growth Factor Binding Protein-5 through a p53-dependent Mechanism C.-H. Heldin, ed. *Molecular Biology of the Cell*, 18(11), pp.4543–4552. Available at: <http://www.ncbi.nlm.nih.gov/pmc/articles/PMC2043568/>.
- Kim, S.R. et al., 2013. Anti-Wrinkle and Anti-Inflammatory Effects of Active Garlic Components and the Inhibition of MMPs via NF- κ B Signaling. *PLoS ONE*, 8(9), pp.1–12.
- Kirkland, J.L. & Tchkonja, T., 2015. Clinical Strategies and Animal Models for Developing Senolytic Agents. *Experimental gerontology*, 68, pp.19–25.
- Kleijmeer, M. et al., 2001. Reorganization of multivesicular bodies regulates MHC class II antigen presentation by dendritic cells. *The Journal of cell biology*, 155(1), pp.53–63. Available at: <http://www.jcb.org/lookup/doi/10.1083/jcb.200103071> [Accessed March 6, 2017].
- Kligman, L.H., 1989. Photoaging. Manifestations, prevention, and treatment. *Clinics in geriatric medicine*, 5(1), pp.235–251.

Kocijan, R. et al., 2016. Circulating microRNA signatures in patients with idiopathic and postmenopausal osteoporosis and fragility fractures. *The Journal of Clinical Endocrinology & Metabolism*, (October), p.jc.2016-2365. Available at: <http://press.endocrine.org/doi/10.1210/jc.2016-2365>.

Kogure, T. & Lin, W.-L., 2011. Inter-cellular nanovesicle mediated microRNA transfer: a mechanism of environmental modulation of hepatocellular cancer cell growth. , 100(2), pp.130–134.

Koppers-Lalic, D. et al., 2014. Nontemplated Nucleotide Additions Distinguish the Small RNA Composition in Cells from Exosomes. *Cell reports*, pp.1649–1658. Available at: <http://www.ncbi.nlm.nih.gov/pubmed/25242326> [Accessed September 24, 2014].

Kosaka, N. et al., 2013. Neutral sphingomyelinase 2 (nSMase2)-dependent exosomal transfer of angiogenic micrornas regulate cancer cell metastasis. *Journal of Biological Chemistry*, 288(15), pp.10849–10859.

Kosaka, N. et al., 2010. Secretory mechanisms and intercellular transfer of microRNAs in living cells. *The Journal of biological chemistry*, 285(23), pp.17442–52. Available at: <http://www.pubmedcentral.nih.gov/articlerender.fcgi?artid=2878508&tool=pmcentrez&rendertype=abstract> [Accessed November 10, 2013].

Kosar, M. et al., 2011. Senescence-associated heterochromatin foci are dispensable for cellular senescence, occur in a cell type- and insult-dependent manner and follow expression of p16(ink4a). *Cell cycle (Georgetown, Tex.)*, 10(3), pp.457–468.

Kottke, M.D., Delva, E. & Kowalczyk, A.P., 2006. The desmosome: cell science lessons from human diseases. *Journal of cell science*, 119(Pt 5), pp.797–806. Available at: <http://www.ncbi.nlm.nih.gov/pubmed/16495480>.

Kowal, J. et al., 2016. Proteomic comparison defines novel markers to characterize heterogeneous populations of extracellular vesicle subtypes. *Proceedings of the National Academy of Sciences of the United States of America*, 113(8), pp.E968-77. Available at: <http://www.ncbi.nlm.nih.gov/pubmed/26858453><http://www.pubmedcentral.nih.gov/articlerender.fcgi?artid=PMC4776515><http://www.ncbi.nlm.nih.gov/pubmed/26858453><http://www.pubmedcentral.nih.gov/articlerender.fcgi?artid=PMC4776515>.

Kowal, J., Tkach, M. & Théry, C., 2014. Biogenesis and secretion of exosomes. *Current Opinion in Cell Biology*, 29(1), pp.116–125.

Kowalczyk, A.P. et al., 1999. Desmosomes: intercellular adhesive junctions specialized for attachment of intermediate filaments. *International review of cytology*, 185, pp.237–302.

Krichevsky, A.M. & Gabriely, G., 2009. miR-21: a small multi-faceted RNA. *Journal of cellular and molecular medicine*, 13(1), pp.39–53. Available at: <http://www.ncbi.nlm.nih.gov/pubmed/19175699> [Accessed March 7, 2013].

Krishnamurthy, J. et al., 2004. Ink4a/Arf expression is a biomarker of aging. *The Journal of clinical investigation*, 114(9), pp.1299–1307.

Krizhanovsky, V. et al., 2008. Senescence of activated stellate cells limits liver fibrosis. *Cell*, 134(4), pp.657–667.

Krunic, D. et al., 2009. Tissue context-activated telomerase in human epidermis correlates with little age-dependent telomere loss. *Biochimica et biophysica acta*, 1792(4), pp.297–308.

Kurinna, S. et al., 2014. A novel Nrf2-miR-29-desmocollin-2 axis regulates desmosome function in keratinocytes. *Nature Communications*, 5, p.5099. Available at: <http://www.nature.com/doifinder/10.1038/ncomms6099>.

Kutsukake, M. et al., 2008. Circulating IGF-binding protein 7 (IGFBP7) levels are elevated in patients with endometriosis or undergoing diabetic hemodialysis. *Reproductive biology and endocrinology : RB&E*, 6, p.54.

Laberge, R.-M. et al., 2012. Glucocorticoids Suppress Selected Components of the Senescence-Associated Secretory Phenotype. *Aging Cell*, 11(4), pp.569–578. Available at: <http://www.ncbi.nlm.nih.gov/pmc/articles/PMC3387333/>.

Laberge, R.-M. et al., 2015. MTOR regulates the pro-tumorigenic senescence-associated secretory phenotype by promoting IL1A translation. *Nature cell biology*, 17(8), pp.1049–1061.

References

- Lahmann, C. et al., 2001. Matrix metalloproteinase-1 and skin ageing in smokers. *Lancet*, 357(9260), pp.935–936.
- Lai, R.C. et al., 2010. Exosome secreted by MSC reduces myocardial ischemia/reperfusion injury. *Stem cell research*, 4(3), pp.214–222.
- Lamouille, S., Xu, J. & Derynck, R., 2014. Molecular mechanisms of epithelial–mesenchymal transition. *Nat Rev Mol Cell Biol*, 15(3), pp.178–196. Available at: <http://dx.doi.org/10.1038/nrm3758>.
- Lamparski, H.G. et al., 2002. Production and characterization of clinical grade exosomes derived from dendritic cells. *Journal of immunological methods*, 270(2), pp.211–226.
- Lang, A. et al., 2016. MicroRNA-15b regulates mitochondrial ROS production and the senescence-associated secretory phenotype through sirtuin 4/SIRT4. *Aging*, 8(3), pp.484–505.
- Langton, A.K. et al., 2010. A new wrinkle on old skin: The role of elastic fibres in skin ageing. *International Journal of Cosmetic Science*, 32(5), pp.330–339.
- Lawlor, K.T. & Kaur, P., 2015. Dermal contributions to human interfollicular epidermal architecture and self-renewal. *International Journal of Molecular Sciences*, 16(12), pp.28098–28107.
- Laws, P.M. & Young, H.S., 2012. Current and emerging systemic treatment strategies for psoriasis. *Drugs*, 72(14), pp.1867–1880.
- Lee, B.Y. et al., 2006. Senescence-associated β -galactosidase is lysosomal β -galactosidase. *Aging Cell*, 5(2), pp.187–195. Available at: <http://doi.wiley.com/10.1111/j.1474-9726.2006.00199.x> [Accessed March 24, 2017].
- Lee, R.C., Feinbaum, R.L. & Ambros, V., 1993. The *C. elegans* heterochronic gene *lin-4* encodes small RNAs with antisense complementarity to *lin-14*. *Cell*, 75(5), pp.843–854. Available at: <http://www.ncbi.nlm.nih.gov/pubmed/8252621>.
- Lehmann, B.D. et al., 2008. Senescence-associated exosome release from human prostate cancer cells. *Cancer Research*, 68(19), pp.7864–7871.
- Lena, A.M. et al., 2012. MicroRNA-191 triggers keratinocytes senescence by SATB1 and CDK6 downregulation. *Biochemical and Biophysical Research Communications*, 423(3), pp.1763–1768. Available at: <http://www.ncbi.nlm.nih.gov/pmc/articles/PMC3400053/>.
- Lena, a M. et al., 2008. miR-203 represses “stemness” by repressing DeltaNp63. *Cell death and differentiation*, 15, pp.1187–1195.
- de Lencastre, A. et al., 2010. MicroRNAs both promote and antagonize longevity in *C. elegans*. *Current biology : CB*, 20(24), pp.2159–2168. Available at: <http://www.ncbi.nlm.nih.gov/pmc/articles/PMC3023310/>.
- Lener, T. et al., 2015. Applying extracellular vesicles based therapeutics in clinical trials - an ISEV position paper. *Journal of Extracellular Vesicles*, 4(January 2016), pp.1–31. Available at: http://www.journalofextracellularvesicles.net/index.php/jev/article/view/30087/xml_44.
- Leoni, G. et al., 2015. Annexin A1 – containing extracellular vesicles and polymeric nanoparticles promote epithelial wound repair. , 125(3), pp.1215–1227.
- Lewis, B.P., Burge, C.B. & Bartel, D.P., 2005. Conserved seed pairing, often flanked by adenosines, indicates that thousands of human genes are microRNA targets. *Cell*, 120(1), pp.15–20.
- Lewis, D.A. et al., 2010. The IGF-1/IGF-1R signaling axis in the skin: a new role for the dermis in aging-associated skin cancer. *Oncogene*, 29(10), pp.1475–1485. Available at: <http://www.ncbi.nlm.nih.gov/pmc/articles/PMC2837099/>.
- Lewis, D.A. et al., 2008. UVB-induced Senescence in Human Keratinocytes Requires a Functional Insulin-like Growth Factor-1 Receptor and p53 J. S. Gutkind, ed. *Molecular Biology of the Cell*, 19(4), pp.1346–1353. Available at: <http://www.ncbi.nlm.nih.gov/pmc/articles/PMC2291419/>.
- Li, D. et al., 2015. MicroRNA-31 Promotes Skin Wound Healing by Enhancing Keratinocyte Proliferation and Migration. *Journal of Investigative Dermatology*, 135(October 2014), pp.1676–1685. Available at:

References

- <http://www.nature.com/doi/10.1038/jid.2015.48>.
- Li, G. et al., 2009. Alterations in microRNA expression in stress-induced cellular senescence. *Mechanisms of Ageing and Development*, 130(11–12), pp.731–741. Available at: <http://www.pubmedcentral.nih.gov/articlerender.fcgi?artid=2795064&tool=pmcentrez&rendertype=abstract> [Accessed December 3, 2015].
- Li, G. et al., 2010. Modulation of Inflammatory Markers by miR-146a during Replicative Senescence in Trabecular Meshwork Cells. *Investigative Ophthalmology & Visual Science*, 51(6), pp.2976–2985. Available at: <http://www.ncbi.nlm.nih.gov/pmc/articles/PMC2891460/>.
- Li, N. et al., 2011. Increased expression of miR-34a and miR-93 in rat liver during aging, and their impact on the expression of Mgst1 and Sirt1. *Mechanisms of Ageing and Development*, 132(3), pp.75–85. Available at: <http://www.sciencedirect.com/science/article/pii/S0047637411000029>.
- Li, N. et al., 2012. Suppression of type I collagen expression by miR-29b via PI3K, Akt, and Sp1 pathway in human Tenon's fibroblasts. *Investigative ophthalmology & visual science*, 53(3), pp.1670–1678.
- Li, P. et al., 2015a. Differentially expressed miRNAs in acute wound healing of the skin: a pilot study. *Medicine*, 94(7), p.e458. Available at: <http://www.pubmedcentral.nih.gov/articlerender.fcgi?artid=4554165&tool=pmcentrez&rendertype=abstract>.
- Li, P. et al., 2015b. Differentially expressed miRNAs in acute wound healing of the skin: a pilot study. *Medicine*, 94(7), p.e458.
- Li, T. et al., 2016. The comparison of microRNA profile of the dermis between the young and elderly. *Journal of Dermatological Science*, 82(2), pp.75–83. Available at: <http://www.sciencedirect.com/science/article/pii/S0923181116300068>.
- Liu, N. et al., 2012. The microRNA miR-34 modulates aging and neurodegeneration in Drosophila Nan. *Nature.*, 482(7386), pp.519–523.
- Liu, W. & Sharpless, N.E., 2012. Senescence-escape in melanoma. *Pigment cell & melanoma research*, 25(4), pp.408–409. Available at: <http://www.ncbi.nlm.nih.gov/pmc/articles/PMC3710671/>.
- Livingston, M.J. & Wei, Q., 2016. MicroRNAs in extracellular vesicles protect kidney from ischemic injury: from endothelial to tubular epithelial. *Kidney international*, 90(6), pp.1150–1152.
- Loesch, M.M. et al., 2016. Insulin-like growth factor-1 receptor regulates repair of ultraviolet B-induced DNA damage in human keratinocytes in vivo. *Molecular oncology*, 10(8), pp.1245–1254.
- López-Camarillo, C. et al., 2012. Protein kinases and transcription factors activation in response to UV-radiation of skin: Implications for carcinogenesis. *International Journal of Molecular Sciences*, 13(1), pp.142–172.
- López-Otín, C. et al., 2013. The hallmarks of aging. *Cell*, 153(6).
- Luo, Z. et al., 2015. Mir-23a induces telomere dysfunction and cellular senescence by inhibiting TRF2 expression. *Aging cell*, (November 2014), pp.1–9. Available at: <http://www.ncbi.nlm.nih.gov/pubmed/25753893> [Accessed March 15, 2015].
- Lynch, S.F. & Ludlam, C.A., 2007. Plasma microparticles and vascular disorders. *British journal of haematology*, 137(1), pp.36–48.
- Maes, O.C., Sarojini, H. & Wang, E., 2009. Stepwise up-regulation of MicroRNA expression levels from replicating to reversible and irreversible growth arrest states in WI-38 human fibroblasts. *Journal of Cellular Physiology*, 221(1), pp.109–119. Available at: <http://dx.doi.org/10.1002/jcp.21834>.
- Mancini, M. et al., 2012. MicroRNA-152 and -181a participate in human dermal fibroblasts senescence acting on cell adhesion and remodeling of the extra-cellular matrix. *Aging*, 4(11), pp.843–853.
- Mancini, M. et al., 2014. MicroRNAs in human skin ageing. *Ageing research reviews*, 17, pp.9–15. Available at: <http://www.ncbi.nlm.nih.gov/pubmed/24784027> [Accessed April 20, 2015].
- Manda, K.R. et al., 2016. NFATc1 promotes prostate tumorigenesis and overcomes PTEN loss-induced senescence. *Oncogene*,

References

- 35(25), pp.3282–3292.
- Mannava, S. et al., 2013. Depletion of Deoxyribonucleotide Pools Is an Endogenous Source of DNA Damage in Cells Undergoing Oncogene-Induced Senescence. *The American Journal of Pathology*, 182(1), pp.142–151. Available at: <http://www.ncbi.nlm.nih.gov/pmc/articles/PMC3532713/>.
- Marasa, B.S. et al., 2010. MicroRNA profiling in human diploid fibroblasts uncovers miR-519 role in replicative senescence. *Aging (Albany NY)*, 2(6), pp.333–343. Available at: http://www.ncbi.nlm.nih.gov/entrez/query.fcgi?cmd=Retrieve&db=PubMed&dopt=Citation&list_uids=20606251.
- Marcelo, C.L. & Tong, P.S., 1983. Epidermal keratinocyte growth: changes in protein composition and synthesis of keratins in differentiating cultures. *The Journal of investigative dermatology*, 80(1), pp.37–44. Available at: <http://www.ncbi.nlm.nih.gov/pubmed/6184421>.
- Marekov, L.N. & Steinert, P.M., 1998. Ceramides are bound to structural proteins of the human foreskin epidermal cornified cell envelope. *The Journal of biological chemistry*, 273(28), pp.17763–17770.
- Marenholz, I. et al., 2001. Identification of Human Epidermal Differentiation Complex (EDC)-Encoded Genes by Subtractive Hybridization of Entire YACs to a Gridded Keratinocyte cDNA Library. *Genome Research*, 11(3), pp.341–355. Available at: <http://www.ncbi.nlm.nih.gov/pmc/articles/PMC311024/>.
- Martin, A. et al., 2010a. BisoGenet: a new tool for gene network building, visualization and analysis. *BMC Bioinformatics*, 11, p.91.
- Martin, A. et al., 2010b. BisoGenet: a new tool for gene network building, visualization and analysis. *BMC Bioinformatics*, 11, p.91. Available at: <http://www.ncbi.nlm.nih.gov/pmc/articles/PMC3098113/>.
- Martin, F. et al., 2005. Tetraspanins in viral infections: a fundamental role in viral biology? *Journal of virology*, 79(17), pp.10839–10851.
- Martinez, T. et al., 2014. In vitro and in vivo efficacy of SYL040012, a novel siRNA compound for treatment of glaucoma. *Molecular therapy : the journal of the American Society of Gene Therapy*, 22(1), pp.81–91.
- Mathivanan, S., Ji, H. & Simpson, R.J., 2010. Exosomes: extracellular organelles important in intercellular communication. *Journal of proteomics*, 73(10), pp.1907–20. Available at: <http://www.ncbi.nlm.nih.gov/pubmed/20601276> [Accessed July 12, 2014].
- Maurer, B. et al., 2010. MicroRNA-29, a key regulator of collagen expression in systemic sclerosis. *Arthritis & Rheumatism*, 62(6), pp.1733–1743. Available at: <http://doi.wiley.com/10.1002/art.27443>.
- McGrath, J.A. & Uitto, J., 2008. Anatomy and Organization of Human Skin. *Rook's Textbook of Dermatology Volume 1*, p.3.1-3.6.
- McKenzie, A.J. et al., 2016. KRAS-MEK Signaling Controls Ago2 Sorting into Exosomes. *Cell Reports*, 15(5), pp.978–987. Available at: <http://dx.doi.org/10.1016/j.celrep.2016.03.085>.
- Melo, S.A. et al., 2014. Cancer Exosomes Perform Cell-Independent MicroRNA Biogenesis and Promote Tumorigenesis. *Cancer Cell*, 26(5), pp.707–721. Available at: <http://dx.doi.org/10.1016/j.ccell.2014.09.005>.
- Mendez, M. V et al., 2017. Fibroblasts cultured from venous ulcers display cellular characteristics of senescence. *Journal of Vascular Surgery*, 28(5), pp.876–883. Available at: [http://dx.doi.org/10.1016/S0741-5214\(98\)70064-3](http://dx.doi.org/10.1016/S0741-5214(98)70064-3).
- Menon, G.K. et al., 1992. Localization of calcium in murine epidermis following disruption and repair of the permeability barrier. *Cell and tissue research*, 270(3), pp.503–12.
- Mestdagh, P. et al., 2009. A novel and universal method for microRNA RT-qPCR data normalization. *Genome biology*, 10(6), p.R64. Available at: <http://www.ncbi.nlm.nih.gov/pubmed/19531210>.
- Metsalu, T. & Vilo, J., 2015. ClustVis: A web tool for visualizing clustering of multivariate data using Principal Component Analysis and heatmap. *Nucleic Acids Research*, 43(W1), pp.W566–W570.

References

- Micutkova, L. et al., 2011. Insulin-like growth factor binding protein-6 delays replicative senescence of human fibroblasts. *Mechanisms of Ageing and Development*, 132(10), pp.468–479. Available at: <http://dx.doi.org/10.1016/j.mad.2011.07.005>.
- Mildner, M. et al., 2006. Gene silencing in a human organotypic skin model. *Biochemical and biophysical research communications*, 348(1), pp.76–82.
- Miller, K. et al., 1986. Localization of the epidermal growth factor (EGF) receptor within the endosome of EGF-stimulated epidermoid carcinoma (A431) cells. *The Journal of cell biology*, 102(2), pp.500–9. Available at: <http://www.ncbi.nlm.nih.gov/pubmed/2868013> [Accessed March 6, 2017].
- Miller, K.J. et al., 2015. MicroRNAs in skin tissue engineering. *Advanced Drug Delivery Reviews*, 88, pp.16–36. Available at: <http://linkinghub.elsevier.com/retrieve/pii/S0169409X15000824>.
- Millis, A.J. et al., 1992. Differential expression of metalloproteinase and tissue inhibitor of metalloproteinase genes in aged human fibroblasts. *Experimental cell research*, 201(2), pp.373–379.
- Min, P.-K. & Chan, S.Y., 2015. The Biology of Circulating MicroRNAs in Cardiovascular Disease. *European journal of clinical investigation*, 45(8), pp.860–874. Available at: <http://www.ncbi.nlm.nih.gov/pmc/articles/PMC4514545/>.
- Minamino, T., 2002. Endothelial Cell Senescence in Human Atherosclerosis: Role of Telomere in Endothelial Dysfunction. *Circulation*, 105(13), pp.1541–1544. Available at: <http://circ.ahajournals.org/cgi/doi/10.1161/01.CIR.0000013836.85741.17> [Accessed March 29, 2013].
- Mine, S. et al., 2008. Aging alters functionally human dermal papillary fibroblasts but not reticular fibroblasts: a new view of skin morphogenesis and aging. *PLoS one*, 3(12), p.e4066. Available at: <http://www.pubmedcentral.nih.gov/articlerender.fcgi?artid=2605251&tool=pmcentrez&rendertype=abstract> [Accessed November 14, 2014].
- Mischke, D. et al., 1996. Genes encoding structural proteins of epidermal cornification and S100 calcium-binding proteins form a gene complex (“epidermal differentiation complex”) on human chromosome 1q21. *The Journal of investigative dermatology*, 106(5), pp.989–992.
- Mittelbrunn, M. et al., 2011. Unidirectional transfer of microRNA-loaded exosomes from T cells to antigen-presenting cells. *Nature communications*, 2, p.282.
- Miyado, K. et al., 2008. The fusing ability of sperm is bestowed by CD9-containing vesicles released from eggs in mice. *Proceedings of the National Academy of Sciences of the United States of America*, 105(35), pp.12921–12926.
- Miyoshi, H. et al., 1996. Calpain activation in plasma membrane bleb formation during tert-butyl hydroperoxide-induced rat hepatocyte injury. *Gastroenterology*, 110(6), pp.1897–904. Available at: <http://www.ncbi.nlm.nih.gov/pubmed/8964416> [Accessed March 6, 2017].
- Montecalvo, A. et al., 2012. Mechanism of transfer of functional microRNAs between mouse dendritic cells via exosomes. *Blood*, 119(3), pp.756–766.
- Moon, H.-G. et al., 2015. Lung epithelial cell-derived extracellular vesicles activate macrophage-mediated inflammatory responses via ROCK1 pathway. *Cell death & disease*, 6(12), p.e2016. Available at: <http://www.ncbi.nlm.nih.gov/pubmed/26658190> <http://www.pubmedcentral.nih.gov/articlerender.fcgi?artid=P4720875>.
- Moreau, J.-F. et al., 2016. The emerging role of ECM crosslinking in T cell mobility as a hallmark of immunosenescence in humans. *Ageing Research Reviews*. Available at: <http://dx.doi.org/10.1016/j.arr.2016.11.005>.
- Moulin, V.J. et al., 2010. Shedding of microparticles by myofibroblasts as mediator of cellular cross-talk during normal wound healing. *Journal of Cellular Physiology*, 225(3), pp.734–740.
- Mudhasani, R. et al., 2008. Loss of miRNA biogenesis induces p19Arf-p53 signaling and senescence in primary cells. *Journal of Cell Biology*, 181(7), pp.1055–1063.
- Mulcahy, L.A., Pink, R.C. & Carter, D.R.F., 2014. Routes and mechanisms of extracellular vesicle uptake. *Journal of extracellular*

References

- vesicles, 3, pp.1–14. Available at: <http://www.pubmedcentral.nih.gov/articlerender.fcgi?artid=4122821&tool=pmcentrez&rendertype=abstract%5Cnhttp://www.ncbi.nlm.nih.gov/pubmed/25143819%5Cnhttp://www.pubmedcentral.nih.gov/articlerender.fcgi?artid=PMC4122821>.
- Mulloikandov, G. et al., 2013. High-throughput assessment of microRNA activity and function using microRNA sensor and decoy libraries. , 9(8), pp.840–846.
- Muñoz-Espín, D. & Serrano, M., 2014. Cellular senescence: From physiology to pathology. *Nature Reviews Molecular Cell Biology*, 15(7), pp.482–496. Available at: <https://www.scopus.com/inward/record.uri?eid=2-s2.0-84904702784&partnerID=40&md5=9f4f0c44981d3b1277fb51eb67825b80>.
- Munro, J. et al., 2004. Histone deacetylase inhibitors induce a senescence-like state in human cells by a p16-dependent mechanism that is independent of a mitotic clock. *Experimental cell research*, 295(2), pp.525–538.
- Muralidharan-Chari, V. et al., 2009. ARF6-Regulated Shedding of Tumor Cell-Derived Plasma Membrane Microvesicles. *Current Biology*, 19(22), pp.1875–1885. Available at: <http://www.ncbi.nlm.nih.gov/pubmed/19896381> [Accessed March 6, 2017].
- Muturi, H.T. et al., 2013. Tumor and endothelial cell-derived microvesicles carry distinct CEACAMs and influence T-cell behavior. *PloS one*, 8(9), p.e74654.
- Nakano, H., 2004. Signaling crosstalk between NF-κB and JNK. *Trends in Immunology*, 25(8), pp.402–405. Available at: <http://dx.doi.org/10.1016/j.it.2004.05.007>.
- Napolitano, M. et al., 2014. Comparative analysis of gene expression data reveals novel targets of senescence-associated microRNAs. *PloS one*, 9(6), p.e98669. Available at: <http://www.pubmedcentral.nih.gov/articlerender.fcgi?artid=4048207&tool=pmcentrez&rendertype=abstract> [Accessed April 20, 2015].
- Naylor, E.C., Watson, R.E.B. & Sherratt, M.J., 2011. Molecular aspects of skin ageing. *Maturitas*, 69(3), pp.249–256. Available at: <http://dx.doi.org/10.1016/j.maturitas.2011.04.011>.
- Neault, M., Mallette, F.A. & Richard, S., 2016. MiR-137 Modulates a Tumor Suppressor Network-Inducing Senescence in Pancreatic Cancer Cells. *Cell Reports*, 14(8), pp.1966–1978.
- Nedoszytko, B. et al., 2014. Chemokines and cytokines network in the pathogenesis of the inflammatory skin diseases: Atopic dermatitis, psoriasis and skin mastocytosis. *Postepy Dermatologii i Alergologii*, 31(2), pp.84–91.
- Negrini, M., Nicoloso, M.S. & Calin, G. a, 2009. MicroRNAs and cancer--new paradigms in molecular oncology. *Current opinion in cell biology*, 21(3), pp.470–9. Available at: <http://www.ncbi.nlm.nih.gov/pubmed/19411171> [Accessed March 26, 2013].
- Nemes, Z. et al., 1999. A novel function for transglutaminase 1: attachment of long-chain omega-hydroxyceramides to involucrin by ester bond formation. *Proceedings of the National Academy of Sciences of the United States of America*, 96(15), pp.8402–8407.
- Nollet, F., Kools, P. & van Roy, F., 2000. Phylogenetic analysis of the cadherin superfamily allows identification of six major subfamilies besides several solitary members. *Journal of molecular biology*, 299(3), pp.551–572.
- Nolte’T Hoen, E.N.M. et al., 2012. Deep sequencing of RNA from immune cell-derived vesicles uncovers the selective incorporation of small non-coding RNA biotypes with potential regulatory functions. *Nucleic Acids Research*, 40(18), pp.9272–9285.
- Offord, E.A., Chappuis, P.O. & Beard, P., 1993. Different stability of AP1 proteins in human keratinocyte and fibroblast cells: possible role in the cell-type specific expression of human papillomavirus type 18 genes. *Carcinogenesis*, 14(12), pp.2447–2455.
- Ogryzko, V. V et al., 1996. Human fibroblast commitment to a senescence-like state in response to histone deacetylase inhibitors is cell cycle dependent. *Molecular and cellular biology*, 16(9), pp.5210–5218.

References

- Ohshima, K. et al., 2010. Let-7 microRNA family is selectively secreted into the extracellular environment via exosomes in a metastatic gastric cancer cell line. *PLoS ONE*, 5(10), pp.1–10.
- Olivieri, F. et al., 2014. Age - and glycemia - related miR - 126 - 3p levels in plasma and endothelial cells. , 6(9), pp.771–787.
- Olivieri, F. et al., 2015. DNA damage response (DDR) and senescence: shuttled inflamma-miRNAs on the stage of inflamm-aging. *Oncotarget*, 6(34).
- Olivieri, F. et al., 2013. MicroRNAs linking inflamm-aging, cellular senescence and cancer. *Ageing Research Reviews*, 12(4), pp.1056–1068. Available at: <http://www.sciencedirect.com/science/article/pii/S1568163713000238>.
- Olsen, C.L. et al., 2002. Raf-1-induced growth arrest in human mammary epithelial cells is p16-independent and is overcome in immortal cells during conversion. *Oncogene*, 21(41), pp.6328–6339.
- Ortega-Molina, A. & Serrano, M., 2013. PTEN in cancer, metabolism and aging. *Trends in endocrinology and metabolism: TEM*, 24(4), p.10.1016/j.tem.2012.11.002. Available at: <http://www.ncbi.nlm.nih.gov/pmc/articles/PMC3836169/>.
- Ostenfeld, M.S. et al., 2014. Cellular disposal of miR23b by RAB27-dependent exosome release is linked to acquisition of metastatic properties. *Cancer Research*, 74(20), pp.5758–5771.
- Ostrowski, M. et al., 2010. Rab27a and Rab27b control different steps of the exosome secretion pathway. *Nature cell biology*, 12(1), pp.13–19.
- Ovadya, Y. & Krizhanovsky, V., 2016. Senescent cell death brings hopes to life. *Cell Cycle*, 4101(October), pp.1–2. Available at: <https://www.tandfonline.com/doi/full/10.1080/15384101.2016.1232088>.
- Overhoff, M.G. et al., 2014. Cellular senescence mediated by p16INK4A-coupled miRNA pathways. *Nucleic Acids Research*, 42(3), pp.1606–1618.
- Özcan, S. et al., 2016. Unbiased analysis of senescence associated secretory phenotype (SASP) to identify common components following different genotoxic stresses. *Ageing*, 8(7), pp.1316–29. Available at: <http://www.ncbi.nlm.nih.gov/pubmed/27288264> <http://www.pubmedcentral.nih.gov/articlerender.fcgi?artid=PMC4993333>.
- Pallet, N. et al., 2013. A comprehensive characterization of membrane vesicles released by autophagic human endothelial cells. *Proteomics*, 13(7), pp.1108–1120.
- Parrinello, S. et al., 2005. Stromal-epithelial interactions in aging and cancer: senescent fibroblasts alter epithelial cell differentiation. *Journal of cell science*, 118(Pt 3), pp.485–496.
- Payne, A.S. et al., 2004. Desmosomes and disease: pemphigus and bullous impetigo. *Current opinion in cell biology*, 16(5), pp.536–543.
- Pegtel, D.M. et al., 2010. Functional delivery of viral miRNAs via exosomes. *Proc. Natl. Acad. Sci. USA*, 107(14), pp.6328–6333. Available at: <http://www.pubmedcentral.nih.gov/articlerender.fcgi?artid=2851954&tool=pmcentrez&rendertype=abstract>.
- Perrotta, I. & Aquila, S., 2016. Exosomes in human atherosclerosis: An ultrastructural analysis study. *Ultrastructural pathology*, 40(2), pp.101–106.
- Pienimaeki-Roemer, A. et al., 2015. Lipidomic and proteomic characterization of platelet extracellular vesicle subfractions from senescent platelets. *Transfusion*, 55(3), pp.507–521.
- Pigati, L. et al., 2010. Selective release of MicroRNA species from normal and malignant mammary epithelial cells. *PLoS ONE*, 5(10).
- Pols, M.S. & Klumperman, J., 2009. Trafficking and function of the tetraspanin CD63. *Experimental cell research*, 315(9), pp.1584–1592.
- Poumay, Y. et al., 1999. High-cell-density phorbol ester and retinoic acid upregulate involucrin and downregulate suprabasal keratin 10 in autocrine cultures of human epidermal keratinocytes. *Molecular cell biology research communications* :

References

- MCBRC*, 2(2), pp.138–144.
- Poumay, Y. & Pittelkow, M.R., 1995. Cell density and culture factors regulate keratinocyte commitment to differentiation and expression of suprabasal K1/K10 keratins. *The Journal of investigative dermatology*, 104(2), pp.271–276.
- Prattichizzo, F., Giuliani, A., et al., 2016. Anti-TNF- α treatment modulates SASP and SASP-related microRNAs in endothelial cells and in circulating angiogenic cells. *Oncotarget*, 7(11), pp.11945–58. Available at: <http://www.ncbi.nlm.nih.gov/pubmed/26943583> <http://www.ncbi.nlm.nih.gov/pubmed/26943583>.
- Prattichizzo, F., De Nigris, V., et al., 2016. “Inflammaging” as a Druggable Target: A Senescence-Associated Secretory Phenotype—Centered View of Type 2 Diabetes. *Oxidative Medicine and Cellular Longevity*, 2016, p.1810327. Available at: <http://www.ncbi.nlm.nih.gov/pmc/articles/PMC4908264/>.
- Puizina-Ivić, N., 2008. Skin aging. *Acta dermatovenerologica Alpina, Pannonica, et Adriatica*, 17(2), pp.47–54. Available at: <http://www.ncbi.nlm.nih.gov/pubmed/18709289>.
- Ragan, C., Zuker, M. & Ragan, M.A., 2011. Quantitative prediction of miRNA-mRNA interaction based on equilibrium concentrations. *PLoS Computational Biology*, 7(2).
- Rames, M., Yu, Y. & Ren, G., 2014. Optimized Negative Staining: a High-throughput Protocol for Examining Small and Asymmetric Protein Structure by Electron Microscopy. *Journal of Visualized Experiments : JoVE*, (90), p.51087. Available at: <http://www.ncbi.nlm.nih.gov/pmc/articles/PMC4710468/>.
- Rani, S. et al., 2015. Mesenchymal Stem Cell-derived Extracellular Vesicles: Toward Cell-free Therapeutic Applications. *Molecular Therapy*, 23(5), pp.812–823. Available at: <http://www.nature.com/doifinder/10.1038/mt.2015.44>.
- Rani, S. & Ritter, T., 2016. The Exosome - A Naturally Secreted Nanoparticle and its Application to Wound Healing. *Advanced Materials*, 28(27), pp.5542–5552. Available at: <http://dx.doi.org/10.1002/adma.201504009>.
- Raposo, G. & Stoorvogel, W., 2013. Extracellular vesicles: Exosomes, microvesicles, and friends. *Journal of Cell Biology*, 200(4), pp.373–383.
- Record, M. et al., 2014. Exosomes as new vesicular lipid transporters involved in cell-cell communication and various pathophysiologicals. *Biochimica et biophysica acta*, 1841(1), pp.108–120.
- Reinhardt, T.A. et al., 2012. Bovine milk exosome proteome. *Journal of Proteomics*, 75(5), pp.1486–1492.
- Reinhart, B.J. et al., 2002. MicroRNAs in plants. *Genes & Development*, 16(13), pp.1616–1626. Available at: <http://www.ncbi.nlm.nih.gov/pmc/articles/PMC186362/>.
- Ressler, S. et al., 2006. p16INK4A is a robust in vivo biomarker of cellular aging in human skin. *Aging Cell*, 5(5), pp.379–389.
- Ridder, K. et al., 2014. Extracellular Vesicle-Mediated Transfer of Genetic Information between the Hematopoietic System and the Brain in Response to Inflammation. *PLoS Biology*, 12(6).
- Rinnerthaler, M. et al., 2013. Age-related changes in the composition of the cornified envelope in human skin. *Experimental dermatology*, 22(5), pp.329–35.
- Rippe, C. et al., 2012. MicroRNA changes in human arterial endothelial cells with senescence: Relation to apoptosis, eNOS and inflammation. *Experimental Gerontology*, 47(1), pp.45–51.
- Ritschka, B. et al., 2017. The senescence-associated secretory phenotype induces cellular plasticity and tissue regeneration. *Genes & Development*, pp.1–12. Available at: <http://genesdev.cshlp.org/lookup/doi/10.1101/gad.290635.116>.
- Rittié, L. & Fisher, G.J., 2002. UV-light-induced signal cascades and skin aging. *Ageing Research Reviews*, 1(4), pp.705–720.
- Rivetti di Val Cervo, P. et al., 2012. p63–microRNA feedback in keratinocyte senescence. *Proceedings of the National Academy of Sciences of the United States of America*, 109(4), pp.1133–1138. Available at: <http://www.ncbi.nlm.nih.gov/pmc/articles/PMC3268329/>.
- Robbins, P.D. & Morelli, A.E., 2014. Regulation of Immune Responses by Extracellular Vesicles. *Nature reviews. Immunology*,

References

- 14(3), pp.195–208. Available at: <http://www.ncbi.nlm.nih.gov/pmc/articles/PMC4350779/>.
- Robinson, N.A., LaCelle, P.T. & Eckert, R.L., 1996. Involucrin Is a Covalently Crosslinked Constituent of Highly Purified Epidermal Corneocytes: Evidence for a Common Pattern of Involucrin Crosslinking in Vivo and in Vitro. *Journal of Investigative Dermatology*, 107(1), pp.101–107. Available at: <http://www.sciencedirect.com/science/article/pii/S0022202X15426326>.
- Röck, K. et al., 2012. Estradiol protects dermal hyaluronan/versican matrix during photoaging by release of epidermal growth factor from keratinocytes. *Journal of Biological Chemistry*, 287(24), pp.20056–20069.
- Röck, K. et al., 2014. miR-23a-3p Causes Cellular Senescence by Targeting Hyaluronan Synthase 2: Possible Implication for Skin Aging. *Journal of Investigative Dermatology*, 135(August), pp.369–377. Available at: <http://www.sciencedirect.com/science/article/pii/S0022202X15370755%5Cnhttp://www.nature.com/doi/10.1038/jid.2014.422> [Accessed October 1, 2014].
- Rodemann, H.P. et al., 1989. Selective enrichment and biochemical characterization of seven human skin fibroblasts cell types in vitro. *Experimental cell research*, 180(1), pp.84–93.
- Rodier, F. & Campisi, J., 2011. Four faces of cellular senescence. *The Journal of Cell Biology*, 192(4), pp.547–556. Available at: <http://www.pubmedcentral.nih.gov/articlerender.fcgi?artid=3044123&tool=pmcentrez&rendertype=abstract>.
- Roos, C.M. et al., 2016. Chronic senolytic treatment alleviates established vasomotor dysfunction in aged or atherosclerotic mice. *Aging Cell*, (February), pp.973–977.
- Ruhrberg, C. et al., 1996. Envoplakin, a novel precursor of the cornified envelope that has homology to desmoplakin. *The Journal of cell biology*, 134(3), pp.715–729.
- Ruhrberg, C. et al., 1997. Periplakin, a Novel Component of Cornified Envelopes and Desmosomes That Belongs to the Plakin Family and Forms Complexes with Envoplakin. *The Journal of Cell Biology*, 139(7), pp.1835–1849. Available at: <http://www.ncbi.nlm.nih.gov/pmc/articles/PMC2132639/>.
- Sanders, Y.Y. et al., 2013. Histone modifications in senescence-associated resistance to apoptosis by oxidative stress. *Redox biology*, 1, pp.8–16.
- Santangelo, L. et al., 2016. The RNA-Binding Protein SYNCRIP Is a Component of the Hepatocyte Exosomal Machinery Controlling MicroRNA Sorting. *Cell Reports*, 17(3), pp.799–808. Available at: <http://dx.doi.org/10.1016/j.celrep.2016.09.031>.
- Sarnow, P. et al., 2006. MicroRNAs: expression, avoidance and subversion by vertebrate viruses. *Nature reviews. Microbiology*, 4(9), pp.651–659.
- Schafer, I.A. et al., 1985. Comparative observation of fibroblasts derived from the papillary and reticular dermis of infants and adults: growth kinetics, packing density at confluence and surface morphology. *Mechanisms of ageing and development*, 31(3), pp.275–293.
- Schageman, J. et al., 2013. The Complete Exosome Workflow Solution : From Isolation to Characterization of RNA Cargo. , 2013.
- Schmitt, C.A. et al., 2002. A senescence program controlled by p53 and p16INK4a contributes to the outcome of cancer therapy. *Cell*, 109(3), pp.335–346.
- Schroder, J. et al., 2009. Deficiency of the tetraspanin CD63 associated with kidney pathology but normal lysosomal function. *Molecular and cellular biology*, 29(4), pp.1083–1094.
- Scott, C.T. & DeFrancesco, L., 2015. Selling long life. *Nature biotechnology*, 33(1), pp.31–40. Available at: <http://www.scopus.com/inward/record.url?eid=2-s2.0-84923267605&partnerID=40&md5=0f90391e394d15ca73ec8ea60980f75a%5Cnhttp://www.ncbi.nlm.nih.gov/pubmed/25654547%5Cnhttp://www.pubmedcentral.nih.gov/articlerender.fcgi?artid=PMC4382265%5Cnhttp://www.ncbi.nlm.nih.gov/pmc/articles/PMC4382265/>.
- Seluanov, A. et al., 2001. Change of the Death Pathway in Senescent Human Fibroblasts in Response to DNA Damage Is Caused by an Inability To Stabilize p53. *Molecular and Cellular Biology*, 21(5), pp.1552–1564. Available at: <http://www.ncbi.nlm.nih.gov/pmc/articles/PMC86701/>.

References

- Serna, E. et al., 2012. Centenarians, but not octogenarians, up-regulate the expression of microRNAs. *Scientific reports*, 2, p.961.
- Serrano, M. et al., 1997. Oncogenic ras Provokes Premature Cell Senescence Associated with Accumulation of p53 and p16INK4a. *Cell*, 88(5), pp.593–602. Available at: <http://www.sciencedirect.com/science/article/pii/S0092867400819029>.
- Setzer, S. V et al., 2004. Comparative analysis of armadillo family proteins in the regulation of a431 epithelial cell junction assembly, adhesion and migration. *The Journal of investigative dermatology*, 123(3), pp.426–433.
- Severino, V. et al., 2013. Insulin-like growth factor binding proteins 4 and 7 released by senescent cells promote premature senescence in mesenchymal stem cells. *Cell Death & Disease*, 4(11), p.e911. Available at: <http://www.ncbi.nlm.nih.gov/pmc/articles/PMC3847322/>.
- Sevilla, L.M. et al., 2007. Mice deficient in involucrin, envoplakin, and periplakin have a defective epidermal barrier. *The Journal of Cell Biology*, 179(7), pp.1599–1612. Available at: <http://www.ncbi.nlm.nih.gov/pmc/articles/PMC2373502/>.
- Sharghi-Namini, S. et al., 2014. DLL4-containing exosomes induce capillary sprout retraction in a 3D microenvironment. *Scientific Reports*, 4, p.4031. Available at: <http://dx.doi.org/10.1038/srep04031>.
- Shin, K.-H. et al., 2011. Identification of senescence-inducing microRNAs in normal human keratinocytes. *International journal of oncology*, 100(2), pp.130–134.
- Shurtleff, M.J. et al., 2016. Y-box protein 1 is required to sort microRNAs into exosomes in cells and in a cell-free reaction. *eLife*, 5(AUGUST).
- Sidhu, S.S. et al., 2004. The microvesicle as a vehicle for EMMPRIN in tumor-stromal interactions. *Oncogene*, 23(4), pp.956–63. Available at: <http://www.ncbi.nlm.nih.gov/pubmed/14749763>.
- Singer, A. & Clark, R.A., 1999. Cutaneous Wound Healing. *The New England Journal of Medicine*, 341(10), pp.738–746.
- Skog, J. et al., 2008. Glioblastoma microvesicles transport RNA and proteins that promote tumour growth and provide diagnostic biomarkers. *Nature cell biology*, 10(12), pp.1470–6. Available at: <http://www.ncbi.nlm.nih.gov/pubmed/19011622>.
- Smoot, M.E. et al., 2011. Cytoscape 2.8: new features for data integration and network visualization. *Bioinformatics*, 27(3), pp.431–432. Available at: <http://www.ncbi.nlm.nih.gov/pmc/articles/PMC3031041/>.
- Smyth, G.K., 2005. Limma: linear models for microarray data R. Gentleman et al., eds. , pp.397–420. Available at: http://dx.doi.org/10.1007/0-387-29362-0_23.
- Sódar, B.W. et al., 2016. Low-density lipoprotein mimics blood plasma-derived exosomes and microvesicles during isolation and detection. *Scientific Reports*, 6(April), p.24316. Available at: <http://www.nature.com/articles/srep24316>.
- Sonkoly, E. et al., 2007. MicroRNAs: novel regulators involved in the pathogenesis of psoriasis? *PloS one*, 2(7), p.e610.
- Sonkoly, E. et al., 2010. Protein Kinase C-Dependent Upregulation of miR-203 Induces the Differentiation of Human Keratinocytes. *Journal of Investigative Dermatology*, 130(1), pp.124–134.
- Sorkin, A. & Goh, L.K., 2009. Endocytosis and intracellular trafficking of ErbBs. *Experimental cell research*, 315(4), pp.683–96. Available at: <http://www.ncbi.nlm.nih.gov/pubmed/19278030> [Accessed March 6, 2017].
- Sorrell, J.M., 2004. Fibroblast heterogeneity: more than skin deep. *Journal of Cell Science*, 117(5), pp.667–675. Available at: <http://jcs.biologists.org/cgi/doi/10.1242/jcs.01005>.
- Sorrell, J.M., Baber, M.A. & Caplan, A.L., 2004. Site-matched papillary and reticular human dermal fibroblasts differ in their release of specific growth factors/cytokines and in their interaction with keratinocytes. *Journal of Cellular Physiology*, 200(1), pp.134–145.
- Spivak, G., 2015. New developments in comet-FISH. *Mutagenesis*, 30(1), pp.5–9. Available at: <http://www.ncbi.nlm.nih.gov/pubmed/25527722> [Accessed February 11, 2015].

References

- Spivak, G. & Hanawalt, P.C., 2015. Photosensitive Human Syndromes. *Reviews in Mutation Research*, June(776), pp.24–30.
- Squadrito, M.L. et al., 2014. Endogenous RNAs Modulate MicroRNA Sorting to Exosomes and Transfer to Acceptor Cells. *Cell Reports*, 8(5), pp.1432–1446.
- Stein, G.H. et al., 1999. Differential roles for cyclin-dependent kinase inhibitors p21 and p16 in the mechanisms of senescence and differentiation in human fibroblasts. *Molecular and cellular biology*, 19(3), pp.2109–2117.
- Stern, R. & Maibach, H.I., 2008. Hyaluronan in skin: aspects of aging and its pharmacologic modulation. *Clinics in dermatology*, 26(2), pp.106–122.
- Stevanato, L. et al., 2016. Investigation of content, stoichiometry and transfer of miRNA from human neural stem cell line derived exosomes. *PLoS ONE*, 11(1), pp.1–13.
- Stevenson, S. & Thornton, J., 2007. Effect of estrogens on skin aging and the potential role of selective estrogen receptor modulators. *clinical interventions in Aging*, 10(4), pp.289–297.
- Stuffers, S. et al., 2009. Multivesicular endosome biogenesis in the absence of ESCRTs. *Traffic (Copenhagen, Denmark)*, 10(7), pp.925–937.
- Sugimoto, M., Yamashita, R. & Ueda, M., 2017. Telomere length of the skin in association with chronological aging and photoaging. *Journal of Dermatological Science*, 43(1), pp.43–47. Available at: <http://dx.doi.org/10.1016/j.jdermsci.2006.02.004>.
- Szabowski, A. et al., 2000. c-Jun and JunB antagonistically control cytokine-regulated mesenchymal-epidermal interaction in skin. *Cell*, 103(5), pp.745–755.
- Tachibana, I. & Hemler, M.E., 1999. Role of transmembrane 4 superfamily (TM4SF) proteins CD9 and CD81 in muscle cell fusion and myotube maintenance. *The Journal of cell biology*, 146(4), pp.893–904.
- Taganov, K.D. et al., 2006. NF- κ B-dependent induction of microRNA miR-146, an inhibitor targeted to signaling proteins of innate immune responses. *Proceedings of the National Academy of Sciences of the United States of America*, 103(33), pp.12481–12486. Available at: <http://www.ncbi.nlm.nih.gov/pmc/articles/PMC1567904/>.
- Takahashi, H. et al., 2001. In vitro and in vivo transfer of bcl-2 gene into keratinocytes suppresses UVB-induced apoptosis. *Photochemistry and photobiology*, 74(4), pp.579–586.
- Takahashi, M. et al., 2012. Reduction of Type IV Collagen by Upregulated miR-29 in Normal Elderly Mouse and klotho-Deficient, Senescence-Model Mouse. *PLOS ONE*, 7(11), p.e48974. Available at: <http://dx.doi.org/10.1371/journal.pone.0048974>.
- Takeda, Y. et al., 2003. Tetraspanins CD9 and CD81 function to prevent the fusion of mononuclear phagocytes. *The Journal of cell biology*, 161(5), pp.945–956.
- Tavakkol, A. et al., 1992. Expression of growth hormone receptor, insulin-like growth factor 1 (IGF-1) and IGF-1 receptor mRNA and proteins in human skin. *The Journal of investigative dermatology*, 99(3), pp.343–349.
- Tchkonia, T. et al., 2013. Cellular senescence and the senescent secretory phenotype: therapeutic opportunities. *The Journal of Clinical Investigation*, 123(3).
- Théry, C. et al., 2006. Isolation and characterization of exosomes from cell culture supernatants. *Current Protocols in Cell Biology*, p.3.22.1-3.22.29.
- Thomason, H.A. et al., 2012. Direct evidence that PKC positively regulates wound re-epithelialization: Correlation with changes in desmosomal adhesiveness. *Journal of Pathology*, 227(3), pp.346–356.
- Tigges, J. et al., 2014. The hallmarks of fibroblast ageing. *Mechanisms of Ageing and Development*, 138, pp.26–44. Available at: <http://www.ncbi.nlm.nih.gov/pubmed/24686308> [Accessed November 14, 2014].
- Tobin, D.J., 2006. Biochemistry of human skin--our brain on the outside. *Chemical Society reviews*, 35, pp.52–67.

References

- Tosar, J.P. et al., 2015. Assessment of small RNA sorting into different extracellular fractions revealed by high-throughput sequencing of breast cell lines. *Nucleic Acids Research*, 43(11), pp.5601–5616.
- Toussaint, O., Houbion, A. & Remacle, J., 1994. Effects of modulations of the energetic metabolism on the mortality of cultured cells. *Biochimica et biophysica acta*, 1186(3), pp.209–220.
- Toussaint, O., Medrano, E.E. & Von Zglinicki, T., 2000. Cellular and molecular mechanisms of stress-induced premature senescence (SIPS) of human diploid fibroblasts and melanocytes. *Experimental Gerontology*, 35, pp.927–945.
- Trajkovic, K. et al., 2008. Ceramide Triggers Budding of Exosome Vesicles into Multivesicular Endosomes. *Science*, 319(5867), p.1244 LP-1247. Available at: <http://science.sciencemag.org/content/319/5867/1244.abstract>.
- Turchinovich, A. et al., 2011. Characterization of extracellular circulating microRNA. *Nucleic acids research*, 39(16), pp.7223–33. Available at: <http://www.pubmedcentral.nih.gov/articlerender.fcgi?artid=3167594&tool=pmcentrez&rendertype=abstract> [Accessed November 9, 2013].
- Turchinovich, A., Tonevitsky, A.G. & Burwinkel, B., 2016. Extracellular miRNA: A Collision of Two Paradigms. *Trends in Biochemical Sciences*, 41(10), pp.883–892. Available at: <http://dx.doi.org/10.1016/j.tibs.2016.08.004>.
- Turchinovich, A., Weiz, L. & Burwinkel, B., 2012. Extracellular miRNAs: The mystery of their origin and function. *Trends in Biochemical Sciences*, 37(11), pp.460–465. Available at: <http://www.ncbi.nlm.nih.gov/pubmed/22944280> [Accessed November 13, 2013].
- Valadi, H. et al., 2007. Exosome-mediated transfer of mRNAs and microRNAs is a novel mechanism of genetic exchange between cells. *Nature cell biology*, 9(6), pp.654–659.
- Valeski, J.E. et al., 1992. Differentiation of bullous pemphigoid from epidermolysis bullosa acquisita on frozen skin biopsies. *International journal of dermatology*, 31(1), pp.37–41.
- van Niel, G. et al., 2017. The Tetraspanin CD63 Regulates ESCRT-Independent and -Dependent Endosomal Sorting during Melanogenesis. *Developmental Cell*, 21(4), pp.708–721. Available at: <http://dx.doi.org/10.1016/j.devcel.2011.08.019>.
- Verzijl, N. et al., 2000. Effect of collagen turnover on the accumulation of advanced glycation end products. *The Journal of biological chemistry*, 275(50), pp.39027–39031.
- Vickers, K.C. et al., 2011a. MicroRNAs are transported in plasma and delivered to recipient cells by high-density lipoproteins. *Nat Cell Biol*, 13(4), pp.423–433.
- Vickers, K.C. et al., 2011b. MicroRNAs are transported in plasma and delivered to recipient cells by high-density lipoproteins. *Nat Cell Biol*, 13(4), pp.423–433. Available at: <http://dx.doi.org/10.1038/ncb2210>.
- Vikos, T.S. et al., 2016. A serum miRNA profile of human longevity : findings from the Baltimore Longitudinal Study of Aging (BLSA). , 8(11), pp.2971–2987.
- Villarroya-Beltri, C. et al., 2013. Sumoylated hnRNP A2B1 controls the sorting of miRNAs into exosomes through binding to specific motifs. *Nature communications*, 4, p.2980. Available at: <http://www.pubmedcentral.nih.gov/articlerender.fcgi?artid=3905700&tool=pmcentrez&rendertype=abstract>.
- Vollgraf, U., Wegner, M. & Richter-Landsberg, C., 1999. Activation of AP-1 and nuclear factor-kappaB transcription factors is involved in hydrogen peroxide-induced apoptotic cell death of oligodendrocytes. *Journal of neurochemistry*, 73(6), pp.2501–2509.
- Waaijer, M.E.C. et al., 2015. P16INK4a Positive Cells in Human Skin Are Indicative of Local Elastic Fiber Morphology, Facial Wrinkling, and Perceived Age. *The journals of gerontology. Series A, Biological sciences and medical sciences*, p.glv114-. Available at: <http://biomedgerontology.oxfordjournals.org/content/early/2015/08/18/gerona.glv114>.
- Wagner, E.F. et al., 2010. Psoriasis: what we have learned from mouse models. *Nature reviews. Rheumatology*, 6(12), pp.704–714.
- Wallis, S. et al., 2000. The alpha isoform of protein kinase C is involved in signaling the response of desmosomes to wounding

References

- in cultured epithelial cells. *Molecular biology of the cell*, 11(3), pp.1077–1092.
- Wang, E., 1995. Senescent Human Fibroblasts Resist Programmed Cell Death, and Failure to Suppress bcl2 Is Involved. *Cancer Research*, 55(11), pp.2284–2292. Available at: <http://cancerres.aacrjournals.org/content/55/11/2284>.
- Wang, G. et al., 2012. Astrocytes secrete exosomes enriched with proapoptotic ceramide and prostate apoptosis response 4 (PAR-4): potential mechanism of apoptosis induction in Alzheimer disease (AD). *The Journal of biological chemistry*, 287(25), pp.21384–21395.
- Wang, K. et al., 2010. Export of microRNAs and microRNA-protective protein by mammalian cells. *Nucleic Acids Research*, 38(20), pp.7248–7259.
- Wang, T. et al., 2012. miR-21 regulates skin wound healing by targeting multiple aspects of the healing process. *The American journal of pathology*, 181(6), pp.1911–20. Available at: <http://www.sciencedirect.com/science/article/pii/S0002944012006645>.
- Wang, X.-L. et al., 2015. MiR-378b Promotes Differentiation of Keratinocytes through NKX3.1. *PloS one*, 10(8), p.e0136049.
- Wang, Y. et al., 2016. Discovery of piperlongumine as a potential novel lead for the development of senolytic agents. *Aging*, 8(11), pp.2915–2926. Available at: <http://www.ncbi.nlm.nih.gov/pubmed/27913811><http://www.aging-us.com/full/101100>.
- Wang, Z. & Lieberman, P.M., 2016. The crosstalk of telomere dysfunction and inflammation through cell-free TERRA containing exosomes. <http://Dx.Doi.Org/10.1080/15476286.2016.1203503>, 6286(July), pp.0–19.
- Warburg, O., 1956. On the origin of cancer cells. *Science (New York, N.Y.)*, 123(3191), pp.309–314.
- Wäster, P. et al., 2016. Extracellular vesicles are transferred from melanocytes to keratinocytes after UVA irradiation. *Scientific Reports*, 6(May), p.27890. Available at: <http://www.nature.com/articles/srep27890>.
- Watson, R.E.B. et al., 1999. Fibrillin-rich microfibrils are reduced in photoaged skin. Distribution at the dermal-epidermal junction. *Journal of Investigative Dermatology*, 112(5), pp.782–787. Available at: <http://dx.doi.org/10.1046/j.1523-1747.1999.00562.x>.
- Watt, F.M. & Green, H., 1981. Involucrin synthesis is correlated with cell size in human epidermal cultures. *The Journal of cell biology*, 90(3), pp.738–742.
- Watt, F.M., Matthey, D.L. & Garrod, D.R., 1984. Calcium-induced reorganization of desmosomal components in cultured human keratinocytes. *The Journal of cell biology*, 99(6), pp.2211–5. Available at: <http://www.pubmedcentral.nih.gov/articlerender.fcgi?artid=2113584&tool=pmcentrez&rendertype=abstract>.
- Weber, J.A. et al., 2010. The MicroRNA Spectrum in 12 Body Fluids. *Clinical chemistry*, 56(11), pp.1733–1741. Available at: <http://www.ncbi.nlm.nih.gov/pmc/articles/PMC4846276/>.
- Weebadda, W.K.C., Jackson, T.J. & Lin, A.W., 2005. Expression of p16INK4A variants in senescent human fibroblasts independent of protein phosphorylation. *Journal of cellular biochemistry*, 94(6), pp.1135–1147.
- Weilner, S., Schraml, E., et al., 2016a. Secreted microvesicular miR-31 inhibits osteogenic differentiation of mesenchymal stem cells. *Aging Cell*, 15(4), pp.744–754.
- Weilner, S., Schraml, E., et al., 2016b. Secreted microvesicular miR-31 inhibits osteogenic differentiation of mesenchymal stem cells. *Aging Cell*, 15(4), pp.744–754.
- Weilner, S. et al., 2013. Secretion of microvesicular miRNAs in cellular and organismal aging. *Experimental Gerontology*, 48(7), pp.626–633. Available at: <http://dx.doi.org/10.1016/j.exger.2012.11.017>.
- Weilner, S. et al., 2015. The role of microRNAs in cellular senescence and age-related conditions of cartilage and bone. *Acta Orthopaedica*, 86(1), pp.92–99. Available at: <http://informahealthcare.com/doi/abs/10.3109/17453674.2014.957079>.
- Weilner, S., Keider, V., et al., 2016. Vesicular Galectin-3 levels decrease with donor age and contribute to the reduced osteo-inductive potential of human plasma derived extracellular vesicles. *Aging*, 8(1), pp.16–33. Available at:

References

- <http://www.pubmedcentral.nih.gov/articlerender.fcgi?artid=4761711&tool=pmcentrez&rendertype=abstract>.
- Wen, S. et al., 2016. Mesenchymal stromal cell-derived extracellular vesicles rescue radiation damage to murine marrow hematopoietic cells. *Leukemia*, 30(11), pp.2221–2231.
- West, M.D., Pereira-Smith, O.M. & Smith, J.R., 1989. Replicative senescence of human skin fibroblasts correlates with a loss of regulation and overexpression of collagenase activity. *Experimental cell research*, 184(1), pp.138–147.
- White, S.D. & Yager, J.A., 1995. Resident Dendritic Cells in the Epidermis: Langerhans Cells, Merkel Cells and Melanocytes. *Veterinary Dermatology*, 6(1), pp.1–8.
- Wiley, C.D. & Campisi, J., 2016. From Ancient Pathways to Aging Cells—Connecting Metabolism and Cellular Senescence. *Cell Metabolism*, 23(6), pp.1013–1021. Available at: <http://linkinghub.elsevier.com/retrieve/pii/S1550413116302285>.
- Wilson, S.L. et al., 2014. A microscopic and macroscopic study of aging collagen on its molecular structure, mechanical properties, and cellular response. *FASEB journal : official publication of the Federation of American Societies for Experimental Biology*, 28(1), pp.14–25.
- Winter, J. et al., 2009. Many roads to maturity: microRNA biogenesis pathways and their regulation. *Nature cell biology*, 11(3), pp.228–234.
- Wisgrill, L. et al., 2016. Peripheral blood microvesicles secretion is influenced by storage time, temperature, and anticoagulants. *Cytometry Part A*, 89(7), pp.663–672. Available at: <http://doi.wiley.com/10.1002/cyto.a.22892>.
- Witwer, K.W. et al., 2013. Standardization of sample collection, isolation and analysis methods in extracellular vesicle research. *Journal of extracellular vesicles*, 2, pp.1–25. Available at: <http://www.pubmedcentral.nih.gov/articlerender.fcgi?artid=3760646&tool=pmcentrez&rendertype=abstract>.
- Wu, N. et al., 2012. The miR-17 family links p63 protein to MAPK signaling to promote the onset of human keratinocyte differentiation. *PloS one*, 7(9), p.e45761. Available at: <http://www.pubmedcentral.nih.gov/articlerender.fcgi?artid=3454365&tool=pmcentrez&rendertype=abstract> [Accessed March 22, 2015].
- Wubbolts, R. et al., 2003. Proteomic and biochemical analyses of human B cell-derived exosomes. Potential implications for their function and multivesicular body formation. *The Journal of biological chemistry*, 278(13), pp.10963–72. Available at: <http://www.jbc.org/cgi/doi/10.1074/jbc.M207550200> [Accessed March 6, 2017].
- Wylie, D. et al., 2011. A novel mean-centering method for normalizing microRNA expression from high-throughput RT-qPCR data. *BMC research notes*, 4(1), p.555. Available at: <http://bmcresearchnotes.biomedcentral.com/articles/10.1186/1756-0500-4-555>.
- Wyss-Coray, T., 2016. Ageing, neurodegeneration and brain rejuvenation. *Nature*, 539(7628), pp.180–186. Available at: <http://www.nature.com/doi/10.1038/nature20411>.
- Xiao, D. et al., 2012. Identifying mRNA, MicroRNA and Protein Profiles of Melanoma Exosomes. *PLoS ONE*, 7(10).
- Xiao, J. et al., 2016. Cardiac progenitor cell-derived exosomes prevent cardiomyocytes apoptosis through exosomal miR-21 by targeting PDCD4. *Cell death & disease*, 7(6), p.e2277.
- Xiao, Z.-Q. & Majumdar, A.P.N., 2000. Induction of transcriptional activity of AP-1 and NF-κB in the gastric mucosa during aging. *American Journal of Physiology - Gastrointestinal and Liver Physiology*, 278(6), p.G855 LP-G865. Available at: <http://ajpgi.physiology.org/content/278/6/G855.abstract>.
- Xu, J. et al., 2013. A novel role of EMMPRIN/CD147 in transformation of quiescent fibroblasts to cancer-associated fibroblasts by breast cancer cells. *Cancer letters*, 335(2), pp.380–386. Available at: <http://www.ncbi.nlm.nih.gov/pmc/articles/PMC3927232/>.
- Xu, J.-F. et al., 2014. Altered microRNA expression profile in exosomes during osteogenic differentiation of human bone marrow-derived mesenchymal stem cells. *PloS one*, 9(12), p.e114627. Available at: <http://www.pubmedcentral.nih.gov/articlerender.fcgi?artid=4263734&tool=pmcentrez&rendertype=abstract>.

References

- Xu, L. et al., 2014. Downregulation of miR-21 increases cisplatin sensitivity of non-small-cell lung cancer. *Cancer genetics*, 207(5), pp.214–20. Available at: http://www.researchgate.net/publication/261598809_Down-regulation_of_miR-21_increases_cisplatin_sensitivity_of_non-small-cell_lung_cancer.
- Xu, M. et al., 2015. JAK inhibition alleviates the cellular senescence-associated secretory phenotype and frailty in old age. *Proceedings of the National Academy of Sciences of the United States of America*, 112(46), pp.E6301-10.
- Xu, N. et al., 2012. MicroRNA-31 Is Overexpressed in Psoriasis and Modulates Inflammatory Cytokine and Chemokine Production in Keratinocytes via Targeting Serine/Threonine Kinase 40. *The Journal of Immunology*, 190(2), pp.678–688. Available at: <http://www.jimmunol.org/cgi/doi/10.4049/jimmunol.1202695>.
- Xu, S. et al., 2015. Exosome-mediated microRNA transfer plays a role in radiation-induced bystander effect. *RNA biology*, 12(12), pp.1355–1363. Available at: <http://www.tandfonline.com/doi/full/10.1080/15476286.2015.1100795> <http://www.ncbi.nlm.nih.gov/pubmed/26488306>.
- Yàñez-Mo, M. et al., 2015. Biological properties of extracellular vesicles and their physiological functions. *Journal of extracellular vesicles*, 4, p.27066.
- Yang, H.H. et al., 2011. Involvement of IGF binding protein 5 in prostaglandin E(2)-induced cellular senescence in human fibroblasts. *Biogerontology*, 12(3), pp.239–252.
- Yang, J. et al., 2013. MiR-34 modulates *Caenorhabditis elegans* lifespan via repressing the autophagy gene *atg9*. *AGE*, 35(1), pp.11–22. Available at: <http://dx.doi.org/10.1007/s11357-011-9324-3>.
- Yang, S. et al., 2013. miR-21 confers cisplatin resistance in gastric cancer cells by regulating PTEN. *Toxicology*, 306, pp.162–168. Available at: <http://linkinghub.elsevier.com/retrieve/pii/S0300483X13000607>.
- Yang, X.X. et al., 2011. miR-21 promotes keratinocyte migration and re-epithelialization during wound healing. *International Journal of Biological Sciences*, 7(5), pp.685–690.
- Yentrapalli, R. et al., 2017. Quantitative changes in the protein and miRNA cargo of plasma exosome-like vesicles after exposure to ionizing radiation. *International Journal of Radiation Biology*, 0(0), pp.1–37. Available at: <https://www.tandfonline.com/doi/full/10.1080/09553002.2017.1294772>.
- Yeo, R.W.Y. et al., 2013. Mesenchymal stem cell: an efficient mass producer of exosomes for drug delivery. *Advanced drug delivery reviews*, 65(3), pp.336–341.
- Yi, R. et al., 2008. A skin microRNA promotes differentiation by repressing 'stemness'. *Nature*, 452(7184), pp.225–229. Available at: <http://dx.doi.org/10.1038/nature06642>.
- Yi, R. et al., 2006. Morphogenesis in skin is governed by discrete sets of differentially expressed microRNAs. *Nature genetics*, 38(3), pp.356–362.
- Yin, L., Morita, A. & Tsuji, T., 2000. Alterations of extracellular matrix induced by tobacco smoke extract. *Archives of Dermatological Research*, 292(4), pp.188–194. Available at: <http://dx.doi.org/10.1007/s004030050476>.
- Yoo, J.K. et al., 2014. Discovery and characterization of miRNA during cellular senescence in bone marrow-derived human mesenchymal stem cells. *Experimental gerontology*, 58, pp.139–45. Available at: <http://www.ncbi.nlm.nih.gov/pubmed/25087724>.
- Yosef, R. et al., 2016. Directed elimination of senescent cells by inhibition of BCL-W and BCL-XL. *Nature communications*, 7, p.11190. Available at: <http://www.nature.com/ncomms/2016/16046/ncomms11190/full/ncomms11190.html>.
- Yu, J. et al., 2015. Suppression of Type I Collagen Expression by miR-29b Via PI3K, Akt, and Sp1 Pathway, Part II: An In Vivo Investigation. *Investigative ophthalmology & visual science*, 56(10), pp.6019–6028.
- Yu, X., Harris, S.L. & Levine, A.J., 2006. The regulation of exosome secretion: A novel function of the p53 protein. *Cancer Research*, 66(9), pp.4795–4801.
- Zeringer, E. et al., 2013. Methods for the extraction and RNA profiling of exosomes. *World Journal of Methodology*, 3(1), pp.11–

References

- 18.
- von Zglinicki, T., 2000. Role of oxidative stress in telomere length regulation and replicative senescence. *Annals of the New York Academy of Sciences*, 908, pp.99–110.
- Zhang, A. et al., 2011. miR-21 Modulates Cell Apoptosis by Targeting Multiple Genes in Renal Cell Carcinoma. *Urology*, 78(2), p.474.e13-e19. Available at: <http://www.ncbi.nlm.nih.gov/pubmed/21820586>.
- Zhang, B. et al., 2016. Focus on extracellular vesicles: Therapeutic potential of stem cell-derived extracellular vesicles. *International Journal of Molecular Sciences*, 17(2).
- Zhang, J. et al., 2015. Exosome and exosomal microRNA: Trafficking, sorting, and function. *Genomics, Proteomics and Bioinformatics*, 13(1), pp.17–24.
- Zhang, J. et al., 2016. MiR-23a-depressed autophagy is a participant in PUVA- and UVB-induced premature senescence. *Oncotarget*, 7(25), pp.37420–37435.
- Zhang, J., Patel, J.M. & Block, E.R., 2002. Enhanced apoptosis in prolonged cultures of senescent porcine pulmonary artery endothelial cells. *Mechanisms of ageing and development*, 123(6), pp.613–625.
- Zhang, L. et al., 2013. Optimized Negative-Staining Electron Microscopy for Lipoprotein Studies. *Biochimica et biophysica acta*, 1830(1), pp.2150–2159. Available at: <http://www.ncbi.nlm.nih.gov/pmc/articles/PMC3508368/>.
- Zhao, L. et al., 2017. Exosomes Derived from Human Pulmonary Artery Endothelial Cells Shift the Balance between Proliferation and Apoptosis of Smooth Muscle Cells. *Cardiology*, 137(1), pp.43–53.
- Zhavoronkov, A. & Bhullar, B., 2015. Classifying aging as a disease in the context of ICD-11. *Frontiers in Genetics*, 6(NOV), pp.1–8.
- Zhou, B.R. et al., 2013. Elevated miR-34c-5p mediates dermal fibroblast senescence by ultraviolet irradiation. *International Journal of Biological Sciences*, 9(7), pp.743–752.
- Zhou, Y. et al., 2013. Exosomes released by human umbilical cord mesenchymal stem cells protect against cisplatin-induced renal oxidative stress and apoptosis in vivo and in vitro. *Stem cell research & therapy*, 4(2), p.34.
- Zhu, Y. et al., 2016. Identification of a novel senolytic agent, navitoclax, targeting the Bcl-2 family of anti-apoptotic factors. *Aging Cell*, 15(3), pp.428–435.
- Zhu, Y. et al., 2017. New agents that target senescent cells: the flavone, fisetin, and the BCL-X_L inhibitors, A1331852 and A1155463. *Aging*, 9, pp.1–9. Available at: <http://www.ncbi.nlm.nih.gov/pubmed/28273655><http://www.aging-us.com/article/101202>.
- Zhu, Y. et al., 2017. Overexpression of miR-29b reduces collagen biosynthesis by inhibiting heat shock protein 47 during skin wound healing. *Translational Research*, 178, p.38–53.e6. Available at: <http://dx.doi.org/10.1016/j.trsl.2016.07.001>.
- Zhu, Y. et al., 2015. The Achilles' heel of senescent cells: From transcriptome to senolytic drugs. *Aging Cell*, (March), pp.644–658.
- Zomer, A. et al., 2015. In vivo imaging reveals extracellular vesicle-mediated phenocopying of metastatic behavior. *Cell*, 161(5), pp.1046–1057.
- Zomer, A. et al., 2016. Studying extracellular vesicle transfer by a Cre-loxP method. *Nature protocols*, 11(1), pp.87–101. Available at: <http://www.ncbi.nlm.nih.gov/pubmed/26658469>.
- Zouboulis, C.C. & Makrantonaki, E., 2011. Clinical aspects and molecular diagnostics of skin aging. *Clinics in Dermatology*, 29(1), pp.3–14. Available at: <http://dx.doi.org/10.1016/j.clindermatol.2010.07.001>.

8. Appendix A

8.1. Cells

Table 44 Overview of human dermal fibroblasts

Donor	Age of donor	Derived from	Approx. replicative lifespan (PD)
HDF161	65 years	abdominoplasty post liposuction - dermis	40
HDF85	49 years	abdominoplasty post liposuction - dermis	35
HDF76	58 years	abdominoplasty post liposuction - dermis	55

Table 45 Foreskin fibroblast used for optimization of transfections

	Age of donor	Derived from	Approx. replicative lifespan (PD)
fHDF166	< 10 years	foreskin	N/A

Table 46 Overview of primary keratinocytes

Donor	Age of donor	Derived from	Used for experiments before PD
'Lonza'	N/A	Adult epidermal tissue	< 6
'MedUni'	N/A	Adult epidermal tissue	< 6
50A	N/A	Adult epidermal tissue	< 6
37W	37	Adult epidermal tissue	< 6
	N/A	Adult epidermal tissue	< 6

8.2. List of Figures

Figure 1 Different building blocks involved in the terminal differentiation of keratinocytes.....	9
Figure 2 The desmosomes between two cells are formed.....	10
Figure 3 Adherens junction between adjacent cells.....	10
Figure 4 Hyper-adhesive Ca ²⁺ -independent	11
Figure 5 binding partners of IGF-BP. Adapted from (Beattie et al. 2006).....	18
Figure 6 miRNA biogenesis, secretory miRNAs and their regulatory functions from Turchinovich et al. 2012	25
Figure 7 Donor depended impact of paraquat-induced stress.....	38
Figure 8 Annexin-V/PI staining shows an i.....	38
Figure 9 Long term follow up of paraquat treated cells (HDF76) show a delayed response to the agent.	39
Figure 12 Vesicles from quiescent/contact inhibited control (Q) and SIPS	42
Figure 13 Representative image of negative stain preparations for Transmission electron microscopy.....	42
Figure 14 Images of contrast stain preparations for Transmission electron microscopy (TEM)	43
Figure 15 Representative Western blot image shows expression).....	43
Figure 16 Senescent cells secrete more small EVs per cell than Q cells.;	44
Figure 17 Quantity of secreted vesicular miRNAs	45
Figure 18 Monitoring of synthetic RNA-spike-ins confirms	45
Figure 19 (A) % of detected miRNAs and number of total miRNAs detected within the discovery study. In total 375 miRNAs were screened. miRNAs with an average Ct-value < 31, between 31 and 35, between 35 and 38, > 38 and not detectable are shown. (B) For statistical analysis, 353 miRNAs detected in both conditions were further analyzed. Averages from D7 and D21 are presented. 81% (285) of miRNAs were detectable in all 3 donors SIPS and Q control. 10% (37) of miRNAs were detected in at least 2 donors and 9% (30) of miRNAs were detected in one donor.....	46

Appendix A

Figure 20 Average differences i	46
Figure 21 Principal Component analysis of extracellular miRNAs from SIPS and Q control cells from	47
Figure 22 Bar chart of significantly higher secreted miRNAs).	48
Figure 23 Differences in size between Q and	49
Figure 24 Bar chart of the top 20 abundant and highly secreted miRNAs.	50
Figure 25 Secreted miRNAs regulate a dynamic crosstalk.....	51
Figure 26 Average raw Ct-values used for global mean normalization.	51
Figure 27 Changes in miRNA composition per vesicle.....	52
Figure 28 Venn diagram shows miRNAs more a.....	52
Figure 29 Venn diagram shows a balanced secretion o.	53
Figure 30 Scheme of experimental design.	53
Figure 31 Data quality control of cDNA library preparation.....	54
Figure 32 Total mapped reads of sequencing.'	55
Figure 33 Descriptive statics by Principal component analysis.	56
Figure 34 Volcano plot of differentially transcribed miRNAs.	56
Figure 35 Venn diagram shows significant miRNAs	56
Figure 36 Venn diagram of significantly higher	57
Figure 37 Correlation of intracellular and extracellular miRNAs	58
Figure 38 Venn diagram of top 16 retained (A) and secreted	58
Figure 39 Specifically SA- secreted (high values) or retained (low values).	59
Figure 40 $\Delta\Delta$ rank values were calculate from Δ rank values.....	59
Figure 41 $\Delta\Delta$ rank and $\Delta\Delta$ ratio were correlated and, s	60
Figure 42 corresponds to Figure 24A. Bar chart of the top 20 abundant a	60
Figure 43 Experimental setup of the EV-miRNA crosstalk.....	61
Figure 44 qPCR confirms transfer of cel-miR-39 e.....	61
Figure 45 Cel-miR-39 and scrambled control overexpressing HDF.....	62
Figure 46 qPCR confirms overexpression of cel-miR39 in HDF.....	62
Figure 47 Samples from HSE were harvested a	63
Figure 48 Agarose gel electrophoresis of qPCR products.	64
Figure 49 Washing and digestion solution	64
Figure 50 sEVs harvested from incubation	65
Figure 51 EVs from skin sections were	65
Figure 52 probably individual EVs between	66
Figure 53 MVB in the basal layer of epidermal cells.....	66
Figure 54 Fibroblasts in the dermal layer and keratinocytes in the epidermis	67
Figure 55 Left: MVB within fibroblasts that are secreted or taken up i	67
Figure 56 Immunogold labelling with TSG101 of skin sections.	68
Figure 57 Enhanced wound healing capacity	69
Figure 58 Enhanced wound healing capacity of primary NHEK after incubation.	70
Figure 59 Expression of involucrin in primary keratinocytes.....	71
Figure 60 MiR-23a-3p levels in NHEK after incubation	72
Figure 61 MiR-23a-3p overexpression in keratinocytes was confirmed.....	73
Figure 62 MiR-23a-3p overexpression accelerates wound closure in keratinocytes. row.	74
Figure 63 Involucrin expression	75
Figure 64 Differences in animal weight	76
Figure 65 growth advantage of knockout (-/-) miR-21	77
Figure 66 relative growth curves of littermates 251 and 253.	78
Figure 67 Relative growth curves of littermates 86 and 85.....	79
Figure 68 absolute growth curves of both littermates 251/253 and 86/85 after 6 hours 25 μ g/ml UV-PAPC.	79
Figure 69 Experimental setup to assess the stress resistance of wt and KO miR-21 tail keratinocytes.	80
Figure 70 Growth advantage of miR-21 knockout.....	81
Figure 71 Growth advantage of miR-21 knockout.....	82
Figure 72 Proliferative capacity of miR-21 knockout cells.....	83
Figure 73 Hypothesis on the role of the miR-SASP.....	92
Figure 74 ibidi® wound healing and migration assay format (A) and work-flow (B). Adapted from ibidi®	103

8.3. List of Tables

Table 1 Overview of RNA packaging mechanism into EVs (Gibbings <i>et al.</i> , 2009; Wang <i>et al.</i> , 2010; Villarroya-Beltri <i>et al.</i> , 2013; Koppers-Lalic <i>et al.</i> , 2014; Melo <i>et al.</i> , 2014; Jaé <i>et al.</i> , 2015; Iavello <i>et al.</i> , 2016; McKenzie <i>et al.</i> , 2016; Santangelo <i>et al.</i> , 2016; Shurtleff <i>et al.</i> , 2016).....	31
Table 2 Characteristics of fibroblast (HDF) cell strains: Confirmation of characteristics of cellular senescence after 7 (D7) and 21 days (D21) after the last H ₂ O ₂ application in cells of three donors.	41
Table 3 Summary of miRNA next generation sequencing (NGS) and data quality control.....	55
Table 4 Summary of 2 Way ANOVA after 24 hours stress treatments..	80
Table 5 Summary of 2 Way ANOVA after 6 hour stress treatment..	82
Table 6 Background and details to miR-21 knockout and wildtype from C57Bl/6J mice.	97
Table 7 Primary antibodies used	105
Table 8 Reaction mix of the High-Capacity cDNA Reverse Transcription kit.	106
Table 9 Thermal cycler temperature profile for reverse transcription.....	107
Table 10 ExiLent SYBR® Green master mix for miRNA based qPCR analysis.	107
Table 11 Temperature profile for the use of ExiLent SYBR® Green master mix in qPCR.	108
Table 12 5x HOT FIREPol™ EvaGreen™ qPCR Mix Plus (ROX) reaction components and respective amounts per reaction.	108
Table 13 Temperature profile for 5x HOT FIREPol™ EvaGreen™ qPCR Mix Plus (ROX) qPCR.....	108
Table 14 Summary and evaluation of secreted miRNAs by qPCR panel.....	112
Table 15 Customized qPCR panel for the screening of secretory miRNAs	113
Table 16 Significantly higher secreted miRNAs per cell from D7.....	120
Table 17 Significantly higher secreted miRNAs per cell from D21.....	124
Table 18 miRNAs significantly more abundant in SIPS on D7 rel. Q.....	130
Table 19 miRNAs significantly more abundant in SIPS on D21 rel. Q.....	130
Table 20 miRNAs significantly less abundant in SIPS on D7 rel. Q.....	130
Table 21 miRNAs significantly less abundant in SIPS on D21 rel. Q.....	130
Table 22 more abundant on D21 in Q rel. D7.....	131
Table 23 less abundant on D21 in Q rel. D7.....	131
Table 24 more abundant on D21 in SIPS rel. D7.....	132
Table 25 less abundant on D21 in SIPS rel. D7.....	132
Table 26 Differentially higher transcribed miRNAs of SIPS cells after 7 days post treatment (upregulated in SIPS)	132
Table 27 Differentially higher transcribed miRNAs after 21 days post stress treatment (upregulated in SIPS D21).....	133
Table 28 Differentially lower transcribed miRNAs after 7 days post stress treatment (downregulated in SIPS D7).....	135
Table 29 Differentially lower transcribed miRNAs after 21 days post stress treatment (downregulated in SIPS D21).....	136
Table 30 Differentially higher transcribed miRNAs in SIPS on day 21 post stress treatment rel. D7).....	137
Table 31 Differentially lower transcribed miRNAs in SIPS on day 21 post stress treatment rel. D7.....	137
Table 32 Differentially higher transcribed miRNAs in Q on day 21 post stress treatment rel. D7 (Up on D21 in Q rel. D7).....	137
Table 33 Differentially lower transcribed miRNAs in Q on day 21 post stress treatment rel. D7 (Down on D21 in Q rel. D7).....	137
Table 34 Top 20 most abundant miRNAs in cells of Q and SIPS	138
Table 35 Top 20 most abundant miRNAs in EVs of Q and SIPS	Fehler! Textmarke nicht definiert.
Table 36 Top 20 retained miRNAs in Q and SIPS as determined after calculating t	139
Table 37 Top 20 secreted miRNAs in Q and SIPS as determined after calculating the differences (Δranks).....	139
Table 38 Top selectively secreted miRNAs from SIPS cells after calculating the differences of the Δ ranks.....	140
Table 39 Top 20 selectively secreted miRNAs from SIPS cells as determined.....	Fehler! Textmarke nicht definiert.
Table 40 selectively secreted miRNAs out of the top20 from SIPS cells determined with ratio and rank method.....	141
Table 42 Top selectively retained miRNAs from SIPS cells after calculating the differences of the Δ ranks.....	Fehler! Textmarke nicht definiert.
Table 43 Top 20 selectively retained miRNAs from SIPS cells as determined	142
Table 44 selectively retained miRNAs out of the top 20 from SIPS cells determined with ratio and rank method	142
Table 45 Overview of human dermal fibroblasts	172
Table 46 Foreskin fibroblast used for optimization of transfections.....	172
Table 47 Overview of primary keratinocytes	172

8.4. Abbreviations

%	percent
α -SMA	α -smooth muscle actin
μ L	microlitre
μ M	micromolar
μ M	mikroliter
3'	three prime end
3D	three dimensional
5'	five prime end
6-4PP	(6–4) pyrimidine-pyrimidone photoproducts
8-oxoG	8-hydroxyguanine (8-oxo-7,8-dihydroguanine)
A	
A	adenine
ATP	Adenosine triphosphate
AGO	argonaut protein
AP-1	Activator protein
APAF-1	Apoptotic protease activating factor 1,
ARF-6	ADP-ribosylation factor 6
ATM	Ataxia telangiectasia mutated
AU	arbitrary units
B	
base pairs	bp
bp	base pair
BrdU	bromodeoxyuridine
C	
c	concentration
C.elegans	Caenorhabditis elegans
c/cm ²	cells per square centimeter
Ca ²⁺	calcium
CaCl ₂	calcium chloride
cancer associated fibroblasts	CAF
CCL	C-C motif chemokine
CCR4-NOT	C-C chemokine receptor type 4 -NOT transcription complex
CDK	cyclin-dependent kinases
CDKI	cyclin-dependent kinase inhibitor
CDKN1A	cyclin-dependent inhibitor 1A, p16 ^{INK4a}
CDKN2A	cyclin-dependent inhibitor 2A, p21 ^{CIP1}
cDNA	complementary DNA
CE	cornified envelope
cm ²	square centimeter
CO ₂	carbon dioxide
COX-2	cyclooxygenase-2
CPD	cylobutane pyrimidine dimers (CPDs)
Cq	quantification cycle
Ct	threshold cycle
ctrl	control
CXCL	C-X-C motif chemokine
D	
d	day
D21	day 7 after stress treatment/recovery
D7	day 7 after stress treatment/recovery

DDR	DNA damage response system (DDR)
DEJ	dermal epidermal junctions
DGCR8	DiGeorge syndrome critical region gene 8
DMEM	Dulbecco's modified eagle medium
DMSO	dimethylsulfoxid
DNA	deoxyribonucleic acid
dNTP	deoxynucleoside triphosphate
ds	double strand
Dsc	desmocollin
Dsg	desmoglein
E	
ECM	extracellular matrix
EDC	epidermal-differentiation complex
EDTA	ethylenediamine tetraacetic acid
EGTA	ethylene glycol-tetraacetic acid
EMT	epithelial to mesenchymal transition
ESCRT	<i>endosomal sorting complexes required for transport</i>
EV	extracellular vesicle
EV-miRNAs.	miRNA enclosed in extracellular vesicle
F	
FACS	fluorescence activated cell sorting
FC	fold change
FCS	fetal calf serum
FDR	false discovery rate
G	
g	gravitational acceleration
G	guanine
G1-phase	gap 1 phase of the cell cycle
GAPDH	glyceraldehyde-3-phosphate dehydrogenase
GTP	guanosine-5'-triphosphate
GTP	guanosine tri phosphate
H	
h	hour
H ₂ O ₂	hydrogen peroxide
HA	hyaluronic acid, hyaluronan
HAS2	hyaluronic acid synthase 2
HBBS	<i>Hank's Balanced Salt Solution</i>
HCl	hydrogen chloride
HDF	human dermal fibroblast
HDL	high-density lipoprotein
hpt	hours post transfection
HSE	human skin equivalents
I	
IGF	Insulin growth factor
IGF-BP	insulin growth factor binding proteins (IGF-BP).
IgG	immunoglobulin G
IL	Interleukin
ILV	intraluminal vesicles
iNOS	nitric oxide synthase
IPC	interplate calibrator
ISEV	international society for extracellular vesicles
JNK	Jun amino-terminal kinase
K	
K	keratin
kb	kilobase
KIF	keratin intermediate filament

KO	knockout
L	
LD	loading dye
lncRNAs	long noncoding RNA
M	
m	mass
MAPK	mitogen-activated protein <i>kinas</i>
MCR	mean-centering restricted
MEKK1	mitogen-activated protein kinases/ERK kinase-1
MEM	modified eagle medium
MHC	Major Histocompatibility Complex
min	minute
miRISC	microRNA RISC complex
miRNA	micro RNA
miRNP	micro-ribonucleoprotein complex
ml	millilitre
mM	millimolar
MMP	matrix metalloproteinases
mRNA	messenger RNA
MSC	<i>mesenchymal stem</i> cell-
mTOR	mammalian target of rapamycin
mtRNA	mitochondrial RNA
MVB	multivesicular body
MVE	multivesicular endosome
N	
n.s	not significant
NADPH	Nicotinamide adenine dinucleotide phosphate
NTA	nanoparticle tracking analysis
NaOH	sodium hydroxide
NER	nucleotide excision repair
nSmase	neutral sphingomyelinase
NGS	next generation sequencing
NFW	nuclease free water
NF- κ B	nuclear factor kappa-B
NHEK	normal human epidermal keratinocyte
nm	nanometer
nM	nanomolar
nmol	nanomol
NT	non-transfected control
nt	nucleotide
NTC	no template control
O	
O/N	overnight
P	
p	p-value
p16 ^{INK4a}	cyclin-dependent kinase inhibitor 2A
p21 ^{CIP1}	cyclin-dependent kinase inhibitor 1A
p53	cellular tumor antigen p53
PBMC	Peripheral Blood Mononuclear Cell
PBS	phosphate buffer saline
PCA	Principal component analysis
PCR	polymerase chain reaction
PD	population doubling
PDGF	platelet derived growth factor
pg	picogram

pH	potential hydrogenii
PI	propidium iodine
PKC- α	protein kinase C
PM	plasmamembrane
PPI	protein-protein interaction
PQ	paraquat
pre-miRs	precursor miRNA
pri-miR	primary miRNA
PRT	papillary to reticular transition
ps	post stress
PTEN	phosphatase tensin homologue
Q	
Q	quiescent
Q	quiescent/quiescence
qPCR	quantitative PCR
R	
RAF	rapidly accelerated fibrosarcoma
Ran	androgen receptor-associated protein 24
RAS	rat sarcoma
Rab	Ras-related in brain
Rb	retinoblastoma
RISC	RNA-induced silencing complex
RN3	ribonuclease type III (also: Drosha)
RNA	ribonucleic acid
RNAi	<i>RNA interference</i>
RNases	ribonuclease
ROS	reactive oxygen species
ROS	reactive oxygen species (ROS)
rpm	rounds per minute
rRNA	ribosomal RNA
RT	reverse transcription
RT	room temperature
RT-	no reverse transcriptase control
S	
S	senescent
S.	Stratumderm/stratum
SA EV-miRNA	senescence associated miRNA enclosed in extracellular vesicles
SAHF	senescence associated heterochromatin foci
SASP	senescence associated secretory phenotype
SASP	senescence-associated secretory phenotype
SA- β -gal	senescence associated β -galactosidase
SDS	sodium dodecylsulfate
sec	seconds
shRNA	short hairpin RNA
SIPS	stress induced premature senescence
siRNA	small interfering RNA
snoRNA	small nucleolar ribonucleic acid
snRNA	small non-coding RNA
S-Phase	synthesis phase of the cell cycle
sphingomyelinase	Smase
β -Gal	beta galactosidase
STAT3	<i>Signal transducer and activator of transcription 3</i>
stdev	standard deviation
SVD	singular value decomposition
T	
T	thymidine

Appendix A

TAE	Tris base, acetic acid, EDTA buffer
TAR	human immunodeficiency virus transactivating response
t-BHP	tert-Butyl hydroperoxide
TEM	transmission electron microscopy
TG	transglutaminase
TGF- β	transforming growth factor β
TNE	Tris base, natrium chloride, EDTA
TNF- α	tumor necrosis factor alpha
TPM	tags per million
TRBP	human immunodeficiency virus transactivating response RNA-binding protein
tRNA	transfer RNA
TSG101	tumour-susceptibility protein
U	
U	<i>enzyme unit</i>
UniSP	universal spike in
UTR	untranslated region
UV	Ultraviolet
V	
Volt	Volt
vRNA	vault RNA
Wt	wildtype
X -gal	5-bromo-4-chloro-3-indolyl- β -D-galactopyranoside

9. Appendix B Manuscripts

9.1. Accepted and published Manuscripts

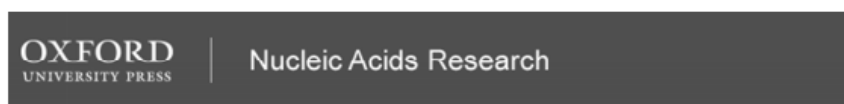
Khan A, Dellago H, **Terlecki-Zaniewicz** L, Karbiener M, Weilner S, Hildner F, Steininger V, Gabriel C, Mück C, Jansen-Dürr P, Hacopian A, Scheideler M, Grillari-Voglauer R, Schosserer M, Grillari J. SNEV^{hPrp19/hPso4} Regulates Adipogenesis of Human Adipose Stromal Cells. Stem Cell Reports. 2017 Jan 10;8(1):21-29. doi: 10.1016/j.stemcr.2016.12.001.

Song X, Narzt M, Nagelreiter IM, Hohensinner P, **Terlecki-Zaniewicz** L, Tschachler E, Grillari J, Gruber F. Autophagy deficient keratinocytes display increased DNA damage, senescence and aberrant lipid composition after oxidative stress in vitro and in vivo. Redox Biol. 2016 Dec 18;11:219-230. doi: 10.1016/j.redox.2016.12.015.

Dellago H, Preschitz-Kammerhofer B, **Terlecki-Zaniewicz** L, Schreiner C, Fortschegger K, Chang MW, Hackl M, Monteforte R, Kühnel H, Schosserer M, Gruber F, Tschachler E, Scheideler M, Grillari-Voglauer R, Grillari J, Wieser M. High levels of oncomiR-21 contribute to the senescence-induced growth arrest in normal human cells and its knock-down increases the replicative lifespan. Aging Cell. 2013 Jun;12(3):446-58. doi: 10.1111/accel.12069.

9.2. Submitted Manuscript

Nucleic Acids Research



Some supplementary files may need to be viewed online via your Referee Centre at <http://mc.manuscriptcentral.com/nar>.

Specifically packaged miRNAs in extracellular vesicles are novel members of the senescence-associated secretory phenotype

Journal:	<i>Nucleic Acids Research</i>
Manuscript ID	Draft
Manuscript Type:	1 Standard Manuscript
Key Words:	Cellular senescence, skin aging, extracellular vesicle (EV) packaging, microRNA (miRNA), senescence-associated secretory phenotype (SASP)

SCHOLARONE™
Manuscripts

Specifically packaged miRNAs in extracellular vesicles are novel members of the senescence-associated secretory phenotype

Lucia Terlecki-Zaniewicz^{1,2}, Ingo Lämmermann², Julie Latreille³, Madhusudhan Reddy Bobbili², Vera Pils^{1,2}, Markus Schosserer², Regina Weinmüllner^{1,2}, Susanna Skalicky⁹, Dietmar Pum¹⁰, Hanna Dellago⁹, Juan Carlos Higareda Almaraz^{5,6,7,8}, Marcel Scheideler^{5,6,7,8}, Frédérique Morizot³, Matthias Hackl⁹, Florian Gruber^{1,4}, Johannes Grillari^{1,2}

¹Christian Doppler Laboratory for Biotechnology of Skin Aging, Vienna, Austria

² Department of Biotechnology, University of Natural Resources and Life Sciences, Vienna, Austria

³ Department of Biology and Women Beauty, Chanel R&T, Pantin, France

⁴ Division for Biology and Pathobiology of the Skin, Department of Dermatology, Medical University of Vienna, Vienna, Austria

⁵ Institute for Diabetes and Cancer (IDC), Helmholtz Zentrum München, German Research Center for Environmental Health, Neuherberg, Germany

⁶ Joint Heidelberg-IDC Translational Diabetes Program, Heidelberg University Hospital, Heidelberg, Germany

⁷ Molecular Metabolic Control, Medical Faculty, Technical University Munich, Germany

⁸ German Center for Diabetes Research (DZD), Neuherberg, Germany

⁹TAmiRNA GmbH, Muthgasse 18, 1190 Vienna, Austria;

¹⁰ Department of Nanobiotechnology, University of Natural Resources and Life Sciences, Vienna, Austria

Address correspondence to:

Prof. Johannes Grillari

Department of Biotechnology

BOKU - University for Natural Resources and Applied Life Sciences Vienna

Muthgasse 18

A-1190 Vienna, Austria

Phone: +43-1-47654-79067

E-mail: johannes.grillari@boku.ac.at

short title: miRNAs are part of the SASP and selectively packed into EVs

Keywords

Cellular senescence, skin aging, extracellular vesicle (EV) packaging, exosomes, microRNA (miRNA), senescence-associated secretory phenotype (SASP)

Abstract

MiRNAs within extracellular vesicles (EV) participate in intercellular communication during normal, aged and diseased conditions. Here, we investigate whether EV-miRNAs from human dermal fibroblasts are part of the senescence-associated secretory phenotype (SASP) and if particular miRNAs are preferentially packaged into EVs in stress-induced premature senescence. A four-fold increased secretion of small EVs by senescent cells was observed and consequently an elevated abundance of more than 80% of all secreted miRNAs. Interestingly, the most highly secreted miRNAs collectively target five pro-apoptotic mediators, suggesting an anti-apoptotic activity of the SASP.

Differences in miRNA composition of EVs from senescent cells versus quiescent nontreated controls revealed increased abundance of two (miR-23a-5p, miR-137), and decrease abundance of five (miR-625-3p, miR-766-3p, miR-199b-5p, miR-381-3p, miR-17-3p) miRNAs. Furthermore, changes in EV-miRNA composition between early and late stages of senescence were observed, while not intracellularly, indicating a dynamic change of secretory activity with deep senescence. Finally, 24% of miRNAs were selectively secreted or retained in response to cellular senescence, indicating a specific, cell condition dependent packaging of miRNAs into EVs. Concluding, we suggest EV-miRNAs to be novel, *bona fide* members of the SASP that might contribute to the detrimental effects of accumulating senescent cells in tissues.

Abbreviations

HDF = human dermal fibroblasts

SIPS = stress-induced premature senescence

D7 = seven days post stress treatment = 1 week recovery

D21 = 21 days post stress treatment = 3 weeks recovery

PD = population doublings

EV = extracellular vesicles

sEV= small extracellular vesicles (< 220nm)

miRNAs = micro RNAs

sncRNAs = small noncoding RNAs

(s)EV-miRNAs = miRNAs enclosed in (small) extracellular vesicles

SASP = senescence-associated secretory phenotype

SA = senescence-associated

SA EV-miRNAs= senescence-associated miRNAs enclosed in extracellular vesicles

FCS = fetal calf serum

BrdU = bromodeoxyuridine

PI = propidium iodide

ISEV = international society for extracellular vesicles

NFW = nuclease free water

TSG101 = tumor susceptibility gene 101

GAPDH = glyceraldehyde 3-phosphate dehydrogenase

qPCR = quantitative real-time PCR

Cq = quantification cycle

SA- β -Gal = senescence-associated- β -galactosidase

TEM = transmission electron microscopy

NTA = nano particle tracking analysis,

NGS = next generation sequencing

TPM = tags per million

SVD = singular value decomposition

MCR = mean-centering restricted normalization

min = minutes

h = hours

Introduction

Cellular senescence has by now passed from being regarded as a mere cell culture phenomenon (1) to the conviction that senescent cells do indeed exist *in vivo* (2) at sites of age-associated diseases (3). Importantly their accumulation with age (2, 4–6) contributes to benign lesions, cardiovascular diseases (7, reviewed by 8), neurodegenerative disease (9, reviewed by 10), cutaneous conditions (11) and others. Contrary, their removal in transgenic mice (12) or by senolytics (13–18) Roos et al. 2016; Zhu et al. 2015) has a beneficial impact on the healthy lifespan (12) and leads to later onset of several age-associated diseases (20). Thus, strategies to remove senescent cells in humans are currently under investigation (reviewed by 19, reviewed by 20).

Cellular senescence can be triggered by various stimuli such as progressive telomere-shortening (23, 24), hyperoncogenic signaling (25), accumulation of DNA damage (reviewed by 26) or oxidative stress (27). All of them inducing an irreversible growth arrest mediated by the key cell cycle inhibitors CDKN1A and CDKN2A (28, reviewed by 29). In comparison to nontreated contact-inhibited quiescent cells in monolayers, senescent cells are not able to re-enter cell cycle at a later time point, although they remain metabolically active (reviewed by 30). Interestingly, senescent cells contribute to an imbalanced tissue metabolism by being more active than corresponding early passage or nonstressed cells (31–33). This metabolic switch is accompanied by loss of cell type specific functionality and partial de- or transdifferentiation (34, 35), loss of replicative potential required for tissue regeneration and the acquisition of a senescence-associated secretory phenotype (SASP) (reviewed by 36).

The SASP is characterized by the secretion of persistent growth factors, pro-inflammatory cytokines and chemokines (37, 38), as well as extracellular matrix (ECM) remodeling enzymes (39, 40). These SASP factors are considered to over-proportionally exert negative effects on tissue homeostasis and regeneration *in vivo* by acting in a paracrine manner on the neighboring cells and ECM (reviewed by 41, reviewed by 42). Attenuation of the negative effects of the SASP have been shown to restore the formation of functional human skin equivalents (Lämmermann et al., in preparation) and has been suggested as a putative target in preventing age-associated diseases and frailty (43) (reviewed by 44, reviewed by 45). Recently, extracellular vesicles (EVs) with their cargo have recently gained increasing interest, since they have been reported to act in a manner similar to hormones or cytokines during intercellular communication (reviewed by 46, reviewed by 47). In addition, EVs were reported to be increasingly secreted in response to various acute or chronic stress stimuli such as hypoxia (48), oxidative burden (49) diseases (50) or pathophysiological processes (51, 52). Three classes of EVs are currently discriminated based on their biogenesis, yet lacking clear biomarkers (53, 54). ‘Apoptotic bodies’ are released as blebs from apoptotic cells, whereas ‘shedding microvesicles’ or ‘ectosomes’ are produced by outward budding and pinching off from the plasma membrane. Both types appear very heterogeneous in size and shape and can differ between 50 nm – 1000 nm (reviewed by 55). Among the smallest EVs are ‘exosomes’. They are of endocytic origin and formed by inward budding of endosomal membranes, forming intraluminal vesicles (IVL) enclosed in multivesicular bodies (MVB) that are released upon fusion with the plasma membrane (reviewed by 56).

EVs are secreted by many, if not all cells, and by encapsulation of cytosolic cargo they transport mRNAs, lipids and non-coding RNAs, specifically miRNAs, over short or long distances (reviewed by 57, 58). When

taken up by recipient cells, the cargo is considered to be still active and to regulate the behavior of recipient cells (59, 60). Thus, transfer of EV-miRNAs adds another holistic regulatory function to the cell autonomous and non-autonomous trafficking and communication.

Together with others, we have postulated a role for miRNAs in cellular senescence and organismal aging (61–69) that was recently further extended to EV packaged miRNAs (68, reviewed by 70, reviewed by 71, 72) and proteins (73, 74) playing important roles during the process of aging. Thus the secretion of specific miRNAs enclosed in EVs and their impact on the senescent environment is of high interest (51, 72, 75, 76)

Therefore, here we investigate whether small EVs and their miRNA cargo (EV-miRNAs) are part of the SASP of senescent human dermal fibroblasts (HDFs). In addition, intracellular miRNA expression was used for correlation to extracellular miRNA abundance, as an indicator of selective packaging of miRNAs into EVs. We found around 24% of selectively secreted and specifically retained miRNAs in dependence of cellular senescence and evaluation of putative pathways, targeted by the most abundant secreted EV-miRNAs identified pro-apoptotic mediators. Taken together, our findings introduce small extracellular vesicles and EV-miRNAs to be *bona fide* members of the SASP, and therefore we suggest to use the term ‘miR-SASP’.

Materials and method

Cell culture

HDF isolated from adult skin of three healthy donors were provided by Evercyte GmbH. Cells were grown in DMEM/Ham's F-12 (1:1 mixture) (Biochrome GmbH, Berlin, Germany, F4815) supplemented with 10 % fetal calf serum (FCS) (Sigma Aldrich GmbH, St Louis, MO, USA, F7524) and 4 mM L-Glutamine (Sigma Aldrich GmbH St Louis, MO, USA, G7513) at 95% air humidity, 7% CO₂ and 37°C. HDFs were routinely passaged twice a week with a split ratio of 1:2. For induction of stress-induced premature senescence (SIPS) (77, 78), cells between population doublings (PD) 14 and PD26 were seeded with 3500 cells/cm² in culture flasks. They were chronically stressed with low doses of 100 µM H₂O₂ for one hour per day, according to the following scheme: 4 days treatment – 2 days recovery – 5 days treatment. After each treatment, media was exchanged to normal growth media. Media change of nontreated control cells was performed twice a week and cells reach quiescence (Q) by contact inhibition.

Seven (D7) and 21 days (D21) after the last stress treatment, bromodeoxyuridine (BrdU) incorporation, senescence associated (SA)-β-Gal staining, qPCR for the detection of CDKN1A (p21) and GAPDH and apoptosis assays were performed to confirm major hallmarks of cellular senescence (79, 80). On the same days, small extracellular vesicles (sEV) below 220 nm were harvested by differential centrifugation (81, 82). Intracellular and corresponding EV-RNA was isolated for small RNA next generation sequencing (NGS) and qPCR panels provided by Exiqon (Denmark) (FigS1A) (83).

Annexin-V/-PI staining

For staining of apoptotic cells, the Pacific Blue™ Annexin-V Kit (Biolegend, San Diego, CA, USA, 640918) was used. Cells and supernatants were harvested, pooled, centrifuged at 200 x g for 10 minutes (min) and pellets were washed twice with Annexin-V binding buffer (10 mM Hepes/NaOH pH 7.4, 140 mM NaCl, 5 mM CaCl₂). After centrifugation at 500 x g, the pellet was resuspended and incubated for 15 min in Annexin-V/PI staining solution (250 ng/mL propidium iodide PI, Sigma Aldrich GmbH, St Louis, MO, USA

P4864, 200 ng/mL Pacific Blue, diluted in Annexin-V binding buffer). The analysis was performed on a Gallios flow cytometer (Beckman coulter, Brea, CA, USA) using an excitation wavelength of 488 nm and a 600 nm emission filter for detection of PI (FL-3) and an excitation of 405 nm and a 450/50nm emission filter for Pacific-Blue-Annexin (FL-9). Cells treated with 300 nM Staurosporin for 24 hours were used as a positive control. Flow cytometry data were analyzed with Kaluza software (Beckman Coulter, Brea, CA, USA, Version 1.2).

BrdU incorporation

In order to verify growth arrest, cells were incubated for 24 hours with 10 μ M BrdU (Sigma Aldrich GmbH, St Louis, MO, USA, B5002). The cells were harvested by trypsinization, centrifuged at 170 x g for 5 min and the pellet was fixed with ice cold 70% ethanol for at least one hour at 4°C. Cells were permeabilized for 30 min with 2 M HCl and 1% Triton X-100 (Sigma Aldrich GmbH, St Louis, MO, USA, X100), followed by neutralization with 0.1 M Na-Borat, pH 8.5. Pellets were resuspended in TBS (0.5% Tween20, 1% BSA in 1 x PBS) containing anti-BrdU antibody 1:50 (BD Biosciences, USA, 347580) and incubated for 30 min. After washing with TBS and counterstaining with anti-mouse FITC-conjugated antibody 1:100 (Sigma Aldrich GmbH, St Louis, MO, USA F8264) for 30 minutes, the pellet was washed with TBS and resuspended in 1 x PBS with 2.5 μ g/ml PI (Sigma Aldrich GmbH, St Louis, MO, USA, P4864). For compensation, cells were stained with either PI or BrdU alone. The analysis was performed by flow cytometry (Gallios Beckman coulter, Brea, CA, USA), using an excitation wavelength of 488 nm and a 600 nm emission filter for detection of PI (FL-3) and a 535 nm filter for BrdU-FITC (FL-1). Proliferating cells were used as positive controls. Flow cytometry data were analyzed with Kaluza software (Beckman Coulter, Brea, CA, USA, Version 1.2).

Senescence associated (SA) β -Gal staining

SIPS HDF and sub-confluent HDF at the middle of their replicative lifespan were stained according to the standard protocol described by Dimri et al. 1995 (84). 15 pictures per well were taken at 100 x magnification and after randomization and blinding, SA- β -Gal positive and negative cells were counted.

Isolation of small extracellular vesicles (sEVs)

Isolation of sEV by differential centrifugation was performed according to standards recommended from the international society for extracellular vesicles (ISEV) and published by Hill et al. 2013 (85). Growth media containing fetal calf serum (FCS) was depleted of EVs by ultracentrifugation at 100,000 x g overnight, followed by filtration with 0.22 μ m filter cups (Millipore, Germany, SCGPU05RE). The cells were allowed to secrete in EV depleted media for 48 hour and the supernatant was then centrifuged for 15 minutes at 500 x g (Eppendorf, 5804R) to remove cellular debris. By a second centrifugation step at 14,000 x g (Beckmann, Coulter, Brea, CA, USA, Avanti JXN-26) for 15 minutes, large EVs were excluded by filtration using 0.22 μ m filter cups (Millipore, Germany, SCGPU05RE). Finally, on average 92 ml supernatant from SIPS and 75 ml supernatant from Q cells were filled into Quick-Seal, Polyallomer, 39ml, 25 x 89 mm tubes (Beckman, Brea, CA, USA, 342414). Small EVs were enriched using a 70Ti Rotor Beckman coulter at 100,000 x g for 90 min (Beckman, Brea, CA, USA, I8-80M) and pellets in different tubes but from the same samples were pooled. Dependent on the subsequent analysis, the pellet was either resuspended in QIAzol reagent (Qiagen) or in filtered 1 x PBS. For TEM freezing and thawing was avoided.

Nanoparticle tracking analysis

For determination of size and concentration of vesicles, the Zetaview system (Particle Metrix, Meerbusch, Germany) was used. After calibrating the system with 110 nm polystyrene standard beads (Particle Metrix, Meerbusch, Germany), vesicles were diluted in filtered 1 x PBS and three consecutive measurements were performed. For optimized performance, camera sensitivity was adjusted to fit the highest and lowest concentrated sample into the dynamic range and all samples were measured with the same dilution and settings. Settings: Gain 904, 98; Offset 0. Measurements were taken at two different camera positions. Particles secreted per cell were calculated using the cell number measured with an automated cell counter, Vi-CELL XR (Beckman Coulter, Brea, CA, USA). Categories of particle size determination was defined by the device. Categories below 15 nm, 15 nm, 45 nm, 105 nm, 135 nm, 165 nm, 195 nm and bigger than 225 nm are shown.

Electron microscopy

Vesicles for Transmission Electron microscopy (TEM) were freshly prepared. Solutions used for the staining procedure were pre-filtered using 0.22 µm filter units ((Millipore, Germany, SCGPU05RE). EVs were adhered on Athene Old 300 mesh copper grids (Agar Scientific, Stansted, Essex, UK) and fixed with 1% glutaraldehyde. After washing three times with nuclease free water (NFW), vesicles were stained for 5 minutes with 2% phosphotungstic acid hydrate (Carl Roth, Karlsruhe, Germany). The grids were left to dry and the specimens were visualized using TEM (FEI Tecnai T20, FEI Eindhoven, Netherlands) operated at 160 kV.

Protein quantification, western blot and antibodies

Vesicles and corresponding cells were lysed in 1 x TNE buffer (2 x TNE: 100 mM Tris/HCl, pH 8.0, 300 mM NaCl, 1 mM EDTA, 2 % Triton X-100) to quantify membrane markers of sEVs. Protein content of lysates was quantified with the Pierce® BCA Protein Assay Kit (Thermo Scientific, USA, 23227) according to manufacturer's recommendations. For SDS page and subsequent western blotting, samples were resuspended in SDS loading dye (4 x SDS loading dye: 240 mM Tris/HCl, pH 6.8, 8% SDS, 40% glycerol, 0.05% bromophenolblue, 5% β-Mercaptoethanol), sonicated and heated to 95°C. Then, samples were separated on a NuPAGE 4–12% Bis/Tris polyacrylamide gel (Invitrogen/Thermo Scientific, USA, 10472322) at 200 V. Subsequently, proteins were transferred to a PVDF membrane (Biorad, Hercules, CA, USA, 170-4156) in a BioRad SemiDry Blotting System at 1.3A 25V for 7 minutes. Membranes were incubated with antibodies targeting TSG101 1:2000 (Abcam, ab125011) and GAPDH 1:1000 (Pierce, MA5-15738). Proteins were detected using secondary antibodies for IRDye® 800CW Donkey anti-Rabbit IgG, 0.5 mg (LI-COR Biosciences, USA, 926-32213) and IRDye® 680RD Donkey anti-Mouse IgG, 0.5 mg (LI-COR Biosciences, USA, 926-68072) with a 1:10000 dilution using the Odyssey (LI-COR Biosciences, USA) infrared image system. All antibodies were diluted in 3% milk-powder dissolved in 1x PBS with 0.1% Tween-20 (Sigma Aldrich GmbH, St Louis, MO, USA, P2287).

RNA Isolation, Illumina small RNA library preparation and cDNA synthesis

Cell pellets and EV were lysed in QIAzol Reagent (Qiagen) and RNA was automatically extracted by miRNeasy Mini kit (Qiagen, 217004) based on QIAcube technology. Intracellular total RNA concentration and quality was controlled using Nanodrop spectrometer (ND-1000) and 2100 Bioanalyzer (Agilent) according to manufacturer's recommendations of the RNA-6000 Nano Kit. Average RNA concentration

as determined by Nanodrop and Bioanalyzer revealed an average concentration ($n = 6$) of $Q = 955 \text{ ng}/\mu\text{l}$ SIPS = $234 \text{ ng}/\mu\text{l}$ in a volume of $20 \mu\text{l}$, and RIN of intracellular RNAs was determined with 2100 Bioanalyzer yielding for $Q = 7.3$ SIPS = 7.5 .

Intracellular small RNA cDNA library for Illumina Sequencing was synthesized according to the manual provided by NEBNext® Small RNA Library Prep Set for Illumina® (Multiplex Compatible) (NEB, E7330S). From initially $1 \mu\text{g}$ of total RNA, small RNA fragments from approximately 18 – 36 nucleotides were gel purified on a 10% TBE Gel (Invitrogen/ Thermo Scientific, EC62752), quantified by 2100 Bioanalyzer (Agilent, Santa Clara, CA, USA) and equimolar amounts were pooled and sent to Exiqon (Denmark) for Illumina RNA-Seq (Fig. S4).

To monitor isolation efficiency of EV-RNA, spike -ins (UniSp2, UniSp4, UniSp5, Exiqon, Denmark, 203203) were added before RNA isolation. Then, equal volumes of EV-RNA were used for cDNA synthesis according to the protocol provided by Universal cDNA Synthesis Kit II (Exiqon, Denmark, 203301). Samples were supplemented and spiked with UniSp6 and cel-miR-39 (Exiqon, Denmark) to control for enzyme activity. cDNA was synthesized by 42°C for 60 min, followed by heat inactivation of enzyme for 5 min at 95°C .

For determination of the senescence markers CDKN1A, cDNA was synthesized from 500 ng of total RNA with the High-Capacity cDNA Reverse Transcription Kit including RNase inhibitor, according to manual provided by the manufacturer (Applied Biosystems, USA, 10400745) with the following conditions: 10 min 25°C , 120 min 37°C , 5 min 85°C .

CDNAs were stored at -20°C in low DNA binding tubes (Eppendorf, 30108051).

Quantitative Real Time PCR (qPCR)

MiRNA qPCR analyses were performed using ExiLent SYBR® Green master mix (Exiqon, Denmark, 203403) and LNA-enhanced miRNA primer (Exiqon, Denmark) on a LC 480 Real Time PCR system (Roche, Germany) according to the following cycling condition's: Activation: Cycles 1, Analysis Mode: None, 95°C , 10min, Ramp $4.4^\circ\text{C}/\text{s}$. Cycles: Cycles 45, Analysis Mode: Quantification 95°C , 10s, Ramp $4.4^\circ\text{C}/\text{s}$, 60°C , 60s, Acquisition Mode: Single, Ramp $1.6^\circ\text{C}/\text{s}$. Melting Curve: Cycles 1, Analysis Mode: Melting Curves, 95°C , 10s, Ramp $4.4^\circ\text{C}/\text{s}$; 55°C , 60s, Ramp $2.2^\circ\text{C}/\text{s}$; 99°C , Acquisition Mode: Continuous, Ramp $0.11^\circ\text{C}/\text{s}$, Acquisition per $^\circ\text{C}$: 5. Cooling: Cycles 1, Analysis Mode: None.

The second derivative method was used to calculate the cycle of quantification values (Cq-values). A preliminary screening for secreted miRNAs was conducted using two 384-well plates covering 752 human miRNAs (microRNA, Ready-to-Use PCR, Human panel I+II, V3.R, Exiqon, Denmark, 203612), with samples derived from one HDF donor in two conditions (SIPS and Q). Based on that, a customized qPCR panel was designed comprising 375 miRNAs and internal and negative controls (Supplemental Table S2.). Experiments were performed in biological triplicates in two conditions (Q and SIPS) and two timepoints (D7 and D21). In total, 12 qPCR panels were set up on three consecutive days. MiRNA analysis was performed according to the ddCT method.

QPCR for the determination of CDKN1A and GAPDH was performed with 5x HOT FIREPol® EvaGreen® qPCR Mix Plus with ROX (Medibena, Austria, SB_08-25-00020) using a Rotor-Gene Q cycler (Qiagen). Standard curves for determination of copy numbers was done in duplicates. Average expression values from quadruplicates were normalized to GAPDH as a reference gene and fold changes were calculated.

Negative controls tested as NFW only, and no template control derived from cDNA synthesis, were below detection limit of qPCR (> 40).

Primer used for qPCR:

Gene name	Sense primer	Anti-sense primer
GAPDH	CGACCACTTTGTCAAGCTCA	TGTGAGGAGGGGAGATTTCAG
CDKN1A (p21)	GGCGGCAGACCAGCATGACAGATT	GCAGGGGGCGGCCAGGGTAT

Illumina, miRNA next generation sequencing

The cDNA library pool was used to generate the clusters on the surface of a flowcell before sequencing with NextSeq 500 (Exiqon, Denmark). The collected reads were quality controlled, aligned and annotated to miRBase20 by Exiqon. Differential expression analysis was done using the R (version 3.2.2)/Bioconductor software package DESeq (86). Low expressed miRNAs were first excluded from the analysis (Tags Per Million (TPM) < 5 for all the samples). Then, the raw read counts were normalized using the DESeq normalization and a model based on negative binomial distribution and local regression was fitted for each miRNA. In the model, 'fibroblast cell strains' ($n = 3$) were defined as a 'block effect' and 'day' and 'condition' as factor of 2 levels. The Benjamini and Hochberg (BH) procedure (87) was applied to adjust the raw p-values into false discovery rate (FDR). A FDR < 0.05 was chosen as the cut-off value.

qPCR panel, analysis of EVs- miRNAs

Spike-ins were detected in all 384-well plates to monitor purification efficiency of RNA Isolation (UniSp2, UniSp4, UniSp5), the presence of enzyme inhibitors during cDNA synthesis (Unisp6 and cel-miR-39–3p) and equal processing of RT-qPCR amplification (interplate calibrator IPC - UniSp3). Additionally, NFW was used to determine background levels of each miRNA. Constant expression of all spike-ins was evaluated with a range calculated by the difference of the highest and lowest and interplate calibration was performed with GenEX 6.0. Cq-values were either normalized to total number of cells used for secretion or by the mean-centering restricted (MCR) normalization (88, 89), also known as the global mean normalization. Thereby, the mean Ct-value across all detected miRNAs of a single sample was subtracted from each individual miRNA. Differences in global mean are presented in Fig. S3A.

Both datasets were subjected to differential expression analysis with the R (version 3.2.2)/Bioconductor software package Limma (90). A linear model was applied for each miRNA and moderated t-tests were computed. In the model, fibroblast cell strains ($n = 3$) were defined as a 'block effect' and 'day' and 'condition' as factor of 2 levels. The raw p-values were corrected using BH method to control FDR.

Statistical analysis

Descriptive statistics were performed using ClustVis, a web tool for the preparation of principal component 2D-biplots and heatmap analysis based on multivariate datasets using different R packages (91). For all exploratory analyses, normalized Cq-values and TPM values were used. Principal component analysis (PCA) of 371 extracellular miRNAs (out of 375) was calculated by iteration of missing values with Nipals PCA and unit variance scaling was applied to rows. Heatmap preparation and hierarchical clustering of secreted miRNAs was performed by applying correlation distance and Ward linkage. Samples in columns are clustered using Euclidean distance and Ward linkage method.

PCA for intracellular miRNAs was done for 432 miRNAs with TPM > 5 in at least one donor. We used Singular Value Decomposition (SVD) for imputation and unit variance scaling was applied on TPM values. Expression matrix and hierarchical clustering of 432 intracellularly transcribed miRNAs was done by applying unit variance scaling and rows were clustered using Euclidean distance and Ward linkage. Columns are clustered using correlation distance and Ward linkage.

Correlation of intracellular and extracellular miRNAs

Only miRNAs, included in the customized qPCR panels for determination of extracellular miRNA abundance (375) were selected. Prior correlation of intracellular and extracellular miRNAs, quartiles from Cq-values and TPM values were calculated and miRNAs being low expressed (quartile 1 corresponds to the lowest 25% of data) in NGS and qPCR were excluded from analysis (330 miRNAs). Then miRNAs giving no signal in NGS experiment (TPM = 0) were excluded (291 miRNAs), and finally all miRNAs not present in all three donors and conditions were excluded. Therefore, correlation was done on 228 miRNAs. Rank from averages were calculated from SIPS and Q separately. Rank order was done according to intracellular TPM values to identify most abundant miRNAs transcribed intracellularly, or according to extracellular Cq-values, to discover most abundantly present miRNAs in EVs. By calculating $\Delta rank$ ($rank_{intra} - rank_{extra}$) from Q and SIPS separately, retained (negative value of $\Delta rank$) and secreted miRNAs (positive value of $\Delta rank$) were identified. By further calculating $\Delta\Delta rank$ ($\Delta rank_{SIPS} - \Delta rank_Q$) and the 25% and 75% percentiles, selectively higher secreted (high value of $\Delta\Delta rank$) or retained (low value of $\Delta\Delta rank$) miRNAs in SIPS were discovered. Next, we analyzed the same dataset with a different method to review our data, using the 'ratio-approach'. For a better visualization, Cq-values were transformed to arbitrary units, defining a Ct-value of 40 to '10' arbitrary units – assuming around 10 miRNA copies. $\Delta ratios$ were calculated from values $intra_{SIPS}/extra_{SIPS}$ and $intra_Q/extra_Q$ separately. Then $\Delta\Delta ratios$ from $\Delta ratios_{SIPS}/\Delta ratios_Q$ were calculated and normalized to the global mean of those ratios. Again, the 25% and 75% percentiles were calculated, and selectively higher secreted (high value of $\Delta\Delta ratio$) or retained (low value of $\Delta\Delta ratio$) miRNAs in SIPS were discovered. For Fig. 6D miRNAs were sorted according to $\Delta\Delta ratio$ values from smallest to largest values and they were plotted on y-axis, $\Delta\Delta rank$ values were then plotted in another diagram (Fig. 6E) in the same order as it was sorted before.

Pathway analysis of extracellular miRNAs

MiRWalk 'microRNA- gene target' tool (92) was used to find all validated targets for each of the 20 most highly abundantly secreted miRNAs. To evaluate the putative network on pathway level, enrichment analysis of pathway-based sets of the common regulated genes (targets) was performed using ConsensusPathDB (93), with the overrepresentation analysis tool. As input, HGNC symbol identifiers of our dataset were used and search was done against pathways with a minimal overlap of a p-value cutoff of 0.0001. Cytoscape (94) and the BisoGenet plug-in (95) was then used to generate a potential miRNA-regulated network using the list of validated targets and the modules obtained in the previous step. Crosstalk maps were created, linking curated pathways to metapathways where several pathways modules share a common set of genes.

Results

Senescent fibroblasts secrete more small extracellular vesicles than nontreated control cells

The senescence-associated secretory phenotype (SASP) is thought to be a crucial driver of age-associated diseases and thus an attractive target to alleviate age-related dysfunctions and to promote healthy aging. While the transient presence of senescent cells and their secretion of protein SASP factors have been shown to act beneficially on wound healing (96, 97), their chronic presence contributes to tissue remodeling and to an impaired homeostasis of the surrounding environment. In order to test if miRNAs enclosed in extracellular vesicles (EV-miRNAs) are part of the SASP of primary human dermal fibroblasts (HDF), stress-induced premature senescence (SIPS) was triggered by repeated low doses of H₂O₂ on nine days (77, 78). Major hallmarks of cellular senescence were confirmed in cells of three different HDF cell strains, at early (after one week/seven days post stress = D7) and late stages (after three weeks/21 days post stress = D21) of cellular senescence. Senescent cells acquired a flattened and enlarged morphology, while nontreated control cells reached quiescence (Q) by contact inhibition (Fig. S1B). Induction of cell cycle inhibitor CDKN1A (Fig. S1E), significantly increased activity of SA- β -Gal (Fig. 1A) and irreversible growth arrest (Fig. S1D) in senescent versus young cells confirmed SIPS in the early and fully developed senescent cells. In addition, no significant differences in the basal amount of apoptotic cells could be measured over time (Fig. S1C) and consequently we can exclude the presence of apoptotic bodies in the purified EV fractions. We summarized detailed data of the characteristics of all SIPS and nontreated control Q HDF cell strains in Table 1 and continued with the evaluation of the extracellular miRNA environment.

Protection and preservation of stability of extracellular miRNAs is guaranteed by either incorporation into high-density lipoprotein particles (98), binding to nucleophosmin (99) and Argonaut associated proteins (100), or they are enclosed in several types of extracellular vesicles (reviewed by 102). To reduce the source of extracellular miRNA carrier, supernatants of SIPS and Q control cells were filtrated and subsequently ultracentrifugated to enrich small EVs below 220 nm. Characterization was performed using nanoparticle tracking analysis (NTA), transmission electron microscopy (TEM) and immunoblotting. TEM confirmed the purification of small EVs surrounded by a visible lipid bilayer (Fig. 1B). Size distribution as assessed by NTA clearly showed the mere presence of small EVs below 220 nm (Fig. 1C) and revealed a median size (X50) between 65 to 80 nm in vesicles derived from Q and SIPS cells, each from two timepoints (Fig. 1D). In addition, we tested for the presence of TSG101, a known marker for exosome-like vesicles synthesized via the endosomal network and found it enriched in equally loaded samples of SIPS and Q cells (Fig. 1E). Presumably, these characteristics and the particular isolation procedure pointed towards exosome-like vesicles, hereinafter collectively called, small EVs (sEVs) that we further used for miRNA-profiling.

In order to determine differences in vesicle secretion between Q and SIPS cells, we quantified the amount of sEVs using NTA and found an elevated secretion of sEVs by 4 fold in all three donors from both timepoints tested (Fig. 1F). Considering the phenomenon of increased senescence-associated secretion of proteins summarized under the term SASP, our data strongly support the idea that sEVs are *bona fide* members of the SASP. We next decided to focus on their miRNA composition and to identify specific senescence-associated EV-miRNAs. EV-miRNAs are members of the senescence-associated secretory

phenotype (SASP) of primary human dermal fibroblasts – the ‘miR-SASP’. In order to identify the coverage of secreted EV-miRNAs, we first performed a preliminary screening covering 752 ubiquitously expressed miRNAs using qPCR panels with EV-RNA derived from SIPS and Q cells from one donor. In total, we detected 542 (72%) miRNAs giving signals above the detection limit (Fig. S2A, B). In order to include only reliably detectable miRNAs for further analysis, we selected 368 miRNAs with Cq-values below 38 in either condition. In addition, we included seven miRNAs detectable just in one condition, but with interesting publication records. Accordingly, we designed a customized qPCR panel comprising 375 miRNAs (Supplementary List S1). This set was used to quantify EV-miRNAs in HDF cell strains from three different donors in Q control and SIPS cells at two different timepoints (D7 and D21) after the last H₂O₂ treatment. Technical robustness was monitored using five synthetic spike-ins (Unisp2, Unisp4, Unisp5, Unisp6, cel-miR39) controlling for RNA extraction, cDNA synthesis, and qPCR efficiency. Additionally, each plate included two interplate calibrator (IPC) and a negative control. Signals of spike-ins and IPC revealed a robust signal within all 12 samples (Fig. S2C). From 375 miRNAs screened, 371 were detected under both conditions (Fig. 2A). Within this subset, 285 miRNAs were found in all three HDF cell strains under both conditions and at both timepoints, respectively (Fig. 2B). Due to the absence of a robust extracellular housekeeping miRNA, we used standardized secretion times and volumes for vesicle preparation and subsequent RNA isolation and normalized the data to the total viable cell number of each sample (see averages of Q and SIPS separately in Table S2). Senescence could be clearly distinguished from quiescence by multivariate statistics on the 371 EV-miRNAs present in all donors, as depicted by principal component analysis (PCA) in Fig. 2C and hierarchical clustering in Fig. 2D. Intriguingly, almost all miRNAs appear to be more secreted by SIPS compared to Q control cells as indicated by the heatmap (Fig. 2D). Statistical evaluation identified 221 (59%) miRNAs significantly higher secreted on day 7, and 321 (85%) on day 21, while none were found to be downregulated (Fig. 2E, F and Supplementary List S2). Altogether, these findings suggest miRNAs within in EVs as new members of the SASP. Thus, as already discussed (70, 71), but not experimentally validated before, we and others propose that secreted miRNAs are active components of the senescent secretome and that they might be able to influence the surrounding microenvironment in a similar manner as protein SASP factors. Therefore, we introduce the terms ‘miR-SASP’ and ‘senescence-associated EV-miRNAs (SA EV-miRNAs)’. The miR-SASP targets pro-apoptotic mediators as predicted by pathway analysis. Bearing in mind that senescent HDF do secrete high amounts of sEVs in comparison to nontreated cells, we were interested in the most abundant and highly secreted miRNAs, which we consider to have the highest functional impact on recipient cells when taken up. To obtain an unbiased view on the top 20 most abundantly secreted miRNAs (Fig. 3A), we screened for validated miRNA/mRNA target pairs and identified in total 11,588 interactions comprising in total 5,437 target genes (Supplementary List S3). To evaluate potential regulated pathways, enrichment analysis of all annotated interactions between miRNAs and genes, discovered 125 GO terms with an adjusted p-value below 0.0001, among those, 54 comprise more than 50% of all associated genes (Fig. 3B). Interestingly, we detected several gene modules that participate repeatedly in several pathways, indicating a crosstalk of pleiotropic genes involved in various cellular activities. In addition, we also observed series of cellular activities such as signaling, which use more than one gene module. Based on that finding, we built large metapathways (102–104) and identified a complex network that pinpoints to an

interplay between signaling, longevity and cancer pathways, which are supposed to be orchestrated by the secreted miRNAs and their target genes (Fig. 3C). Finally, we identified the prominent master regulators PTEN, P53, APAF-1, CDKN1B and MYC as putative targets of the top 20 secreted miRNAs involved in the dynamic crosstalk of all three cellular activities (Fig. 3C). Encountering only pro-apoptotic miRNA targets strengthens the hypothesis that the miR-SASP and EVs confer a protective function on target cells (105, 106) and miR-21-5p, highly secreted from senescent fibroblasts in our study, might be a key mediator of this process (107, 108). Changes in miRNA composition of SIPS-derived EVs reflect the dynamic progression of the SASP. We next addressed the question, if the miRNA composition per sEV changes after entry into SIPS (D7), as well as after senescence is fully established (D21). In order to achieve this, we normalized raw-Cq-values to the global mean of each sample, which we assume to reflect the average miRNA content of a sEV. Volcano plot of all analyzed miRNAs revealed a typical symmetric distribution showing 31 SA EV-miRNAs differentially present per sEV at an early timepoint of cellular senescence (Fig. 4A), and 32 when senescence was fully established (Fig. 4B). However, none of those reached the 0.05 cut-off value for the FDR of an adjusted p-value (Supplementary List S4) and we took only those into account that pass a p – value < 0.05 . Thus, we consistently found two SA EV-miRNAs (miR-23a-5p, miR-137) preferentially present per sEV at both timepoints (Fig. 4C) and five SA miRNAs (miR-17-3p, miR-625-3p, miR-766-3p, miR-199b-5p, miR-381-3p) that were less abundant per sEV at both, 7 and 21 days after SIPS treatment (Fig. 4D). To investigate if the composition of a vesicle changes between early and late timepoints of senescence, we evaluated differences between day 21 relative to day 7 in SIPS and Q separately. In total, we observed a balanced miRNA secretion over time between SIPS (6 miRNAs) and Q cells (6 miRNAs) (Fig. 4E). However, we found 14 miRNAs that were less abundant in SIPS derived vesicles on D21 relative to D7, while only three miRNAs were identified in Q cells (Fig. 4F). Taken together, these results indicate that senescent cells do not only secrete more miRNA containing sEVs as part of the SASP, but that they also differ in the miRNA composition per vesicle compared to nontreated control cells. Since differential secretion of miRNAs might be caused either by differential transcription, processing or packaging into EVs, we decided to quantify also the intracellular miRNA composition of all cell strains and conditions.

Analysis of intracellular miRNA transcription identifies a robust signature at early and late stages of cellular senescence

In order to quantify intracellular miRNA transcription of SIPS versus Q HDF, we performed small RNA next generation sequencing (NGS) using RNA extracted from the same cells at the same timepoints, as for the miRNA analysis of EVs (Fig. S1A).

RNA isolation and cDNA library preparation were quality controlled prior to NGS (Fig. S4 A, B, C). After adapter trimming and mapping, on average 17.6 million reads per sample were obtained (Fig. S4G, H). Identified miRNAs were annotated according to miRBase 20.0 and the dataset was evaluated (Table S4 and Fig. S4D, E, F), normalized to the number of total reads and 432 miRNAs that reached at least five tags per million (TPM) in one donor were included into the analysis.

Multivariate statistics by principal component analysis (PCA) separated samples derived from Q and SIPS cells by components 1 and 2, which account for 59% total variability (Fig. 5A). This result was further

confirmed by unsupervised hierarchical clustering, depicting two clearly separated clades for SIPS and Q cells (Fig. 5B).

Differentially transcribed miRNAs were identified (Supplementary List S5) and visualized by Volcano plot (Fig. 5 C, D). Comparison of up- (Fig. 5E) and downregulated (Fig. 5F) miRNAs from early and deep senescent HDF revealed senescence-associated miRNAs, which have also been identified earlier, either in senescent fibroblasts (63, 109–113) or in the dermis of elderly (Li et al. 2016) and thus point to a very robust miRNA signature of senescent dermal cells. Furthermore, in order to evaluate differences in miRNA transcription over time, we compared D21 relative to D7 and found only two miRNAs less transcribed in Q and SIPS cells (Fig. 5G), while none were significantly upregulated in both conditions (Fig. 5H).

We conclude that once senescence-signaling induces a specific intracellular miRNA pattern, it does not change significantly over time. Contrary, we observed significant changes in the miRNA composition of vesicles between early and late timepoints of SIPS (Fig. 2E, F and Fig. 4E, F).

Correlation of intracellular and extracellular miRNAs identifies specifically secreted and retained miRNAs in cellular senescence

Next, we addressed whether all miRNAs with high transcriptional abundance are also highly abundant in sEVs. Similarly, we tested if physiological stimuli, such as the induction of cellular senescence modulates the selective secretion or retention of specific miRNAs. Thus, we correlated the intracellular NGS dataset with the extracellular qPCR data by including only miRNAs present in both conditions and timepoints (228 miRNAs, Q = 6, SIPS = 6, see Material and Methods for filtering criteria). To group the most abundant miRNAs present in sEVs or in cells, they were ranked from the lowest to their highest abundance and the top 20 miRNAs respectively, were then compared and visualized by Venn diagrams (Fig. 6A, B and Supplementary List S6). Thereby, we identified 26.5% matching miRNAs and it became clear that particular miRNAs are indeed selectively secreted or retained in the two conditions (Fig. 6C).

In order to identify those miRNAs that are differentially present, we calculated the differences of ranks ($\Delta rank = rank_{intra} - rank_{extra}$) for Q and SIPS separately (Supplementary List S6 and Fig. S5A, B). Further calculation of $\Delta\Delta rank (\Delta rank_{SIPS} - \Delta rank_Q)$ of SIPS versus Q, allowed us to identify specifically packaged SA-EV-miRNAs in dependence on the senescence stimulus, whereby the higher the value, the higher is the selective secretion, and vice versa, the lower the value, the likelihood grows for retention (Supplementary List S6 and Fig. S5C).

In order to compare the $\Delta\Delta rank$ results to a statistical analysis based on the quantitative content of qPCR and NGS and not on the rank, we also calculated ratios between extracellular and intracellular miRNA levels from quiescent ($\Delta ratio_Q$) and SIPS ($\Delta ratio_{SIPS}$), respectively. Therefore, we transformed Cq-values to arbitrary units, by defining a Ct-value of 40 to 10 arbitrary units (AU). We then calculated $\Delta\Delta ratios (\Delta ratio_{SIPS} / \Delta ratio_Q)$ and normalized obtained values to the global means (Fig. S5C). Consequently, the result was then correlated with $\Delta\Delta rank$ values and plotted in a xy-diagram, revealing ~80% of total variability as determined by Spearman correlation (Fig. 6D) (Spearman R = 0.81 95% confidence interval 0.76 to 0.85 p-value (two-tailed) < 0.0001). Indeed, comparison of the top 20 from the $\Delta\Delta rank$ and the $\Delta\Delta ratio$ - approach confirmed a similar range of selectively secreted (Fig. 6D) or retained miRNAs after entry into cellular senescence. However, some miRNAs were only detected with one of the

two methods (Fig. 6F). Finally, we identified about 24% of the total EV contained miRNAs to be selectively packaged or retained in response to senescence, as defined by a cut-off of the 25% and 75% percentiles from both approaches, while the remaining ones seem to be evenly distributed between cells and EVs. To sum up, the 'ratio-' and 'rank-' approach allowed the correlation of extracellular and intracellular data independently and disclosed a set of specific miRNAs associated for retention or secretion in response to SIPS. Whether the highly abundantly secreted miRNAs (Fig. 3 A and Fig. 6 B) are the ones that confer a biological effect on recipient cells, or if the selectively secreted miRNAs are those to regulate the signaling during the miR-SASP, remains to be elucidated.

Discussion

Accumulation of senescent cells is considered to drive several age-associated diseases. One of the characteristic of senescent cells that is considered to contribute to this phenomenon, is the cumulative secretion of several proteins involved in inflammation, growth promoting signaling (37) and extracellular matrix remodeling (39, 40), which is generally summarized under the term SASP (reviewed by 115). With increasing numbers of reports on secretory miRNAs describing their almost 'hormonal' action on recipient cells (115) and their potential as biomarkers (116) or therapeutic targets for age-associated diseases (reviewed by 118, reviewed by 119), the question emanates whether secreted miRNAs, especially those enclosed in EVs, might also be part of the SASP.

Therefore, we focused on the vesicular environment of senescent human dermal fibroblast and discovered a 4-fold higher secretion of small EVs compared to nontreated control cells. This observation is in line with a reported increase in EV secretion in replicative senescent fibroblasts, as well as in irradiation-induced senescent prostate cancer cells (51), which might be mediated by p53 activation in response to DNA damage (119). Such an increase of EVs has also been observed in tissues of atherosclerotic aortas (115), where senescent endothelial and vascular smooth muscle cells are known to accumulate (3, 12). Similarly, EV increase in cerebrospinal fluid of Alzheimer's disease patients was found (121), where also senescent astrocytes were reported to contribute to the SASP (9). It is therefore intriguing to speculate that senescent cells might also secrete more EVs *in vivo*.

As a consequence of elevated small EV secretion, we found in senescent fibroblasts an increased abundance of almost all EV-miRNAs compared to nontreated control cells. The most abundantly secreted miRNAs, seem to target pro-apoptotic mediators involved in longevity, nutrient sensing pathways and cancer signaling, thereby conferring protective functions on their environment, as recently suggested (49, 105, 122, 123).

In addition, we identified differences in miRNA composition per sEVs from senescent versus control cells, whereby miR-23a-5p and miR-137 were more abundant, while five miRNAs, including miR-17-3p and miR-199b-5p, were less abundant per vesicle from senescent cells. Several of these miRNAs were found to be regulated intracellularly in the same manner. While miR-23a-5p is also upregulated in senescence induced by PUVA treatment (124), miR-137 was induced in senescent fibroblasts (125) and keratinocytes (126). MiRNA-17-3p is also commonly downregulated in several models of replicative and organismal aging (62, reviewed by 128), as well as miR-199b-5p in skin of elderly (62) and in senescence of mesenchymal stem cells (128).

Comparing intracellular miRNA transcription of senescent versus quiescent fibroblasts, we confirmed several miRNAs that were reported as differentially expressed in replicative or UVB induced senescence of fibroblasts (63, 109–113). Several of these are also found in the dermis of elderly (65), where estimates from a non-human primate study suggest up to 20% of cells to be senescent (2). In addition, several miRNAs were identified so far not yet described in fibroblast senescence, such as miR-1197 and miR-450-2-3p.

Furthermore, we addressed here, whether, specific EV-miRNA packaging is influenced by changes in cell physiology. So far it is known that some miRNAs are selectively packaged into EVs depending on the cell

type (129–137), but only one study has compared miRNA packaging in isogenic cell lines differing in KRAS mutation status (138). However, no reports exist that cover changes due to external stimuli including induction of senescence. Therefore, we correlated intra- versus extracellular miRNA levels. Overall, most miRNAs are as abundant intracellularly as extracellularly, suggesting that for the majority of miRNAs the extracellular environment seems to mirror the cytoplasm. However, we also provide evidence that around 24% of all miRNAs included in the correlation approaches, are selectively packaged into small EVs in response to cellular senescence, while the remaining ones are evenly distributed between cells and EVs. This finding supports the idea that some miRNAs are sorted into EVs in a selective and regulated manner and is in line with several reports showing an active mechanism of miRNA packaging into exosomes (60, 130–133, 136, 138–140). Several factors contributing to a selective packaging have been reported so far: (i) It can be orchestrated by sumoylation on ribonucleoproteins (141) and their binding to specific sequence motifs (141), often with non-template terminal nucleotide additions rich in 3' uridylation (142). (ii) It can be directed by Y-box proteins (143) or (iii) the phosphorylation of Ago2, a component of the RNA-induced silencing complex (RISC) (144). Furthermore, (iv) a miRNA sequence independent mechanism guided by distinct (v) ribonucleoproteins relevant for RNA stability and transport (145) and (vi) accessory proteins involved in biogenesis of multivesicular bodies such as Alix (146) and neural sphingomyelinase 2 (nSMase2) (147) have been described as necessary for specific miRNA loading. Finally, (v) even miRNAs as endogenous stimuli can influence specific loading, as has been shown by overexpression of miR-146a-5p in HEK293 cells, which resulted in enrichment of several EV-miRNAs, while others remained constant (130). However, if this mechanism is dependent and directed by downstream target regulations or on transcriptional level has not been addressed.

To date, specific EV packaging of selected miRNAs is still a matter of debate and a passive form of garbage disposal as an alternative way of bulk miRNA degradation has also been suggested (discussed in 149). Still, our data in addition to the many changes in recipient cell behavior after EV mediated uptake of miRNAs (58–60, 75, reviewed by 149, 150) would support the idea of a specifically regulated packaging mechanism.

Which miRNAs are now selectively secreted and thus able to send distinct messages to their environment? What effect on the microenvironment might such specifically packaged miRNAs have?

One prominent example to address these questions is miR-15b-5p, which we identified here to be selectively packaged and secreted by senescent cells. Intracellularly, we found miR-15b-5p to be downregulated in senescence as it was reported before (151). The fact that it is preferential packaged and secreted in senescence might be an additional mechanism to keep miR-15b-5p levels low within fibroblasts. Decrease of miR-15b-5p de-represses SIRT4, which has a regulatory role in stress-induced senescence-associated mitochondrial dysfunction (151) and in driving a NF- κ B mediated induction of the SASP (152). This is consistent with our data, where we see an induction of NF- κ B signaling in SIPS cells, as determined by biostatistical pathway analysis and in addition, the de-repression of known SASP components such as IL-8 (CXCL8), MCP-1 (CCL2), RANTES (CCL5), GRO α (CXCL1), INHBA (Lämmermann et al. in preparation). Specifically, miR-15b-5p seems to confer a crucial fine-tuning mechanism, similar to the 'inflamma-miR' miR-146a/b (153, 154), by dampening excessive secretion and

transcription of SASP components (155). In accordance to these *in vitro* data, miR-15b-5p was also found to be down-regulated *in vivo* in photo aged and non-photo aged skin (151). Interestingly, it is lowly abundant in the dermis of skin biopsies derived from young individuals and elderly, while it appears highly enriched in the epidermis (151). Thus, it is tempting to speculate that the low dermal levels versus high epidermal levels are caused by an EV-miRNA crosstalk between fibroblast vesicles and keratinocytes. Such miRNA dependent crosstalk has also been described between senescent endothelial cells and mesenchymal stem cells (75) and thus strengthening our speculation.

Additionally, miR-17-3p, a member of the miR-17-92 cluster, described as oncogene as well as a factor modulating the life span of mice (reviewed by 156) is preferentially retained by senescent cells, but not in quiescent. The same is true for miR-199b-5p, which was also found significantly down regulated intracellularly in senescent cells (157), less abundant per vesicle from senescent cells, and selectively retained in SIPS.

Interestingly, several miRNAs including miR-122-5p (158, 159), miR-21-3p (160), miR-376a-5p (161), miR-378b which is highly similar to miR-378a-3p (162) and miR-17-3p (163) are connected to keratinocyte differentiation and/or proliferation, suggesting that senescent fibroblasts might impact on epidermal function.

Taken together, we conclude that miRNAs are specifically packaged depending on cellular conditions and/or external stimuli. The specific molecular mechanism of selective release and retention of senescence-associated EV-miRNAs and the miR-SASP crosstalk between different cell types and its consequences in the context of aging and age-associated diseases, however, remains largely to be discovered. Finally, we suggest that small EVs and EV-miRNAs are novel, *bona fide* members of the SASP, for which we suggest to use the term 'miR-SASP'.

Accession Number

miRNA NGS data from differentially transcribed miRNAs in stress-induced premature senescence (SIPS) have been deposited to the GEO repository under the accession number GSE95354 <https://www.ncbi.nlm.nih.gov/geo/query/acc.cgi?token=ytojsgmknpgbtix&acc=GSE95354>

Supplementary Data

Supplementary Data are available at NAR online.

Fig. S1 Stress-induced premature senescence (SIPS) in fibroblasts mirrors hallmarks of cellular senescence

Fig. S2 Statistics of preliminary screening and the quality control of final screening

Fig. S3 Quantification of global mean from Q and SIPS HDF

Fig. S4 Data quality control of cDNA library preparation and NGS carried out by Exiqon

Fig. S5 Correlation of intracellular and extracellular miRNAs

Supplementary Lists in one Excel spreadsheet 2017_Terlecki_HDF_H2O2_SIPS_Supplementary_Lists

S1 S1_customized_QPCR_panel

S2_Secreted_per_cell

S3_pathway_miRNA_gene_interact

S4__secreted_per_vesicle_MCR

S5_Intracellular

S6_Correlation_Top20

Funding

This work was funded by the Christian Doppler Society. The financial support by the Austrian Federal Ministry of Economy, Family and Youth; the National Foundation for Research, Technology and Development is also gratefully acknowledged, as is funding by the Austrian Science Fund (FWF: I2514 to JG). In addition, we gratefully acknowledge the FP7 EU projects Frailomics and Sybil and FWF RiboDACH.

Conflict of interest

MH and JG, are co-founders of TAmiRNA GmbH. JG is co-founder of Evercyte GmbH. FM and JL are employees of Chanel Research and Technology.

Acknowledgements

We wish to thank Sylvia Weilner, Severin Mühleder and Jacqueline Friedmann for technical support and helpful advices, Selma Osmanagic-Myers for reading the manuscript critically, as well as Matthias Mattanovich and Jennifer Schwestka for experimental support.

Author contributions

LTZ, JG, FG, FM: planned the study; LTZ, JG, IL and FG: designed experiments, interpreted the results. LTZ, JG: prepared and wrote the manuscript, designed the figures. LTZ, JL: performed bioinformatics and statistics. LTZ, MRB, VP, RW performed experiments. MScho, HD: contributed to planning of experiments and interpreted the data. SK, MH: contributed to cDNA library preparation and qPCR analysis. JCHA, MSche: performed pathway analysis and prepared the figures. DP: performed electron microscopy. JG and MScho supervised the writing of the manuscript. All authors read, edited and approved the final manuscript

9.3. Submitted Manuscript – Co-author

Blocking negative effects of senescence in human skin fibroblasts with a plant extract

Ingo Lämmermann^{1,2}, Lucia Terlecki-Zaniewicz^{1,2}, Regina Weinmüllner^{1,2}, Markus Schosserer², Hanna Dellago^{1,2}, André Dargen de Matos Branco^{1,2}, Dominik Autheried^{1,2}, Benjamin Sevcnikar^{1,2}, Lisa Kleissl^{1,2}, Irina Berlin³, Frédérique Morizot³, Francois Lejeune³, Nicola Fuzzati⁴, Sandra Forestier⁴, Alix Toribio⁴, Anaïs Tromeur⁴, Lionel Weinberg⁴, Juan Carlos Higareda Almaraz^{5,6,7,8}, Marcel Scheideler^{5,6,7,8}, Marion Rietveld⁹, Abdoel El Ghalbzouri⁹, Erwin Tschachler¹⁰, Florian Gruber^{1,10} and Johannes Grillari¹

1 Christian Doppler Laboratory for Biotechnology of Skin Aging, Vienna, Austria

2 Department of Biotechnology, University of Natural Resources and Life Sciences, Vienna, Austria

3 Department of Biology and Women Beauty, Chanel R&T, Pantin, France

4 Actives Department, Chanel R&T, Pantin, France

5 Institute for Diabetes and Cancer (IDC), Helmholtz Zentrum München, German Research Center for Environmental Health, Neuherberg, Germany

6 Joint Heidelberg-IDC Translational Diabetes Program, Heidelberg University Hospital, Heidelberg, Germany

7 Molecular Metabolic Control, Medical Faculty, Technical University Munich, Germany

8 German Center for Diabetes Research (DZD), Neuherberg, Germany

9 Department of Dermatology, Leiden University Medical Centre, Leiden, The Netherlands

10 Division for Biology and Pathobiology of the Skin, Department of Dermatology, Medical University of Vienna, Vienna, Austria

Abbreviations

ECM (extracellular matrix)

HDF (human dermal fibroblast)

HSE (human skin equivalent)

PBMC (peripheral blood mononuclear cell)

PD (population doubling)

PRT (papillary to reticular transition)

RPT (reticular to papillary transition)

SA- β -gal (senescence-associated β -galactosidase)

SASP (senescence-associated secretory phenotype)

SIPS (stress-induced premature senescence)

Keywords

Skin aging, senescence, senescence-associated secretory phenotype, senolytic, plant extract, *Solidago virgaurea*, papillary fibroblast, reticular fibroblast, papillary to reticular transition, reticular to papillary transition, SNEV, PRPF19, PSO4

ABSTRACT

There is increasing evidence, that senescent cells are a driving force behind many age-related pathologies and that their selective elimination increases the life- and healthspan of mice. Senescent cells negatively affect their surrounding tissue by losing their cell specific functionality and by secreting a pro-tumorigenic and pro-inflammatory mixture of growth hormones, chemokines, cytokines and proteases, termed the senescence-associated secretory phenotype (SASP). Here we identified an extract from the plant *Solidago virgaurea* subsp. *alpestris*, which exhibited weak senolytic activity, delayed the acquisition of a senescent phenotype and induced a papillary phenotype with improved functionality in human dermal fibroblasts. When administered to stress-induced premature senescent fibroblasts, this extract changed their global mRNA expression profile and particularly reduced the expression of various SASP components, thereby ameliorating the negative influence on nearby cells. Thus, the investigated plant extract represents a promising possibility to block age-related loss of tissue functionality.

INTRODUCTION

Cellular senescence was long hypothesised to be involved in the development of age-related diseases and the loss of tissue functionality with age [1,2]. Senescent cells indeed accumulate in vivo and their selective elimination has been shown to increase the healthspan of mice and to decrease various age-related pathologies [3–11]. Although senescence is a tumour suppressive mechanism and the transient presence of senescent cells has beneficial functions in wound healing [12,13], they are considered to negatively affect the surrounding tissue by secreting pro-inflammatory cytokines and chemokines, extracellular matrix (ECM) remodelling proteases and growth factors as soon as they chronically accumulate within the tissues. This so-called senescence-associated secretory phenotype (SASP) creates a chronically inflamed, pro-tumorigenic environment and is able to induce senescence in a paracrine manner resulting in a vicious cycle of progressive functional loss in tissues and organs [14–18]. Senescent cells are characterised by an irreversible cell-cycle arrest induced via the p53-p21CIP1 or the p16INK4a-Rb axis, the accumulation of senescence-associated β -galactosidase (SA- β -gal) and the acquisition of a flattened and enlarged cell morphology [19]. One of the first organs where senescent cells have been identified in vivo, is the skin [20], which contains up to 20% senescent fibroblasts in elderly primates [21,22].

The dermis of human skin can be divided into two distinct layers, the upper papillary dermis and the lower reticular dermis. Fibroblasts isolated from the papillary dermis have a lean spindle-like morphology, a higher proliferative capacity and a lower sensitivity towards contact inhibition than their flat and irregular-shaped reticular counterparts [23]. They also differ in the production of ECM and growth factors [23,24], their response to growth factors and epidermal signalling [25,26] and only papillary fibroblasts seem to be able to support the formation of a fully differentiated human skin equivalent (HSE) [27,28]. When aged in vitro or in vivo, changes in cell characteristics are almost exclusively seen in papillary fibroblasts, which led to the hypothesis that ageing of human skin fibroblasts might involve a gradual de- or trans-differentiation process of the papillary to the reticular phenotype [27,28]. We suggest to term this process “papillary to reticular transition” (PRT). It seems that the PRT is accompanying serial passaging in vitro, since fibroblasts approaching senescence do resemble the reticular phenotype [28].

In order to avoid the negative effects of cellular senescence, three strategies have been proposed: (i) to delay the acquisition of a senescent cell phenotype and the loss of cell type specific functionality mediated by de- or trans-differentiation (like by PRT), (ii) to attenuate the negative effects of the senescent phenotype once it is established and (iii) to selectively eliminate senescent cells with senolytic substances [29].

Indeed, several clinically approved drugs including glucocorticoids, metformin, rapamycin and JAK inhibitors have been postulated to attenuate the SASP [30–33] and thus the negative effects of senescence. In addition, the quest for substances with senolytic properties resulted in the identification of quercetin, dasatinib, navitoclax and piperlongumine [4,6,9,10,34] with promising impact on the removal of senescent cells in vivo.

Here we report, to our knowledge, the first plant extract, an alcoholic extract of *Solidago alpestris* (1201), with the ability to block on one hand the negative effects of senescence in human skin fibroblasts and on the other hand to block PRT in vitro to maintain a functional papillary phenotype of fibroblasts.

RESULTS

Long-term treatment with 1201 slightly delays replicative senescence and maintains a papillary-like morphology of human dermal fibroblasts (HDF)

To investigate the consequences of long-term exposure to 1201, we cultivated HDF from population doubling (PD) 32 onwards in the presence of 1201, during which RNA samples and cell counts were taken at regular intervals. When treated with 1201, the cells retained a papillary-like morphology and a cell density comparable to replicatively young cells for up to 160 days in culture, whereas the control cells were only able to retain a papillary-like morphology until day 95 (Fig. 1a and S1 Fig.). In addition, 1201 slightly extended the replicative lifespan of the cells by 11% before they entered senescence (Fig. 1b).

Figure 1 1201 delays the acquisition of a senescent phenotype. (a) HDF were cultivated with growth medium supplemented with 1201 from day 71 (PD 32) of the replicative lifespan experiment onwards. Control cells were cultivated with normal growth medium. Microscopic pictures were taken at 100 x magnification. Scale bar, 100 μ m. (b) Growth curve of the replicative lifespan experiment. At the end of the replicative lifespan the cell number was determined at regular intervals and population doublings were adjusted to compensate for decreasing cell density. (c) At regular intervals during the lifespan experiment RNA samples were prepared and the transcript levels of the senescence markers p21 and SNEV were determined with RT-qPCR. Expression levels of replicatively young (PD 11.5) control cells were set to 1. (d) At regular intervals during the lifespan experiment RNA samples were prepared and the transcript levels of markers for the papillary phenotype were determined with RT-qPCR. Expression levels of replicatively young (PD 11.5) control cells were set to 1. (e) At regular intervals during the lifespan experiment RNA samples were prepared and the transcript levels of markers for the reticular phenotype were determined with RT-qPCR. Expression levels of replicatively young (PD 11.5) control cells were set to 1. Data represents one experiment.

To test the hypothesis that PRT and the aging process are indeed related, we compared the expression of mRNA markers for papillary/reticular fibroblasts [35] with a marker for early passage cells, SNEV (PRPF19) [36], as well as for cellular senescence, p21 (CDKN1A). We observed a similar expression pattern for p21 and the reticular markers with a marked increase at the end of the replicative lifespan, which was prevented by treatment with 1201 (Fig.

1c,e). Moreover, treatment with 1201 resulted in a modest increase of SNEV throughout the lifespan except for the last time point at day 172 (Fig. 1c). In line with the observed morphology of the cells, the papillary markers, podoplanin (PDPN) and netrin-1 (NTN1), were increased in cells treated with 1201 compared to the respective control throughout the replicative life span, except for the last time point on day 172 where the treated cells started to display a reticular phenotype (Fig. 1d and S1 Fig.). On the other hand, the reticular markers, protein phosphatase 1 regulatory subunit 14A (PPP1R14A) and alpha-2-macroglobulin (A2M), were decreased in the treated cells at all time points, except for the first time point at day 94, where the changes in morphology were not yet obvious (Fig. 1a,e).

1201 reverses PRT

In order to confirm that 1201 reverts PRT or at least maintains the papillary phenotype, HDF cells were cultivated in the presence of 1201 over five PDs. The cells were counted, seeded at defined cell numbers for SA- β -gal staining and proliferation assay and RNA samples were prepared. 1201 altered the morphology of HDF, resembling papillary-shaped replicatively young cells (Fig. 2a), and the cells reached higher cell densities and/or displayed increased proliferation (Fig. 2b). Next, we quantified the expression levels of mRNAs used as markers for the papillary and reticular phenotype, to confirm that the observed changes in morphology and growth characteristics represent a transition to a papillary-like phenotype. The levels of papillary markers PDPN and NTN1 were significantly induced, while reticular markers PPP1R14A and A2M were significantly reduced in cells treated with 1201 (Fig. 2c). Additionally, 1201 treatment for only 48 hours resulted already in morphological alterations, which implies that the effect seen for 1201 is not due to a selection process in which the survival of papillary fibroblast is favoured (S2 Fig.). Exposing HDF cells to the solvent propanediol or two major components of 1201, chlorogenic acid and isochlorogenic acid A, did not induce any changes morphology or the expression of PDPN, NTN1 and PPP1R14A, suggesting that other compounds present in 1201 are alone or in combination responsible for the observed effects (S3 Fig.).

Figure 2 1201 reverses the papillary to reticular transition. (a) HDF were cultivated at the middle of their replicative lifespan in growth medium supplemented with 1201 for the duration of five passages. Control cells were cultivated with normal growth medium. Microscopic pictures at 100 x magnification were taken at the end of the treatment. Scale bar, 100 μ m. (b) After cultivation with 1201 for the duration of three passages, the cells were counted and 40,000 cells were seeded per well. The cells were cultivated in growth medium supplemented with 1201 and counted after the indicated time period. Control cells were always cultivated with normal growth medium. (c) Cells were treated as described in a and transcript levels of markers for the papillary (PDPN, NTN1) and the reticular (PPP1R14A, A2M) phenotype were analysed with RT-qPCR. Expression levels of untreated control cells were set to 1 (dashed line). (d) Transcript levels of SNEV were analysed with RT-qPCR (as in c). Expression levels of replicatively young (PD 10) control cells were set to 1 (dashed line). (e) The cells were treated as described in a, counted and 40,000 cells were seeded per well. The cells were stained for SA- β -gal after 3 days of cultivation in growth medium supplemented with 1201. Replicatively young cells (PD 10) served as a young control. Control cells were always cultivated with normal growth medium. Ten microscopic pictures per sample were taken at 100 x magnification at random positions in the well and after randomisation and blinding, the SA- β -gal positive and negative cells were counted. (f) Full thickness human skin equivalents (HSE) were constructed as described in the methods section.

Sections of HSEs were stained with hematoxylin and eosin. The average of the epidermal thickness was calculated from at least 50 measurements per HSE and the epidermal thickness of untreated HSEs was set to 1. (g) Representative pictures from one experiment as described in f are shown. Scale bar, 50 μ m. For a, pictures from one representative of three experiments are shown. For b to e, data represents the average of three experiments. For f, data represents the average of two experiments.

Hypothesizing that PRT represents an early stage in the aging process of HDF cells, we aimed at confirming the effects of 1201 on the expression of senescence markers, we did observe in the long-term treatment. Indeed, the expression of SNEV was significantly induced (Fig. 2d), whereas the number of SA- β -gal positive cells was significantly reduced (Fig. 2e). Now, if PRT resembles the process of cellular senescence in HDF, its reversion should result in a recovery of cell functionality. We addressed this question by constructing full thickness HSEs, which were cultured with 1201 supplemented medium during the formation of the epidermal layer. The epidermal thickness was increased by 55% compared to untreated control HSEs (Fig. 2f,g).

In addition, we isolated papillary and reticular fibroblasts from the dermis as described [37] and confirmed mRNA marker expression (S4 Fig.). Exposure of these reticular fibroblasts to 1201 for two PDs resulted in visible morphological changes towards a papillary-like phenotype (Fig. 3a). Cells exposed to 1201 reached higher cell densities (Fig. 3b) and both papillary markers were significantly induced while the reticular markers were reduced (Fig. 3c). There was no significant change in SNEV levels or in the number of SA- β -gal positive cells detectable (Fig. 3c,d). Taken together, these results indicate that 1201 is indeed able to block PRT in papillary fibroblasts and to induce a reticular to papillary transition (RPT) in reticular fibroblasts.

Figure 3 1201 induces a reticular to papillary transition in reticular fibroblasts. (a) Reticular HDF cells were cultivated at the beginning of their replicative lifespan (PD 5) in growth medium supplemented with 1201 for the duration of three passages. Control cells were cultivated with normal growth medium. Microscopic pictures at 100 x magnification were taken after 2 passages. Scale bar, 100 μ m. (b) After cultivation with 1201 for the duration of three passages, the cells were counted and 40,000 cells were seeded per well. The cells were cultivated in growth medium supplemented with 1201 and counted after the indicated time period. Control cells were always cultivated with normal growth medium. (c) Cells were treated as described in a and transcript levels of markers for the papillary (PDPN, NTN1) and the reticular (PPP1R14A, A2M) phenotype and SNEV were analysed with RT-qPCR. Expression levels of untreated control cells were set to 1 (dashed line). (d) The cells were treated as described in a, counted and 40,000 cells were seeded per well. The cells were stained for SA- β -gal after 3 days of cultivation in growth medium supplemented with 1201. Control cells were always cultivated with normal growth medium. Ten microscopic pictures per sample were taken at 100 x magnification at random positions in the well and after randomisation and blinding, the SA- β -gal positive and negative cells were counted. For a, pictures from one representative of three experiments are shown. For b to d, data represents the average of three experiments.

1201 attenuates the senescent phenotype in stress-induced premature senescent (SIPS) fibroblasts

SIPS was induced in HDF cells [38] as described recently by us (Terlecki et al. in preparation) and subsequently 1201 was added to the medium. Confluent quiescent cells served as a control. 1201 treatment had no effect on SIPS-induced expression changes of p21 and SNEV (Fig. 4a), whereas the number of SA- β -gal positive SIPS cells was significantly reduced already after 4 and 11 days of 1201 treatment (Fig. 4b).

Figure 4 1201 attenuates the senescent phenotype in SIPS HDF cells. (a) Premature senescence was induced by chronic oxidative stress in HDF cells. As a control for the SIPS treatment cells were cultivated with normal growth medium, grew to confluency during the treatment and entered a quiescent state (Q). Subsequent to the SIPS treatment cells were cultivated for 4 days with 1201 supplemented to the growth medium. Transcript levels of senescence markers (p21, SNEV) were analysed with RT-qPCR. Expression levels of untreated quiescent control cells were set to 1. (b) SIPS was induced as described in a. The cells were stained for SA- β -gal after 4, 11 and 18 days of cultivation in growth medium supplemented with 1201. Control cells were always cultivated with normal growth medium. Ten microscopic pictures per sample were taken at 100 x magnification at random positions in the well and after randomisation and blinding, the SA- β -gal positive and negative cells were counted. (c) Cells were treated as described in a and PCA analysis and hierarchical clustering was performed with the transcript levels derived from next generation sequencing (RNA-Seq). PC-1 separates SIPS from Q and comprises 96 % of the transcripts. PC-2 separates SIPS from Q and cells treated with 1201 and comprises 4 % of the transcripts. (d) Shows two Venn diagrams identifying the genes which are differential expressed in SIPS compared to Q and are regulated contrariwise by treatment of SIPS with 1201. The pie chart illustrates the identified SASP factors and their response to the treatment with 1201. Data used for analysis was derived as described in c. (e) Transcript levels of all upregulated SASP factors, which were regulated contrariwise by treatment with 1201. Expression levels were derived from RNA-Seq data and are displayed as Fragments Per Kilobase of transcript per Million mapped reads (FPKM). Error bars indicate confidence intervals (95 %). (f) Six genes were quantified with RT-qPCR from the same RNA samples which were used for RNA-Seq. Expression levels relative to GAPDH were correlated with transcript levels derived from RNA-Seq. For a to f, data represents the average of three experiments.

In order to analyse the effect of 1201 on the whole transcriptome level, RNA sequencing (RNA-Seq) was performed after four days of 1201 treatment in SIPS and quiescent control cells. For visualisation of differences in the data sets, principle component analysis (PCA) was performed and revealed that treatment with 1201 changed the expression profile of SIPS cells to closely resemble quiescent cells (Fig. 4c).

The hierarchical clustering of the samples confirmed this result by showing a closer relationship of SIPS cells treated with 1201 to quiescent cells than to their untreated counterparts (Fig. 4c). After identifying genes, which were significantly regulated in SIPS compared to quiescent cells and 'rescued' by treatment with 1201 (Fig. 4d), functional annotation clustering was performed and revealed a strong correlation with processes of the immune response (S5 Data). Since many of the deleterious effects of senescent cells are considered to be caused by components of the SASP, which comprises many pro-inflammatory cytokines and chemokines, we specifically looked for SASP-mRNAs within our RNA-Seq dataset, which were regulated by 1201. Therefore, the list of genes upregulated by the SIPS treatment was cross-referenced with 89 secreted factors considered as members of SASP [18,39,40] (S5 Data). We were able to identify 30 of these SASP members, which were detectable in our dataset, 9 of which were significantly reduced by 1201 (Fig. 4d,e).

By filtering for the keyword "secreted" (KW-0964) in the list of genes upregulated by the SIPS treatment, additional 193 genes were identified as potentially novel members of the SASP. 21 of these putative SASP factors were significantly downregulated by 1201 (Fig. 4d and S5 Data). The RNA-Seq results were confirmed by RT-qPCRs

against selected targets. Calculation of the Pearson's correlation coefficient between RNA-Seq and RT-qPCR data revealed a strong correlation, with R-values ranging from 0.88 to 0.99 (Fig. 4f).

A detailed pathway analysis revealed several prominent SASP-related pathways, which were all inhibited by treatment with 1201 (Fig. 5a and S6 Table). In addition, ConsensusPathDB [41] (for complete results refer to S7 Fig.) revealed that 1201 downregulates pathways related to the immune system in senescent cells, including the JAK-STAT pathway (Fig. 5d). Searching for pathways upregulated by 1201 in both, quiescent and SIPS cells, we identified pathways related to the ECM and ECM interacting proteins (Fig 5c), which might be seen in accordance to our data showing increased epidermal thickness in HSEs. Also, Wnt/ β -catenin signalling, one of the few pathways activated by 1201, was previously shown to induce a remodelling of adult dermis to neonatal-like dermis [42], which might be interpreted as a kind of 'rejuvenation' (Fig. 5a).

Figure 5 Analysis of pathways and upstream regulators affected by 1201 treatment. (a) List of selected canonical pathways and (b) upstream regulators derived from Ingenuity pathway analysis of RNA-Seq data (for complete lists refer to S6 Table and S8 Table). (c) Pathway enrichment analysis of genes upregulated by 1201 in both, Q and SIPS cells, and (d) of genes downregulated by 1201 in SIPS cells. Gene expression levels were derived from RNA-Seq data (for complete results of the analysis refer to S7 Fig.).

Predicted upstream regulators inhibited by 1201 were either related to inflammatory responses, growth factors or transcriptional regulators controlling genes involved in stress response and aging (Fig. 5b and S8 Table). PTPN6, KDM5B and PTEN were all activated by treatment with 1201 and are factors that might mediate the observed attenuation of the SASP by potentially inhibiting the JAK/STAT, GATA4 and PI3K/AKT pathway respectively [43–45]. Interestingly, curcumin and resveratrol, two polyphenolic compounds with anti-tumorigenic and anti-inflammatory properties were also identified as predicted upstream regulators, indicating that the polyphenolic components of 1201 might have similar modes of action as these well-known substances [46].

1201 attenuates deleterious effects of senescent fibroblasts on other cells

In order to see if 1201 is able to attenuate age-associated changes of intercellular communication, a hallmark of aging [47], we tested if 1201 is able to decrease the pro-proliferative effect of senescent fibroblasts on the tumour cell line HaCaT [15]. Therefore, SIPS HDF cells were pre-treated for four days with 1201 and subsequently co-cultured with pre-neoplastic HaCaT cells for eight days in growth factor-deficient medium without the addition of 1201. HaCaT cell number was determined by counting the cells positive for keratinocyte-specific K14 staining. Indeed, the treatment with 1201 resulted in a significant reduction of HaCaT cell growth by 26%, compared to HaCaT cells co-cultured with untreated SIPS HDF (Fig. 6a,c). Similarly, when HaCaT cells were cultivated with conditioned medium derived from SIPS HDF, supernatants of 1201 treated cells significantly reduced HaCaT cell growth by 52% (Fig. 6b).

Figure 6 1201 blocks the negative effects of SIPS HDF cells on other cells. (a) Premature senescence was induced by chronic oxidative stress in HDF. Following the SIPS treatment fibroblasts were cultivated for 4 days with 1201 supplemented to the growth medium and subsequently, HaCaT cells pre-conditioned in growth factor deficient keratinocyte medium were seeded on top and the cell mixture was co-cultured for 8 days in growth factor deficient keratinocyte medium. Control fibroblasts were always cultivated with normal growth medium. Cells were fixed and stained for K14 and DAPI, 15 pictures per condition were taken at 50 x magnification and K14 positive cells

were counted. The seeding cell number of HaCaT cells was subtracted from the number of K14 positive cells. The cell number of HaCaTs co-cultured with untreated control cells was set to 1. (b) HDF cells were treated as described in a. Per well 20,000 HaCaT cells pre-conditioned in growth factor deficient keratinocyte medium were seeded in a 6-well culture plate and cultured for 8 days with growth factor deficient keratinocyte medium, which was conditioned for 24 hours by SIPS HDF cells. The HaCaT cells were counted and after subtracting the seeding cell number the resulting cell number of untreated control cells was set to 1. (c) Representative pictures from one experiment as described in a are shown. Scale bar, 100 μ m. (d) HDF cells were treated as described in a. RPMI 1640 medium was conditioned for 24 hours by SIPS HDF cells and analysed for its chemotactic potential on freshly isolated human PBMCs with a migration assay using a μ -Slide Chemotaxis (IBIDI). The setup with both reservoirs filled with unconditioned medium served as an additional control where no directed migration was detectable. The migratory paths of 30 PBMCs per condition were analysed. Graphic illustrates the migratory paths and are coloured in black if migrating towards the conditioned medium and red if migrating towards the reservoir containing unconditioned medium. The blue dot marks the centre of mass. (e) HDF cells were treated as described in a. Full thickness human skin equivalents were constructed as described in the methods section. Sections of skin equivalents were stained with hematoxylin and eosin. Average epidermal thickness was calculated by dividing the total epidermal area by its length and the epidermal thickness of HSE constructed with untreated cells was set to 1. (f) Representative pictures from one experiment as described in e are shown Scale bar, 50 μ m. For a, b and e, data represents the average of three experiments. For d, data represents one experiment.

In order to test pro-inflammatory properties of SIPS HDF cells, a chemotaxis assay with conditioned medium and human peripheral blood mononuclear cells (PBMCs) seeded in a three dimensional collagen matrix was performed. Subsequent live-cell imaging was conducted over a period of 12 hours, 30 cells for each condition were manually tracked and their migration quantified. Pre-treatment of SIPS HDF cells with 1201 abolished the chemotactic property of senescent cell supernatant compared to untreated control (Fig. 6d).

To test the hypothesis that the accumulation of senescent HDF is a driving force of the aging process in human skin, we constructed full thickness HSE using SIPS HDF cells embedded in a collagen matrix and investigated the ability of primary keratinocytes to form a fully differentiated epidermal layer. Additionally, we tested if pre-treatment of senescent fibroblasts with 1201 can rescue the negative effects on the formation of the HSE. This was indeed the case, as 1201 rescued the senescent cell dependent reduction in epidermal thickness and the impaired differentiation of keratinocytes, which we reported earlier (Weinmüller et al. in preparation) (Fig. 6e,f).

Finally, the ability to induce senescence in a paracrine manner was evaluated by cultivation of non-senescent fibroblasts with conditioned media derived from SIPS HDF cells for 8 days. However, conditioned media under the conditions tested here was not able to induce bystander senescence in HDF (data not shown), which is in line with previous findings [16], but contradicts others [17,18]. Thus, effects of 1201 on bystander senescence could not be tested in our experimental set-up.

1201 selectively eliminates senescent cells

In recent studies, it was demonstrated that the selective elimination of senescent cells was able to extend the healthspan of mice[5], and the search for senolytic drugs resulted already in the identification of several senolytic candidate substances [4,6,9,10,34]. To evaluate if 1201 also has senolytic properties, we cultivated SIPS and

quiescent HDF cells with 1201 for 39 days and counted the cells. The treatment with 1201 resulted in a significant reduction of the cell number of senescent cells by 30%, whereas quiescent cells were not significantly affected (S6 Fig.). Treating SIPS HDF cells for only 4 days with 1201 did not result in a significant reduction of the cell number, thus the attenuation of the SASP and its effect on other cells was not caused by a senolytic effect (S9 Fig. and S10 Fig.).

DISCUSSION

Solidago virgaurea, also known as goldenrod, is traditionally used as an anti-inflammatory herbal medicine. Compounds isolated from *Solidago virgaurea* are reported to have cytotoxic, anti-microbial, anti-mutagenic, anti-fungal, analgesic, anti-inflammatory, anti-oxidative and diuretic activity [48–54]. A recent study identified 3,4,5-tri-O-caffeoylquinic acid as the constituent with the highest reduction of TNF- α and IL-1 β concentrations in a carrageenan-induced rat paw oedema model [51]. However, the effect of extracts from *Solidago virgaurea* on cellular senescence and fibroblast subpopulations have not been studied so far.

The plant extract 1201 was not only able to delay the acquisition of a senescent phenotype, but preserved a papillary phenotype and the functionality of human dermal fibroblasts in regard to their ability to stimulate the formation of a full thickness HSE. Furthermore 1201 reverted the gene expression profile of SIPS HDF cells towards one resembling quiescent cells and reduced the expression of various SASP factors. Consequently the negative effects of the SASP on neighbouring cells was ameliorated, namely the growth stimulation of pre-neoplastic HaCaT cells, the pro-inflammatory attraction of immune cells and the impairment of keratinocytes to differentiate and form a fully stratified epidermis. At the same time, 1201 did not override the tumour suppressive senescence mechanism mediated by an irreversible growth arrest.

The identification of a treatment which was able to simultaneously attenuate cellular senescence and induce a papillary phenotype in fibroblasts supports the hypothesis that cellular senescence of fibroblasts is a differentiation process, in which the reticular phenotype represents a transition-stage on the way to the senescent phenotype, whereby senescent cells also seem to resemble the reticular morphology. Cellular senescence of fibroblasts has already been proposed previously to be a differentiation process, but neither the *in vivo* situation, nor the different dermal subpopulations have been considered so far [55–57]. The development of the different fibroblast lineages in mouse skin during embryogenesis was thoroughly investigated, but the fate of the different fibroblast subpopulations during the aging process hasn't been addressed yet [58].

All previous reported substances, which were able to ameliorate the SASP, exerted their effect by targeting NF- κ B, IL1A-signalling or the JAK/STAT-pathway. Pathway analysis of our RNA-Seq data provided evidence that 1201 is able to target multiple pathways involved in inflammation, aging and tumorigenesis. The caffeoylquinic acids with their anti-inflammatory property [51] are likely to be candidates for the SASP-attenuating property of 1201, whereas the three derivatives of quercetin, one of the two naturally occurring senolytics reported so far, could be the driving force behind the slow but significant selective elimination of around one third of the senescent cells. The induction of a papillary phenotype might be due to interference with TGF β -signalling which was shown to be the driving force in PRT [59] or due to inhibition of mTOR/PI3K/AKT-signalling, which reduces SA- β -gal staining and induces a papillary-like morphology [60]. In addition, Wnt and ILK signalling were identified as potential targets that need to be activated to counteract negative effects of senescence. However, the complete characterisation

of 1201 and the identification of the molecules responsible for the identified effects will be the focus of subsequent studies. Considering that senescent cells are linked to age-related pathologies throughout the body, the effect of 1201 will also be investigated in other cell types.

Of course, in vitro cell cultures are artificial systems and are not able to completely reflect the in vivo situation in human skin. Nevertheless, they provide valuable information on the molecular pathways involved in the observed effects, especially if combined with full thickness HSEs. These are a very useful tool to evaluate the functionality of skin cells, and when constructed with SIPS HDF cells, they represent in our opinion currently a valid model for aged human skin.

Taken together, we have identified a plant extract that is able to block detrimental effects of cellular senescence in HDF cells and to maintain their functionality. Furthermore, our results increased the evidence for a connection between cellular senescence and PRT. We have also identified numerous putative novel SASP factors, highlighting that the list of accepted SASP members might not be complete and needs to be curated in a collective effort, like e.g. by the databases available (<http://genomics.senescence.info/cells>).

MATERIALS AND METHODS

Plant extract (1201) preparation and characterisation

1201 was selected for further investigation after showing positive effects on cell morphology, growth characteristics, expression of PRT markers and SA- β -galactosidase activity in a screening experiment including five additional plant extracts (data not shown).

The ethanolic extract of *Solidago virgaurea* subspecies *alpestris* was prepared as follows. 1 kg of finely ground dried aerial parts of *Solidago alpestris* was immersed in 6 kg of 96 % ethanol (v/v) in a glass beaker. The mixture was then heated to 60 °C and extracted twice during 2 hours. The mixture was sieved and filtrated at 100 μ m (Prolabo, France) to remove the plant residue and then let to settle overnight. The ethanolic extract was discolored by mixing with 31 g of 100 mesh Darco activated charcoal (Sigma-Aldrich, France) for 3 hours at room temperature. The mixture was then filtrated at 4 μ m on a K1 BECO (Eaton, France) disc. The filtrate (6.55 g dried extract) was solubilized with 530.5 g of 1, 3-propanediol (Sigma-Aldrich, France) and 59 g of deionized water. The ethanol remaining in the extract was completely removed by evaporation under vacuum leading finally to 655 g of extract (1201).

A high-performance liquid chromatography (HPLC) method with Agilent 1200SL was performed for the identification and quantification of the secondary metabolites in the ethanolic extract of *Solidago alpestris*. Reverse phase chromatography analysis was carried out with an Agilent C18 Zorbax SBRR column (2.1 mm \times 50 mm) packed with 1.8 μ m diameter particles. Fourteen components of 1201 could be identified by diode array detector (DAD) and electrospray ionization tandem mass spectrometry (ESI-MS/MS) techniques. These were chlorogenic acid, two isomers of caffeoylquinic acid, octulosonic acid B & C, isoquercetin, leiocarposide, rutin, quercetin arabinoside, astragalin, cynarin, 3,4- & 3,5-di-caffeoylquinic acid and nicotiflorin.

Cell isolation and Ethics

Fibroblasts and keratinocytes were isolated from skin biopsies. HaCaT cells were obtained from the German Cancer Research Center (Heidelberg, Germany). HDF cells were provided by Evercyte (Vienna, Austria) and FL. Site-matched papillary and reticular HDF were kindly provided by AEG and their identity was confirmed by

measurement of the expression levels of three papillary and three reticular mRNA markers. PBMCs were isolated from a blood sample donated by a healthy male donor. Primary human keratinocytes were kindly provided by FG and FL. The isolation of the cells was approved by the respective local ethics commission and all donors gave informed consent. Thus, this study was performed in compliance with the declaration of Helsinki.

Cell culture

Primary human keratinocytes were cultured in Dermalife K Keratinocyte Medium (LL-0007, CellSystems). Fibroblasts and HaCaT cells were cultured with DMEM/Ham's F-12 (1:1 mixture) (F4815, Biochrome) supplemented with 10% FCS (F7524, Sigma) and 4 mM L-Glutamine (G7513, Sigma) under ambient oxygen, 7% CO₂ and 37 °C.

Proliferation assay

Cells were washed twice with 1 x PBS (L1820, Biochrome) detached by incubation with 0.1% trypsin with 0.02% EDTA at 37 °C for 5 min. After determining the viable cell number with a Vi-CELL XR (Beckman Coulter) automated cell counter, the cells were seeded in a 6-well culture plate (657160, Greiner Bio-One) at 40,000 cells/cm². Media was changed every three to five days and cells were detached and counted at the indicated time point.

RNA isolation and RT-qPCR

Cells were lysed in TRI Reagent (T9424, Sigma) and RNA was isolated following the manufacturer's protocol. RNA concentration and quality were measured with a Nanodrop spectrometer (ND-1000). cDNA was synthesised from 500 ng of total RNA with the High-Capacity cDNA Reverse Transcription Kit (4368814, Applied Biosystems) and quantified with the 5x HOT FIREPol® EvaGreen® qPCR Mix Plus with ROX (SB_08-24-GP, Solis BioDyne) using a Rotor-Gene Q cyclor (Qiagen). Expression values were normalised to GAPDH.

Table 1 Sequences of RT-qPCR primers.

Gene name	Sense primer	Anti-sense primer
GAPDH	CGACCACTTTGTCAAGCTCA	TGTGAGGAGGGGAGATTCAG
PDPN	GCATCGAGGATCTGCCAACT	CCCTTCAGCTCTTAGGGCG
NTN1	TGCCATTACTGCAAGGAGGG	TTGCAGGTGATACCCGTCAC
PPP1R14A	GTGGAGAAGTGGATCGACGG	CCCTGGATTTCCGGCTTCT
A2M	AGAGCAGCATAAAGCCAGT	TCTCAGTGGTCTCAGTGTGGA
CDKN1A (p21)	GGCGGCAGACCAGCATGACAGATT	GCAGGGGGCGGCCAGGGTAT
PRPF19 (SNEV)	TCATTGCCCGTCTCAACAAG	GGCACAGTCTTCCCTCTCTTC
CCL2	GAAAGTCTCTGCCGCCCTTC	ACAGATCTCCTTGCCACAA
CXCL1	TCAATCCTGCATCCCCATAG	CAGGAACAGCCACCAAGTGAG
CXCL8	CTCTTGGCAGCCTTCTGATTT	ACAGAGCTCTTCCATCAGA
IL11	ATGAACTGTGTTTGCCGCCT	GGGAATCCAGGTTGTGGTCC

SA-β-gal staining

SA-β-gal staining was performed according to the standard protocol [20]. 15 random pictures were taken per well at 100 x magnification and after randomisation positive and negative cells were counted in blinded fashion.

Full thickness human skin equivalent with HDF cells and normal human keratinocytes

On day one, 330,000 HDF per skin equivalent were embedded in a collagen matrix containing rat tail collagen type I (Corning), 10X DMEM (fish), sodium bicarbonate (Gibco/Invitrogen), filled into 6-well-culture inserts (Thermofisher) and placed in deep 6-well culture plates (Thermofisher). After 2 hours of polymerisation at 37 °C, dermal equivalents were equilibrated in DMEM medium supplemented with 10% fetal bovine serum (Sigma Aldrich) and placed at 37 °C, 5% CO₂. After 3 days, 150,000 keratinocytes were seeded on top of each skin equivalent and submerged for 7 days in DMEM medium supplemented with 10% fetal calf serum and growth factors (EGF, isoproterenol, hydrocortisone). Then the inserts were placed at the air-liquid interface for 7 days. 1201 was supplemented to the culture medium for the last 7 days and the medium was changed every second day. HSE were fixed in 10% formalin before embedding in paraffin and cutting into 5 µm-thick sections. Hematoxylin and eosin staining was performed using a standard protocol. Hematoxylin and Eosin-stained sections were photographed under microscope and a minimum of 50 measurements of epidermal thickness were done for each HSE.

Stress-induced premature senescence

Cells were seeded at a cell density of 3,500 cells/cm² one day prior to the start of the chronic oxidative stress treatment used to induce premature senescence. The cells were treated nine times with 100 µM H₂O₂ supplemented to their growth media for the duration of one hour followed by a media change. Induction of premature senescence was verified by SA-β-gal staining, p21 expression and absence of BrdU incorporation. Additionally AnnexinV/PI staining was performed to assure that the treatment was non-lethal and SIPS HDF cells were cultured and monitored for over 50 days to assure that the induced growth arrest was permanent (Terlecki et al. in preparation).

Next generation sequencing and data analysis

Quality and concentration of the RNA was assessed using a Bioanalyzer 2100 with the RNA 6000 Nano Kit (Agilent Technologies) before the samples were sent for next generation sequencing. Library preparation and transcriptome sequencing on an Illumina HighSeq 2000 Platform were performed by GATC Biotech AG (Konstanz, Germany). All analysis steps were done according to the Tuxedo Suite Pipeline [61]. Briefly, Illumina Casava 1.8.2 software was used for basecalling. RNA-seq reads were aligned to hg19 genome assembly using TOPHAT Version 2.0.13 with default parameters. Table 2 indicates the number of mapped reads.

Table 2 Information on reads from RNA-Seq data.

Sample code	Total reads	Mapped to genome [%]
Q1	48,912,062	95.8
Q2	35,231,599	94.0
Q3	30,695,013	96.6
Q1201_1	36,822,399	96.1
Q1201_2	53,613,886	58.8
Q1201_3	48,975,121	95.6
SIPS1	40,406,275	93.8
SIPS2	4,479,584	92.3
SIPS3	32,505,280	75.2

Appendix B Manuscripts

SIPS1201_1	36,343,341	95.6
SIPS1201_2	31,555,227	95.5
SIPS1201_3	4,688,330	93.5

Transcripts were assembled in Cufflinks Version 2.1.1 and differentially expressed genes were predicted by Cuffdiff. Finally, tables and figures were assembled with R using the CummRbund package and with The Unscrambler X software (Camo). Functional clustering analysis and filtering for the keyword secreted (KW-0964) was done using the Database for Annotation, Visualization and Integrated Discovery (DAVID v6.8). Pathway analysis was realised with the Ingenuity pathway analysis software (Qiagen). Pathway enrichment analysis was performed employing ConsensusPathDB, by using the overrepresentation analysis tool. As input, we use the HGNC symbol identifiers of our datasets. We searched against pathways in all databases with a minimal overlap with a p-value cutoff of 0.0001. The raw data is available at the Gene Expression Omnibus (GEO) website under accession number GSE93535 (<https://www.ncbi.nlm.nih.gov/geo/query/acc.cgi?token=kzobciauftyfnfml&acc=GSE93535>).

Growth stimulation of HaCaT cells in co-culture with SIPS HDF

After being cultured for 48 hours in KGM minimal medium, comprising basal KGM medium (CC-3101, Lonza) supplemented only with insulin and hydrocortisone from the BulletKit (CC-3111), HaCaT cells were seeded at a cell density of 2,000 cells/cm² in a 6-well culture plate containing SIPS HDF. The cells were co-cultured in KGM minimal medium for eight days with a media change after two and five days. Subsequently the cells were fixed with 4% formaldehyde (F8775, Sigma) in PBS for 10 min and permeabilized with 0.3% Triton X-100 (X100, Sigma) in PBS for 10 min. Cells were then incubated O/N at 4 °C with α -K14 (ab7800, Abcam) diluted 1:200 in 0.3% Triton X-100 + 10% FCS in PBS. On the next day cells were incubated for 1 hour at RT with α -mouse Alexa Fluor 488 (715-545-150, Jackson ImmunoResearch) diluted 1:1000 in 0.3% Triton X-100 + 10% FCS in PBS. Finally the cells were stained for 10 min at RT with DAPI (62248, Thermo Fisher Scientific) diluted 1:10,000 in PBS. After each step the cells were washed at least twice with PBS. 15 pictures per condition were taken at 50 x magnification using a DMI6000 CS fluorescence microscope (Leica) and K14 positive cells were counted. For determination of the HaCaT cell growth the initial seeding cell density was subtracted from the cell density calculated from the images.

Growth stimulation of HaCaT cells with conditioned medium from SIPS HDF

SIPS HDF cells were cultivated for 24 hours with KGM minimal medium to generate conditioned medium. HaCaT cells were seeded at a cell density of 2,000 cells/cm² in a 6-well culture plate and cultivated for 48 hours with KGM minimal to deprive the cells of growth factors. Subsequently, the cells were cultivated with conditioned medium for 8 days with a media change after four days. Finally, the cells were trypsinized, collected in 1 ml and counted with a Vi-CELL XR cell counter. For determination of HaCaT cell growth the initial seeding cell density was subtracted from the cell density calculated from the cell concentrations.

Chemotaxis assay

SIPS HDF cells were cultivated for 24 hours with RPMI 1640 medium (FG1215, Biochrome) to generate conditioned medium. PBMCs were isolated from fresh blood by creating a gradient using Biocoll (L6115, Biochrome) and centrifugation (400 g for 40 min). After collecting the PBMC containing phase, erythrocyte lysis buffer (156 mM NH₄Cl, 12 mM NaHCO₃, 100 μ M EDTA, pH = 7.43) was added and again centrifuged (400 g for 10 min). Cells were

washed once with PBS and after another round of centrifugation (400 g for 10 min) resuspended in RPMI 1640 medium and counted with a hemocytometer. Chemotaxis assay was done using a μ -Slide Chemotaxis (80326, IBIDI) according to the manufacturer's manual (Application Note 17 and 23). The collagen matrix consisted of 4 μ l L-glutamine (G7513, Sigma), 20 μ l 10 x MEM (M0275, Sigma), 53.5 μ l nuclease free water (10977035, Thermo Fisher Scientific), 10 μ l 7.5 % sodium bicarbonate solution (S8761, Sigma), 50 μ l RPMI 1640 medium, 112.5 μ l collagen G (L7213, Biochrome) and 50 μ l PBMC cell suspension containing 18×10^6 cells/ml. Life cell imaging was performed using a DMI6000 CS microscope (Leica) equipped with a heated CO₂ chamber (OKOLAB) and an automated stage. Over the course of 12 hours, every 2.5 minutes a picture of every condition was taken. For each condition 30 cells were manually tracked using the manual tracking plugin and analysed with the chemotaxis and migration tool plugin (IBIDI) in ImageJ.

Full thickness human skin equivalents with SIPS HDF cells and normal human keratinocytes

The HSE were constructed as recently published [62]. Briefly, on day one 250,000 SIPS HDF per skin equivalent were embedded in a collagen matrix consisting of eight parts collagen G (L7213, Biochrome), one part 10 x HBSS (14060-040, ThermoFisher Scientific) and one part FCS (F7524, Sigma) and equilibrated with KGM-2 (CC-3103, Lonza) supplemented with the BulletKit (CC-4152) overnight. On day two 1.5 million primary human keratinocytes were seeded on top of each skin equivalent. On day three differentiation of the keratinocytes was induced by lifting the skin equivalents to the air-liquid interface and changing the cultivation medium to differentiation medium consisting of KGM (CC-3101, Lonza) supplemented with the BulletKit (CC-3111) except for the bovine pituitary extract, 1.3 mM CaCl₂ (21115, Sigma), 50 μ g/ml L-ascorbic acid (A4544, Sigma), 0.1% bovine serum albumin (A7906, Sigma) and 10 μ g/ml transferrin (T8158, Sigma). The medium was replaced daily throughout the whole differentiation process (day 3-10). On day ten the skin equivalents were harvested, fixed with Roti®-Histofix 4% (P087, Carl Roth), and paraffin-embedded for further histological analysis. Hematoxylin and eosin staining was performed using a standard protocol.

Statistical analysis

Error bars are presented as mean \pm standard deviation. Statistical significance was evaluated using a two-tailed Student's t-test and assumption of equal variance. Significance levels were denoted as: *P < 0.05, **P < 0.01 and ***P < 0.001.

ACKNOWLEDGEMENTS

We thank Marina Wagesreither and the BOKU-VIBT Imaging Center for technical support. This work was funded by the Christian Doppler Society. The financial support by the Austrian Federal Ministry of Economy, Family and Youth, the National Foundation for Research, Technology and Development is also gratefully acknowledged, as is funding by the Austrian Science Fund (FWF: I2514 to JG).

Competing financial interests

JG is co-founder and CSO of Evercyte GmbH. IB, FM, FL, NF, SF, ATo, ATr and LW are employees of Chanel R&T. CHANEL filed a patent for the cosmetic use of 1201 and IL, JG, FG, IB and AT are listed as inventors.

Author contributions

JG, IL, FM and FG planned the study; IL, LTZ, RW, MScho, MR, AEG, FM, FL, IB and JG designed experiments; IL, LTZ, RW, ADMB, DA, BS, MScho, MR, IB, FL and LK performed experiments, analysed and interpreted data; JCHA and MSche performed bioinformatics analyses; AEG, MR, FG, ET and FL helped with cell culture experimentation; NF, SF, ATo, ATr and LW generated the plant extracts; IL and JG designed figures and wrote the manuscript; JG and MScho supervised the writing of the manuscript. All authors read, edited and approved the final manuscript.

REFERENCES

1. Grillari J, Grillari-Voglauer R. Novel modulators of senescence, aging, and longevity: Small non-coding RNAs enter the stage. *Exp Gerontol*. Elsevier Inc.; 2010;45: 302–311. doi:10.1016/j.exger.2010.01.007
2. Campisi J, Robert L. Cell senescence: Role in aging and age-related diseases. *Aging: Facts and Theories*. 2014. pp. 45–61. doi:10.1159/000358899
3. van Deursen JM. The role of senescent cells in ageing. *Nature*. Nature Publishing Group; 2014;509: 439–446. doi:10.1038/nature13193
4. Zhu Y, Tchkonja T, Fuhrmann-Stroissnigg H, Dai HM, Ling YY, Stout MB, et al. Identification of a novel senolytic agent, navitoclax, targeting the Bcl-2 family of anti-apoptotic factors. *Aging Cell*. 2016;15: 428–435. doi:10.1111/acer.12445
5. Baker DJ, Childs BG, Durik M, Wijers ME, Sieben CJ, Zhong J, et al. Naturally occurring p16 Ink4a - positive cells shorten healthy lifespan. *Nature*. Nature Publishing Group; 2016; 1–20. doi:10.1038/nature16932
6. Chang J, Wang Y, Shao L, Laberge R-M, Demaria M, Campisi J, et al. Clearance of senescent cells by ABT263 rejuvenates aged hematopoietic stem cells in mice. *Nat Med*. Nature Publishing Group; 2016;22: 78–83. doi:10.1038/nm.4010
7. Baker DJ, Wijshake T, Tchkonja T, LeBrasseur NK, Childs BG, van de Sluis B, et al. Clearance of p16Ink4a-positive senescent cells delays ageing-associated disorders. *Nature*. Nature Publishing Group; 2011;479: 232–6. doi:10.1038/nature10600
8. Xu M, Palmer AK, Ding H, Weivoda MM, Pirtskhalava T, White TA, et al. Targeting senescent cells enhances adipogenesis and metabolic function in old age. *Elife*. 2015; 1–20. doi:10.7554/eLife.12997
9. Zhu Y, Tchkonja T, Pirtskhalava T, Gower AC, Ding H, Giorgadze N, et al. The Achilles' heel of senescent cells: From transcriptome to senolytic drugs. *Aging Cell*. 2015; 644–658. doi:10.1111/acer.12344
10. Childs BG, Baker DJ, Wijshake T, Conover CA, Campisi J, van Deursen JM. Senescent intimal foam cells are deleterious at all stages of atherosclerosis. *Science* (80-). 2016;354: 472–477. doi:10.1126/science.aaf6659
11. Roos CM, Zhang B, Palmer AK, Ogronik MB, Pirtskhalava T, Thalji NM, et al. Chronic senolytic treatment alleviates established vasomotor dysfunction in aged or atherosclerotic mice. *Aging Cell*. 2016;15: 973–977. doi:10.1111/acer.12458
12. Jun J-I, Lau LF. The matricellular protein CCN1 induces fibroblast senescence and restricts fibrosis in cutaneous wound healing. *Nat Cell Biol*. 2010;12: 676–85. doi:10.1038/ncb2070
13. Demaria M, Ohtani N, Youssef S, Rodier F, Toussaint W, Mitchell J, et al. An essential role for senescent cells in optimal wound healing through secretion of PDGF-AA. *Dev Cell*. 2014;31: 722–733. doi:10.1016/j.devcel.2014.11.012
14. Coppé J-P, Patil CK, Rodier F, Sun Y, Muñoz DP, Goldstein J, et al. Senescence-associated secretory phenotypes reveal cell-nonautonomous functions of oncogenic RAS and the p53 tumor suppressor. *PLoS Biol*. 2008;6: 2853–68. doi:10.1371/journal.pbio.0060301
15. Krtolica A, Parrinello S, Lockett S, Desprez PY, Campisi J. Senescent fibroblasts promote epithelial cell growth and tumorigenesis: a link between cancer and aging. *Proc Natl Acad Sci U S A*. 2001;98: 12072–7. doi:10.1073/pnas.211053698
16. Nelson G, Wordsworth J, Wang C, Jurk D, Lawless C, Martin-Ruiz C, et al. A senescent cell bystander effect: Senescence-induced senescence. *Aging Cell*. 2012;11: 345–349. doi:10.1111/j.1474-9726.2012.00795.x
17. Hubackova S, Krejčíková K, Bartek J, Hodny Z. IL1 - and TGF β - Nox4 signaling , oxidative stress and DNA damage response are shared features of replicative , oncogene - induced , and drug - induced paracrine “ Bystander senescence .” *Aging* (Albany NY). 2012;4: 932–951.
18. Acosta JC, Banito A, Wuestefeld T, Georgilis A, Janich P, Morton JP, et al. A complex secretory program orchestrated by the inflammasome controls paracrine senescence. *Nat Cell Biol*. 2013;15: 978–90. doi:10.1038/ncb2784
19. Campisi J, d'Adda di Fagagna F. Cellular senescence: when bad things happen to good cells. *Nat Rev Mol Cell Biol*. 2007;8: 729–740. doi:10.1038/nrm2233
20. Dimri GP, Lee XH, Basile G, Acosta M, Scott C, Roskelley C, et al. A Biomarker That Identifies Senescent Human-Cells in Culture and in Aging Skin in-Vivo. *Proc Natl Acad Sci U S A*. 1995;92: 9363–9367. doi:DOI 10.1073/pnas.92.20.9363
21. Herbig U, Ferreira M, Condel L, Carey D, Sedivy JM. Cellular Senescence in Aging Primates.pdf. 2006; 1–2. doi:10.1126/science.1122446
22. Jeyapalan JC, Ferreira M, Sedivy JM, Herbig U. Accumulation of senescent cells in mitotic tissue of aging primates. *Mech Ageing Dev*. 2007;128: 36–44. doi:10.1016/j.mad.2006.11.008

23. Sorrell JM, Baber M a., Caplan a. I. Site-matched papillary and reticular human dermal fibroblasts differ in their release of specific growth factors/cytokines and in their interaction with keratinocytes. *J Cell Physiol.* 2004;200: 134–145. doi:10.1002/jcp.10474
24. Izumi T, Tajima S, Nishikawa T. Differential expression of alpha 1 and alpha 2 chains of type VI collagen in the upper, middle, and lower dermal fibroblasts in vitro. *J Biochem.* 1995;117: 1004–7. Available: <http://www.ncbi.nlm.nih.gov/pubmed/8586611>
25. Lichtenberger BM, Mastrogiannaki M, Watt FM. Epidermal β -catenin activation remodels the dermis via paracrine signalling to distinct fibroblast lineages. *Nat Commun. Nature Publishing Group;* 2016;7: 10537. doi:10.1038/ncomms10537
26. Feldman SR, Trojanowska M, Smith EA, Leroy EC. Differential responses of human papillary and reticular fibroblasts to growth factors. *Am J Med Sci.* 1993;305: 203–7. Available: <http://www.ncbi.nlm.nih.gov/pubmed/8475944>
27. Mine S, Fortunel NO, Pigeon H, Asselineau D. Aging alters functionally human dermal papillary fibroblasts but not reticular fibroblasts: A new view of skin morphogenesis and aging. *PLoS One.* 2008;3. doi:10.1371/journal.pone.0004066
28. Janson D, Saintigny G, Mahé C, Ghalbzouri A El. Papillary fibroblasts differentiate into reticular fibroblasts after prolonged in vitro culture. *Exp Dermatol.* 2013;22: 48–53.
29. Naylor RM, Baker DJ, van Deursen JM. Senescent cells: a novel therapeutic target for aging and age-related diseases. *Clin Pharmacol Ther.* 2013;93: 105–16. doi:10.1038/clpt.2012.193
30. Xu M, Tchkonja T, Ding H, Ogronik M, Lubbers ER, Pirtskhalava T, et al. JAK inhibition alleviates the cellular senescence-associated secretory phenotype and frailty in old age. *Proc Natl Acad Sci U S A.* 2015;112: E6301–E6310. doi:10.1073/pnas.1515386112
31. Laberge RM, Zhou L, Sarantos MR, Rodier F, Freund A, de Keizer PLJ, et al. Glucocorticoids suppress selected components of the senescence-associated secretory phenotype. *Aging Cell.* 2012;11: 569–578. doi:10.1111/j.1474-9726.2012.00818.x
32. Moiseeva O, Deschênes-Simard X, St-Germain E, Igelmann S, Huot G, Cadar AE, et al. Metformin inhibits the senescence-associated secretory phenotype by interfering with IKK/NF- κ B activation. *Aging Cell.* 2013;12: 489–498. doi:10.1111/accel.12075
33. Laberge R-M, Sun Y, Orjalo A V, Patil CK, Freund A, Zhou L, et al. MTOR regulates the pro-tumorigenic senescence-associated secretory phenotype by promoting IL1A translation. *Nat Cell Biol.* 2015;17: 1049–1061. doi:10.1038/ncb3195
34. Wang Y, Chang J, Liu X, Zhang X, Zhang S, Zhang X, et al. Discovery of piperlongumine as a potential novel lead for the development of senolytic agents. *Aging (Albany NY).* 2016;8: 2915–2926. doi:10.18632/aging.101100
35. Janson DG, Saintigny G, van Adrichem A, Mahé C, El Ghalbzouri A. Different Gene Expression Patterns in Human Papillary and Reticular Fibroblasts. *Journal of Investigative Dermatology.* 2012. pp. 2565–2572.
36. Voglauer R, Chang MWF, Dampier B, Wieser M, Baumann K, Sterovsky T, et al. SNEV overexpression extends the life span of human endothelial cells. *Exp Cell Res. Elsevier Inc.;* 2006;312: 746–759. doi:10.1016/j.yexcr.2005.11.025
37. Janson DG, Saintigny G, van Adrichem A, Mahé C, El Ghalbzouri A. Different Gene Expression Patterns in Human Papillary and Reticular Fibroblasts. *J Invest Dermatol.* 2012;132: 2565–2572. doi:10.1038/jid.2012.192
38. Fripiat C, Chen QM, Zdanov S, Magalhaes J-P, Remacle J, Toussaint O. Subcytotoxic H₂O₂ Stress Triggers a Release of Transforming Growth Factor- 1, Which Induces Biomarkers of Cellular Senescence of Human Diploid Fibroblasts. *J Biol Chem.* 2001;276: 2531–2537. doi:10.1074/jbc.M006809200
39. Freund A, Orjalo A V., Desprez PY, Campisi J. Inflammatory networks during cellular senescence: causes and consequences. *Trends Mol Med.* 2010;16: 238–246. doi:10.1016/j.molmed.2010.03.003
40. Coppé J-P, Desprez P-Y, Krtolica A, Campisi J. The senescence-associated secretory phenotype: the dark side of tumor suppression. *Annu Rev Pathol.* 2010;5: 99–118. doi:10.1146/annurev-pathol-121808-102144
41. Kamburov A, Stelzl U, Lehrach H, Herwig R. The ConsensusPathDB interaction database: 2013 update. *Nucleic Acids Res. Oxford University Press;* 2013;41: D793-800. doi:10.1093/nar/gks1055
42. Collins CA, Kretschmar K, Watt FM. Reprogramming adult dermis to a neonatal state through epidermal activation of β -catenin. *Development.* 2011;138: 5189–99. doi:10.1242/dev.064592
43. Wu C, Guan Q, Wang Y, Zhao ZJ, Zhou GW. SHP-1 suppresses cancer cell growth by promoting degradation of JAK kinases. *J Cell Biochem.* 2003;90: 1026–37. doi:10.1002/jcb.10727
44. Dey BK, Stalker L, Schnerch A, Bhatia M, Taylor-Papadimitriou J, Wynder C. The histone demethylase KDM5b/JARID1b plays a role in cell fate decisions by blocking terminal differentiation. *Mol Cell Biol.* 2008;28: 5312–27. doi:10.1128/MCB.00128-08
45. Gustin JA, Maehama T, Dixon JE, Donner DB. The PTEN tumor suppressor protein inhibits tumor necrosis factor-induced nuclear factor kappa B activity. *J Biol Chem.* 2001;276: 27740–4. doi:10.1074/jbc.M102559200
46. Pavan A, Silva G, Jornada D, Chiba D, Fernandes G, Man Chin C, et al. Unraveling the Anticancer Effect of Curcumin and Resveratrol. *Nutrients.* 2016;8: 628. doi:10.3390/nu8110628
47. López-Otín C, Blasco MA, Partridge L, Serrano M, Kroemer G. The Hallmarks of Aging. *Cell.* 2013;153: 1194–1217. doi:10.1016/j.cell.2013.05.039
48. Kołodziej B, Kowalski R, Kedzia B. Antibacterial and antimutagenic activity of extracts aboveground parts of three *Solidago* species: *Solidago virgaurea* L., *Solidago canadensis* L. and *Solidago gigantea* Ait. *J Med Plants Res.* 2011;5: 6770–6779. doi:10.5897/JMPR11.1098

49. Choi SZ, Choi SU, Lee KR. Phytochemical constituents of the aerial parts from *Solidago virga-aurea* var. *gigantea*. Arch Pharm Res. 2004;27: 164–8. Available: <http://www.ncbi.nlm.nih.gov/pubmed/15022716>
50. Bader G, Seibold M, Tintelnot K, Hiller K. Cytotoxicity of triterpenoid saponins. Part 2: Relationships between the structures of glycosides of polygalacic acid and their activities against pathogenic *Candida* species. Pharmazie. 2000;55: 72–4. Available: <http://www.ncbi.nlm.nih.gov/pubmed/10683877>
51. Abdel Motaal A, Ezzat SM, Tadros MG, El-Askary HI. In vivo anti-inflammatory activity of caffeoylquinic acid derivatives from *Solidago virgaurea* in rats. Pharm Biol. 2016;54: 2864–2870. doi:10.1080/13880209.2016.1190381
52. Chodera A, Dabrowska K, Sloderbach A, Skrzypczak L, Budzianowski J. [Effect of flavonoid fractions of *Solidago virgaurea* L on diuresis and levels of electrolytes]. Acta Pol Pharm. 1991;48: 35–7. Available: <http://www.ncbi.nlm.nih.gov/pubmed/1669338>
53. Apáti P, Szentmihályi K, Kristó ST, Papp I, Vinkler P, Szoke E, et al. Herbal remedies of *Solidago*-- correlation of phytochemical characteristics and antioxidative properties. J Pharm Biomed Anal. 2003;32: 1045–53. Available: <http://www.ncbi.nlm.nih.gov/pubmed/12899992>
54. Sampson JH, Phillipson JD, Bowery NG, O'Neill MJ, Houston JG, Lewis JA. Ethnomedicinally selected plants as sources of potential analgesic compounds: indication of in vitro biological activity in receptor binding assays. Phytother Res. 2000;14: 24–9. Available: <http://www.ncbi.nlm.nih.gov/pubmed/10641043>
55. Bell E, Marek LF, Levinstone DS, Merrill C, Sher S, Young IT, et al. Loss of Division Potential in vitro: Aging or Differentiation. Science (80-). 1978;202: 1158–1163.
56. Bayreuther K, Rodemann HP, Hommel R, Dittmann K, Albiez M, Francz PI. Human skin fibroblasts in vitro differentiate along a terminal cell lineage. Proc Natl Acad Sci U S A. 1988;85: 5112–6. doi:10.1073/pnas.85.14.5112
57. Seshadri T, Campisi J. Repression of c-fos transcription and an altered genetic program in senescent human fibroblasts. Science. 1990;247: 205–209. doi:10.1126/science.2104680
58. Driskell RR, Lichtenberger BM, Hoste E, Kretschmar K, Simons BD, Charalambous M, et al. Distinct fibroblast lineages determine dermal architecture in skin development and repair. Nature. 2013;504: 277–81. doi:10.1038/nature12783
59. Janson D, Saintigny G, Zeypveld J, Mahé C, El Ghalbzouri A. TGF- β 1 induces differentiation of papillary fibroblasts to reticular fibroblasts in monolayer culture but not in human skin equivalents. Eur J Dermatology. 2014;24: 342–348. doi:10.1684/ejd.2014.2312
60. Walters HE, Deneka-Hannemann S, Cox LS. Reversal of phenotypes of cellular senescence by pan-mTOR inhibition. Aging (Albany NY). 2016;8: 231–244. doi:10.18632/aging.100872
61. Trapnell C, Roberts A, Goff L, Pertea G, Kim D, Kelley DR, et al. Differential gene and transcript expression analysis of RNA-seq experiments with TopHat and Cufflinks. Nat Protoc. 2012;7: 562–578. doi:10.1038/nprot.2012.016
62. Mildner M, Ballaun C, Stichenwirth M, Bauer R, Gmeiner R, Buchberger M, et al. Gene silencing in a human organotypic skin model. Biochem Biophys Res Commun. 2006;348: 76–82. doi:10.1016/j.bbrc.2006.07.035

10. Appendix C Contributions during the Phd

10.1. Talks and Posters

Talks

May 2017	ISEV2017 Annual Meeting, Toronto 'miRNAs enclosed in small extracellular vesicles are selectively secreted and retained in cellular senescence and modulate keratinocyte functionality'
December 2016	Menopause - Andropause - Anti Aging 2016, Vienna, Austria 'Modulation der Hautalterung durch extrazelluläre Vesikel'
September 2015	Hyperflow 2015, Vienna, Austria 'Den kleinsten Partikeln auf der Spur. Nanopartikel Tracking Analysis, für die Charakterisierung und Quantifizierung von Partikeln unter 200nm'
March 2015	Geriatrikongress, Vienna 'High levels of oncomiR-21 contribute to the senescence-induced growth arrest in normal human cells and its knock-down increases the replicative lifespan.'
February 2013	Buck Institute for Research on Aging, Novato, CA Host Judy Campisi 'Novel factors modulating the life span of cells and organism'

Short Poster talks

September 2016	ESDR 2016, The European Society for Dermatological Research, Annual Meeting, Munich, Germany 'The extravesicular miRNome of senescent human fibroblasts and its impact on keratinocyte functionality'
May 2016	IEV 2016, International society for extracellular vesicles, Rotterdam 'The extravesicular miRNome of senescent human fibroblasts and its impact on keratinocyte functionality'
September 2015	ESDR 2015, The European Society for Dermatological Research, Annual Meeting Rotterdam 'The microvesicular miRNOME of senescent human fibroblasts'

Posters and Abstracts

Poster

Abstracts and Poster from cooperative studies

IEV2017

Transfer of extracellular vesicles between fibroblasts and keratinocytes in cellular senescence

Madhusudhan Reddy Bobbili, **Lucia Terlecki-Zaniewicz**, Markus Schosserer, Vera Pils, Dietmar Pum, Johannes Grillari

SFRRE2016

A' multi-omic investigation of the effects of long wavelength ultraviolet light on primary human keratinocytes.

Marie-Sophie Narzt^{1,2}, Ionela M. Nagelreiter^{1,2}, Valery N. Bochkov³, Julie Latreille⁴, Maria Fedorova⁵, Zhixu Ni⁵, Manuel Filzwieser², Haihong Qin¹, Lucia Terlecki^{2,6}, Matthias Hackl⁷, Johannes Grillari^{2,6}, Lucian Beer⁸, Martin Bilban⁹, Erwin Tschachler¹, Florian Gruber^{1,2}

¹ Department of Dermatology Medical University of Vienna, Austria

² Christian Doppler Laboratory for Biotechnology of Skin Aging, Austria

³ Department of Pharmaceutical Chemistry, University of Graz, Austria

⁴ ChanelPB, Pantin, France

⁵ Institute of Bioanalytical Chemistry, Faculty of Chemistry and Mineralogy, Universität Leipzig, Germany

⁶ VIBT-BOKU Vienna, Austria

⁷ TAmiRNA Vienna, Austria

⁸ Department of Biomedical Imaging and Image-guided Therapy, Medical University of Vienna, Austria

⁹ Core Facility Genomics, Medical University of Vienna, Austria

EMBL 2016

Glioblastoma microenvironment modulation via extracellular vesicles containing a RGS family member

Bernadette Blauensteiner, Klara Soukupa, Angela Halfmanna, Friedrich Erharta, Barbara Dillingera, Lucia **Terlecki-Zaniewicz**, Johannes Grillari, Alexander Dohnala

a Department of Tumor Immunology, St Anna Kinderkrebsforschung, Children's Cancer Research Institute Vienna (CCRI), Vienna, Austria

b GrillariLABS, Vienna Institute of BioTechnology, University of Natural Resources and Life Sciences Vienna, Vienna, Austria

OEGAI 2016

Characterization of RGS16 in the tumor-promoting immunosuppressive niche of glioblastoma multiforme

B Blauensteiner 1, K Soukup 1, A Halfmann 1, F Erhart 1, B Dillinger 1, G Zirkovits 1, **L Terlecki-Zaniewicz** 2, L Zopf 3, J Grillari 2, J Zinnanti 3, AM Dohnal 1

1 Department of Tumor Immunology, St Anna Kinderkrebsforschung, Children's Cancer Research Institute Vienna (CCRI), Vienna, Austria

2 GrillariLABS, Vienna Institute of BioTechnology, University of Natural Resources and Life Sciences Vienna, Vienna, Austria

3 PciMAG Facility, The Vienna Biocenter Core Facilities GmbH (VBCF), Vienna, Austria

Geriatriskongress 2015

The role of miR-663 and PP5 in the oxidative stress response and cell cycle control of human dermal fibroblasts (HDF)

Ingo Lämmermann, Lucia Terlecki-Zaniewicz, Kathrin Garschall, Harald Kühnel, Matthias Wieser and Johannes Grillari

ESDR2015

Development of a three-dimensional tissue model for skin aging

Regina Weinmüllner, Michael Mildner, Lucia Terlecki-Zaniewicz, Markus Schosserer, Ingo Lämmermann, Erwin Tschachler, Florian Gruber and Johannes Grillari

10.2. Prizes and Scholarships

May 2017	IEV2017 Junior Member Scholarship For the attendance at the IEV2017 Annual Meeting, May 2017 Toronto
January 2017	Best Talk award and Scholarship for visiting and learning abroad Science Days 2017, of the Austrian Society of Dermatology and Venereology ÖGDV, Salisbury, Austria “The extravesicular miRnome of senescent fibroblasts and its impact on keratinocyte functionality”

10.3. Visits abroad

01/2014 – 03/2014 **Visiting Scientific Researcher, at Phil Hanawalt Lab**, Stanford University, USA.

Objective: ‘Is SNEV a transcription coupled repair factor? Application of the Comet-FISH’ (J. Guo et al. 2013; reviewed by Spivak 2015)

Funding: OEFG Öster. Forschungsgemeinschaft and KUWI (Boku)

10.4. Students

Co-supervision of Bachelor and Master students

Jennifer Schwestka, 28.1.2016 Bachelor Thesis: Evaluation of the paracrine miRNA crosstalk between dermal and epidermal cells

Vera Pils, 25.1.2017 Master Thesis: The impact of senescence associated extravesicular microRNAs on keratinocyte functionality

Tonja Grillenberger Bachelor thesis ongoing

Michaele Hauser Master thesis ongoing

Co-supervision

Matthias Mattanovic – Bachelor part time for 6 months

Cristina Morsiani – PhD, visiting student for 6 months

Riccardo Paone – PhD, visiting student for 6 months

Damita Jevapatarakul – Master - visiting student for 6 months

11. Appendix D Curriculum vitae

DIPL. ING. LUCIA TERLECKI - ZANIEWICZ

Date and place of birth	20.01.1984, Vienna,
Address	Corvinusgasse 4/4/14, 1230 Vienna
Phone number	+ 43 6505824228
Email	lucia.terlecki@gmail.com ,



QUALIFICATIONS AND PROFESSIONAL EXPERIENCE

07/2013 till present	PhD thesis , University of Natural Resources and Life Sciences, Vienna <i>Thesis: Differentially secreted miRNAs from senescent human fibroblasts and their impact on primary keratinocytes</i> <u>Supervisor</u> : Assoc. Prof. Dr. Johannes Grillari
Since 2015	Co-supervision for Bachelor and Masterstudents, Guest students and cooperations (Italy and Vienna) Project planning and coordination
01/2014 – 03/2014	Visiting Scientific Researcher, at Phil Hanawalt Lab , Stanford University, USA. Funding: OEFG Öster. Forschungsgemeinschaft and KUWI (Boku)
01/2012-11/2012	Master thesis , University of Natural Resources and Life Sciences, Vienna <i>Thesis: miR-663 & miR-21 converging on the p53 pathway in cellular senescence</i> <u>Supervisor</u> : Assoc. Prof. Dr. Johannes Grillari
03/2011-03/2012	Tutor for molecular biology exercises II -part time, University of Natural Resources and Life Sciences, Vienna
03/2011-07/2013	Junior Scientist/technician - part time Supervision: Dr. Christian Kaisermayer and Univ.Prof. Dipl.-Ing. Dr.nat.techn. Renate Kunert GE healthcare in cooperation with University of Natural Resources and Life Sciences, Vienna
07 - 09/2008	Practical Bachelor thesis and internship Department of Internal Medicine I, Division of Hematology - Medical University Vienna,

Bachelor thesis: *Comparison of two bisulfite treatment methods for determination of methylation status in hemophilia*

Supervisor: Univ.Prof.ⁱⁿ DI.ⁱⁿ Dr.ⁱⁿ Christine Mannhalter

Ao.Univ.Prof. Dipl.-Ing. Dr.nat.techn. Lukas Mach

10/2006-10/2010

Tutor employment at the center of IT-services– part time
University of Natural Resources and Life Sciences, Vienna

08/2007-10/2010

Assistant of the management of mechanical engineering consultant
MEC© TERZA, Vienna -part-time

08/2005

Internship chemical laboratory and office at the Austrian
Competence Centre of Food Safety, Vienna

EDUCATION

08/2013 till present

PhD student in the Christian Doppler Laboratory for Biotechnology of Skin Aging, University of Natural Resources and Life Sciences, Vienna

10/2010-07/2013

Master program Biotechnology, University of Natural Resources and Life Sciences, Vienna

09/2002-09/2010

Bachelor program food and biotechnology, University of Natural Resources and Life Sciences, Vienna and Department of Internal Medicine I, Division of Hematology - Medical University Vienna,

09/1994-06/2002

High school of cath. Private school of the Dominican nuns, Vienna

LABORATORY SKILLS

***In-vitro* studies**

- Animal cell culture: primary cells, stem cells, differentiation, senescence, 3D tissue culture
- optimization of transient and stable miRNA/siRNA/plasmid based transfection systems; Lipid based transfection methods; Electroporation; Viral Transduction
- extracellular vesicles as transport vehicles,

***In-vivo* studies**

- Mice; Isolation of cells, RNA, bone

Biotechnology production

- Mammalia cell culture, adherent monolayer and suspension culture, preparation for fermentation processes
- Process monitoring and assessment of parameter
- Carrier cultivation of serum-free cultures

- | | |
|--------------------------|---|
| Molecular biology | <ul style="list-style-type: none"> • FACS, nanoparticle tracking analysis (NTA), workshop to NTA in cooperation with particle metrix • standard molecular biology methods (Protein and RNA based) • DNA damage COMET-FISH assay (Stanford Phil Hanawalt lab) • blood/plasma, RNA/miRNA isolation from liquids and NGS library preparation for RNA-Seq |
|--------------------------|---|

Dry Lab	<p>Computational data analysis with a focus on miRNA analysis. ANOVA, Benjamini Hochberg FDR, Exploratory Data analysis (PCA; Hierarchical Clustering), parametric and nonparametric tests, Spearman, Rank, Pearson correlation</p>
----------------	---

FURTHER SKILLS

- | | |
|-------------------------|--|
| EDV | <p><u>Programs:</u>
MS Office package professional, special Excel features for large datasets, Corel Draw, Graph Pad,</p> |
| Languages | <p><u>German</u>: mother tongue
<u>English</u>: fluent in speech and writing, <i>English III, IV, and technical English</i> at the University of Natural Resources and Life Sciences, Vienna (2012-2013)
<u>Italian</u>: Basic knowledge</p> |
| Driver's license | <p>Class B</p> |

EXTRACURRICULAR ACTIVITIES

- | | |
|---|--|
| <p>Club Biotech
2007 - 2013</p> | <p>in cooperation with <i>YEBN (young european biotech network)</i>, an intercultural communication workshops among scientists
President of Club Biotech, 10/2012 - 06/2013
Vicepresident of Club Biotech, 10/2011 – 10/2012</p> |
| <p>Tutoring
2002 – 2003,
2010 - 2012</p> | <p>Tutoring in mechanical engineering, molecular biology and chemistry
Learning support for hearing impaired students</p> |
| <p>Athletic training
1998 - ongoing</p> | <p>Gymnastics instructor for children and adults,
Coordinator of summer camps for children and young adults
Member of the management board of sports and gymnastic club Gersthof</p> |

PUBLICATIONS AND INVITED TALKS

Khan A, Dellago H, **Terlecki-Zaniewicz** L, Karbiener M, Weilner S, Hildner F, Steininger V, Gabriel C, Mück C, Jansen-Dürr P, Hacobian A, Scheideler M, Grillari-Voglauer R, Schosserer M, Grillari J.

SNEV^{hPrp19/hPso4} Regulates Adipogenesis of Human Adipose Stromal Cells.
Stem Cell Reports. 2017 Jan 10;8(1):21-29. doi: 10.1016/j.stemcr.2016.12.001.

Song X, Narzt M, Nagelreiter IM, Hohensinner P, **Terlecki-Zaniewicz** L, Tschachler E, Grillari J, Gruber F.
Autophagy deficient keratinocytes display increased DNA damage, senescence and aberrant lipid composition after oxidative stress in vitro and in vivo.

Redox Biol. 2016 Dec 18;11:219-230. doi: 10.1016/j.redox.2016.12.015.

Dellago H, Preschitz-Kammerhofer B, **Terlecki-Zaniewicz** L, Schreiner C, Fortschegger K, Chang MW, Hackl M, Monteforte R, Kühnel H, Schosserer M, Gruber F, Tschachler E, Scheideler M, Grillari-Voglauer R, Grillari J, Wieser M.

High levels of oncomiR-21 contribute to the senescence-induced growth arrest in normal human cells and its knock-down increases the replicative lifespan

Aging Cell. 2013 Jun;12(3):446-58. doi: 10.1111/accel.12069.

December 2016

Menopause - Andropause - Anti Aging 2016, Vienna, Austria

„Modulation der Hautalterung durch extrazelluläre Vesikel“

September 2015

Hyperflow 2015, Vienna, Austria

„Den kleinsten Partikeln auf der Spur. Nanopartikel Tracking Analysis, für die Charakterisierung und Quantifizierung von Partikeln unter 200nm“

February 2013

Buck Institute for Research on Aging, Novato, CA

Host Judy Campisi

“Novel factors modulating the life span of cells and organism”

AWARDS

May 2017

IEV2017 Junior Member Scholarship

For the attendance at the IEV2017 Annual Meeting, May 2017 Toronto

January 2017

Best Talk award and Scholarship for visiting and learning abroad

Science Days 2017, of the Austrian Society of Dermatology and Venereology ÖGDV, Salisbury, Austria

“The extravesicular miRnome of senescent fibroblasts and its impact on keratinocyte functionality”

Academic year 2010/11

Performance scholarship

University of Natural Resources and Life Sciences, Vienna